# Design and Sensitivity of Buckling Restrained Braces

Audsley Sarah Jones

A thesis submitted in partial fulfilment of the requirements for the degree, Doctor of Philosophy in Civil and Natural Resources Engineering

The University of Canterbury

Christchurch

New Zealand

January 2020

*For my dad, Warren, thank you for walking this journey with me, with steadfast support and belief.*

# Abstract

This thesis evaluates the design of Buckling Restrained Braces (BRBs) based on freely available information with respect to design, qualification and implementation. Key sensitivity areas of the BRB are evaluated through experimental testing, numerical analysis and the development of a theoretical model. 37 specimens were experimentally tested to current accepted standards evaluating the key sensitivity areas: restraining mechanism; stroke length; transition gradient; embedment length; and yielding to non-yielding radii. Among the 37 experimental specimens, three were nominally identical, for evaluating the reliability in design performance.

The nominally identical specimens were successful in completing the minimum testing protocol, with the design of these specimens used as the foundation for the development of the empirical and semi-empirical models. Two empirical models were developed, evaluating the design, irrespective of experimental results. These models were unsuccessful. Two further models were investigated, calibrating the yielding core cyclic hardening to that observed experimentally. The final model was successful in response up to 1.0 x drift.

A theoretical model was developed predicting first yield and the maximum compression capacity. The results of this theoretical model, based on the geometric and measured material magnitudes showed that it was conservative in estimating the critical values. The tensile strength of the BRB was 103 % of that measured experimentally and 90 % of the maximum compression strength. This model can be used to develop a backbone curve for BRB assessment.

# Acknowledgements

Firstly, thank you to Professor Stephen Hicks of University of Warwick (formerly New Zealand Heavy Engineering Research Association, HERA). Your support, persistent encouragement and belief in the completion of the research have been a solid foundation. Without your support this PhD would not have succeeded.

To the lab technicians at the University of Canterbury. Thank you for always bringing joy and laughter to long days in the lab. John Maley, thank you for being involved from day one; the concept, design and application. Your time and dedication exceeded the norm. To Alan Thirlwell, for supporting not only in the lab, but also outside. Your problem solving, execution and moral support went above and beyond. Thank you also to Dave MacPherson, Gavin Keats and Russell McConchie, for supporting this project and lending a hand when needed.

To Christina Blackford, thank you for always being available to chat, vent and unconditionally supporting me throughout the past seven years. To Dominic and Kirsty Mahoney, thank you both for keeping me honest, encouraged and supported. Dom, thank you for reviewing the theoretical model, and Kirsty being an amazing rowing partner.

To Anna Winkley Tuck, thank you for being a constant support and for reviewing this thesis.

Thank you to Nandor Mago (HERA) for support in the development of the numerical model. Kevin Cowie (Steel Construction New Zealand) for proofing and adding industry input into this thesis.

And finally, to HEERF, the Building Research Levy and College of Engineering Earthquake Safe Building Scholarship, without whose assistance this research would not have been possible.

# Table of Contents

# List of Figures

# List of Tables

# Nomenclature

| | |
|---|---|
| $a$ | Fabrication imperfection of core |
| | Maximum deflection (amplitude) of that mode |
| $A_e$ | Cross-sectional area of non-yielding and connection region |
| $A_{ec}$ | Equivalent cross-sectional area |
| $A_o$ | Original cross-sectional area of core |
| $A_{sc}$ | Cross-section area of core |
| $A_{sc}$ | Cross-sectional area of yielding region |
| $A_t$ | Cross-sectional area of transition region |
| $b$ | Isotropic hardening factor |
| $B_c$ | Width of core |
| $B_r$ | Width of outer casing |
| $C$ | Kinematic hardening modulus |
| $c_m$ | Restraining medium contribution factor (mortar contribution factor) |
| $DCR$ | Demand to capacity ratio |
| $D_r$ | Depth of outer casing |
| $E$ | Young's modulus of core |
| $e$ | Eccentricity of axial force |
| $f_c'$ | Restraining medium compression strength |
| $f_y$ | Yield stress |
| $f_{yr}$ | Yield strength of outer casing |
| $H$ | Vertical slope component, perpendicular to brace longitudinal axis |
| $I$ | Second moment of area of column |
| $I_1$ | Second moment of area of section one |
| $I_2$ | Second moment of area of section two |
| $I_E$ | Importance level |
| $I_{min}$ | Minimum outer casing axial stiffness |
| $K_F$ | Stiffness modification factor |
| $K_{model}$ | Adjusted BRB stiffness |
| $K_{required}$ | Required member stiffness for design drift |

| | |
|---|---|
| $K_{ysc}$ | Stiffness of core yielding region |
| $l$ | Length of column |
| $L_1$ | Length of section one |
| $L_2$ | Length of section two |
| $L_e$ | Length of non-yielding and connection region |
| $L_t$ | Length of transition region |
| $L_w$ | Buckling length |
| $L_{wp}$ | Member length (work-point to work-point) |
| $L_y$ | Length of yielding region |
| $m$ | Integer |
| $M_B$ | Maximum flexural outer casing demand |
| $M_{casing}$ | Nominal moment capacity of outer casing |
| $M_y^B$ | Flexural strength of outer casing |
| $n$ | Number of half sine waves |
| $N_{c,max}$ | Maximum observed compression strength |
| $N_{cr}^E$ | Euler buckling strength of outer casing |
| $N_{brace}^{oc}$ | Adjusted (overstrength) brace capacity in compression |
| $N_{brace}^{ot}$ | Adjusted (overstrength) brace capacity in tension |
| $N_s$ | Nominal section capacity in compression |
| $N_t$ | Nominal section capacity in tension |
| $N_{t,max}$ | Maximum observed tensile strength |
| $P$ | Axial load |
| $P_{crit}$ | Critical axial load |
| $P_{lb}$ | Outer casing capacity with respect to punching force |
| $Q$ | Isotropic hardening factor |
| $r$ | Radius |
| $s_r$ | Unbonding medium thickness (or required gap) per face |
| $t_c$ | Length of contact between core and restraining medium (assumed to be the core thickness) |
| $t_m$ | Thickness of restraining medium |

| | |
|---|---|
| $t_r$ | Thickness of outer casing |
| $t_{sc}$ | Core thickness |
| $T$ | External work |
| $U_b$ | Bar strain energy |
| $U_f$ | Elastic medium deformation energy |
| $v$ | y axis deflection at length $x$ |
| $w$ | Uniformly distributed load |
| $x$ | x axis |
| | Distance along length, $l$ |
| $y$ | y axis |
| | Initial deflection |
| $y_1$ | Deflection due to section one |
| $y_2$ | Deflection due to section two |

| | |
|---|---|
| $\alpha$ | Angle between x and h axes |
| | Algebraic value |
| | Backstress |
| $\beta$ | Compression strength adjustment factor (determined through observed maximum loads in experimental verification) |
| $\beta_e$ | Modulus of foundation |
| $\delta$ | Maximum y deflection |
| $\delta_{bf}$ | Total axial core deformation |
| $\varepsilon_{max}$ | Maximum expected tensile strain |
| $\varepsilon_{sc}$ | Yielding core strain |
| $\gamma$ | Ratio of yielding core length to total brace length |
| | Kinematic hardening parameter |
| $\lambda$ | External deflection |
| $\lambda_b$ | Ratio of outer casing capacity to critical axial force, local buckling occurs when less than 1.0 |
| $\eta$ | Ratio of average axial stress outside core to average stress within the core |
| $v$ | Poisson ratio |

| | |
|---|---|
| $\phi$ | Strength reduction (capacity) factor |
| $\phi_{om}$ | Overstrength factor, incorporating the statistical variation in yield stress component |
| $\phi_{os}$ | Overstrength factor, incorporating only the strain hardening component |
| $\Delta$ | Deflection |
| $\Delta_b$ | Applied axial deformation |
| $\Delta_{bm}/\delta_i$ | Design storey drift, no less than 0.01 storey height |
| $\Delta_{by}/\delta_e$ | Deformation at elastic yield |
| $\theta_x$ | Design storey drift angle |

# 1 Introduction

## 1.1 Background

Buckling restrained braces (BRB) were conceived in the early 1970s and developed within the 1980s. This established technology has become a common alternative to conventional bracing due to its ability to develop balanced and stable hysteresis loops. The original purpose of BRBs was to be used a secondary lateral load resisting system, however with the availability of the technology, it is more common to see BRBs being used as a primary system.

A buckling restrained brace frame (BRBF) is a frame which contains a BRB. The BRB is composed of a yielding element and restraining mechanism. These elements can be all-steel or composite in nature. A traditional BRB is a combination of steel and grout/concrete, with all-steel BRBs referring to fully steel composition. Traditional BRBs have the ability to utilise the composite material nature, with greater capacity and reliability in high stress environments. The all-steel BRB performance is limited by the steel properties, particularly within lateral restraint of the yielding element.

The yielding element is referred to as the core, and is broken down into specific regions namely: yielding, transition, non-yielding restrained, non-yielding unrestrained (stroke) and a connection region. The non-yielding regions of the core may contain stiffeners for greater connection stability. The core is surrounded by a unbonding medium or gap to prevent friction and to de-bond the core (to act independently) from the restraining mechanism. The restraining mechanism is composed of a restraining medium typically grout/concrete encased in a steel outer casing, providing full lateral restraint to the core, developing equal compression to tension capacity. For all-steel BRBs the restraining mechanism is composed of steel elements, typically bolted along the member length.

The development and availability of the BRB has been predominantly controlled by proprietary providers, and as such, design and sensitivity information is generally unavailable in the public domain. Following the 2011 earthquake in Christchurch, New Zealand, the BRB became a desirable technology, reducing cost and foundation requirements. Within New Zealand, the BRB is used in the primary lateral load resisting system. The BRB is not explicitly defined within New Zealand regulations, and as such ambiguities in design and implementation can be exploited. New Zealand designers commonly design their own BRBs, without experimental verification. Internationally the BRB and BRBF are regulated through design guidance and regulatory bodies. This thesis, although with a New Zealand approach will consider a global perspective of BRB design and evaluation.

The purpose of this thesis is to evaluate the freely available information regarding BRB design, qualification and implementation requirements. Based on this information, experimental testing of the BRB designed based on the available information will be evaluated for sensitivity. Key sensitivity areas of the BRB will be examined, with the intent to provide design parameters. The qualification protocols of those countries (Unites States of America, Canada and Japan) with regulatory qualification requirements will be evaluated, and any recommendations on their use and specified protocol will be discussed.

A theoretical and numerical investigation of BRB design is also carried out. Due to the lack of, and capacity of testing facilities within New Zealand it is desirable for consultants to design the BRB without qualification testing. The viability of using a theoretical and/or numerical model to adequately design a BRB without experimental verification will be evaluated.

This thesis aims to cohesively detail the available information in one source and provide an understanding of the design, behaviour and response of the BRB. It is hoped that the outcomes from this research will lead to regulatory framework within New Zealand, and a re-evaluation of the framework available in other countries.

## 1.2 Outline of thesis

Chapter 2 presents a literature review outlining the history and development of the BRB and its key characteristics. The composition, theory and design of the BRB is detailed based on standards and codes of practice, academic publications and commercially available resources, providing an insight and highlighting areas requiring investigation.

Chapter 3 presents the design, fabrication, experimental testing and dissection of BRBs with a range of sensitivities. Both single bay and V configuration BRB specimens are investigated, both with and without stiffeners. The restraining mechanism, stroke length, transition gradient, embedment length and yielding to non-yielding radii are all investigated for geometric sensitivity. Three nominally identical specimens are compared along with an investigation of experimental rotational verification through eccentric load application.

Chapter 4 presents the development of a theoretical model representing an elastic BRB, which predicts the critical load for first mode buckling with respect to the interaction of the core and restraining mechanism. Both the equilibrium and energy methods are investigated with respect to an elastic foundation and varying cross-sectional area. Numerical modelling (finite element analysis) is also investigated empirically based on the nominally identical specimens investigated within Chapter 3. Three models are considered: the core; core to transition regions; and the reliability of modelling the full BRB.

Chapter 5 presents key findings from the previous chapters. These findings are discussed as well as recommendations and limits for current BRB design. Future work and final conclusions of the current BRB design practices are also presented.

# 2 Buckling Restrained Brace Design and Development

This section presents a literature review examining buckling restrained brace (BRB) conception, composition and development. Proposed behavioural theories and design guidance from codes of practice, research and commercial natures are investigated, along with methods of quantification through experimental testing and numerical modelling of the BRB member.

## 2.1 Conception and early development

The development of the BRB dates back to the early 1970s when steel sections encased in concrete were being investigated for buckling performance (Takeuchi T & Wada A, 2017). The first concept of the BRB originated in 1973 at the Architectural Institute of Japan as a flat steel plate sandwiched between a pair of reinforced concrete panels (Corte G. D et al., 2011). The use of two panels gave a "debonding layer" around the flat plate, allowing the specimen to develop stable hysteresis loops, eventually failing through local buckling. This concept was expanded in 1976 and first published in English in 1988 by (Watanabe A et al., 1988) through use of a cross-shaped steel core member within a concrete filled square steel tube (Figure 2-1). These specimens, using debonding layers of vinyl/mastic tape in the thickness (major axis) direction and polystyrol in the width (minor axis) direction, demonstrated stable hysteresis loops if the yielding load applied to the core member was smaller than the buckling load of the steel tube (Watanabe A et al., 1988).

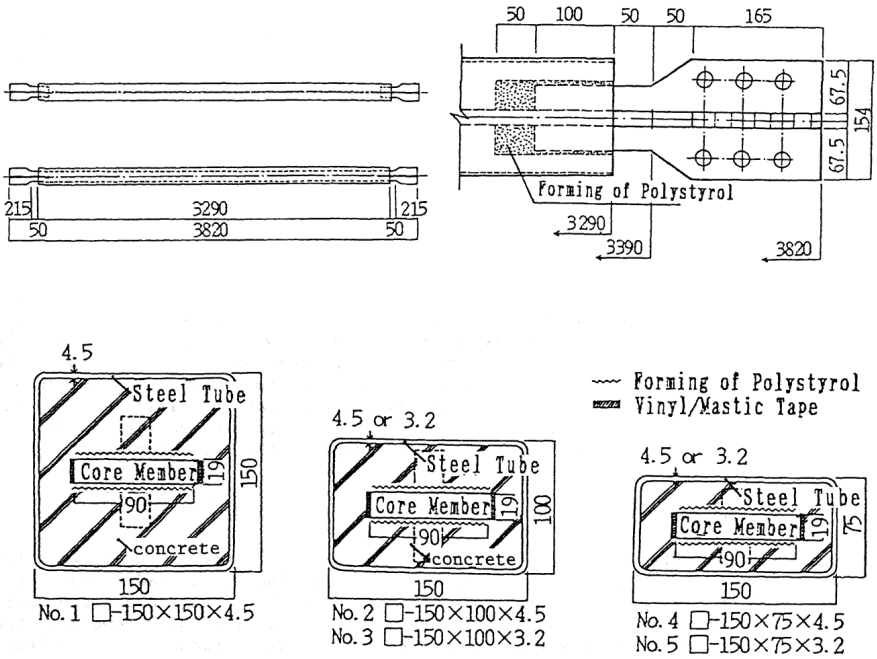


**Figure 2-1: Cross-section of first successful BRB specimens (Watanabe A et al., 1988)**

This form of BRB is that commonly used today, with variances typically to the concrete and steel tube by use of all steel components to restrain the steel core. The concrete can be used with small aggregate, and grout is commonly used in its place due to high flow in small spaces. The core remains to this day lower grade steel (due to its higher ductility), Conversely, as the external steel tube is not restricted by ductility demands, it can be specified as a higher grade. The core is also not restricted to being singular, with double and triple cores embedded in a singular tube common in high demand projects.

BRBs were first used in Japan as a secondary load resisting system in 1989 at the Nippon Steel Second Headquarters (Takeuchi T & Wada A, 2017). An adaption of the BRB was first introduced to New Zealand in 1991 in the retrofit exoskeleton of the University of Canterbury, Christchurch Psychology Building. Further research of BRBs and the first adoption within America was in 1998 at the Plant and Environmental Sciences Building at University of California, Davis (Figure 2-2 (a)) (Jones A. S, 2011), with a shift in application from a secondary to a primary lateral load resisting system (Fussell A, 2010). BRB application has since expanded to Asia, Europe, Canada and South America among other regions. Construction in Christchurch, New Zealand following the 2011 earthquake has favoured the BRB system over concentric and eccentrically braced frames (CBF and EBF respectively) (Figure 2-2 (b)).

**a)** **b)**

**Figure 2-2: a) Plant and Environmental Sciences Building, UC Davis (Univeristy of California Davis, 2018) b) Rutherford Regional Science and Innovation Centre, Canterbury University, NZ (University of Canterbury, 2018)**

The largest scale application of BRBs has been at the Wilshire Grand, situated in downtown Los Angeles (Figure 2-3 and Figure 2-4) which was opened in June 2017. 170 BRBs were used throughout the 73-storey structure with design capacities ranging from 3600 kN to 9800 kN. 40 of these BRBs were in “double-double” configuration (Figure 2-3) giving a combined design capacity of 19600 kN.

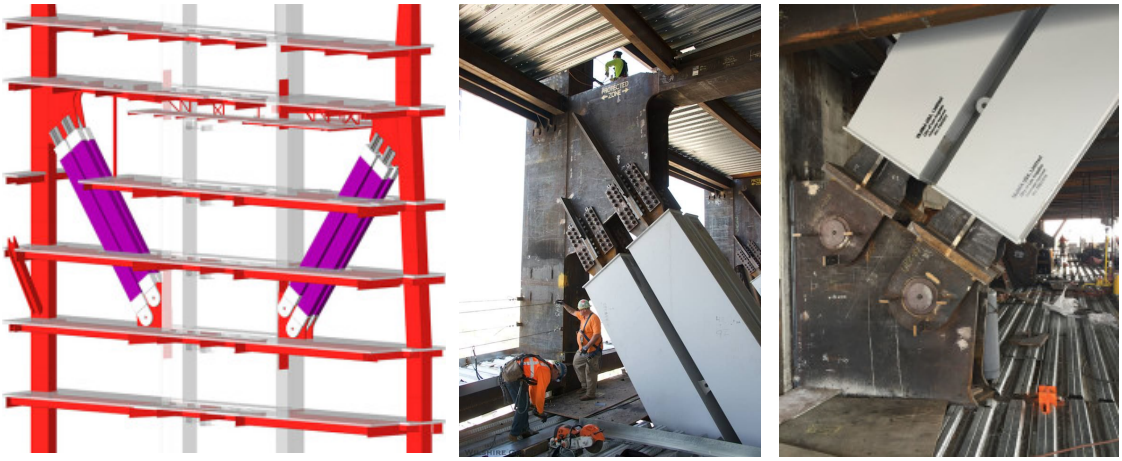

a) b) c)

**Figure 2-3: Wilshire Grand, Los Angeles (Structure Magazine, 2015) a) Lower outrigger design with double-double BRBs b) Bolted connection end c) Pin connection**

a) b)

**Figure 2-4: Wilshire Grand, Los Angeles a) Upper outrigger design (Structure Magazine, 2015) b) Artist interpretation of 70th floor Sky Lobby (Urban Land, 2018)**

Since the mid 1990s BRB development has been in the form of proprietary products provided by commercial suppliers. The increase in patenting and intellectual property surrounding the design of the BRB member has resulted in little information freely available to design engineers regarding the member itself and its influence and interaction with surrounding elements. It is common, even for bespoke projects to be carried out by propriety providers based on this lack on information.

Proprietary providers typically supply general tables of core sizes with respect to axial load and bay dimensions, supplying a stiffness modification factor which can be used in conjunction with Euler buckling to determine the resulting frame deformation (CoreBrace, 2011, 2013a, 2013b, 2014, 2016). The casing can also be preliminarily sized based on the expected core cross-sectional area and work-point length. This initial sizing allows designers to determine key factors (expected drift, adjusted tension and compression design loads, resulting vertical frame forces etc.), however, these dimensions, resulting design loads and drift are confirmed along with gusset plate and connection design from the proprietary provider based on experimental

testing. The true design of the BRB member and surrounding elements is carried out by the propriety provider, with little design documentation passed on due to intellectual property rights.

## 2.2 Key concepts and principles

BRBs are defined by their suppression of buckling through stable and balanced hysteresis response, with compression capacity of the member equal to or slightly greater than that of tension. The BRB is composed of a yielding element carrying the axial load, responding independently to a restraining mechanism.

The BRB is reported to be a simple, economic and reliable alternative to conventional bracing due to its stable hysteretic behaviour and suppression of buckling (Black C. J et al., 2004; Fussell A, 2010; Lopez-Almansa F et al., 2012; Takeuchi T & Wada A, 2017). BRBs are commonly used to control and maintain storey drifts with sustained dissipation and strength allowing elastic behaviour of the surrounding elements and frame (Black C. J et al., 2004; Kim J & Choi H, 2004). BRB members are composed of three elements: the core, unbonding medium, and restraining mechanism (outer casing and restraining medium) (Figure 2-5).

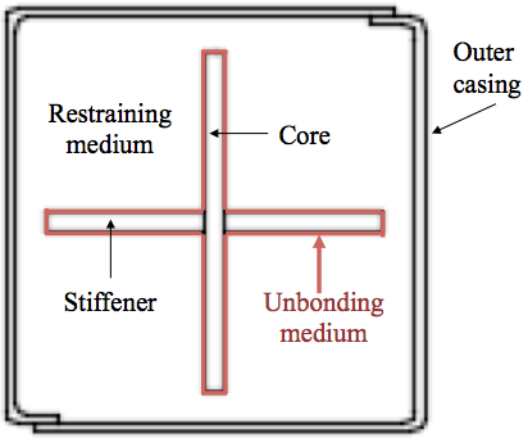


**Figure 2-5: BRB Elements**

The core is typically composed of steel and can be broken down into specific regions namely: yielding, transition, non-yielding restrained, non-yielding unrestrained (stroke), and connection region (Figure 2-6) (Fussell A, 2010). The core can be singular or multiple in nature and is typically of ‘dog bone’ shape (Tremblay R et al., 2006). It can include longitudinal stiffeners preventing local buckling and yielding of the non-yielding and transition regions (Tremblay R et al., 2006).

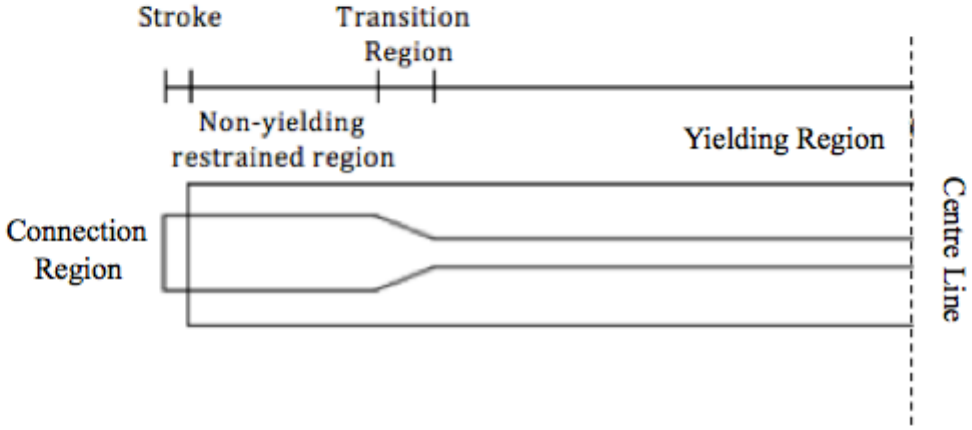


**Figure 2-6: Core Regions**

The primary role of the unbonding medium is to reduce/prevent friction from developing between the core(s) and the restraining mechanism, preventing the transfer of the core axial load (Iwata M & Murai M, 2006; Lin P-C et al., 2012; Tremblay R et al., 2006). The unbonding medium can range in material, and in some countries as a result of patent restrictions, an air gap. The restraining mechanism typically comprises two components, a restraining medium and an outer casing. The restraining medium is typically composed of grout and is used to restrain the core from local buckling. The outer casing that is composed of steel, confines the restraining medium and also supressed global buckling of the member. The BRB term refers to this form of restraining mechanism combination. Research has also been carried out using an all-steel restraining mechanism (commonly referred to as an all-steel BRB, Figure 2-7). The primary reason for employing an all-steel BRB over the traditional BRB is to reduce fabrication quality associated issues and costs (Chou C-C et al., 2012; Tremblay R et al., 2006). To increase the stiffness to be similar to that of a traditional restraining mechanism, multiple steel sections are used, typically bolted along the length of the BRB member. However, the design of all-steel BRBs is out of the scope of this thesis.

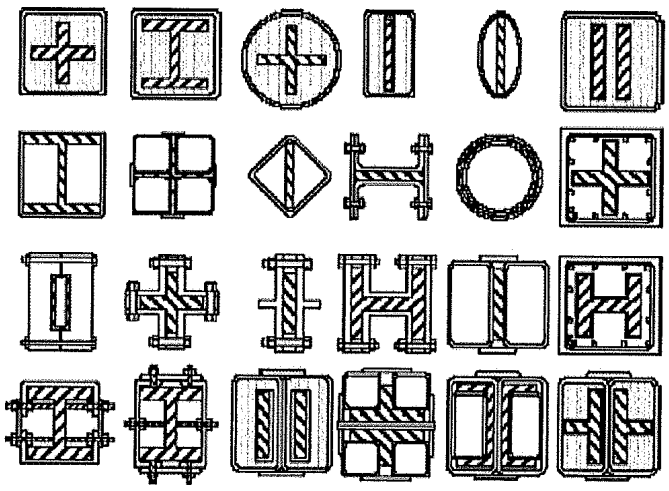

**Figure 2-7: Composite and all-steel BRB schematics (Corte G. D et al., 2011)**

BRBs are known primarily for their restraint from buckling as a result of full lateral support of the core (Choi H & Kim J, 2006; Cowie K et al., 2016; Fussell A, 2010; Lopez-Almansa F et al., 2012). As the core carries the full axial load, significant inelastic deformation is concentrated within the yielding region, enhancing ductility capacity and low cycle fatigue resistance (Andrews B. M, Fahnestock L. A, et al., 2009; Asgarian B & Shokrgozar H. R, 2009; Cowie K et al., 2016; D'Aniello M et al., 2006; Kim J & Choi H, 2004). BRBs are classified by the ability to develop balanced and stable hysteresis loops (Figure 2-8) in both tension and compression loading (Andrews B. M, Fahnestock L. A, et al., 2009; Andrews B. M, Song J, et al., 2009; Asgarian B & Shokrgozar H. R, 2009; Carden L. P et al., 2006; Choi H & Kim J, 2006; Chou C-C & Chen S-Y, 2010; Corte G. D et al., 2011; Cowie K et al., 2016; D'Aniello M et al., 2006; Fussell A, 2010; Iwata M & Murai M, 2006; Kim J & Seo Y, 2003; Mahin S et al., 2004; Mirtaheri M et al., 2011). Due to strain hardening of the core and friction development between the core and restraining mechanism through Poisson's effect (Fussell A, 2010; Kim J & Seo Y, 2003), the compression overstrength will exceed the tension capacity, in some cases by up to 35 % (Corte G. D et al., 2011). The ability of the member to have similar (if not equal) compression and tension capacities allows for stable and concentrated energy dissipation under seismic loading. As the BRB member is not part of the gravity-resisting system of the structure, it can be replaced post event(s) provided the residual drift is small (American Institute of Steel Construction, 2010; Cowie K et al., 2016; Iwata M & Murai M, 2006; Mirtaheri M et al., 2011).

BRBs possess significant ductility before, during and after a seismic event as a result of the core restraint, allowing a large drift capacity and better fatigue loading tolerance when compared to CBFs (Asgarian B & Shokrgozar H. R, 2009; Corte G. D et al., 2011). The ideal response of a BRB is balanced repeatable hysteretic response with positive incremental stiffness and the compression overstrength greater than but close to 1.0. This is difficult to achieve due to frictional effects that build up within

the unbonding layer between the yielding core and restraining mechanism. As frictional effects increase, so does the differing in tension and compression capacities, and strain concentration throughout compression loading leading to larger permanent residual drift.

For qualification of the member a minimum cumulative ductility demand (CDD) must be met. By achieving the minimum CDD, successful designs demonstrate the member is not governed by fatigue (Corte G. D et al., 2011; D'Aniello M et al., 2006; Mahin S et al., 2004). BRBs are susceptible to low post-yield stiffness resulting in large permanent drift when used as the primary lateral load resisting system. When used as a secondary system, such as in conjunction with a moment-resisting frame, self-centring of the structure is possible.

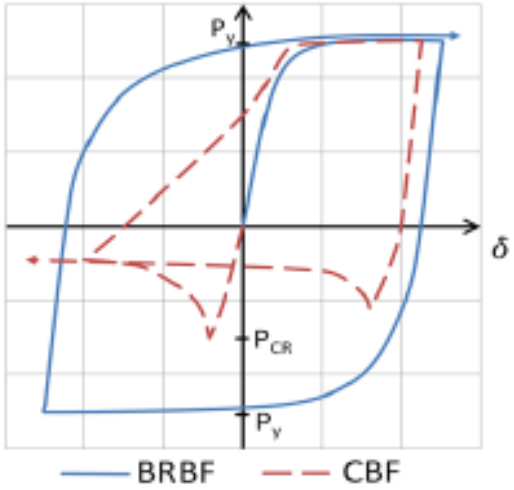


**Figure 2-8: Hysteresis behaviour of BRB frames and concentrically brace frames (Jones A. S, 2011)**

## 2.3 Composition, theory and design

The following sub-section details the compositional elements that form the BRB member, along with theory of their function and design from regulatory, academic and commercial sources.

### Standards and Codes of Practice

The presence of BRB and BRB frame (BRBF) design in regulatory documents is a relatively new adoption. The BRBF is a frame with BRB members connected concentrically to beams and columns (American Institute of Steel Construction, 2010). The American Institute of Steel Construction (AISC) was the first national regulatory body to implement specifications for BRB/BRBF design and qualification. These are found in Section F4 and K3 of ANSI/AISC 341-16 (American Institute of Steel Construction, 2010, 2016). These specifications were built on the regulatory framework developed by the Structural Engineers Association of Northern California (SEAONC), “Recommended Provisions for Buckling-Restrained Braced Frames” published in 2001 (Structural Engineers Association of Northern California, 2001). These were written to be used in conjunction with FEMA 350 and FEMA 450

(Federal Emergency Management Agency & SAC Joint Ventrue, 2000; Program on Improved Seismic Safety Provisions, 2003).

The Canadian Standards Association (CSA) first introduced BRBs within CSA-S16-09. Although experimental testing was specified, provisions for this were not included until the 2014 edition within Annex J (Canadian Standards Authority, 2014; Humar J et al., 2010). BRBs are also mentioned within the National Building Code of Canada (NBCC) as a lateral force resisting system (Humar J et al., 2010), with overstrength and ductility force modifications included.

BRBs are cited in European Standard EN 15129, as a displacement dependent device, requiring quantification of the BRB design through experimental testing (European Standards Committee, 2010). Within the Eurocodes, no specific BRB/BRBF design regulations are present. However, EN 1998-1 (Eurocode 8) has been used by proprietary providers to quantify BRB members in accordance with the requirements of EN 15129 (Dunai L, 2011). This quantification was carried out with experimental analysis for non-conforming buildings using the procedures for seismic no-collapse, through non-linear static (pushover) or non-linear dynamic (time-history) (British Standards Institute, 2004).

New Zealand does not currently have BRB/BRBF specific guidelines, regulatory or other. Although BRBs can fall under ductile CBF design in accordance with NZS 3404:Part 1 (Standards New Zealand, 1997), BRB/BRBF design more commonly falls under Section 1.5, “Use of alternative materials or methods”. Quantification under Section 1.5 requires the use of a special study in accordance with Appendix A of AS/NZS 1170.0, where experimental testing or rational design based on accepted engineering principles needs to be undertaken. Special studies using rational design are the standard preference, with experimental testing being costly and limited by local capacity and appropriate testing facilities.

Within Japan, BRBs must be prequalified and are subject to the approval of the Building Centre of Japan (BCJ) (Takeuchi T & Wada A, 2017). The qualification and approval requirements are not currently available in English, however any insight to these through reviewed literature will be presented in the present chapter.

Although not regulatory documents, the “Seismic Design of Buckling-Restrained Braced Frames” produced by the Structural Steel Education Council (SSEC) (Lopez W. A & Sabelli R, 2004); NEHRP Seismic Design Technical Brief No. 11 “Seismic Design of Steel Buckling Restrained Brace Frames” (Kersting R. A et al., 2015); and NEHRP Professional Fellowship Report “Research on Improving the Design and Analysis of Earthquake-Resistant Steel-Brace Frames”, provide useful supplementary guidance (e.g. BRBF worked examples, evolution of the qualification procedure etc.) (Sabelli R, 2000).

**Research**

The backbone of BRB development has been through academic investigation into the design and performance of the member (and system) since its conception in the late 1970s. Internationally there has been a growing interest in BRB design and behaviour, with research groups forming and focusing on local application with increasing popularity of the system. Japan, Taiwan, Europe, Canada and America (with a focus on proprietary and bridge application) are the key research contributors to BRB development, with groups from New Zealand, Chile, China and the Middle East recently contributing to this body of knowledge.

Research has varied in form from experimental, theoretical and numerical, and can range from BRB member design, connection performance, gusset behaviour, frame interaction and dual systems. The following subsections will focus primarily on academic research on BRB member design and behaviour, with connection interaction excluded for the purpose of understanding the complexity and sensitivity of the member itself. Although out of the scope of this literature review, it is noted in the Japan Society of Seismic Isolation publication "Buckling-Restrained Brace and Applications" that the design of the connection, gusset and frame directly influence the performance of the BRB member and therefore it is desirable for the consultant engineer to understand the behaviour and uniqueness of the BRB member in system-level design (Takeuchi T & Wada A, 2017).

**Commercial**

The commercially available information comes from a limited number of sources. Firstly, the proprietary providers, with basic design information provided to consultant engineers to initially size the required BRB for the design frame. Secondly, qualification-testing reports, where methods of analysis are evaluated for insight into qualification and theory behind commercial design. And thirdly, personal correspondence between the proprietary providers and the present author are also included to further the availability of design information not commonly available in the public domain.

### 2.3.1 Core

The core of a BRB, typically composed of steel, carries the axial load of the member and is the primary dissipating element. It can be singular, multiple in quantity, thickness and grade (and also stiffened) (Lopez W. A & Sabelli R, 2004). The core may be of varying sections and sizes, but is typically a stiffened steel flat plate. The core is divided into five regions (see Figure 2-6), with each region having a function contributing not only to the overall performance of the BRB member, but also the neighbouring regions. If one region is poorly designed and unable to dissipate energy adequately, then subsequent regions must compensate.

The core can be separated into elastic and plastic zones, with the yielding core being the only region in the plastic zone. No welds are permitted in the plastic zone. Multiple plastic zone BRBs have been successfully tested, allowing multiple necking regions, however it is common for the plastic zone to be singular in nature for ease of design. The elastic regions are strengthened against plastic behaviour through increasing the stiffness of the zone. The stiffness is typically adjusted through increasing the cross-sectional area of the core and/or the use of stiffeners in the elastic zone, which also provide connection stability and prevent plastic torsional buckling from occurring. Within this subsection, general design information of the core will be presented, with specific design criteria for the five core regions presented.

**Standards and Codes of Practice**

American and Canadian codes provide identical requirements for the core. AISC 341-16 Section F4.5b (American Institute of Steel Construction, 2010) and CSA-S16-14 Section 27.8.3 (Canadian Standards Authority, 2014) specify that the core be composed of structural steel plate(s), surrounded by a system that prevents buckling. Splices are not permitted within the core. If the plate(s) used is greater than 50 mm in thickness, minimum notch toughness requirements must be met (based on AISC 341-16 Section A3.3 and CSA G40.20, respectively).

Within AISC 341-16, Section F4.2, eccentric loads are permitted through the BRB core, provided they are less than the beam depth. The loads resulting from the eccentricities must be primarily dissipated through the yielding of the member, additional inelastic capacity will be required to resist these loads. Section F4.3 specifies that the BRB does not resist gravity loads and within CSA-S16-14 Section 27.8.5.1 the factored resistance of the surrounding frame elements (including connections) shall be equal to, or exceed the combined load of gravity and adjusted BRB connection forces. Also, within CSA-S16-14 Section 27.8.2 a maximum frame height of 40 m is specified, unless stable inelastic response can be demonstrated. The maximum building height was introduced to prevent soft storey response when BRBs are used in a non-moment-resisting system (primary lateral load resisting system); this consequently also limits the accepted BRB work-point to work-point (wp-wp) length (Canadian Standards Authority, 2014; Humar J et al., 2010).

The adjusted member strength and associated overstrength factors are well agreed upon through provisions with BRB specific design.

The design strength, for design of core regions and qualification, is taken as:

$$\phi N_s = \phi N_t = \phi f_y A_{sc} \qquad \text{Equation 2-1}$$

where:

$N_s$ Nominal section capacity in compression

$N_t$ Nominal section capacity in tension

$\phi$ Strength reduction (capacity) factor

$= 0.9$ for structural steel

$f_y$ Yield stress

Specified as minimum/lower bound yield strength of the steel core or actual yield strength of the steel core determined from an average of 2 coupon tests (American Institute of Steel Construction, 2010; Canadian Standards Authority, 2014)

$A_{sc}$ Cross-section area of core

The adjusted brace strength, for the design of the connection region and surrounding frame members, based on qualification testing is:

$$N_{brace}^{oc} = \beta \phi_{os} \phi_{om} f_y A_{sc} \quad \text{Equation 2-2}$$

$$N_{brace}^{ot} = \phi_{os} \phi_{om} f_y A_{sc} \quad \text{Equation 2-3}$$

Where:

$N_{brace}^{oc}$ Adjusted (overstrength) brace capacity in compression

$N_{brace}^{ot}$ Adjusted (overstrength) brace capacity in tension

$\beta$ Compression strength adjustment factor

This factor is determined through observed maximum compression loads in each cycle above member yield. The greatest value is taken.

$= \frac{N_{c,max}}{N_{t,max}} > 1.0$

but < 1.3 (American Institute of Steel Construction, 2010; Canadian Standards Authority, 2014)

but < 1.1 (Takeuchi T & Wada A, 2017)

Where:

$N_{c,max}$ is the maximum observed compression strength

$N_{t,max}$ is the maximum observed tensile strength

$\phi_{os}$ Overstrength factor, incorporating only the strain hardening component, taken as the ratio between observed maximum tension load in each cycle above member yield to the expected member yield (either based on coupon tests or nominal capacity).

$\phi_{os} = \omega = \frac{N_{t,max}}{f_y A_{sc}}$ (American Institute of Steel Construction, 2010; Canadian Standards Authority, 2014)

$\phi_{om}$ Overstrength factor, incorporating the statistical variation in yield stress component, but not applicable if $f_y$ is determined based on coupon tests (American Institute of Steel Construction, 2010; Canadian Standards Authority, 2014). This value is equivalent to $R_y$ in AISC 341-16 (American Institute of Steel Construction, 2010)

Within New Zealand the following range of overstrength and compression adjustment factors are accepted based on Saxey and Daniels (Saxey B & Daniels M). This report evaluates 23 BRB subassemblage tests of three different proprietary BRB manufacturers. The overstrength and compression adjustment factor equations used in this study are recommended to be evaluated by designers, such that the parameters can realistically be achieved (Cowie K, 2018). Empirical relationships are developed based on the 23 BRB subassemblage tests. Where bolted and pinned equations are presented, these tests were predominantly from one supplier and should be used only where appropriate. The theoretical relationships are developed based on theoretical determination from first principals of the compression overstrength and strain hardening overstrength factor (see Equation 2-15 and Equation 2-16).

| | | |
|---|---|---|
| Empirical | $\phi_{os} = 20.63\varepsilon_{sc} + 1.15$ | Equation 2-4 |
| Theoretical | $\phi_{os} = 27.62\varepsilon_{sc} + 0.98$ | Equation 2-5 |
| Empirical | $\beta_{bolted} = 3.57\varepsilon_{sc} + 1.06$ | Equation 2-6 |
| Empirical | $\beta_{pinned} = 10.54\varepsilon_{sc} + 1.08$ | Equation 2-7 |
| Empirical | $\beta = 4.97\varepsilon_{sc} + 1.10$ | Equation 2-8 |
| Theoretical | $\beta = 10\varepsilon_{sc} + 1.00$ | Equation 2-9 |

where:

$\varepsilon_{sc}$ Yielding core strain

For comparison purposes, the above equations are presented in Table 2-1, and are evaluated for the design range $10\Delta_{by}$ to $20\Delta_{by}$ (1.30 % - 2.61 % strain). It can be observed that the overstrength factor increases as drift (strain increases). The theoretical value increases by 1.3 times with double the strain, whereas the upper bound overstrength factor determined based on subassemblage testing increases by 1.2 times. The theoretical overstrength is conservative at higher strain concentrations. The compression overstrength values only increase slightly with double the strain. The bolted specimens have the smallest increase of 1.04 times with double strain, however this could be attributed to the large number of specimens (130) resulting in less skew of the results. The pinned compression overstrength factor increases by 1.1 times, unlike the bolted specimens, the data points for the pinned specimens was

lower (86) with outliers skewing the results. The upper bound compression overstrength determined from bolted, pinned and welded (22 data points) is 1.05 times with double strain. The theoretical compression overstrength is 1.1 times with half strain, and is conservative in comparison to that of experimentally evaluated subassemblage tests.

**Table 2-1: Overstrength factors summary (Saxey B & Daniels M)**

| Equation | $\phi_{os,10}$ | $\phi_{os,20}$ | $\beta_{10}$ | $\beta_{20}$ |
|---|---|---|---|---|
| Upper bound, $\phi_{os}$ (Equation 2-4) | 1.42 | 1.69 | - | - |
| Theoretical, $\phi_{os}$ (Equation 2-5) | 1.34 | 1.70 | - | - |
| Upper bound (bolted connection), $\beta_{bolted}$ (Equation 2-6) | - | - | 1.10 | 1.15 |
| Upper bound (pinned connection) $\beta_{pinned}$ (Equation 2-7) | - | - | 1.21 | 1.35 |
| Upper bound (all) $\beta$ (Equation 2-8) | - | - | 1.17 | 1.23 |
| Theoretical $\beta$ (Equation 2-9) | - | - | 1.13 | 1.26 |

The core stiffness is taken for modelling purposes, and design of the surrounding elements as an adjusted yielding core stiffness. The brace strength is determined via the cross-sectional area of the yielding core. However, the yielding core stiffness does not adequately capture the member stiffness; to compensate for this, a stiffness modification factor, $K_F$, is adopted (see Equation 2-10) (American Institute of Steel Construction, 2016). The stiffness modification factor is typically set by proprietary providers and is determined based on successful qualification testing designs. The stiffness modification factor accounts for the equivalent stiffness of the member of uniform dimensions and equivalent behaviour.

$$K_{model} = \frac{K_F A_{sc} E}{L_{wp}} \qquad \text{Equation 2-10}$$

where:

$K_{model}$ Adjusted BRB stiffness

$K_F$ Stiffness modification factor, based on qualification testing, unique to each BRB design.

$L_{wp}$ Member length (work-point to work-point)

$E$ Young's modulus of core

**Research**

Prior to BRB adoption within CSA-S16, design of BRBs within Canada was carried out with respect to Tremblay *et al.* (Tremblay R et al., 2006). This research was widely available, with proof testing carried out of the presented designs. This research investigated both composite and all-steel BRB designs through subassemblage verification testing, while also providing theoretical design guidance where appropriate. According to these authors, the total axial core deformation ($\delta_{bf}$) with respect to the design axial stress $\phi f_y$, can be approximated as:

$$\delta_{bf} = \frac{\phi f_y}{E} L_{wp}[\gamma + \eta(1-\gamma)] \qquad \text{Equation 2-11}$$

where:

$\gamma$ Ratio of yielding core length to total brace length

$\eta$ Ratio of average axial stress outside core to average stress within the core

The core strain ($\varepsilon_{sc}$) corresponds to the design storey drift of the frame (it is assumed the core cross-sectional area is adjusted for each floor, such that the resistance is not significantly greater than the factored force for that specific level). The first components of Equation 2-12 approximate the total member deformation based on the importance level of the design structure. The second components approximate the elastic deformation response of the elastic zones (outside of the yielding core).

$$\varepsilon_{sc} = \left[\frac{5.2}{I_E}\delta_{bf} - \eta\phi_{os}\phi_{om}\frac{f_y}{E}(1-\gamma)L_{wp}\right]\frac{1}{L_y} \qquad \text{Equation 2-12}$$

where:

$I_E$ Importance level

$L_y$ Length of yielding region

For use in New Zealand it is recommended the core strain is taken as (Cowie K, 2018):

$$\varepsilon_{sc} = \frac{\theta_x \sin 2\alpha}{2\dfrac{L_y}{L_{wp}}} \qquad \text{Equation 2-13}$$

where:

$\theta_x$ Design storey drift angle

$\alpha$ Angle of BRB inclination with respect to the horizontal

Tremblay *et al*. (Tremblay R et al., 2004) approximated the equivalent cross-sectional area of the core (Equation 2-14) and for preliminary design calculations it was assumed $\frac{A_{sc}}{A_e} = 0.3$ and $\frac{A_{sc}}{A_t} = 0.5$.

$$A_{ec} = \frac{L_{wp}}{\left(\frac{L_y}{A_{sc}}\right) + \left(\frac{L_t}{A_t}\right) + \left(\frac{L_e}{A_e}\right)} = \frac{A_{sc} L_{wp}}{\left(L_y + L_t\left(\frac{A_{sc}}{A_t}\right) + L_e\left(\frac{A_{sc}}{A_e}\right)\right)} \quad \text{Equation 2-14}$$

where:

$L_t$ Length of transition region

$L_e$ Length of non-yielding and connection region

$A_{sc}$ Cross-sectional area of yielding region

$A_t$ Mean across-sectional area of transition region

$A_e$ Cross-sectional area of non-yielding and connection region

It should be noted that Equation 2-12 is considered to be inappropriate for design within New Zealand (Cowie K, 2018). This is due to the method of importance level application within New Zealand's design codes.

**Commercial**

Commercial providers follow, as a minimum, the design requirements outlined above in Standards and Codes of Practice. The three key areas proprietary providers are concerned with are qualification testing, overstrength factors (as a result of strain hardening of the steel core), and member stiffness (Robinson K, 2013). Overstrength factors along with core strain and stiffness can be derived theoretically to aid initial design. The following equations, although determined within research, are specified by proprietary providers as preliminary design guidance for designers, and hence is detailed within the commercial sections of this review.

The compression strength adjustment factor can be broken down into contributing factors of Poisson effects and friction between the core surface and the restraining mechanism, and approximated as (CoreBrace, 2011):

$$\beta = 1 + Poisson + Friction \quad \text{Equation 2-15}$$

where:

$Poisson$ Approximated as

$$\frac{N_{c,max} - N_{t,max}}{N_{t,max}} = \frac{\frac{A_o}{(1-\varepsilon_{sc})} - \frac{A_o}{(\varepsilon_{sc}+1)}}{\frac{A_o}{(\varepsilon_{sc}+1)}} = \frac{2\varepsilon_{sc}}{(1-\varepsilon_{sc})} \approx 2\varepsilon_{sc}$$

$Friction$ Minimum approximated as

$= 1.5(2\varepsilon_{sc}) = 3\varepsilon_{sc}$

According to (Tsai K-C et al., 2004), friction effects range between 1.5 and 9 times Poisson effects

The strain at yield is based on a deflection amplification factor of 5.0 in accordance with ASCE.SEI 7 (American Society of Civil Engineers, 2016), relating the relative brace stiffness to curvature with respect to AISC 341-16. If no information is available with regards to the force at the controlling drift, the strain can be approximated as (CoreBrace, 2011):

$$\varepsilon_{sc} = 2 \cdot \phi \cdot 5 \cdot \left(\frac{f_y}{E}\right) \qquad \text{Equation 2-16}$$

For example, if

$f_y = 250MPa$

$E = 205x10^3 MPa$

The minimum theoretical value of $\beta$ is as follows:

$$\beta = 1 + 2\varepsilon_{sc} + 1.5(2\varepsilon_{sc}) = 1 + 5 \cdot \left[2 \cdot 0.9 \cdot 5\left(\frac{250}{205x10^3}\right)\right]$$

$\beta = 1.05$

If the design force for the controlling drift case is provided, the strain can be approximated as (CoreBrace, 2011):

$$\varepsilon_{sc} = \left(\frac{2 \cdot 5 \cdot \Delta_{by} K_{ysc}}{A_{sc} E}\right) \qquad \text{Equation 2-17}$$

where:

$\Delta_{by}$ Deformation at first yield

$K_{ysc}$ Stiffness of core yielding region

Within the Brace on Demand cloud based system, the compression strength adjustment factor is taken as 1.15 for all cases (for steel $f_y$ ranging from 248 – 345 MPa) (Lin P-C et al., 2013). The Brace on Demand system is an open-source software which designs BRBs based on the research carried out at the National Taiwan University. These BRBs are unique in design, allowing designers to input the required parameters, and an appropriate BRB design produced. The BRBs are fabricated locally with the fabrication licence distributed by the Brace on Demand group.

Proprietary provider CoreBrace (CoreBrace, 2011) have derived the strain-hardening factor based on the stiffness, deformation and load in the plastic and elastic regions for a given strain. This derivation can be summarised as:

$$\phi_{os} = 1 + \frac{E_p\left(2\varepsilon_{sc} - \frac{f_y}{E}\right)}{f_y} \qquad \text{Equation 2-18}$$

$E_p$ is approximated as 2.24 $\%E$ by (CoreBrace, 2011) with $\varepsilon_{sc}$ given by Equation 2-16, so Equation 2-18 can be re-written as:

$$\phi_{os} = 1 + \frac{E_p}{E}\left[(4 \cdot \phi \cdot 5) - 1\right] \qquad \text{Equation 2-19}$$

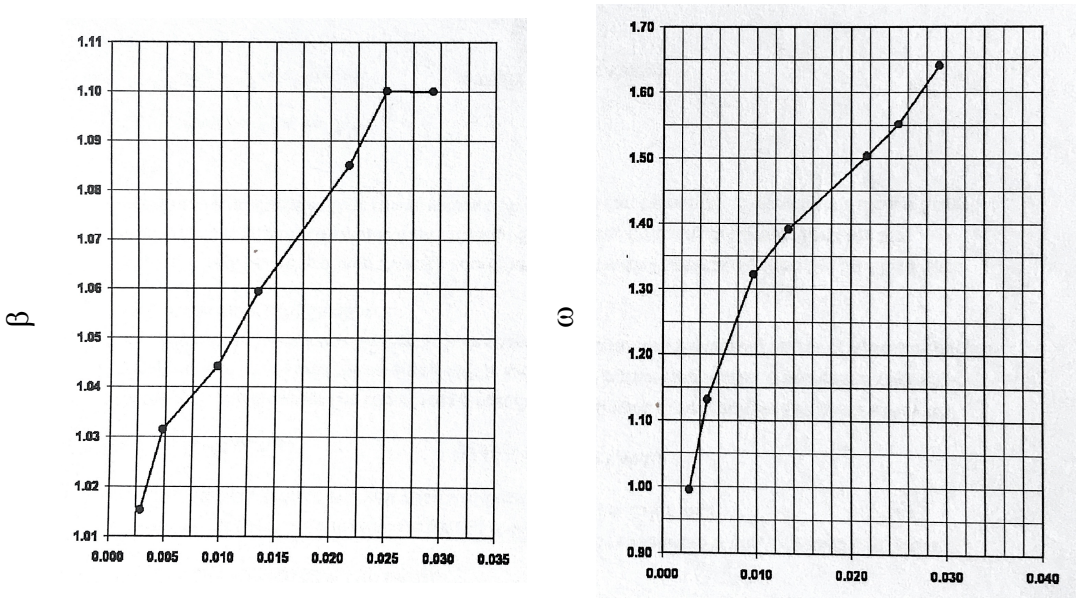


**Figure 2-9: Backbone curves (CoreBrace, 2011)**

It is common for the compression and material overstrength factors to be graphically represented through backbone curves, plotted against strain for a given BRB design (Figure 2-9). These curves are available to designers to aid in the design of the surrounding elements (which are dependent on the adjusted brace strengths taking into consideration these factors).

The core stiffness is approximated by Equation 2-10 (CoreBrace, 2013a, 2013b, 2014; Robinson K). The stiffness modification factor can be initially approximated by the ratio of the member stiffness required for the design drift to the yielding region stiffness (Equation 2-20) (CoreBrace, 2011), proprietary provider supplied graphs (Figure 2-10) or by assuming the elastic regions remain rigid (Equation 2-21):

$$K_F = \frac{K_{required}}{K_{ysc}} \qquad \text{Equation 2-20}$$

where:

$K_{required}$ Required member stiffness for design drift

$$K_F \cong \frac{L_{wp}}{L_y} \qquad \text{Equation 2-21}$$

The stiffness modification factor (Figure 2-10) can be used while modelling the member as a truss element within engineering software (CoreBrace, 2011; Lin P-C et al., 2013). The modification factor can range from 1.2 (for long BRB members) to 1.5 (for short BRB members). It is advised that the stiffness modification factor does not exceed 1.6, as the greater the value, the greater the strain development within the yielding region (Lin P-C et al., 2013).

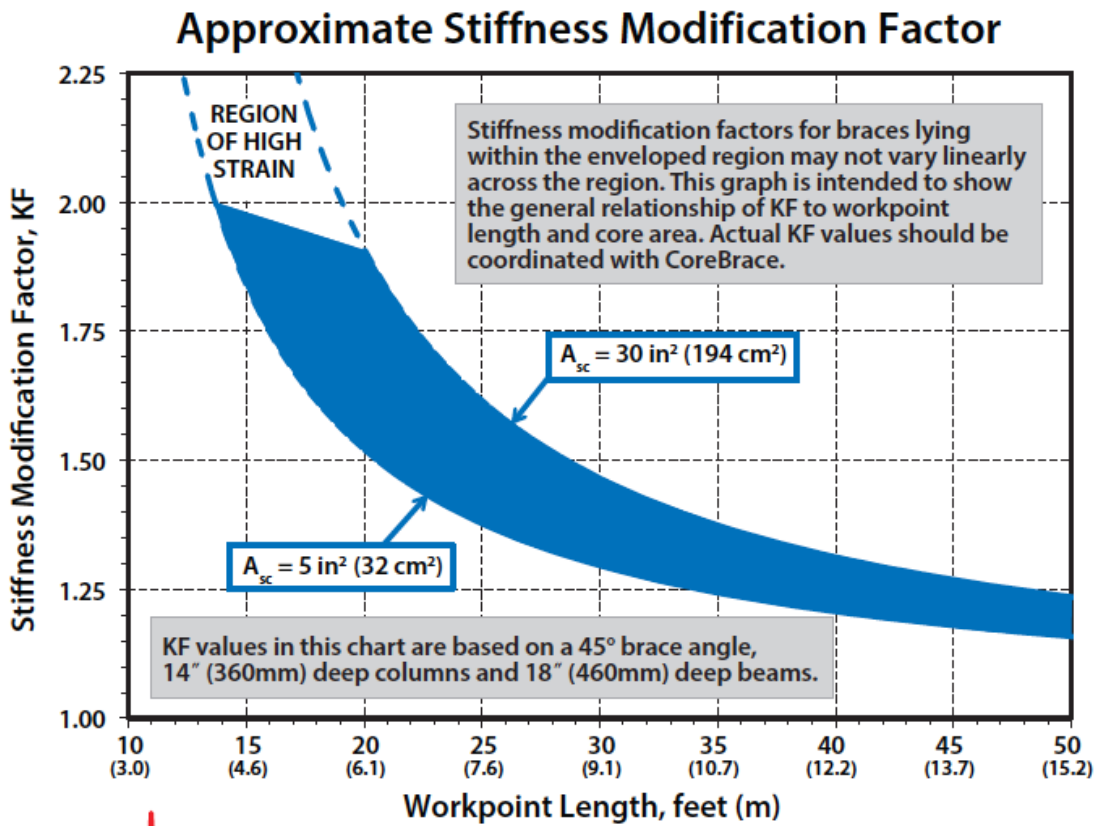
Approximate Stiffness Modification Factor
REGION OF HIGH STRAIN
Stiffness modification factors for braces lying within the enveloped region may not vary linearly across the region. This graph is intended to show the general relationship of KF to workpoint length and core area. Actual KF values should be coordinated with CoreBrace.
$A_{sc}$ = 30 in² (194 cm²)
$A_{sc}$ = 5 in² (32 cm²)
KF values in this chart are based on a 45° brace angle, 14″ (360mm) deep columns and 18″ (460mm) deep beams.
Stiffness Modification Factor, KF
2.25
2.00
1.75
1.50
1.25
1.00
10 (3.0)
15 (4.6)
20 (6.1)
25 (7.6)
30 (9.1)
35 (10.7)
40 (12.2)
45 (13.7)
50 (15.2)
Workpoint Length, feet (m)

a)

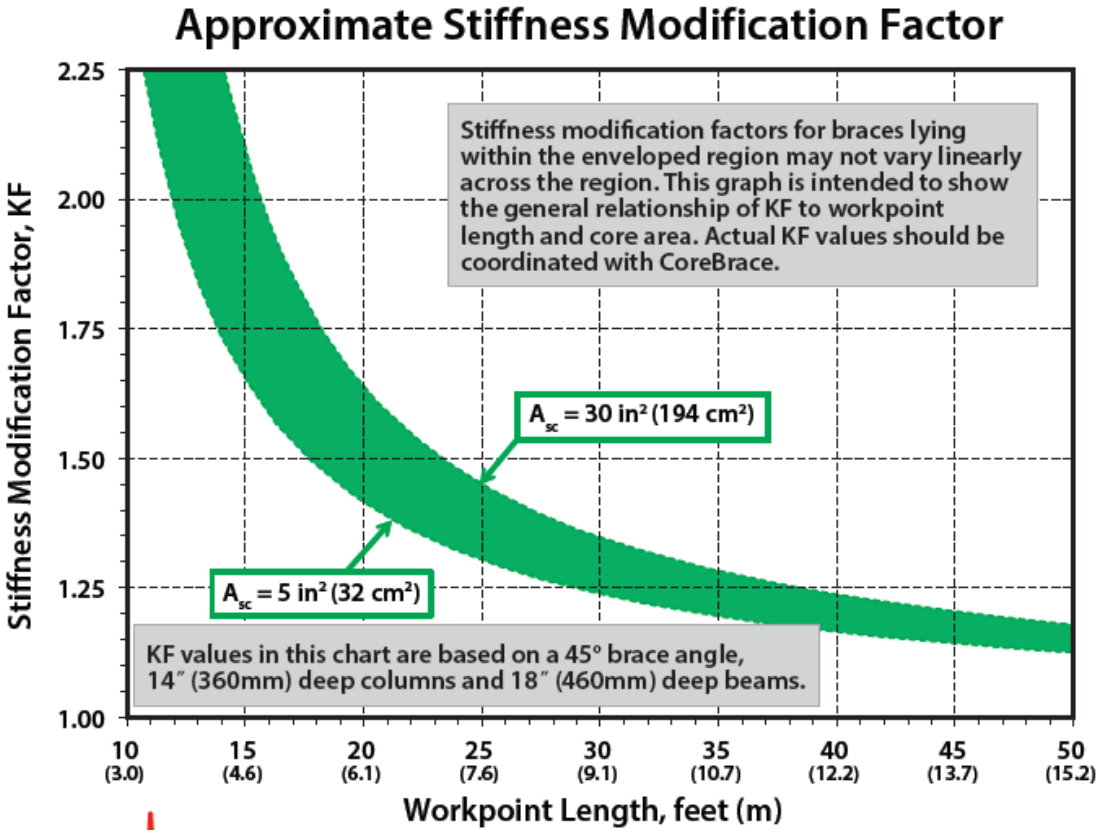
Approximate Stiffness Modification Factor
Stiffness modification factors for braces lying within the enveloped region may not vary linearly across the region. This graph is intended to show the general relationship of KF to workpoint length and core area. Actual KF values should be coordinated with CoreBrace.
$A_{sc}$ = 30 in² (194 cm²)
$A_{sc}$ = 5 in² (32 cm²)
KF values in this chart are based on a 45° brace angle, 14″ (360mm) deep columns and 18″ (460mm) deep beams.
Stiffness Modification Factor, KF
2.25
2.00
1.75
1.50
1.25
1.00
10 (3.0)
15 (4.6)
20 (6.1)
25 (7.6)
30 (9.1)
35 (10.7)
40 (12.2)
45 (13.7)
50 (15.2)
Workpoint Length, feet (m)

b)

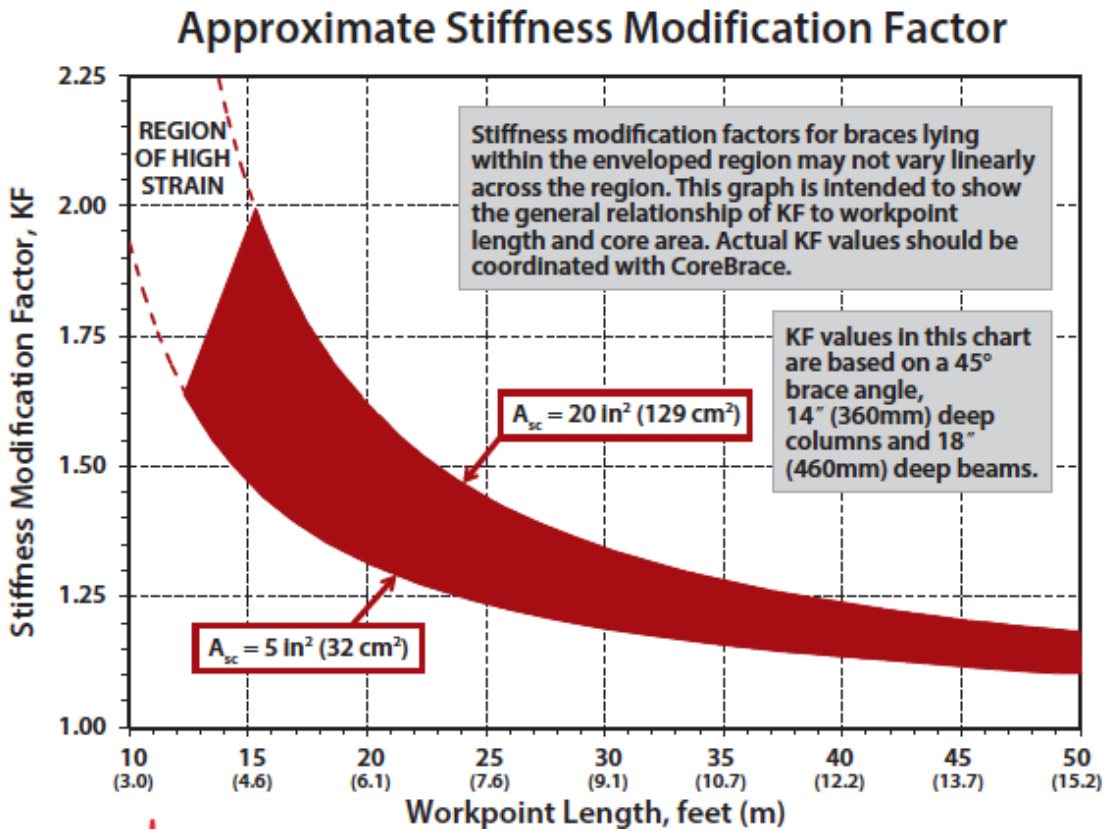


c)

**Figure 2-10: Stiffness modification factors for different connection types a) Welded (CoreBrace, 2013b) b) Pin (CoreBrace, 2014) c) Bolted (CoreBrace, 2013a)**

### *2.3.1.1 Yielding region*

**Standards and Codes of Practice**

AISC 341-16 permits the yielding core to accommodate the expected inelastic deformations through yielding in tension and compression. The expected deformations arising from the inelastic design storey drift and expected brace deformations must also be accommodated in design (including those from beam vertical flexibility). AISC 341-16 and CSA-S16-14 require the entire axial force to be carried by the core (in particular, the yielding region). The cross-sectional area of the yielding region must be sized to be close to the required load as specified by the applicable building code; this is to prevent the development of inelastic deformation concentration between stories.

The design strength of the yielding region is determined by Equation 2-1 when using CSA-S16-14, and without the use of the strength reduction factor for use with AISC 341-16. AISC 341-16 specifies that the axial yield strength (design strength) must be no less than 0.5 and no greater than 1.2 times the prototype used in qualification. This clause allows designers to extrapolate within 0.7 times the axial yield strength with no restrictions on design elements. Provided the axial strength falls within the extrapolation, the design itself could vary considerably from that experimentally

verified (multiple cores, yielding length variation, etc.). Further details on design by qualification are detailed in Subsection 2.3.4.

As discussed above, the length of the yielding region along with the non-yielding regions determines the stiffness of the BRB member. The yielding length alone in conjunction with the angle of inclination within the frame determines the strain demand with respect to the design storey drift (American Institute of Steel Construction, 2010). Typically, the yielding length is ⅔ wp-wp length of the BRB member (Lopez W. A & Sabelli R, 2004).

**Research**

The yielding region length influences the member behaviour (Mirtaheri M et al., 2011; Takeuchi T & Wada A, 2017). As the yielding length decreases, core strains will increase (Tremblay R et al., 2006) as well as susceptibility to low cycle fatigue. However, by decreasing the yielding length in conjunction with increasing the connection area, smaller drifts can be achieved (Takeuchi T & Wada A, 2017). Investigation into the use of short cores was carried out by (Mirtaheri M et al., 2011) (≈1 m), however the design and sensitivity of the yielding region has not been investigated in depth to date.

**Commercial**

The basis for design is based on the minimum yielding region area and strain. The minimum yielding region area controls the overall member strength, with the stiffness adjusted to accommodate the transition and non-yielding regions by use of a stiffness modification factor $K_F$ (described above) (Robinson K, 2013). It is recommended that the core area be greater than 1 $in^2$/13 $cm^2$. Core areas less than or equal to the recommended are known to be sensitive to geometrical design and fabrication tolerances (CoreBrace, 2016; Jones A. S, 2014), with large behavioural changes with small geometrical changes, in comparison to larger cross-sectional areas which require large geometrical changes for small performance gains. The maximum strain permitted within the yielding region of the core is 2.5 % (CoreBrace, 2016).

#### *2.3.1.2 Transition region*

Although intuitive to include a transition region to force plasticity into the defined regions, there are no regulatory provisions requiring its presence (American Institute of Steel Construction, 2010). The transition region is used to transition the plastic zone into the elastic zone. It is common for this region to be a neck shape, with increasing plate width from yielding to non-yielding regions (and subsequently increased cross-sectional area and stiffness). Stiffeners are commonly used within the transition region (along with the non-yielding region) to also aid in increasing the stiffness of the region and to prevent plastic deformation and/or high strains from being transferred from the yielding core to the surrounding elements. The transition

region is not specified with respect to design within regulatory documentation and is scarcely mentioned within academic literature reviewed to date.

This region can be broken into a number of variables: the thickness; initial (yielding region) and final (non-yielding region) width; length; gradient/slope of the transition; and radii of the initial and final junctions. As welding and splices are not permitted, the thickness of the plate remains constant throughout the section. The initial width is that of the yielding region, based on the design strength (Equation 2-1), with the final width typically being connection dependent, based on the adjusted member strength (Equation 2-2).

The length of this region is a function of the gradient/slope of the transition. The length must be proportioned, taking into consideration the required embedment (non-yielding restrained) length required to prevent undesirable connection behaviour (which is out of the scope of this literature review), and also the required yielding length. Small adjustments to each length component will affect the performance of the member. The gradient/slope of the transition can be taken from NZS 3404: Part 1, Clause 12.12.7.2 e), where the slope through the transition zone is not permitted to exceed 1:2.5 vertical:horizontal (horizontal being parallel to the brace longitudinal axis). All changes in slope shall also be rounded to a radius not less than 10 mm.

A review of freely available core designs (with dimensions) is summarised in Table 2-2. Pinned connection cores were likely to use a smaller transition slope due to the lack of additional stress and moment in the non-yielding region. It was found that the radius aligned with BS 5400-10, H2.3 where the presence of an aperture or re-entrant corner implies additional stress concentration, the net section stress should be multiplied by the appropriate stress concentration factor (see Figure 2-11) (British Standards Institute, 1980). BS 5400-10, H2.3 can be applied to determine the required radius between the yielding and the transition region for a given yielding core cross-sectional area, reducing stress concentration and fatigue within this area.

**Table 2-2: Core and transition region design comparison**

| Source | End connection type | Transition ratio (H:W) | Radius (mm) | Yield core width (mm) | Non-yielding core width (mm) | Core thickness (mm) | Change in width, W, (each side) (mm) | Radius/H |
|---|---|---|---|---|---|---|---|---|
| (Dunai L, 2011) | Welded | 1:2 | 56.3 | 40.0 | 130.0 | 20.0 | 45.0 | 1.25 |
| (Benzoni G & Innamorato D, 2007) | Pin | 1:2.5 | 89.0 | 149.6 | 254.0 | 101.6 | 52.2 | 1.70 |
| (Benzoni G & Innamorato D, 2007) | Pin | 1:1 | 100.8 | 135.9 | 254.0 | 114.3 | 59.1 | 1.70 |
| (Wijanto S, 2012) | Pin | 1:4 | 10.0 | 70.0 | 125.0 | 10.0 | 27.5 | 0.36 |
| (Tremblay R et al., 2006) | Bolted | 1:4 | 102.0 | 62.5 | 226.0 | 12.7 | 81.8 | 1.25 |
| (Wijanto S, 2012) | Bolted | 1:4 | 10.0 | 70.0 | 125.0 | 10.0 | 27.5 | 0.36 |

Based on Table 2-2, the following relationships can be determined:

For pinned connections $r = 1.7H$ Equation 2-22

For welded and bolted connections $r = 1.25H$ Equation 2-23

where:

$r$ Radius

$H$ Vertical slope component, perpendicular to brace longitudinal axis

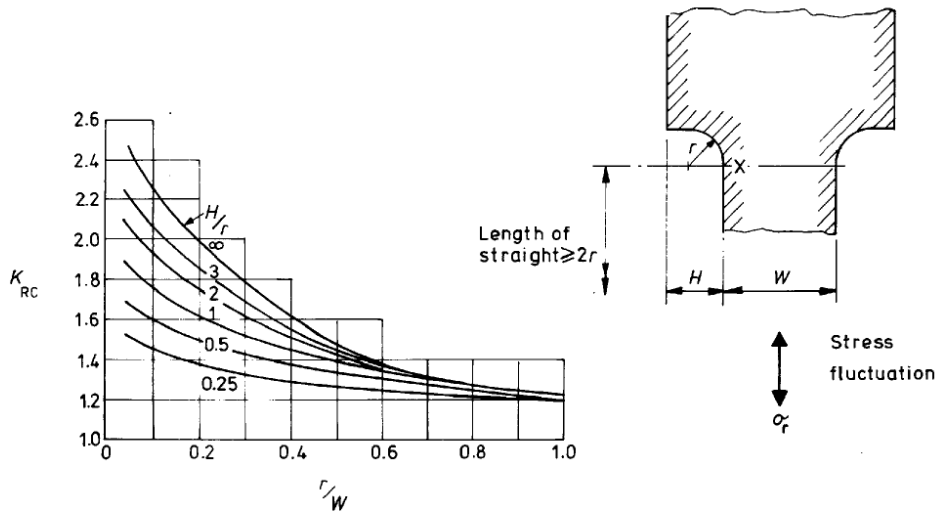


(b) Fatigue stress concentration factor for re-entrant corners $K_{RC}$ (based on net stress at X)

**Figure 2-11: Stress concentration factor BS 5400 (British Standards Institute, 1980)**

Mirtaheri *et al.* (Mirtaheri M et al., 2011) carried out experimental testing on four BRB specimens, optimising their transition lengths with respect to FEMA-450 and the Coffin-Manson relationship for fatigue. It was recommended that further research is required to determine empirical formulas for the transition length relationship within BRBs, as results from the experimental testing were dependent on the specimen's compositional materials and the amount of hardening which occurred, influencing hysteresis behaviour.

#### *2.3.1.3 Non-yielding restrained region*

The non-yielding restrained zone is the elastic portion of the core contained within the restraining mechanism and is commonly referred to as the embedment length. The primary role of this region is to limit rotational effects as a result of connection interaction and, in some cases, reduce the yielding region length. The width of this area is the final transition width and is unlikely to change. The embedment length and its interaction with connection design is a recent development (Zaboli B et al., 2017), and is out of the scope of this literature review.

Proprietary providers have used a minimum embedment of three times the stroke length with success (Jones A. S, 2015). The Japanese Institute of Technology BRB research group, who are one of the key research groups investigating the embedment length and connection interaction, uses an embedment length of two times the non-yielding width (Sitler B, 2016).

#### *2.3.1.4 Non-yielding unrestrained region*

The non-yielding unrestrained region or stroke is the region that projects outside of the restraining mechanism. It is required by AISC 341-16 that the steel core must have projections to establish the connection zone, buckling must be prevented within

this region. Euler buckling theory ($P_{crit} \leq \frac{\pi^2 EI}{L_y^2}$) can be used in conjunction with the adjusted brace strength (Equation 2-2 and Equation 2-3) to approximate vulnerability to buckling, and if stiffeners are required (Humar J et al., 2010). There are no further specifics regarding the length of the stroke; it is commonly taken as the expected drift, conservatively at both ends, or non-conservatively distributed between the two end projections. According to AISC 341-16 Section F4.2 "Expected deformations are those corresponding to a storey drift of at least 2 % of the storey height or two times the design storey drift, whichever is larger, in addition to brace deformations resulting from deformation of the frame due to gravity loading" (American Institute of Steel Construction, 2010). Based on AISC 341-16, the deformation of the BRB is case dependent.

#### *2.3.1.5 Connection region*

The connection region is reviewed for completeness, however the design of the connection itself is out of the scope of this literature review. The connection region must adequately resist the adjusted brace strength (Equation 2-2 and Equation 2-3) (American Institute of Steel Construction, 2010), and it is recommended by one proprietary BRB manufacturer (CoreBrace, 2011) that an additional factor of 1.1 be applied due to the possibility that deformations may exceed those calculated.

### 2.3.2 Unbonding medium

**Standards and Codes of Practice**

The performance of the unbonding medium is directly related to the compression strength adjustment factor applied to the design axial load. This factor takes into consideration the amplification in core compression capacity as a result of frictional interaction between the core and restraining mechanism (American Institute of Steel Construction, 2010).

**Research**

The unbonding medium is a key component in BRB design. The medium (or gap) prevents the transfer of compression axial forces from the core to the restraining mechanism through reducing the friction interface (Iwata M & Murai M, 2006; Takeuchi T & Wada A, 2017). This allows the core to slide relative to the restraining mechanism and maintain full lateral restraint whilst acting as the sole dissipating member (Carden L. P et al., 2006). The medium must be soft to allow transverse (Poisson) expansion of the core, eliminating shear transfer (Black C. J et al., 2004; Corte G. D et al., 2011; D'Aniello M et al., 2006; Fussell A, 2010; Lin P-C et al., 2012). Without (or with poor) design/application of the unbonding medium, composite action between the core and restraining mechanism can develop, or more commonly localised strain build up resulting in local buckling and core fracture (Corte G. D et al., 2011).

The unbonding medium typically ranges between 0.15 – 2 mm in thickness, if it is too thick local buckling will develop (Corte G. D et al., 2011). Common mediums used include epoxy or silicon resin, vinyl tapes, polythene film, silicon or butyl rubber sheets, etc. (D'Aniello M et al., 2006; Fussell A, 2010; Tsai K-C et al., 2004). Successful proof tests were carried out at the University of Auckland, New Zealand, using a neutral petroleum compound, Denso tape, commonly used in pipe protection (Denso, 2011; Wijanto S, 2012). Tsai *et al.* (Tsai K-C et al., 2004) carried out unbonding medium tests through increasing cyclic displacement of ten identical specimens with varying unbonding mediums up to 5 mm in thickness.

The performance was evaluated (Tsai K-C et al., 2004) based on the axial load difference ratio (Poisson portion of the compression overstrength factor), between the compression and tension capacities at a specified axial strain of 2 %. It assumed that perfect unbonding of the core from restraining medium occurs and the final volume of steel is equal to the initial. Theoretically, at an axial strain of 2 %, the axial load difference ratio = 4 %. However, due to imperfect bonding and friction, the maximum axial load difference was found to be ≈ 30 % and the lowest was a 2 mm thick silicon rubber sheet ≈ 10 %.

Rather than evaluating materials on a case-by-case basis, a required unbonding medium thickness per face (gap) to accommodate the maximum expected tensile strain has been developed (Takeuchi T & Wada A, 2017). It was found that with an increase in gap size, the greater the susceptibility of the stress-strain relationship to deviate from a linear relationship, to non-linear, due to localised buckling occurring, effecting the member performance. It was recommended that a small gap be used in design to reduce the effect that the stress-strain behaviour has on the member, with the thickness (gap) required per face given by the following equation:

$$s_r \geq \frac{v\varepsilon_{max}B_c}{2} \qquad \text{Equation 2-24}$$

where:

$s_r$ Unbonding medium thickness (or required gap) per face

$v$ Poisson ratio

= 0.5 (steel)

$\varepsilon_{max}$ Maximum expected tensile strain

$B_c$ Core width

It was also found (Takeuchi T & Wada A, 2017) that the thickness of the unbonding medium is directly related to the higher mode of buckling of the core. Thicker mediums create larger voids for friction to build up, resulting in imperfect debonding and higher modes of buckling. Thin mediums result in the buckling mode stabilising,

similar to ideal axial behaviour, it was found the thinner mediums have negligible effect in the stress-strain behaviour of the core. The greater the mode of buckling, the greater the surface area interacting with the restraining mechanism and, therefore, the greater application of normal force, friction and concentrated strain decreasing the low cycle fatigue life. The relationship between the core thickness and required gap has not been extended out of substituting the core thickness into Equation 2-24. The gap is typically 0.5 – 2.0 % of the core width.

### 2.3.3 Restraining mechanism

**Standards and Codes of Practice**

AISC 341-16 specifies that the buckling-restraining mechanism consists of a casing. The primary role of the restraining mechanism is to prevent local and global buckling of the steel core. Stability of the system as a result of beam, column and gusset interactions must also be accounted for in the restraining mechanism calculations. The specified criteria are demonstrated to conform through mandatory qualification only.

NZS 3404 requires minimum compression restraint provisions (Clause 6.7). These provisions can be summarised as Equation 2-25 (Cowie K, 2018). The outer casing must have adequate moment capacity to resist transverse loading. This load is estimated as the equivalent of 2.5 % of the design axial load applied at midspan (point load). The outer casing is also subject to in-plane and out-of-plane consideration where it is not doubly symmetric (Cowie K, 2018). Based on the relationship between the nominal section capacity and Euler buckling load, the minimum outer casing second moment of inertia can be taken as Equation 2-26 (Watanabe A et al., 1988).

$$\phi M_{casing} = 0.025\beta\phi_{om}\phi_{os}A_{sc}f_y\frac{L_{wp}}{4} \qquad \text{Equation 2-25}$$

where:

$M_{casing}$ Nominal moment capacity of outer casing

$$I_{min} = \frac{1.5{L_{wp}}^2 f_y A_{sc}}{\pi^2 E} \qquad \text{Equation 2-26}$$

where:

$I_{min}$ Minimum outer casing axial stiffness

**Research**

The restraining mechanism is a two-part system consisting of a restraining medium, typically grout, and a restrainer/steel outer casing. In the original BRB research conducted by (Watanabe A et al., 1988), it was proposed that the Euler critical

buckling load of the outer casing should be greater than 1.5 times the core yield load, this ratio considers the global buckling of the BRB (Equation 2-26).

The contribution of the restraining mechanism to confining the steel core from local buckling is not commonly reported but it is a key component. Takeuchi *et al.* (Takeuchi T et al., 2012) proposes a method to calculate whether the restraining mechanism is appropriate in both the major and minor axes of the BRB (Equation 2-27). This method considers the flexural capacity of the restraining medium and the punching force (the force exerted on the outer casing as a result of the steel core "puncturing" through the restraining medium). This is a function of both the outer casing and restraining medium, based on the assumption that the local buckling wavelength of the core plate is approximately 4 times the core plate width.

$$\lambda_b = \frac{P_{lb}}{N_{brace}^{oc}} = \frac{\left( 2t_r^2 \frac{{L_w}/{2}}{2s_r + v\varepsilon_{max}B_c} f_{yr} \frac{B_r}{B_r - t_c - c_m t_m} \right)}{N_{brace}^{oc}} > 1.0 \qquad \text{Equation 2-27}$$

where:

$\lambda_b$ Ratio of outer casing capacity to critical axial force, local buckling occurs when less than 1.0

$P_{lb}$ Outer casing capacity with respect to punching force

$c_m$ Restraining medium contribution factor (mortar contribution factor)

$t_m$ Thickness of restraining medium

$t_r$ Thickness of outer casing

$B_r$ Width of outer casing

$f_{yr}$ Yield strength of outer casing

$L_w$ Buckling length

(Lin P-C et al., 2015) proposes a similar relationship for estimating the maximum outward (punching) force based on the geometrical characteristics of the high mode buckling length and available space between the steel core and the restraining mechanism (Figure 2-12 and Figure 2-13). Both methods assume the restraining medium spreads the outward punching force to the outer casing, with Takeuchi *et al.* proposing a mortar spread factor for both the major and minor axes.

The relationship defined by (Lin P-C et al., 2015) is characterised by an equivalent beam model representing the inner surface of the outer casing (Figure 2-12). The core buckling wave crest/trough contacts with the restraining medium (conservatively assumed to not contribute to resisting the core), spreading the contact force both longitudinally and transversely to the inner surface of the outer casing (represented by

a line load). The outer casing resistance is assumed to be the required force (from the core) which results in the equivalent beam forming plastic hinges at both ends.

(Lin P-C et al., 2015) proposes a demand-to-capacity ratio (Equation 2-28), in where the ratio of the maximum outward force from core high mode buckling to the maximum outward force required to develop flexural capacity of the outer casing must be less than 1.0 to prevent local buckling failure. It was found that a thicker outer casing increases the resistance to the outward force, and that the thicker the unbonding medium, the greater the susceptibility to local buckling. Also, the closer the outer casing depth is to the core plate depth, the greater the resistance to local buckling failure.

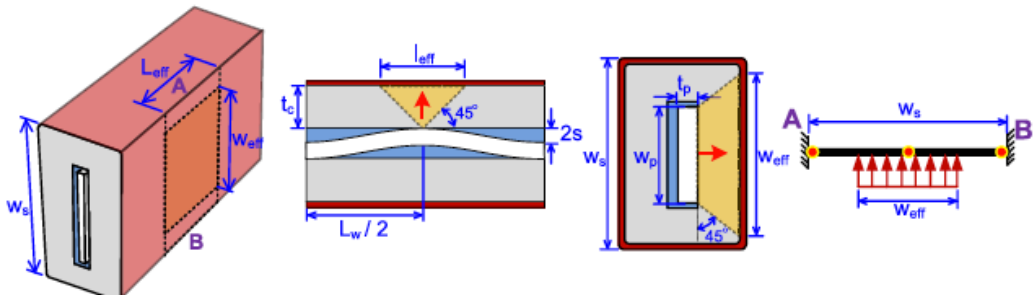


**Figure 2-12: Local buckling projection analysis (Lin P-C et al., 2015)**

$$DCR = \frac{4N_{brace}^{oc}(2s_r + v\varepsilon_{max}t_{sc})\left(1 - \frac{B_c}{B_r}\right)}{L_w t_r^2 f_{yr}\left(2 - \frac{B_c}{B_r}\right)} \qquad \text{Equation 2-28}$$

where:

| | |
|---|---|
| $DCR$ | Demand to capacity ratio |
| $t_{sc}$ | Core thickness |
| $B_c$ | Width of yielding core |

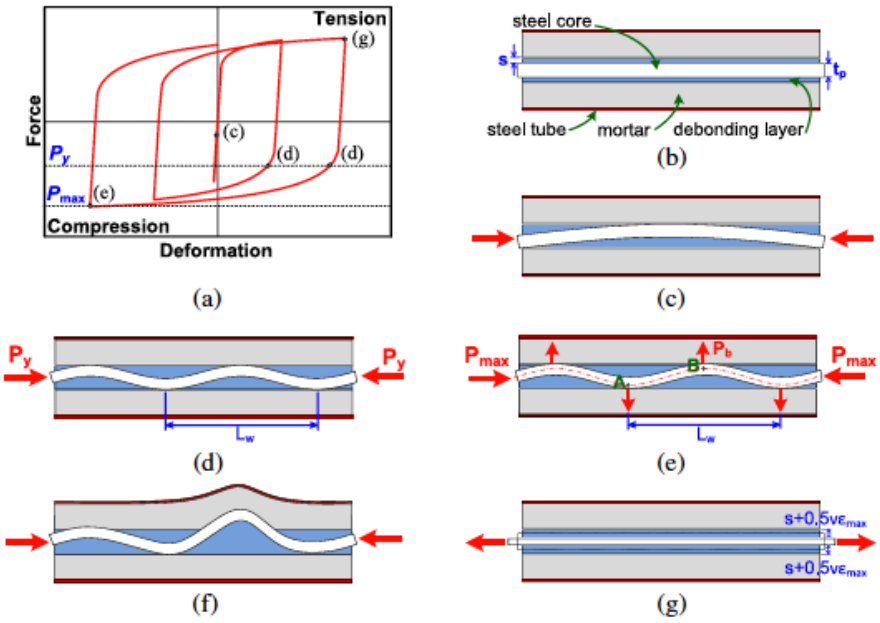


**Figure 2-13: Local buckling process (Lin P-C et al., 2015)**

Figure 2-13 demonstrates the local buckling process based on hysteretic response. The hysteresis loop is shown in (a), with a longitudinal schematic of the BRB shown in (b). As compressive axial load is initiated (c), the core undergoes first mode buckling. Once the restraining medium is engaged (c), higher mode buckling is engaged (d) resulting in outward forces distributed to the restrainer inner surface. When the capacity of the restrainer is less than that of the core force acting on it, local bulging occurs (f). Tension loading is represented by (g), where the gap is developed by the unbonding medium (or fabricated gap) and poisons effect.

Along with local buckling it is acknowledged (Tremblay R et al., 2006) that secondary in-plane bending moments will develop at large displacements, however this is dependent on the interaction between the restraining mechanism and the core. The maximum restrainer flexural demand is a function of the maximum compression force the core can transfer, which is described by Equation 2-29 (Tremblay R et al., 2006) for outer casing design.

$$M_B = \frac{N_{brace}^{oc}(a + 2s_r + e)}{1 - N_{brace}^{oc} / N_{cr}^{E}} \leq M_y^B \qquad \text{Equation 2-29}$$

where:

$M_B$ Maximum flexural outer casing demand

$a$ Fabrication imperfection of core

$e$ Eccentricity of axial force

$M_y^B$ Flexural strength of outer casing

$= 2\left(\frac{I_r}{D_r}\right) f_{yr}$

$D_r$ = depth of outer casing

$N_{cr}^E$ Euler buckling strength of outer casing

No research to date has been undertaken on the mortar strength, as it is assumed conservative when considering the outer casing as the primary resistance to local buckling (Takeuchi T & Wada A, 2017). Based on local buckling research, it is proposed that the mortar infill compression strength resist the stress attributed to contact between the core and the mortar when undergoing buckling (Equation 2-30) (Takeuchi T & Wada A, 2017).

$$f_c' > \frac{\frac{4N_{brace}^{oc}(2s_r + vt_c\varepsilon)}{L_w}}{t_c B_c} \qquad \text{Equation 2-30}$$

where:

$f_c'$ Restraining medium compression strength

$t_c$ Length of contact between core and restraining medium (assumed to be the core thickness)

### 2.3.4 Overall qualification criteria

**Standards and Codes of Practice**

Qualification of BRB member design is typically undertaken through experimental verification testing, with the exception being BRB application in New Zealand. Due to the lack of BRB guidelines in New Zealand, BRBs fall under "Use of alternative materials or methods" (Standards New Zealand, 1997). It is specified that quantification can be carried out experimentally, numerical (special study) or through rational design. Rational design is based on first principals, available research and industry best practice. The associated cost, lack of testing facilities and ability to verify the design based on special studies (numerical or rational) has resulted in the preferred and accepted method of rational design.

CSA-S16-14 refers to AISC 341-16 for experimental verification, which requires cyclic testing of the individual BRB member (including connections) and also a BRB subassemblage test. Within the qualification testing criteria, material requirements are also included such that the member verified is approximately equal in design, fabrication and material strengths to those distributed. The individual member test allows verification of the required strength, expected inelastic deformations and determination of the compression strength adjustment factor. The subassemblage test,

which is not required to be full scale, is used to provide evidence that the BRB member can adequately meet the expected deformation and rotational demands imposed from the system. The subassemblage test is also used to verify the hysteresis behaviour of the BRB member demonstrated within member testing. The 2000 NEHRP Report identified that the BRB response is sensitive to proportioning and that significant bending and shear forces develop in actual application, however this effect on BRB behaviour is unknown (Sabelli R, 2000).

The loading protocol below is a minimum requirement for qualification. Each cycle contains full tension and compression loading; additional programs may be applied post verification protocol.

a) 2 cycles of loading at the deformation corresponding to $\Delta_b = \Delta_{by}$

b) 2 cycles of loading at the deformation corresponding to $\Delta_b = 0.5\,\Delta_{bm}$

c) 2 cycles of loading at the deformation corresponding to $\Delta_b = \Delta_{bm}$

d) 2 cycles of loading at the deformation corresponding to $\Delta_b = 1.5\,\Delta_{bm}$

e) 2 cycles of loading at the deformation corresponding to $\Delta_b = 2.0\,\Delta_{bm}$

f) Additional complete cycles of loading at the deformation corresponding to $\Delta_b = 1.5\,\Delta_{bm}$ as required for the test specimen to achieve a cumulative inelastic axial deformation of at least 200 times the yield deformation.

where:

$\Delta_b$ Applied axial deformation

$\Delta_{bm}$ Design storey drift, no less than 0.01 storey height

The acceptance criteria determined from qualification testing is not limited to the cumulative inelastic ductility deformation of at least 200 times that of yield displacement. The member must demonstrate stable behaviour with positive incremental stiffness, while rupture, member instability and connection failure are not permitted (Figure 2-14). The calculated compression strength adjustment factor must not exceed 1.3 (American Institute of Steel Construction, 2010; Canadian Standards Authority, 2014).

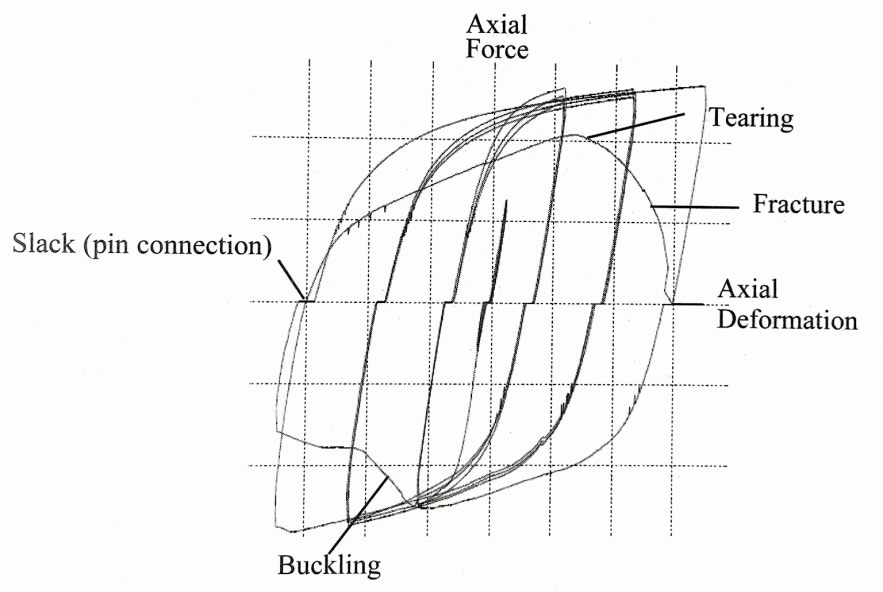


**Figure 2-14: Unstable qualification behaviour (Takeuchi T & Wada A, 2017)**

As described in Section 2.3.1, qualification of all designs is not required provided that cross-sectional shape and orientation of the steel core, unbonding medium and restraining mechanism material are the same as members already verified. The member in question must also fall into the interpolation range specified (Clause K.3.3c), namely no less than 50 % and not greater than 120 % of the member tests of equal axial yield strength. The specification of same cross-sectional shape of the core does not take into consideration multiple cores in place of a single core when the cross-sectional areas and shape are equal. The unbonding medium thickness and its relationship with the core width is also neglected, along with the transition-yielding region radii and other geometry. The performance of an interpolated specimen cannot be guaranteed to match the verified drift/strain of the original specimen. This ambiguity has been raised by proprietary providers to the AISC-341 committee, and continues to be debated.

Within Japan, prequalification and approval must be given by the BCJ. The test specimens must be provided and fabricated by the same organisations that supply the BRBs, and can be no less than half the actual size. The qualification testing protocol is broken into three different tests and is considered to be demanding. The testing protocols are broken down below. As with AISC 341-16, instability and non-ductile failure (fracture) are prohibited. The compression strength adjustment factor must not exceed 1.1 (Takeuchi T & Wada A, 2017) and it is recommended that out of plane displacements in the stroke region be monitored to indicate instability onset and the ideal failure mechanism is fatigue induced fracture.

BSJ loading protocol (summarised)

Test 1 – Cyclic Loading Test

| | |
|---|---|
| 3 cycles of loading at the deformation corresponding to plastic length strain | $\Delta_{by}$ |
| 3 cycles of loading at the deformation corresponding to plastic length strain | 0.5 % |
| 3 cycles of loading at the deformation corresponding to plastic length strain | 1.0 % |
| 3 cycles of loading at the deformation corresponding to plastic length strain | 2.0 % |
| 3 cycles of loading at the deformation corresponding to plastic length strain | 3.0 % |

Test 2 – Cyclic Loading with Initial Out-of-plane Drift

This test is carried out with gussets and transverse beams. It is recommended that an initial out-of-plane storey drift of 1.0 % rad be applied.

Test 3 – Cyclic Loading Test, Constant Amplitude

Three constant amplitude tests should be conducted. Three different amplitudes shall be used, the maximum corresponding to the maximum qualification strain and a subsequent lower and medium amplitude at the discretion of the practitioner.

It is common for BRB gussets within Japan to be stiffened with either full depth edge or centre stiffeners along with fixed end transverse beams. This allows the boundary conditions to be adequately captured within the testing program, providing additional performance certainty. The BSJ testing regime is similar to the AISC-341 protocol, with the exception of gusset and transverse beam requirements and Test 3. Test 3 applies a constant amplitude until failure, providing a low cycle fatigue curve of the specimen. This additional information provides additional certainty of the BRB under fatigue loading.

It is important to note that AISC-341 target displacement (amplitude) is based on the design storey drift, whereas in Japan it is based on the core axial strain (Equation 2-31). The qualification protocols also differ in cumulative inelastic ductility, with a typical AISC 341-16 program producing approximately 47 % plastic strain, where the equivalent Japanese protocol produces a plastic strain of 66 % (Takeuchi T & Wada A, 2017).

$$\varepsilon = \frac{L_{wp}}{L_{sc}} \cdot \frac{\Delta}{\cos\alpha \sin\alpha} \qquad \text{Equation 2-31}$$

where:

$\Delta$ Deflection

$\alpha$ Angle between x and h axes

**Research**

Within academic literature available to date, the member and subassemblage testing is carried out with respect to AISC 341-16 with additional loading protocols, such as local earthquake records carried out as post qualification criteria. Dynamic testing is limited, with testing typically carried out statically (Tremblay R et al., 2006).

## 2.4 General comments

BRB conception occurred nearly 50 years ago, with implementation of the member in construction accepted over the past 30 years. This member, although not new, has significant ambiguity around design and performance. The development and implementation of the member has been dominated by proprietary providers and as such this established system is lacking information for reliable design and response.

The three elements, core, unbonding medium and restraining mechanism are agreed upon as key functions to the characteristic of a BRB member. The core carries the axial load, where the unbonding medium isolates the core from composite effects and allows the restraining mechanism to laterally restrain the core along the members full length. Through the unbonding medium reducing friction between the core and restraining mechanism, the compression capacity of the core can achieve equal, if not higher capacity than that in tension.

Qualification of BRBs to date is carried out through experimental verification. Both AISC and CSA adopt the same qualification loading protocol. The BSJ has a more rigorous loading protocol than that of AISC, where members are used in a secondary lateral load resisting system compared to the AISC (which considers them to be used within a primary system). The BSJ approve case-by-case designs regardless of experimental verification success. Within New Zealand, due to a lack of regulatory requirements, the BRB member can be implemented without experimental verification based on a special study using rational methods.

Where experimental verification is carried out, qualification is achieved by meeting a minimum cumulative inelastic ductility based on the design storey drift of the specific case for AISC, and core strain for BSJ. AISC allows interpolation of results, such that each design does not require experimental verification. The design strength must be no less than 0.5, nor greater than 1.2 times that tested with similar materials and cross-sectional area. This allows variation in the member design from single core to double core, provided the core cross-sectional area is that which was verified. As qualification is carried out to a specific design storey drift, interpolation of this design may not achieve this design drift in application, and the reliability of the member is therefore questionable.

The allowable compression overstrength which is related to the unbonding mediums ability to reduce friction is limited within AISC to 1.3 and BSJ 1.1. The lower this overstrength, the less friction developing between the core and restraining mechanism, and near perfect unbonding. When this overstrength increases, there is an undesirable development of friction between the core and restraining mechanism, and the balanced hysteresis response becomes disproportionate. It is desirable for the compression overstrength to be as close as possible to 1.0, such that tension and compression capacities are similar, and balanced hysteresis is achieved.

AISC, CSA and BSJ all allow verification of a scaled member. The sensitivity of the design of each element is disregarded when this approach is used. Scaling of the unbonding medium is unachievable, and also the core and the divided regions within the element could be susceptible to surrounding (connection, gusset, etc.) interaction affects which cannot be adequately captured. An understanding of the sensitivity of the key elements irrespective of surrounding interaction effects is required to validate this approach.

The literature presented in the previous sections is typically case dependent to a specific design, with relationships then verified through semi-empirical methods (where semi-empirical refers to relationships with specific boundary conditions to mimic or force a result to converge with experimental results). These relationships have not been verified together with a simple, intuitive design. An understanding of the design sensitivity of the BRB member is necessary to fill the void of ambiguity when designing a BRB.

The restraining mechanism is composed of two elements: a medium and an outer-casing. Semi-empirical methods have been used to validate experimental results of the restraining mechanisms contribution to member response, but have not been applied outside the designs that was used to develop them. The stroke length (unrestrained region of the core), although specified in AISC as a required component, has no specific boundaries or subsequent guidance in design. The transition region of the core, although not required in regulation, is a predominant design feature in BRBs that was considered in this literature review. As such, the design sensitivity and how this region affects the performance of the yielding and non-yielding regions of the core is paramount for reliable design.

The presence of stiffeners and how these affect the members performance is also an area which has not been investigated. If stiffeners provide a significant advantage in validation of performance, regulation should specify them, together with design limits over which they remain valid. The loading protocol used for experimental verification can undisclosed the performance of the member. An example of this is failure within a particular cycle, however due to the quantity (typically two cycles), this failure may not be present in the low number of tested cycles. Evaluating the performance of

nominally identical specimens to determine any bias from the experimental program is recommended.

A fully empirical (relationships evaluated without case dependent boundary conditions) method has not been investigated to date. With semi-empirical methods used, modelling only the yielding region of the member. If a full empirical method is achievable, the sensitivity of the member could be evaluated parametrically and aid in initial design. The following chapters aim to address the sensitivity of ambiguous member details, experimental performance and both numerical and analytical approaches to BRB design.

# 3 Experimental Testing

This section presents the experimental parametric testing that was undertaken within the present research programme in order to evaluate how the buckling restrained brace (BRB) member responds to small geometrical changes. This is evaluated by gathering the physical response of small geometrical changes and also the subsequent member response when loaded. The geometrical changes are based on design recommendations to prevent undesirable behaviour, that were identified within the literature review (Chapter 2). The results of the experimental testing program will be used to calibrate and compare numerical and analytical models that will be developed in Chapter 4.

In total, 37 specimens were tested in both concentric (C) and eccentric (E) configurations. Between the unrestrained non-yielding region (stroke) and connection region, an end plate was present (which is significantly stiff, to isolate the BRB member from connection effects). Connection design, performance and behaviour is not considered within the present experimental testing program. Two different BRB lengths are investigated; V or inverted V configuration and a single bay brace (SB). The bay size is the same in design for both configurations. Design of the BRBs is identical for both the V and SB configuration, identifying behavioural variations between the two lengths with identical design principles.

The key geometric sensitivities and corresponding behavioural theories that are investigated within this section are:

- The restraining mechanism geometrical dimensions with respect to the effects on local and global buckling initiation.
- The stroke length, its relationship with the design drift and effects on member response in both concentric and eccentric configurations.
- The presence, and lack thereof of stiffeners within the non-yielding regions and the subsequent effect on member response and failure mechanism.
- The transition gradient for SB configuration, evaluating the response of the member and strain-failure relationship.
- The non-yielding restrained (embedment) length and whether/if this affects member response.
- Reliability of nominally identical specimens.

The design of the specimens, fabrication and determination of applied loading protocol are key control elements, which if executed poorly will introduce undesirable variations to the control. The following subsections detail these steps based on the findings of Chapter 2 and also provide information where no current information is available.

## 3.1 Specimen design

The following sub-section presents the procedure followed for the specimen design. The methodology and premise behind the order and decisions of the design process is included for completeness. The BRB member core was designed first, as it was found that the core elements (yielding, transition and non-yielding regions) directly influenced each other. The core also affected the overall dimensions of the restraining mechanism. Although not investigated within this test program, it is important to note that the connection design directly influences the final dimensions of the non-yielding region, which can subsequently affect the required transition length and remaining available length of the yielding region. Figure 3-1 outlines the order of design that was followed for all specimens, with the corresponding sub-sections. Figure 3-2 visually represents these design elements for clarity, with both un-stiffened and stiffened specimens shown (top and bottom elevation respectively). A summary of the key dimensions for all specimens can be found in Appendix A.

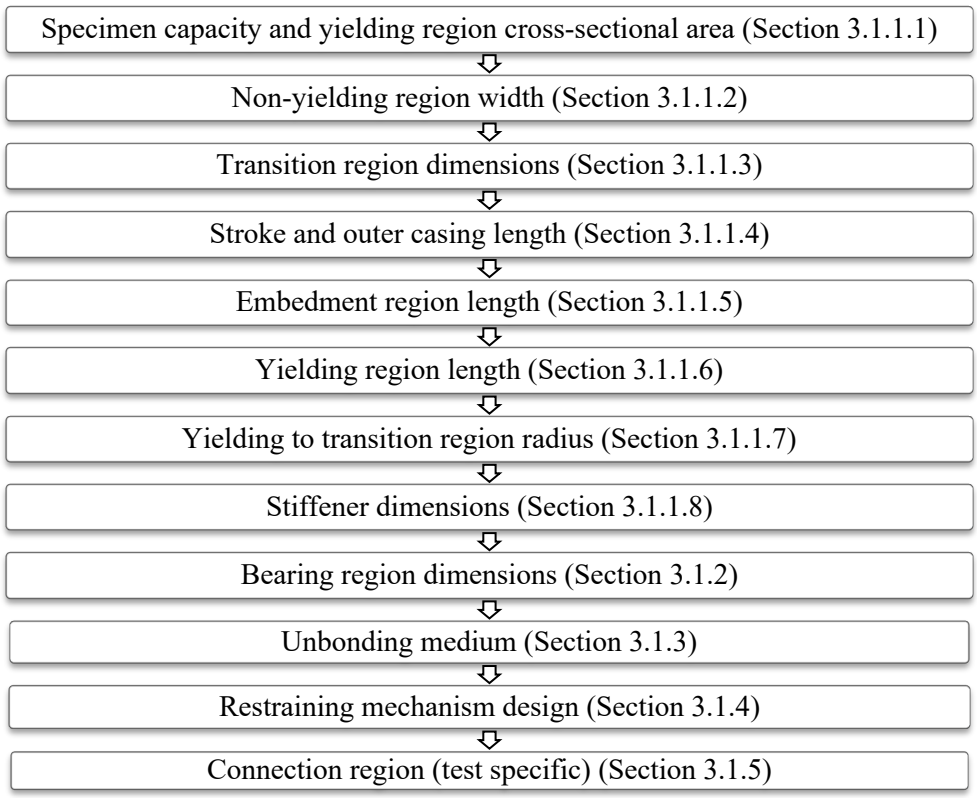


**Figure 3-1: Specimen design overview**

All specimens were designed based on a standard frame with a bay width of 6 m and a height of 3.2 m. The work-point to work-point (wp-wp) for V and SB specimens was 4.4 m and 6.8 m, respectively. It is assumed for all specimens that 1200 mm of the wp-wp length is for connecting the BRB to the frame (600 mm at each end). The BRB member is designed based on the remaining length.

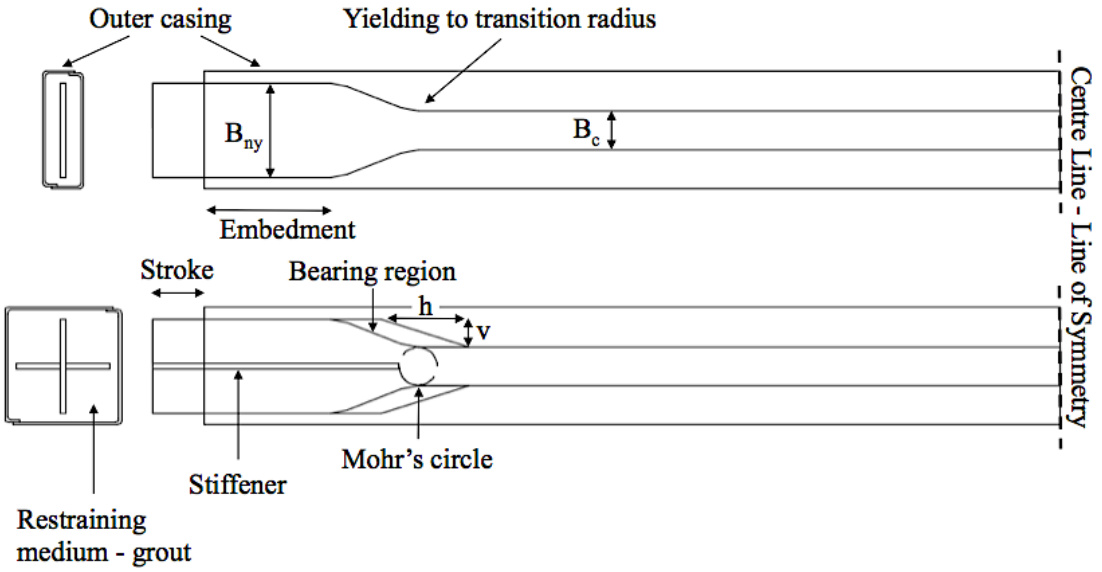


**Figure 3-2: Key design elements**

### 3.1.1 Core

#### *3.1.1.1 Specimen capacity and yielding region cross-dimensions*

The yielding region cross-sectional area determines the available capacity of the specimen, and can also dictate the dimensions for the adjacent elements, and as such is the starting point within member design. Based on personal correspondence with a BRB proprietary provider (Jones A. S, 2014), the cross-sectional area of 1 $in^2$ was known to be sensitive to geometrical design, with performance variabilities and undesirable behavior being displayed with small geometrical variations at a low cross-sectional area.

Low yield strength steel is commonly adopted for the core (Jones A. S, 2014) to ensure significant ductility. The lowest readily available grade flat plate in New Zealand is Grade 250. Based on the recommended cross-sectional area of 1 $in^2 \cong 650$ $mm^2$, and available flat steel plate, the yielding core dimensions of 10 mm x 65 mm was adopted for all specimens (with a nominal yield strength $f_y = 260$ MPa (Standards Australia & Standards New Zealand, 2011)). The thickness of 10 mm is continuous throughout the full specimen length.

#### *3.1.1.2 Non-yielding region cross-sectional dimensions*

The non-yielding width specification is dependent on the weld strength connecting the core (unrestrained non-yielding region/stroke) to the connection plate. A laboratory safety factor of 1.4 was required, resulting in a minimum non-yielding width of 160 mm for all specimens based on 10 mm equal leg fillet weld (Figure 3-3) designed in accordance with NZS 3404 Section 9.7 (Standards New Zealand, 1997). Two secondary checks were also carried out. The first check of brace overstrength $B_c.\beta.\phi_{os}$, where $\beta$ =1.8, and $\phi_{os}$ =1.3 (see Section 2.3.1) resulting in a width of

152.1 mm. The second, based on evaluation of proprietary provider test reports, it was common for the non-yielding width for pin connections to be 2.5 times that of the yielding. This provided a width of 162.5 mm. 160 mm was adopted as the non-yielding width for all specimens.

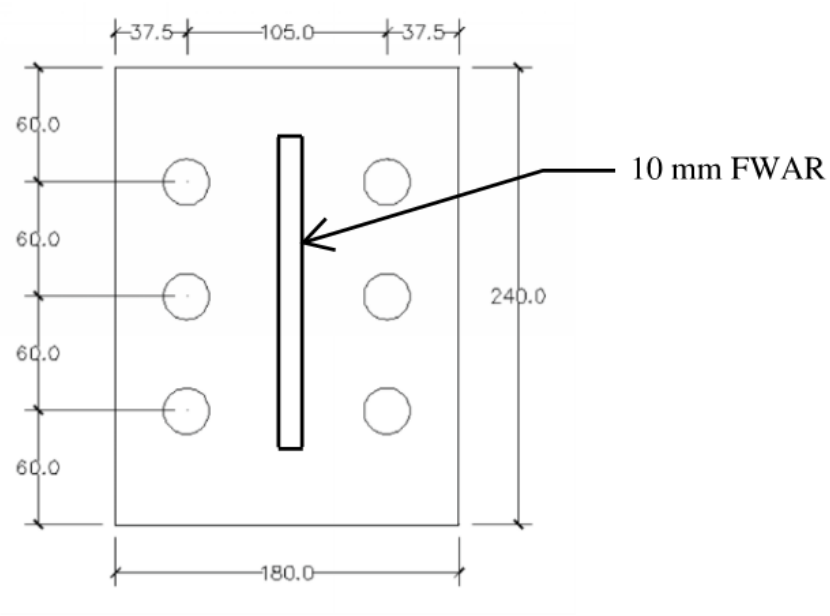


**Figure 3-3: Non-yielding core weld to connection plate detail**

### *3.1.1.3 Transition region dimensions*

The transition gradient is the slope at which the yielding core width transitions into the non-yielding width. A preliminary experimental testing program on ten un-stiffened BRB members was carried out to evaluate three commonly used transition gradients (Jones A. S et al., 2016). The three evaluated transition gradients were 1:2.5, 1:3 and 1:4 (vertical:horizontal). The first gradient is the maximum permitted slope for notched regions with respect to NZS 3404 Clause 12.12.7.2(e). The latter two were determined based on a review of BRB proprietary member designs (Benzoni G & Innamorato D, 2007; Dunai L, 2011). It was found that the larger the transition ratio, the greater the cumulative inelastic ductility demand was required to reach $N_{brace}^{oc}$ in cycles above the design storey drift. Gradient 1:2.5 performed with the highest overall compression capacity, and along with 1:3, performed competitively and remained stable with increasing cumulative inelastic ductility in comparison to the 1:4 transition gradient.

Within this testing program, three specimens (SB configuration) will be evaluated for transition gradient sensitivity. The preliminary testing program evaluated specimens of similar length to V configuration. The three specimens, C-DU2-E2-65-T3, C-DU2-E2-65 and C-DU2-E2-65-T1 will vary by the gradients 1:3, 1:2.5 and 1:1

respectively. The 1:1 gradient was included for completeness based on personal correspondence (Jones A. S, 2015) with a proprietary provider, where the 1:1 gradient is preferred for pin connections. All other specimens within the testing program will adopt a 1:2.5 gradient. The transition length for all specimens is specified as the minimum length for the transition gradient to reach the required non-yielding width from the yielding region width.

#### *3.1.1.4 Stroke and outer casing length*

The stroke length is the length in which the BRB member will contract at the applied drift. To date, there is no guidance with respect to minimum and/or maximum specification. It is assumed that the stroke is proportional to the required design drift, which is project specific due to frame and structural configuration. AISC 341 (American Institute of Steel Construction, 2010) requires that qualification (and the subsequent loading protocol) must be achieved at two times the design storey drift, where the minimum design storey is limited to 0.01 the storey height.

For this experimental program, the stroke is determined based on the loading protocol requirements where 0.01 drift is equivalent to 0.01 the wp-wp length of the specimen. Three sensitivity tests in both V and SB configurations will evaluate the member response at two, four and six times the drift equivalent stroke lengths in both un-stiffened and stiffened specimens (C-VU2-E2-65, C-VU4-E2-65, C-VU6-E2-65, C-VS2-E2-200-R10, C-VS4-E2-200-R10, C-VS6-E2-200-R10, C-DU2-E2-65, C-DU4-E2-65, C-DU6-E2-65, C-DS2-E2-200-R10, C-DS4-E2-200-R10 and C-DS6-E2-200-R80). All other specimens will adopt two times drift equivalent stroke. The stroke is applied at each end of the specimen. This application, rather than equal distribution (splitting the stroke evenly between the two ends) was made due to the non-symmetric engagement of the specimen observed in the preliminary testing program (Jones A. S et al., 2016). For un-stiffened specimens a check for Euler buckling of the stroke length is required to prevent undesirable local buckling in the stroke region. Based on the known stroke length, the subsequent casing length can be determined.

#### *3.1.1.5 Embedment region length*

The non-yielding restrained region, where the non-yielding width is constant is commonly referred to as the embedment region. This length affects the resulting yielding length quantity and is also associated with connection rotational effects. Proprietary providers have used a minimum embedment of three times the stroke length with success (Jones A. S, 2015). In personal correspondence with the Japanese Institute of Technology BRB research group, an embedment length of two times the non-yielding width was recommended (Sitler B, 2016). Six unstiffened specimens, three of each V and SB configuration (C-VU2-E1-65, C-VU2-E2-65, C-VU2-E3-65, C-DU2-E1-65, C-DU2-E2-65 and C-DU2-E3-65) will examine the sensitivity of the embedment length without connection influence. Three embedment lengths proportional to the non-yielding width will be used in the sensitivity analysis for the

properties of equal to, two times and three times the non-yielding width. All other specimens will adopt an embedment length equal to two times the non-yielding width.

#### *3.1.1.6 Yielding region length*

Based on the remaining unallocated length, the yielding region length can be specified. It is recommended that the yielding length should be approximately ⅔ the wp-wp length (Lopez W. A & Sabelli R, 2004). The SB specimens yielding length is approximately ⅔ the wp-wp length, whereas the V specimens are approximately ½.

#### *3.1.1.7 Yielding to transition region radius*

The yielding to transition region radius is the radius connecting the constant area of the yielding region, to the changing slope of the transition region. An initial radius between the end of the yielding region and the beginning of the transition/non-yielding region was taken as 10 mm. This radius was chosen due to its application in New Zealand made BRBs (Wijanto S, 2012) based on NZS 3404. Five stiffened specimens (three V, and two SB configurations) were initially tested; it was found that premature local buckling occurred at the radius upon dissection (Figure 3-4). A review of proprietary BRB designs in conjunction with BS 5400-10, H.2.3 (British Standards Institute, 1980) was found to be applicable (Section 2.3.1.2). All other specimens were fabricated with a radius of 80 mm.

a) b)

**Figure 3-4: Local buckling at radii (10 mm) a) Folding in transition region, fracture within yielding region b) Pinching of steel at radii**

The two specimens tested by (Wijanto S, 2012) consisted of a bearing region of 15 mm and a stroke of 20 mm. The $K_{RC}$ based on BS 5400-10, H.2.3 is equal to 2.0. This equates to two times the stress occurring at the center of the radius circle, this falls 5 mm into the bearing region. This location has an additional 1.25 mm gap, which is likely to have little impact on the local buckling susceptibility at this point. In comparison, the initial specimens in this testing programme have a bearing region equivalent to the stroke (44 mm for 2 % specimens). Based on BS 5400-10, H.2.3 $K_{RC}$

equals approximately 2.05, with and additional gap of 13.6 mm occurring at the point of 2.05 times the stress concentration resulting in local buckling failure.

Note: Specimens with 10 mm radii will be identified within the experimental results and also the specimen name definition (denoted -R10).

#### *3.1.1.8 Stiffener dimensions*

Stiffeners were included in nine specimens (S), three of each length with identical designs as the unstiffened (U) stroke sensitivity specimens, and three nominally identical V configurations with two times the design storey drift stroke length (C-VU2-E2-65, C-VU4-E2-65, C-VU6-E2-65, C-VS2-E2-200-R10, C-VS4-E2-200-R10, C-VS6-E2-200-R10, C-DU2-E2-65, C-DU4-E2-65, C-DU6-E2-65, C-DS2-E2-200-R10, C-DS4-E2-200-R10, C-DS6-E2-200-R80, C-VS2-E2-200-R80A, C-VS2-E2-200-R80B and C-VS2-E2-200-R80C).

Stiffeners were adopted as they are a common method of increasing stiffness of the core non-yielding regions and provide connection stability and prevent plastic torsional buckling, the latter being of interest within this program. Stiffeners are a cost-effective method of providing additional stability within the non-yielding region when welded and bolted connections are adopted. The geometry of the stiffeners was kept similar to the core, such that the non-yielding region was doubly symmetric.

Stiffeners are specified to be in the center of the non-yielding region, at right angles to the core. The stiffeners have equal thickness and transition gradient to the core, are the same total width as the non-yielding region (for a symmetric cruciform shape), and are present throughout the non-yielding unrestrained and restrained region. The transition length varies from the core due to the depth of the stiffener. To prevent weld residual stress within the yielding region, the stiffeners are positioned 32.5 mm from the yielding region-transition region junction. This distance is half that of the yielding width, with the weld stress assumed to distribute radially with respect to Mohr's circle.

### 3.1.2 Bearing region

The bearing region is typically represented by the presence of polystyrene, allowing the non-yielding and yielding region to move, contact and expand without bearing stresses forming against the restraining medium. Due to the lack of available literature specifying the design of this region, the bearing length is taken as equal to the stroke length for this experimental program.

### 3.1.3 Unbonding medium

Denso tape, a synthetic fabric coated in a petrolatum compound, has shown to be a sufficient unbonding medium in previous BRB experimental tests (Wijanto S, 2012). Denso tape was chosen due to its ready availability within the timeframe specified for the experimental testing programme. The tape thickness is taken as 2.0 mm within

theoretical calculations to allow for the preparation paste and variation in tape thickness (1.4 +/- 0.3 mm) (Denso, 2011). The Denso tape is applied to the core and surrounds the polystyrene within the bearing region to prevent the restraining medium from infiltrating this region.

### 3.1.4 Restraining mechanism

The restraining mechanism comprises high strength grout (55 MPa) and a Grade 250 custom steel outer casing. The length of the restraining mechanism as defined above is the length of the core minus the stroke length. Three design checks were carried out on the outer casing to determine the appropriate dimensions. The first check, for global buckling is determined based on the ratio of the core capacity to Euler buckling capacity of the outer casing. The second and third checks evaluate the members susceptibility to local buckling based on the yielding core and outer casing dimensions through the relationships detailed within Equation 2-27 and Equation 2-28, respectively. The width, depth and thickness dimensions were considered. The grout volume was determined based on the required volume to fulfil the outer casing dimension. A summary of the design check ratios and outer casing dimensions can be found in Appendix A.

### 3.1.5 Connection

The connection design is specific for this testing regime. Design for the connection was carried out with respect to NZS 3404 and a laboratory safety factor of 1.8. The core is welded to a significantly stiff connection plate, to isolate the behavior of the member from connection influence. For concentric loading and unstiffened eccentric loading the connection plate is connected to two external brace ply plates, which position around an internal gusset; loading actuator ply or fixed end connection ply (connected to a free-standing reaction frame). The loading actuator and fixed end connection ply plates are connected to the brace ply plates via a pin. A schematic of the connection set up is shown in Figure 3-5. Stiffened eccentric specimens are connected via the connection plate directly to an eccentric testing specific actuator block to form a fixed end connection. The fixed connection to the actuator block is at a specified eccentric displacement from the centerline, and in plane at the opposing end, creating a fixed connection with the freestanding reaction frame.

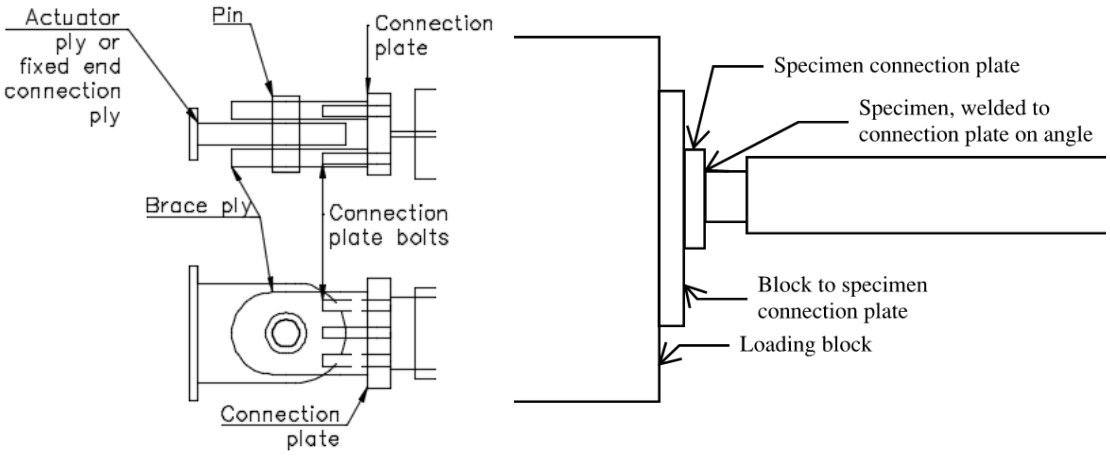


**Figure 3-5: Connection schematic a) Pinned b) Fixed**

## 3.2 Loading protocol determination

The loading protocol was determined based on an evaluation of industry best practice at the time of the experimental testing programme planning and that freely available. Within New Zealand, proprietary providers from the United States of America were the dominant BRB supplier, with a small number of BRBs fabricated within New Zealand making up the remaining demand. The BSJ loading protocol was not available at the time of planning and carrying out of the experimental programme presented here. Due to this, American best practice was evaluated. Two specifications were reviewed, AISC 341-10 (now superseded by AISC 341-16) (American Institute of Steel Construction, 2016) and FEMA 450-1 (Program on Improved Seismic Safety Provisions, 2003).

AISC 341-16 is presented within Section 2.3.4.

Excerpt from FEMA 450-1 Clause 8.6.3.7.6.3

“Loads shall be applied to the test specimen to produce the following deformations, where the deformation is the steel core axial deformation for the Test Specimen and the rotational deformation demand for the subassemblage test specimen brace:

1) 6 cycles of loading at the deformation corresponding to $\Delta_b = \Delta_{by}$

2) 4 cycles of loading at the deformation corresponding to $\Delta_b = 0.5\,\Delta_{bm}$

3) 4 cycles of loading at the deformation corresponding to $\Delta_b = 1.0\,\Delta_{bm}$

4) 2 cycles of loading at the deformation corresponding to $\Delta_b = 1.5\,\Delta_{bm}$

5) Additional complete cycles of loading at the deformation corresponding to $\Delta_b = 1.0\,\Delta_{bm}$ as required for the Brace Test Specimen to achieve a cumulative inelastic axial deformation of at least 140 times the yield deformation (not required for the

subassemblage test specimen).

The design storey drift shall not be taken as less than 0.01 times the storey height for the purposes of calculating $\Delta_{bm}$. $\Delta_{bm}$ need not be taken as greater than 5 $\Delta_{by}$."

The key difference between the two protocols is that FEMA 450-1 applies more cycles of a specified displacement, and requires a lower cumulative inelastic axial deformation (CID, or cumulative inelastic ductility demand, CDD) (140 in comparison to AISC 341 at 200) for qualification. AISC 341 applies a higher level of displacement and does not limit the design storey drift to five times that of yield displacement. It is common for proprietary providers to combine the two loading protocols, increasing the number of cycles within the first three steps. For the purpose of this experimental programme, the AISC 341 loading protocol will be adopted, information regarding sensitivity at higher displacements corresponding to drift are key to the evaluation of the BRB designs within this programme.

The design storey drift is frame dependent and can range in values depending on the member angle of positioning. It is common for proprietary providers to calculate the drift based on a member angle of 45° and 0.01 times that of the corresponding frame height at this angle (Dunai L, 2011). A general approach was adopted, where the design storey drift would equal 0.01 the wp-wp length, resulting in a larger drift if the frame height was taken. This provided a design drift for V and SB configuration of 44 mm and 68 mm respectively.

The first step of the loading protocol is the theoretical equivalent to deformation at first yield. This was calculated based on Hooke's Law for linearly elastic material. The deformation was taken at the material specified yield of 260 MPa, and is a contribution of the yielding core and a portion of the transition region. The transition region portion was taken as the length of the transition region from the yielding core-transition junction to the centroid of the region. The yielding and transition region deformation contributions were combined and rounded to the nearest millimetre.

A summary of applied loading protocol to each specimen can be found in Appendix A and the loading protocols themselves in Appendix B.

## 3.3 Fabrication

The following sub-section details the fabrication process. All specimens were assembled (including welding) and cast at the University of Canterbury, with steel fabrication carried out at specialised external facilities. All cores, stiffener plates and end caps were CNC machined from Grade 250 hot rolled flat plate. The outer casings were custom fabricated from two cold-formed C-sections, longitudinally welded down the major axis. These casings were fabricated at a facility specialising in cold-formed box beams. Prior to assembly, the stiffeners (where applicable) were welded to the core.

All elements were checked prior to fabrication to be within ± 2 mm for length and ± 3 mm for straightness tolerance in accordance with AS/NZS 1365. All geometry was checked prior to fabrication. The casing in some cases slipped during casting, the initial stroke at each end of each specimen is presented within the results.

One end connection plate was welded to the end of the core prior to assembly. Denso MP Primer was applied to the restrained regions of the core by hand, followed by positioning of 10 mm thick polystyrene in the bearing regions. The unbonding medium of Denso Petrolatum Tape was applied to the restrained region surface, encasing the bearing region polystyrene. There was no overlap of the Denso Petrolatum Tape (Figure 3-6 a)). The casing was positioned horizontally over the core using die sliders to prevent the core from touching the outer casing (Figure 3-6 b)); end caps were subsequently welded to the outer casing to hold the core in position. The specimens were then suspended from the strong wall by the welded connection plate, with the remaining connection plate welded at the base of the specimen. All welding was monitored at the end of each pass, such that deformation was prohibited.

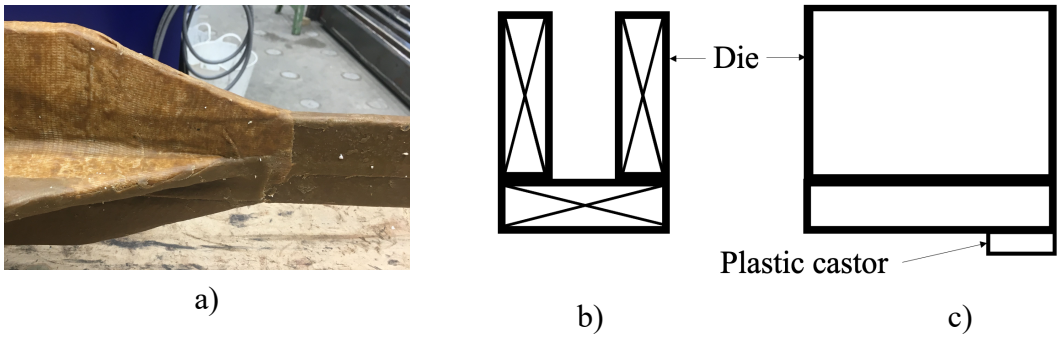


**Figure 3-6: a) Applied Denso Petrolatum Tape b) Die slider, front c) Die slider, side**

Unlike proprietary providers and other researchers who cast from the top, the specimens within this programme were cast from the bottom up in the interest of eliminating the risk of voids forming. The specimens were suspended from the strong wall through welded connection end plates at the ends of the core. One connection plate (top) was fixed to the wall through a custom bracket (Figure 3-7 a)). The other (bottom) was loaded with weight plates or load cells to pre-tension the core (Figure 3-7 b)); these weights were left on throughout casting and the first 24 hours of curing (a summary of the pre-tension weight for each specimen can be found in Appendix A).

Pre-tensioning of the core is common practice by commercial suppliers. The core is pre-tensioned to eliminate the core from bending as the grout is cast within the outer casing, eliminating any out-of-straightness due to grout pressure. As grout forms at the base of the specimen, the pre-tensioning weights themselves become redundant. The pre-tension weight was approximately 2/3 the yield load of the yielding core. Load cells and weights were interchanged based on laboratory availability on the day of casting. All weights and load cells were calibrated prior to pre-tensioning.

Sika 215 grout was pumped through a hose connection ≅ 40 mm from the capping plate, positioned within the non-yielding region (Sika 215 is a high flow grout with positive shrinkage compensation and is used in applications with narrow dimensions). Pumping the grout from the bottom allowed the specimen to pre-tension itself under self-weight, but also prevent segregation, air pockets and the need for compaction aid. Gaps within the top capping plate, allowed the grout to expand post pumping, and also visually identified when the specimens were filled. All specimens were left for at least 24 hours before being moved to a temperature-controlled area for curing in the horizontal position (Figure 3-8).


a) b)

**Figure 3-7: a) Specimens attached to strong wall via custom bracket b) Pre-tensioning weights**

**Figure 3-8: Suspended specimens**

Mill certificates of the hot rolled steel core and cold-formed outer casing can be found in Appendix C. Tensile testing according to AS 1391 (Standards Australia, 2007) was carried out from samples of the core material plate; results can be found in Appendix D. Grout testing in accordance with NZS 3112 (Standards New Zealand, 1986) was carried out at 28 days and on the day of testing; results can be found in Appendix E.

## 3.4 Experimental testing

### 3.4.1 Test rig

Two different test configurations were examined within this testing regime: concentric and eccentric. The concentric configuration consisted of both ends of the specimen being aligned and in plane. One end was connected to the loading actuator (Figure 3-9), with the other being a freestanding reaction frame (Figure 3-10). Both ends were connected via pin as specified in Section 3.1.5. As three pins were in series, the actuator was propped vertically with a single prop at the initiation of actuator extension/contraction to support and prevent rotation occurring out of plane.

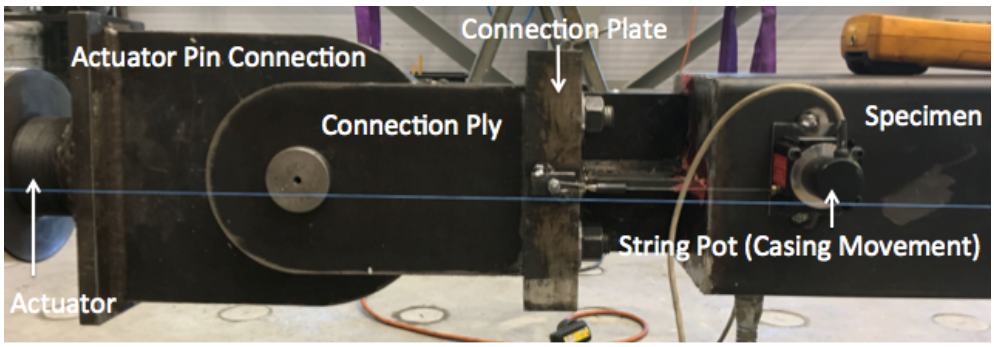


**Figure 3-9: Concentric test configuration actuator end**

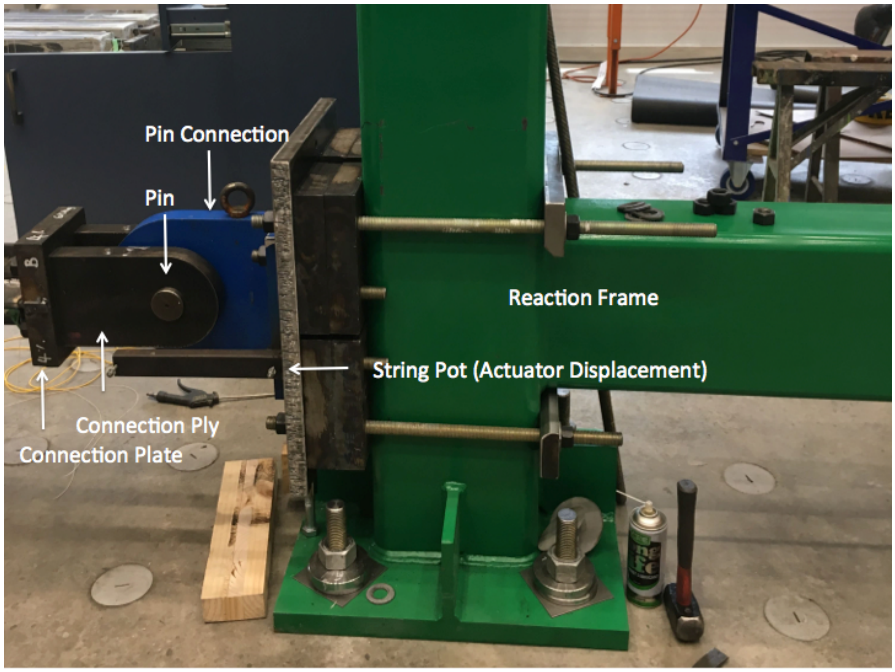


**Figure 3-10: Concentric test configuration freestanding end**

The eccentric configuration involved two setups, one each for unstiffened and stiffened specimens. The unstiffened specimens were prone to buckling in the un-restrained non-yielding region. In accordance with AISC 341, C-K3.2, the use of pins or spherical bearings may be used to limit the flexural yielding and rotational demands of the core extension. A pin connection similar to that used within the concentric configuration was adopted for unstiffened eccentric specimens (E-S/LU) (Figure 3-12). For the stiffened specimens (E-S/LS), the connection plate connected directly to a rigid reinforced concrete application block situated on bearing tracks and at the other end, a freestanding reaction frame (Figure 3-13). This created a fixed end connection, with the connection plate attached to the concrete application block at an out of plane displacement of 128 mm. The out of plane displacement was based on Clause C7.5 of NZS 1170.5 (Standards New Zealand, 2004) where the interstorey deflection limit is taken as 3.75 % for ordinary buildings with an annual period of exceedance of 1/2500, representing the near-collapse limits. The out of plane displacement was the maximum permissible for the concrete application block, equivalent to a frame height of 3.4 m or 4 % deflection limit for a standard frame height of 3.2 m.

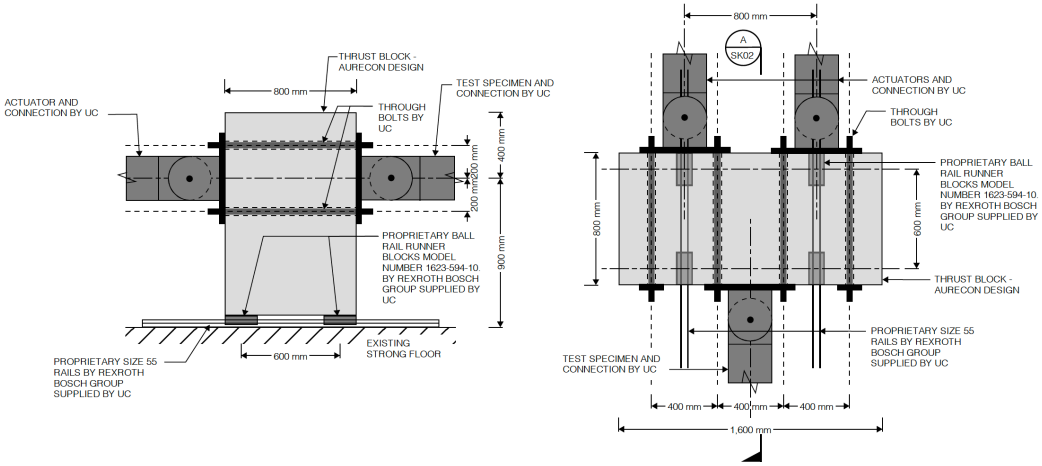


**Figure 3-11: Load application block, side and plan view**

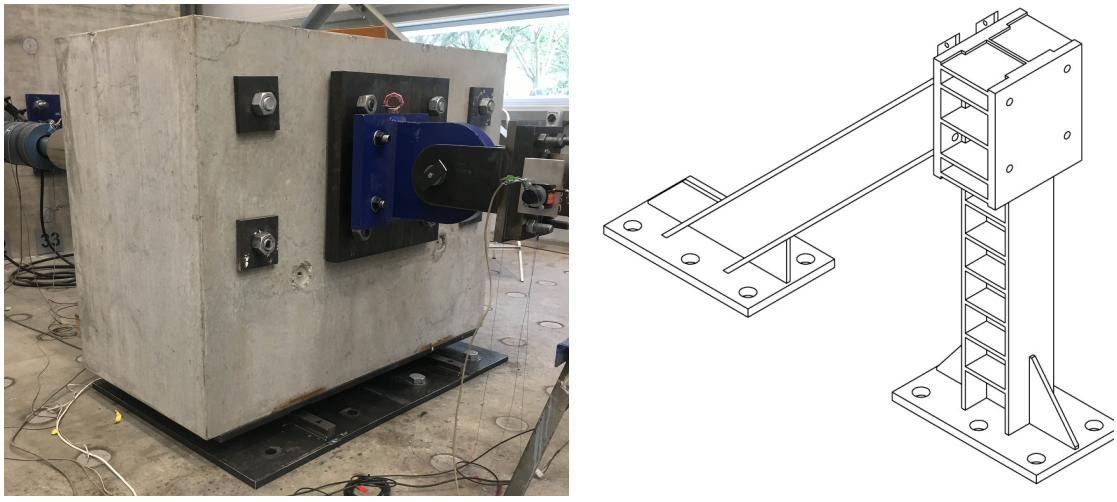

a) b)

**Figure 3-12: Eccentric unstiffened specimen configuration a) Actuator connection b) Free-standing frame**

a) b)

**Figure 3-13: Eccentric stiffened specimen configuration a) Actuator end b) Full specimen**

The actuator(s) used for all test configurations were of ± 300 mm stroke with 1 MN and 750 kN capacity in tension and compression, respectively. A single actuator was used in the concentric testing, with two actuators connected to the concrete application block for eccentric configurations (increasing the combined compression capacity to 1500 kN). Both test types applied the load in the axial direction of the specimen where the specimens were orientated such that the core was perpendicular to the strong floor, and stiffeners (if present) were parallel. The actuator was calibrated prior to testing, with the calibration file and readout reported within Microsoft Excel.

It was found that the connecting bolts for the connection ply impeded the stroke of the stiffened specimens; this was accounted for in later testing. In already fabricated specimens an adaptor was welded to the end of the specimens (Figure 3-14).

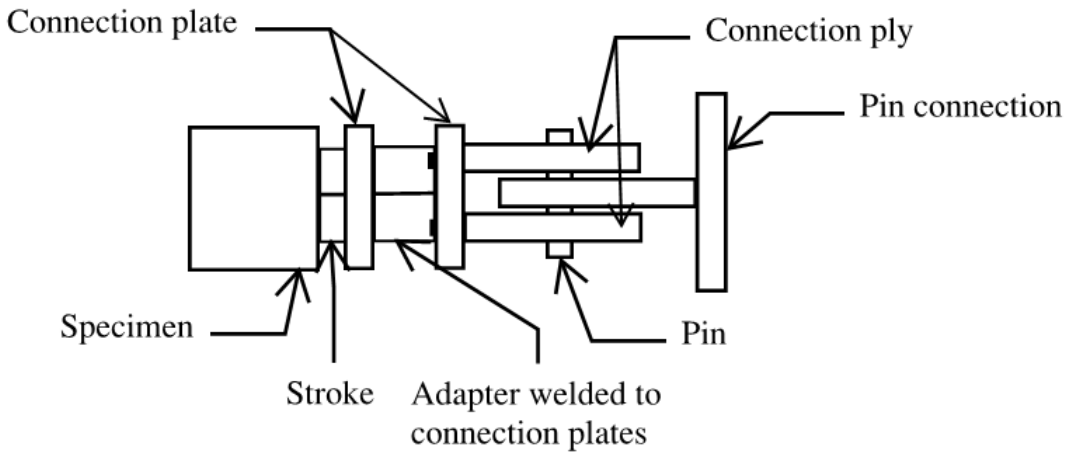


**Figure 3-14: Specimen adaptor**

### 3.4.2 Instrumentation

String pots were used to measure global specimen displacement with respect to the actuator and also specimen displacement with respect to stroke. Two string pots were positioned at each end of the specimen, parallel to the core. By use of two string pots, the outer casing rotation and displacement could be obtained. A global string pot was used to control the actuator displacement; this was connected to the actuator and the reaction frame at the freestanding end. In later testing, inclinometers were placed on each connection plate, and at each end of the specimen, measuring any rotation occurring throughout the length of the specimen (twisting), and also any rotation occurring within the unrestrained non-yielding region (stroke). This information was used to determine effects, if any of rotational, global and localised buckling. The global string pot provided the applied loading protocol on the specimen to 0.001 mm. The above outputs were reported in conjunction with the actuator outputs within a Microsoft Excel sheet, along with any calibration factors, allowing for transformation of the data when required. Figure 3-15 shows a general schematic of the instrumentation. The string pot was positioned 200 mm from the outer casing edge to the centre of the connection plate. The inclinometers were positioned in the centre of the connection plate and also 250 mm from the outer casing edge.

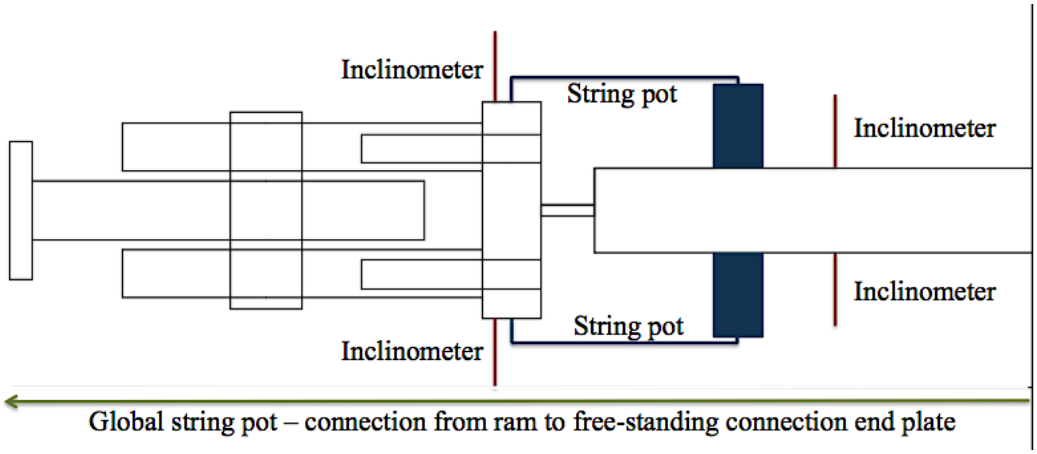


**Figure 3-15: Instrumentation schematic**

### 3.4.3 Summary

Table 3-1 summarises the loading rig, instrumentation and specimen orientation within the rig for all 37 specimens.

**Table 3-1: Specimen testing rig and instrumentation summary**

| Specimen | Configuration Length | Loading Rig | Instrumentation | Specimen end at actuator |
|---|---|---|---|---|
| C-VU2-E2-70 | V | C | 2 | Bottom |
| C-VU2-E1-65 | V | C | 2 | Bottom |
| C-VU2-E2-65 | V | C | 1 | Bottom |
| C-VU2-E3-65 | V | C | 1 | Bottom |
| C-VU2-E2-60 | V | C | 2 | Bottom |
| C-VU4-E2-65 | V | C | 1 | Bottom |
| C-VU6-E2-65 | V | C | 1 | Bottom |
| C-VS2-E2-200-R10 | V | CA | 1 | Bottom |
| C-VS4-E2-200-R10 | V | C | 1 | Bottom |
| C-VS6-E2-200-R10 | V | C | 1 | Bottom |
| C-VS2-E2-200-R80A | V | C | 2 | Bottom |
| C-VS2-E2-200-R80B | V | C | 2 | Bottom |
| C-VS2-E2-200-R80C | V | C | 2 | Top |
| C-DU2-E2-70 | SB | C | 2 | Bottom |
| C-DU2-E1-65 | SB | C | 2 | Bottom |
| C-DU2-E3-65 | SB | C | 2 | Bottom |
| C-DU2-E2-60 | SB | C | 2 | Bottom |
| C-DU2-E2-65-T3 | SB | C | 2 | Bottom |
| C-DU2-E2-65 | SB | C | 2 | Bottom |
| C-DU2-E2-65-T1 | SB | C | 2 | Bottom |
| C-DU4-E2-65 | SB | C | 2 | Bottom |
| C-DU6-E2-65 | SB | C | 2 | Bottom |
| C-DS2-E2-200-R10 | SB | C | 1 | Bottom |
| C-DS4-E2-200-R10 | SB | C | 1 | Bottom |
| C-DS6-E2-200-R80 | SB | C | 2 | Bottom |
| E-VU2-E2-65 | V | EU | 2 | Top |
| E-VU4-E2-65 | V | EU | 2 | Top |
| E-VU6-E2-65 | V | EU | 2 | Bottom |
| E-VS2-E2-200 | V | ES | 2 | Top |
| E-VS4-E2-200 | V | ES | 2 | Top |

| | | | | |
|---|---|---|---|---|
| E-VS6-E2-200 | V | ES | 2 | Top |
| E-DU2-E2-65 | SB | EU | 2 | Top |
| E-DU4-E2-65 | SB | EU | 2 | Top |
| E-DU6-E2-65 | SB | EU | 2 | Top |
| E-DS2-E2-200 | SB | ES | 2 | Top |
| E-DS4-E2-200 | SB | ES | 2 | Top |
| E-DS6-E2-200 | SB | ES | 2 | Bottom |

Key: C = Concentric configuration; E = Eccentric configuration; V = V configuration length; D = Single bay configuration length; A = Adaptor; 1 = String and global pots; U = Unstiffened specimen; S = Stiffened specimen; E = Embedment ratio to non-yielding width; R = Radius; T = Transition slope; 2 = String, global pots and inclinometers

E.g.: C-DS4-E2-200-R10 = Concentric single bay configuration, stiffened specimen with 4 % stroke, embedment ratio 2, 200 mm outer casing depth, 10 mm yielding to transition region radii.

## 3.5 Results and discussion

The following subsection details the results of the experimental testing program. The results are presented with respect to the variables investigated. Where a specimen was included in more than one sensitivity group, the results will be italicised on repeat reporting. Where a normalised force is reported, the force response has been normalised with the average tensile testing yield force at a strain of 0.002 with respect to the appropriate steel batch (see Appendix D for full results). Dissection photos are also included where applicable. The results along with observations throughout the experimental testing and dissection will be discussed with respect to each variable considered within that sensitivity group.

Within each comparison, two tables are presented. The first details the key geometrical details of the specimens, the second, key experimental results. The experimental results summary table presents the failure mode of the specimen, these are summarised as:

- Local buckling, referring to a localised region of buckling within the yielding core (not to be mistaken with high mode wave formation), within slender outer casings this is visually identified through bulging of the outer casing. In some cases the mode of buckling can be visualised, 1$^{st}$ mode buckling refers to a localised buckling forming a wavelength with a crest, 2$^{nd}$ mode buckling refers to locaslised buckling in the form of a wave with both crest and trough.
- Global buckling, referring to the specimen buckling as a single unit
- Hinge, this refers to the stroke bending, forming a hinge between the outer casing and stroke region

The material yield is presented based on the average tensile test results, and specimen yield presented based on experimental testing. The first cycle of testing, to elastic yield was less than that for specimen yield, with the specimen yeild occurring in the 0.5 times drift cycles. The elastic yield was calculated as follows:

$$\Delta_{by}/\delta_e = \frac{f_y L_y}{E} + 2\left(\frac{f_y\left(\frac{2}{3}L_t\right)}{E}\right) \qquad \text{Equation 3-1}$$

The stroke length varied between specimens due to the nature of fabrication, with the initial (prior to loading) and final (post loading) stroke lengths presented for both the actuator end and freestanding frame end. The final stroke lengths give an indication of symmetric loading, where both strokes are engaged equally, or one is engaged over the other resulting in unsymmetrical yielding behaviour. The maximum compression overstrength factor is included for each specimen, and the percent strain of the yielding core this occurs.

The global buckling safety factor evaluates the outer casing Euler buckling capacity with respect to the cores yield capacity. When this exceeds 1.0, the member is susceptible to global buckling (this equation is based on Equation 2-26, without the 1.5 factor). Two local buckling factors are presented, Equation 2-27 and Equation 2-28. The former evaluates a punching force exerted on the inner surface of the outer casing with respect to the restraining mediums contribution, the latter, a more conservative approach, assumes the restraining medium does not contribute to restraining the core from local buckling. Local buckling susceptibility is present when the factors exceed 1.0.

### 3.5.1 Restraining mechanism sensitivity

The restraining mechanisms geometrical dimensions were investigated to evaluate the effects (and the sensitivity, if any) on local and global buckling initiation. Unstiffened BRBs were evaluated due to the ability to vary the restraining mechanisms geometrical dimensions while considering in conjunction the effects of local and global buckling. Stiffened BRBs restraining mechanism is typically dictated by the dimensions of the stiffener, and as such, local buckling sensitivity is suppressed.

**Table 3-2: V configuration unstiffened restraining mechanism sensitivity specimen key geometrical features**

| **Specimen** | | **C-VU2-E2-70** | **C-VU2-E2-65** | **C-VU2-E2-60** |
|---|---|---|---|---|
| Non-yielding length (mm) | Transition | 120 | 120 | 120 |
| | Embedment | 320 | 320 | 320 |
| | Stroke | 44 | 44 | 44 |
| Yielding length (mm) | | 2232 | 2232 | 2232 |
| Radius (mm) | | 80 | 80 | 80 |
| Outer casing depth (mm) | | 70 | 65 | 60 |
| Stiffeners | | No | No | No |

**Table 3-3: V configuration unstiffened restraining mechanism sensitivity results**

| Specimen | | | C-VU2-E2-70 | C-VU2-E2-65 | C-VU2-E2-60 |
|---|---|---|---|---|---|
| Failure mode | | | Local buckling | Local buckling | Global buckling |
| Material yield (kN) | | | 195.1 | 195.1 | 195.1 |
| Specimen yield (kN) | | | 220.0 | 221.5 | 225.1 |
| Compression adjustment factor, $\beta$ | | | 1.13 | 1.05 | 0.83 |
| Percent strain $\beta$ occurs, $\varepsilon_{sc}$ (%) | | | 1.97 | 0.99 | 0.85 |
| Stroke length (mm) | Actuator end | Initial | 46.31 | 51.81 | 47.23 |
| | | Final | 86.73 | 32.12 | 50.46 |
| | Freestanding frame end | Initial | 47.36 | 51.79 | 50.51 |
| | | Final | 61.01 | 107.92 | 53.69 |
| Global buckling safety factor | | | 0.44 | 0.51 | 0.61 |
| Local buckling | Minor axis (Equation 2-27) | | 0.80 | 1.01 | 1.21 |
| | Demand to capacity ratio (Equation 2-28) | | 1.18 | 1.23 | 1.23 |

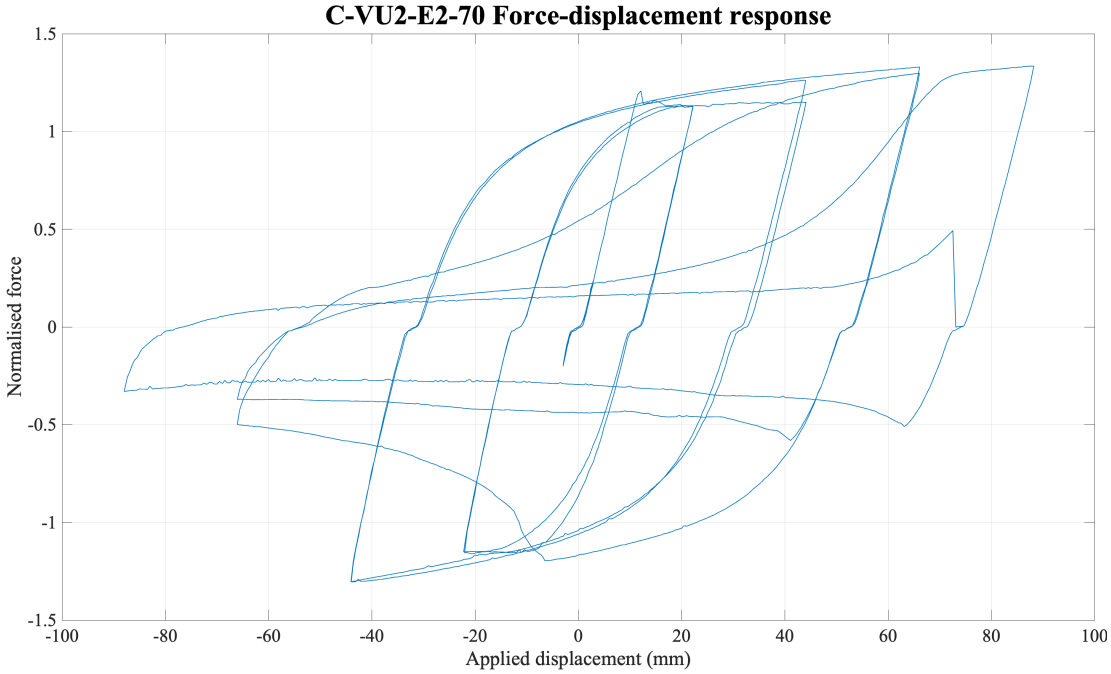


a)

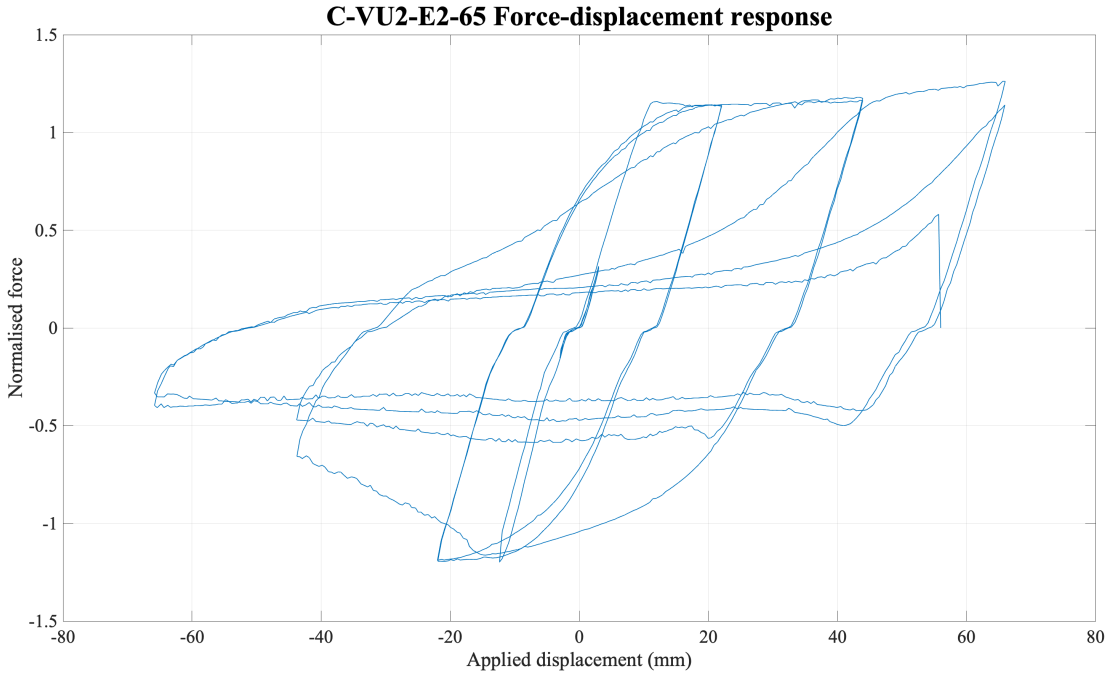
C-VU2-E2-65 Force-displacement response
Normalised force
Applied displacement (mm)
1.5
1
0.5
0
-0.5
-1
-1.5
-80
-60
-40
-20
0
20
40
60
80

b)

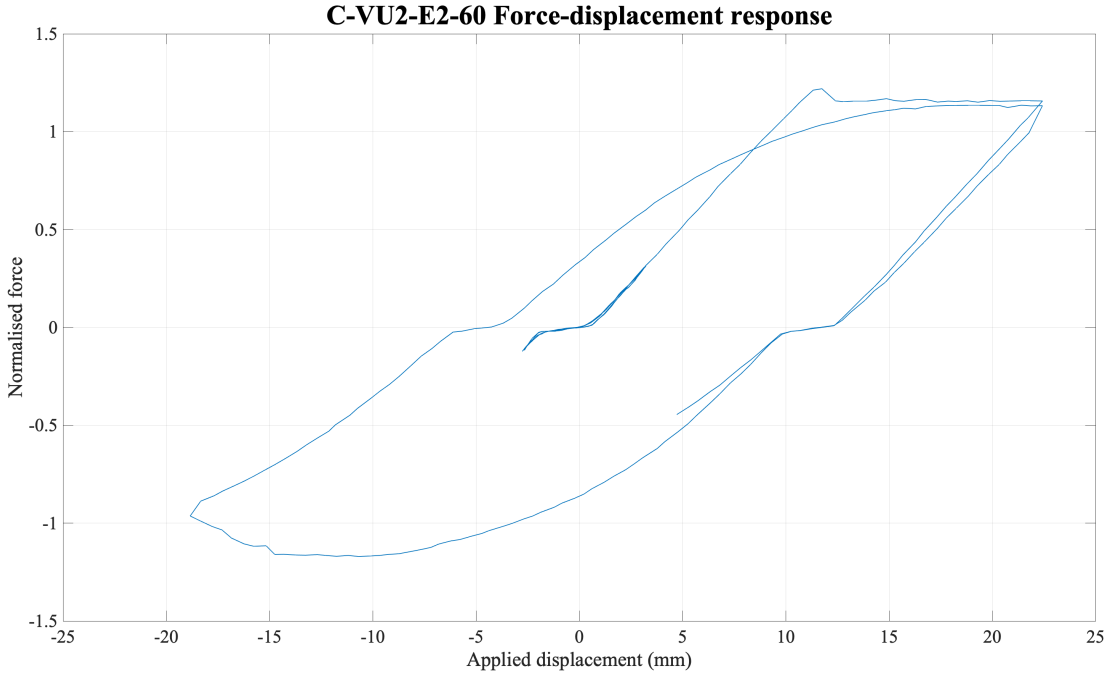
C-VU2-E2-60 Force-displacement response
Normalised force
Applied displacement (mm)
1.5
1
0.5
0
-0.5
-1
-1.5
-25
-20
-15
-10
-5
0
5
10
15
20
25

c)

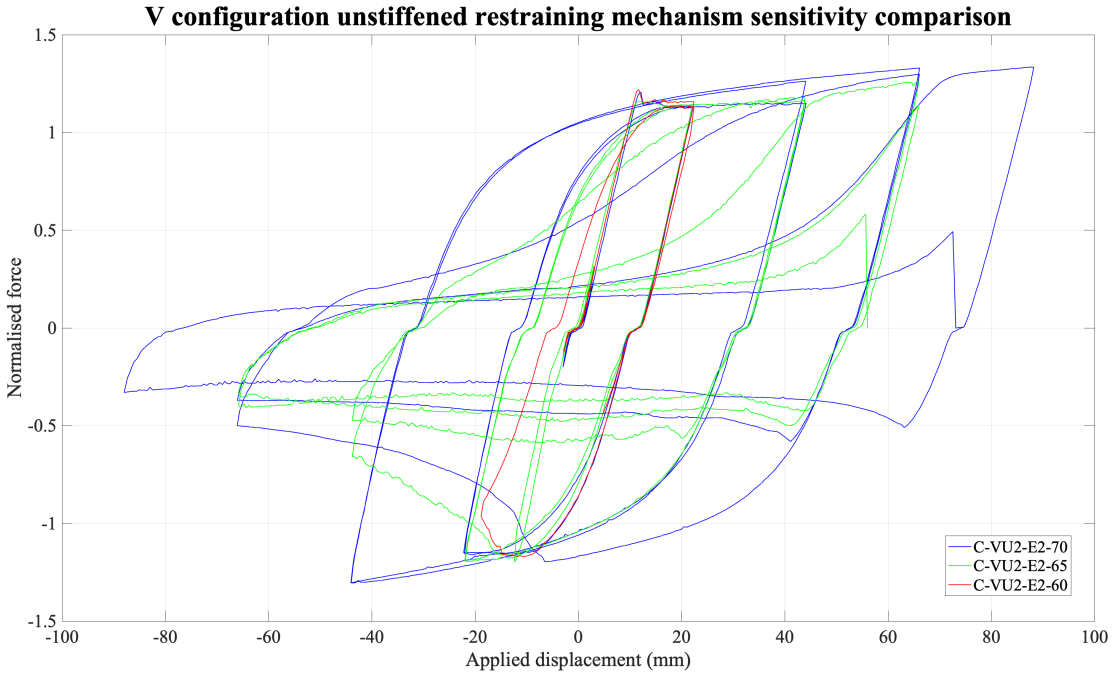


d)

**Figure 3-16: V configuration unstiffened restraining mechanism sensitivity a) Specimen C-VU2-E2-70 b) Specimen C-VU2-E2-65 c) Specimen C-VU2-E2-60 d) Comparison of sensitivity**

a) b)

**Figure 3-17: C-VU2-E2-65 Dissection a) Damaged restraining medium b) Fractured core**

The unstiffened V configuration BRBs were evaluated; C-VU2-E2-70, C-VU2-E2-65 and C-VU2-E2-60. C-VU2-E2-65 was loaded in compression first, engaging global buckling instantly. This global buckling was recovered when unloaded, the test was restarted in tension, with the C-VU2-E2-65 core behaving independently from the restraining mechanism. This observation is discussed in Section 3.6. Based on the

Euler buckling load, all specimens were theoretically supressed from global buckling (global buckling safety factor < 1.0, see Table 3-3), however C-VU2-E2-60 experienced global buckling within the first compression cycle post core yielding (see Figure 3-16). It was found through dissection that the core did not present any yielding bands within the mill scale commonly formed when the core yields independently to the restraining mechanism. Bonding of the restraining medium to the core was not obvious on dissection (Figure 3-17), and if present, was in small to localised regions. Global buckling was likely caused by poor application of the unbonding medium, resulting in a smaller gap required to compression stresses to be distributed through the restraining mechanism.

C-VU2-E2-70 and C-VU2-E2-65 underwent 2$^{nd}$ and 1$^{st}$ mode local buckling respectively. The local buckling was localised and visually present throughout testing with deformation of the restraining mechanism. All local buckling occurred within the yielding core and was located in the vicinity of the bearing region. On local buckling initiation, the tension capacity of the specimen was still achieved while the compression capacity tended to 0 kN on repetitive cycles, providing an indicative response of BRB failure. Based on local buckling of the minor axis (Equation 2-27, Table 3-3) and Demand to Capacity Ratio (DCR) (Equation 2-28, Table 3-3), C-VU2-E2-65 was designed to have higher susceptibility to local buckling than C-VU2-E2-70. This was confirmed through C-VU2-E2-70 performing two more stable cycles (Figure 3-16) than C-VU2-E2-65 and through the engagement of higher mode buckling within the yielding region.

The minor axis buckling ratio and DCR (Table 3-3) for C-VU2-E2-70 and C-VU2-E2-65 are 0.80, 1.18, 1.21 and 1.23, respectively. The DCR for both specimens exceeds 1.0, indicating local buckling susceptibility. The difference between the minor axis and DCR can provide an insight into the sensitivity and influence of local buckling. Both factors take into consideration the ratio of the punching force and the restraining mechanisms capacity with respect to the restraining mediums thickness, distribution throughout this thickness and overall restraining mechanisms dimensions. However, the minor axis ratio assumes a contribution factor of the restraining medium, which when altered significantly affects the minor axis ratio. This contribution factor was assumed to be 2.0 based on advice from the developers of the ratio. The results indicate that a factor less than or equal to 1.8 would be appropriate due to local buckling failure and in the case where experimental testing cannot be afforded to verify this factor, the DCR provides a reasonable prediction of local buckling susceptibility.

**Table 3-4: Single bay configuration unstiffened restraining mechanism sensitivity specimen key geometrical features**

| Specimen | | C-DU2-E2-70 | C-DU2-E2-65 | C-DU2-E2-60 |
|---|---|---|---|---|
| Non-yielding length (mm) | Transition | 120 | 120 | 120 |
| | Embedment | 320 | 320 | 320 |
| | Stroke | 68 | 68 | 68 |
| Yielding length (mm) | | 4584 | 4584 | 4584 |
| Radius (mm) | | 80 | 80 | 80 |
| Outer casing depth (mm) | | 70 | 65 | 60 |
| Stiffeners | | No | No | No |

**Table 3-5: Single bay configuration unstiffened restraining mechanism sensitivity results**

| Specimen | | | C-DU2-E2-70 | C-DU2-E2-65 | C-DU2-E2-60 |
|---|---|---|---|---|---|
| Failure mode | | | Global buckling | Global buckling | Global buckling |
| Material yield (kN) | | | 191.4 | 191.4 | 191.4 |
| Specimen yield (kN) | | | 206.8 | 209.6 | 202.6 |
| Compression adjustment factor, $\beta$ | | | 0.79 | 0.77 | 0.82 |
| Percent strain $\beta$ occurs, $\varepsilon_{sc}$ (%) | | | 0.15 | 0.15 | 0.15 |
| Stroke length (mm) | Actuator end | Initial | 74.42 | 68.89 | 76.25 |
| | | Final | 80.65* | 74.06* | 79.00* |
| | Freestanding frame end | Initial | 70.57 | 74.80 | 68.65 |
| | | Final | 73.79* | 76.55* | 77.01* |
| Global buckling safety factor | | | 1.31 | 1.55 | 1.85 |
| Local buckling | Minor axis (Equation 2-27) | | 0.80 | 1.01 | 1.21 |
| | Demand to capacity ratio (Equation 2-28) | | 1.18 | 1.23 | 1.30 |

* Unloaded displacement

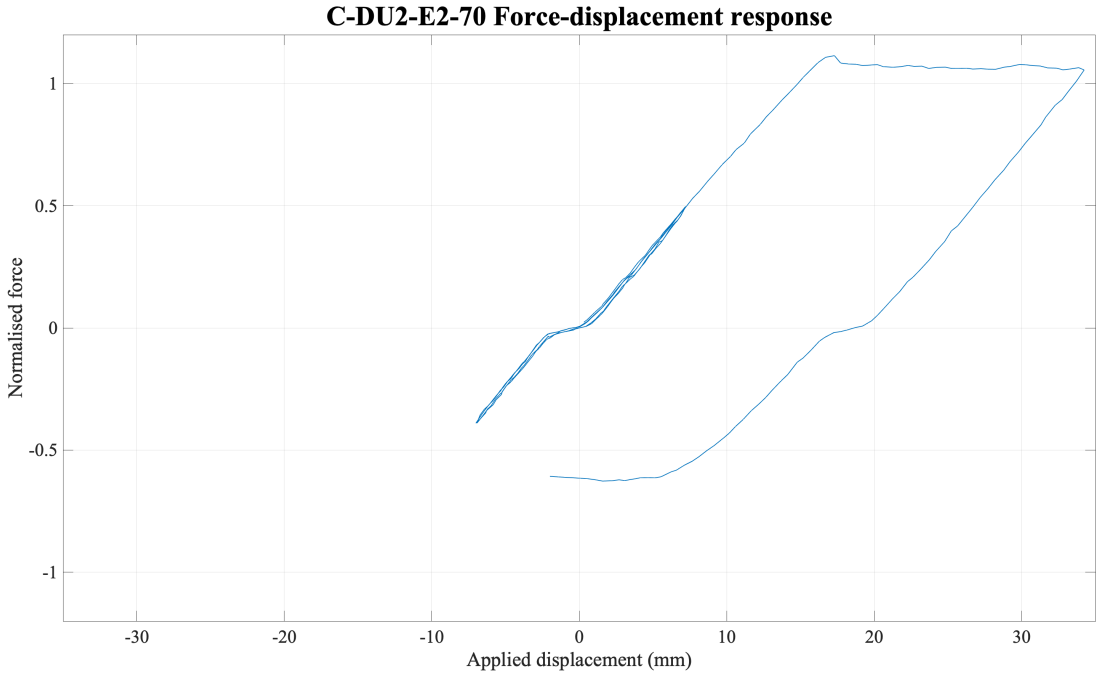
C-DU2-E2-70 Force-displacement response
Normalised force
Applied displacement (mm)
1
0.5
0
-0.5
-1
-30
-20
-10
0
10
20
30

a)

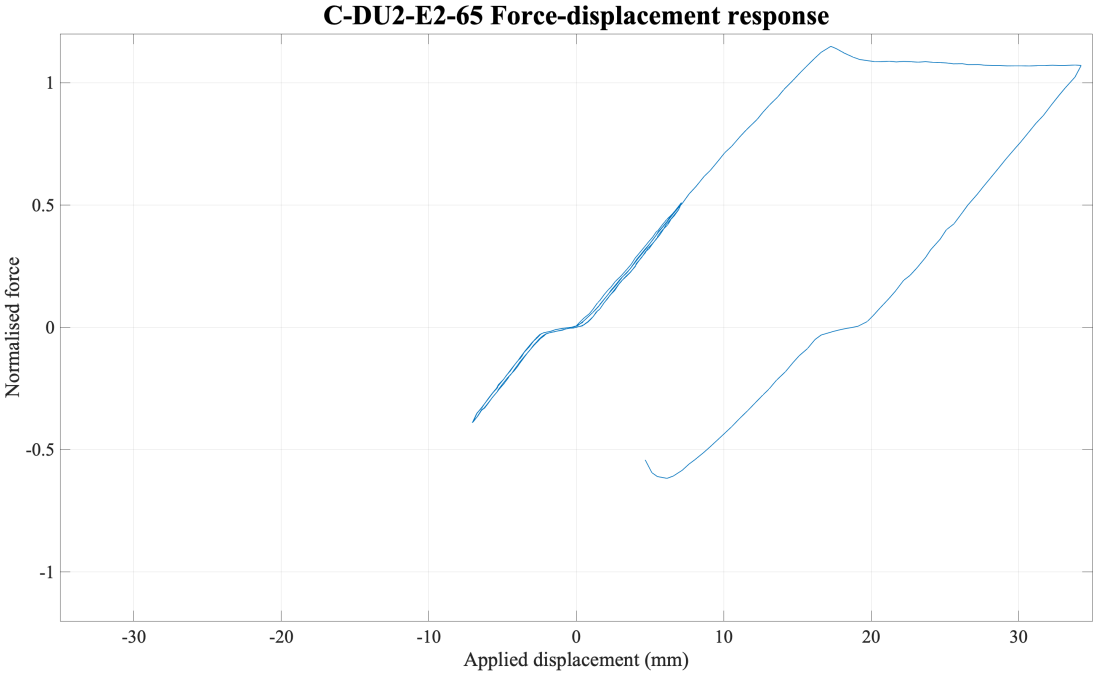
C-DU2-E2-65 Force-displacement response
Normalised force
Applied displacement (mm)
1
0.5
0
-0.5
-1
-30
-20
-10
0
10
20
30

b)

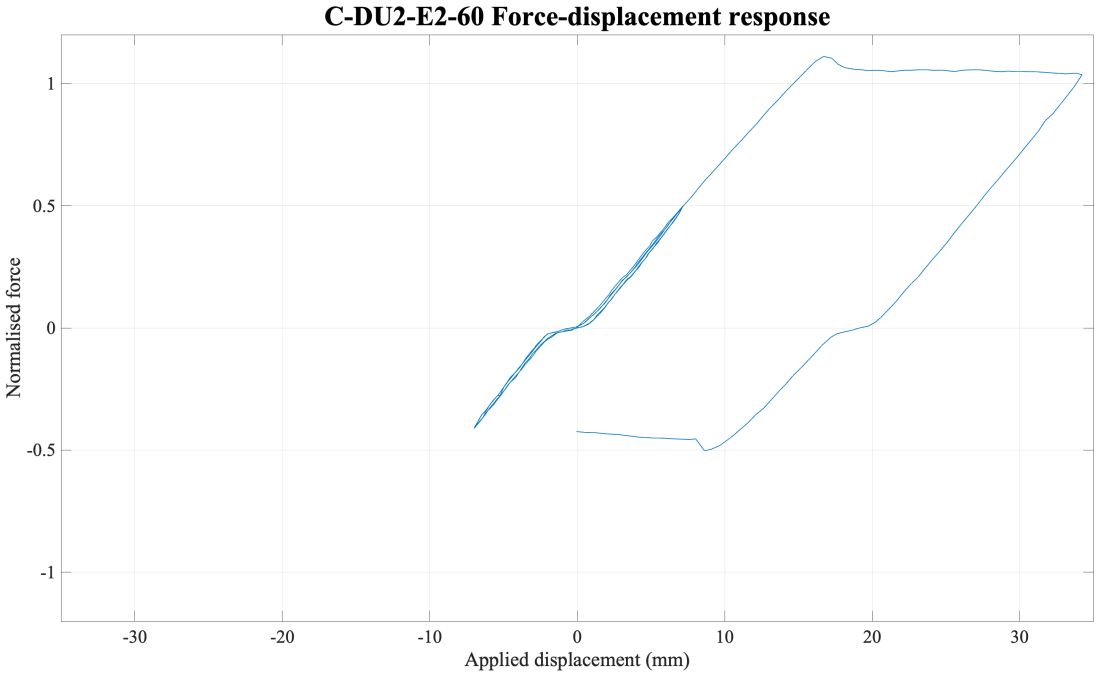


c)

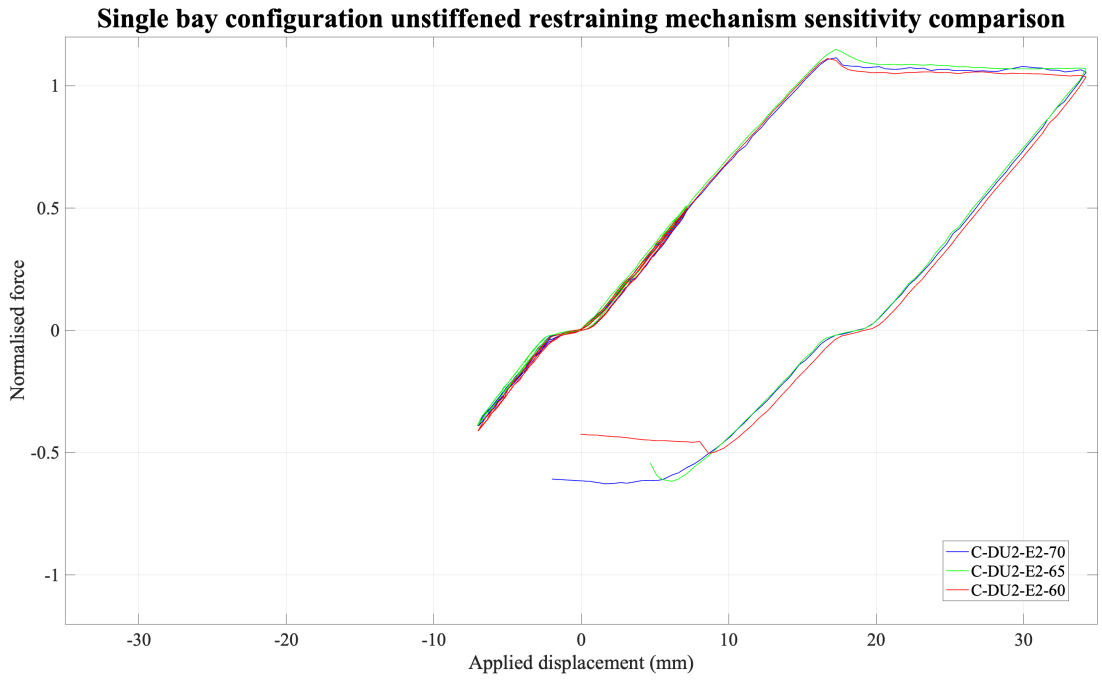


d)

**Figure 3-18: Single bay configuration unstiffened restraining mechanism sensitivity a) Specimen C-DU2-E2-70 b) Specimen C-DU2-E2-65 c) Specimen C-DU2-E2-60 d) Comparison of sensitivity**


a) b) c)

**Figure 3-19: Dissection a) C-DU2-E2-70 undamaged restraining medium b) C-DU2-E2-65 undamaged restraining medium c) C-DU2-E2-60 undamaged core and bearing region polystyrene**

The SB configuration unstiffened BRBs evaluated were C-DU2-E2-70, C-DU2-E2-65 and C-DU2-E2-60. All specimens underwent 1st mode global buckling within the first plastic compression cycle (0.5 x drift). The specimens were designed similar to the V configuration with increases in susceptibility to local and global buckling from C-DU2-E2-70, C-DU2-E2-65 and C-DU2-E2-60 respectively. It was assumed that local buckling would govern performance, and hence the specimens were designed to local buckling sensitivity (mimicking the V configuration specimen design with the only variance the yielding core length). The global buckling safety factor for all specimens exceeded 1.0 (Table 3-5), indicating susceptibility to global buckling and as such it can be determined that the susceptible failure mode factor will govern performance.

All SB configuration specimens reached the specimen yield in tension, and developed a compression strength of approximately ⅓ that of tension, which is typical of unrestrained steel (Figure 3-18). The global safety factors of C-DU2-E2-70, C-DU2-E2-65 and C-DU2-E2-60 are 1.31, 1.55 and 1.85 respectively. It was observed in testing that the higher the global buckling safety factor the more susceptible to global buckling and premature failure, with C-DU2-E2-60 undergoing global buckling at a lower compression displacement. It was also observed that the higher the global buckling safety factor, the more prone the specimen was to torsional rotation from mid-span. All tests were aborted on initiation of global buckling due to out of plane deflection safety concerns. On dissection (Figure 3-19) of all specimens, no damage was present to the cores, however unrecoverable plastic deformation was present in the outer casings.

### 3.5.2 Unrestrained nonyielding region (stroke) response sensitivity

The stroke region was investigated to evaluate any correlation between the region and design drift and also see how the presence of stiffeners affected the member response. Twelve specimens, six each unstiffened and stiffened, with V and SB configuration were evaluated. As in Section 3.5.1, the SB configuration specimens were designed

assuming local bucking governed, mirroring the V bay configuration specimens with the yielding and stroke length being the only differing factors.

**Table 3-6: V configuration unstiffened stroke length sensitivity specimen key geometrical features**

| **Specimen** | | **C-VU2-E2-65** | **C-VU4-E2-65** | **C-VU6-E2-65** |
|---|---|---|---|---|
| Non-yielding length (mm) | Transition | *120* | 120 | 120 |
| | Embedment | *320* | 320 | 320 |
| | Stroke | *44* | 88 | 132 |
| Yielding length (mm) | | *2232* | 2144 | 2056 |
| Radius (mm) | | *80* | 80 | 80 |
| Outer casing depth (mm) | | *65* | 65 | 65 |
| Stiffeners | | *No* | No | No |

**Table 3-7: V configuration unstiffened stroke length sensitivity results**

| **Specimen** | | | **C-VU2-E2-65** | **C-VU4-E2-65** | **C-VU6-E2-65** |
|---|---|---|---|---|---|
| Failure mode | | | *Local buckling* | Rotation – local hinge | Local buckling |
| Material yield (kN) | | | *195.1* | 205.0 | 205.0 |
| Specimen yield (kN) | | | *221.5* | 212.0 | 216.1 |
| Compression adjustment factor, $\beta$ | | | *1.05* | 1.02 | 1.04 |
| Percent strain $\beta$ occurs, $\varepsilon_{sc}$ (%) | | | *0.99* | 1.03 | 1.07 |
| Stroke length (mm) | Actuator end | Initial | *51.81* | 66.67 | 106.12 |
| | | Final | *32.12* | 63.76 59.89 | 117.23 |
| | Freestanding frame end | Initial | *51.79* | 61.21 | 105.64 |
| | | Final | *107.92* | 46.37 49.10 | 135.74 |
| Global buckling safety factor | | | *0.51* | 0.51 | 0.51 |
| Local buckling | Minor axis (Equation 2-27) | | *1.01* | 1.01 | 1.01 |
| | Demand to capacity ratio (Equation 2-28) | | 1.23 | 1.23 | 1.23 |

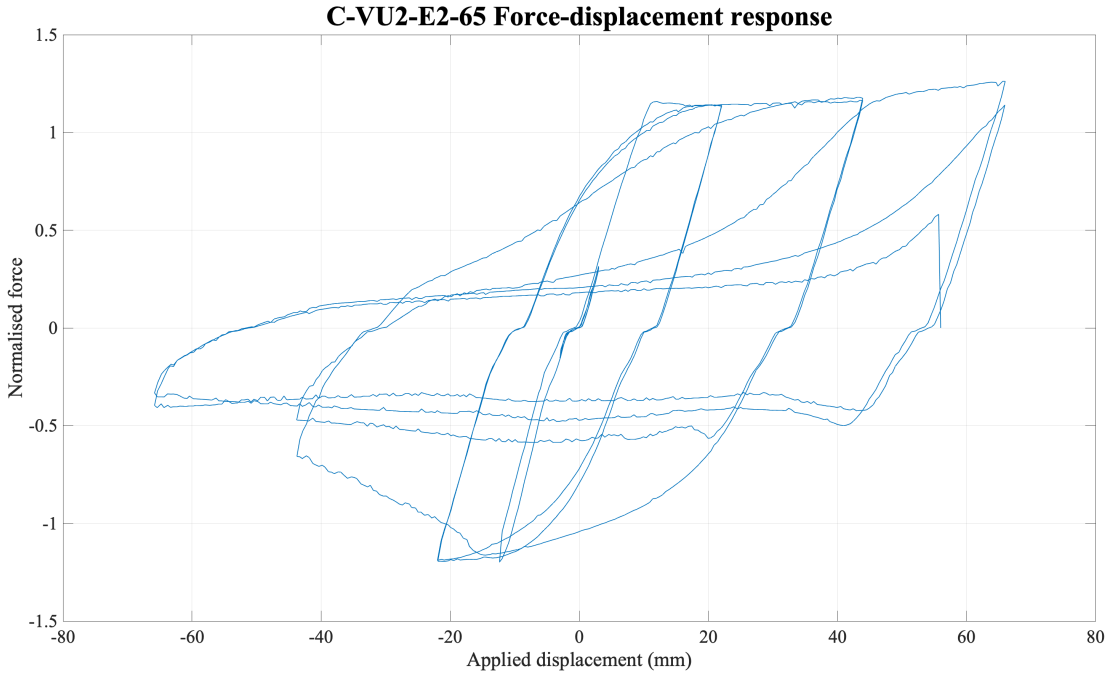
C-VU2-E2-65 Force-displacement response
Normalised force
Applied displacement (mm)
1.5
1
0.5
0
-0.5
-1
-1.5
-80
-60
-40
-20
0
20
40
60
80

a)

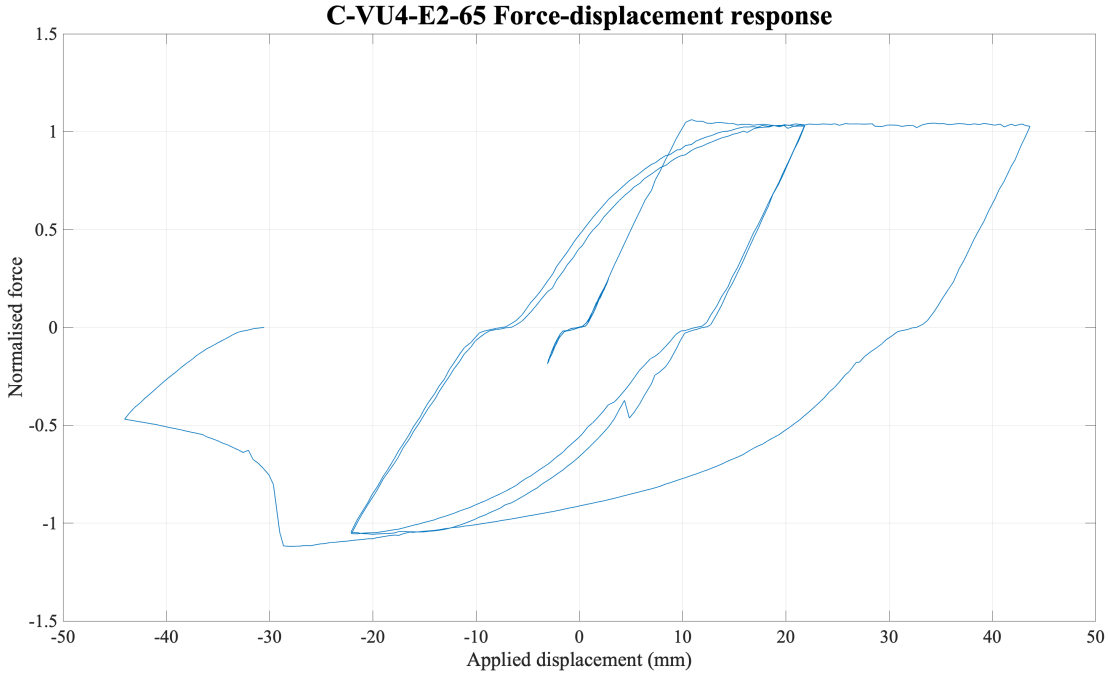
C-VU4-E2-65 Force-displacement response
Normalised force
Applied displacement (mm)
1.5
1
0.5
0
-0.5
-1
-1.5
-50
-40
-30
-20
-10
0
10
20
30
40
50

b)

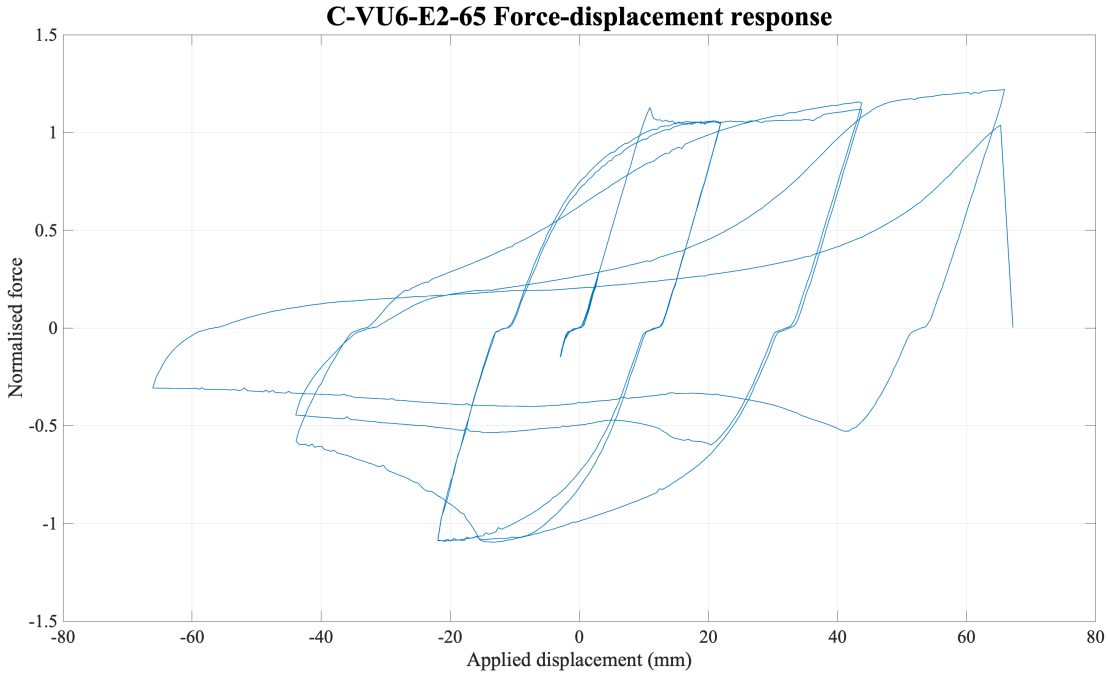


c)

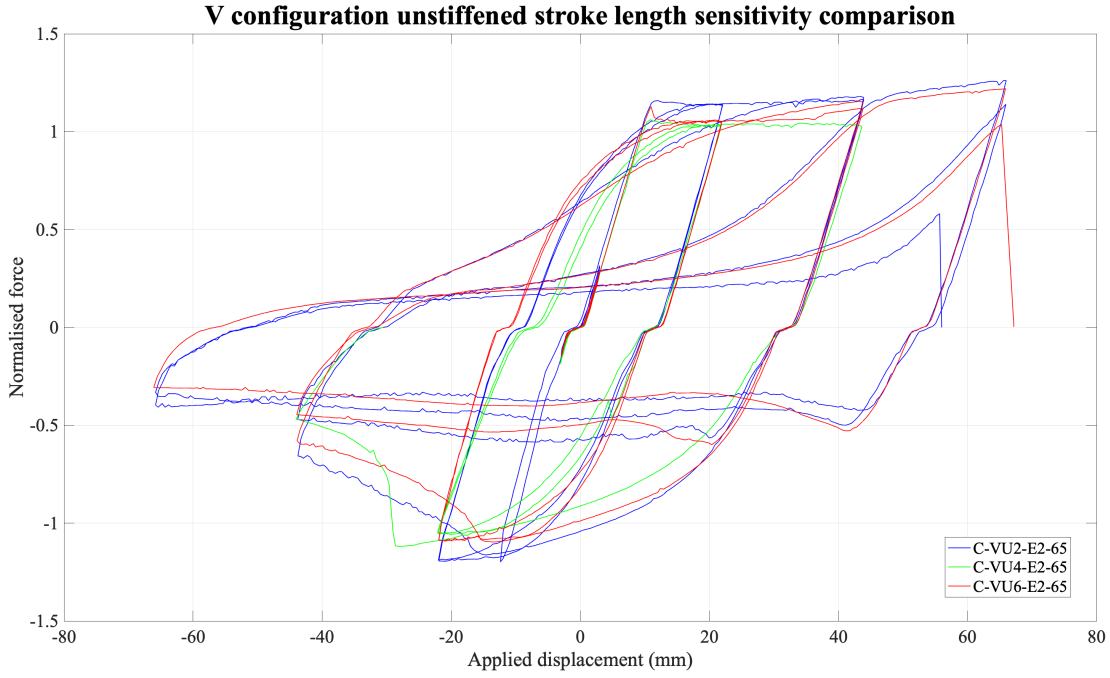


d)

**Figure 3-20: V configuration unstiffened stroke length sensitivity a) Specimen C-VU2-E2-65 b) Specimen C-VU4-E2-65 c) Specimen C-VU6-E2-65 d) Comparison of sensitivity**

**Figure 3-21: C-VU4-E2-65 local hinge in unrestrained non-yielding region**

The V configuration specimens C-VU2-E2-65, C-VU4-E2-65 and C-VU6-E2-65 shared the same global safety factor, minor axis local buckling ratio and DCR, 0.51, 1.01, 1.23 respectively (Table 3-7). The stroke varied between these specimens with 44 mm, 88 mm and 132 mm distributed at each end of C-VU2-E2-65, C-VU2-E4-65 and C-VU6-E2-65, respectively. A greater stroke length also equated to a shorter yielding length. All specimens degraded in compression in the same cycle (1.0 x drift, Figure 3-20) through an increase in required load to meet the applied cycle drift. All specimens once unloaded returned to the yield tension load, degrading again near the end of the compression cycle. C-VU2-E2-65 and C-VU6-E2-65 both failed through core fracture in local buckling at 1.5 x drift, with C-VU2-E2-65 sustaining a marginally larger cycle displacement exhibiting 1$^{st}$ mode buckling (whereas C-VU6-E2-65 presented 2$^{nd}$ mode buckling) (Figure 3-20).

C-VU2-E4-65 failed prematurely through local hinging formed within the stroke region (Figure 3-21). The hinging was initiated in the 0.5 x drift cycle through the stroke moving out of plane until prevented by the capping plate. The hinge occurred in the subsequent cycle (1.0 x drift) with buckling of the stroke region and global buckling response (outer casing no longer in concentric alignment). The test was aborted due to safety concerns. The Euler buckling load of 13.9 N (minor axis buckling) of the stroke was exceeded; this was due to local buckling occurring in the opposite end, restrained region, where the stroke was freely moving. The local buckling of the stroke was likely caused by localised bonding of the restraining medium to the core within the non-yielding restrained region, preventing core movement.

**Table 3-8: Single bay configuration unstiffened stroke length sensitivity specimen key geometrical features**

| Specimen | | C-DU2-E2-65 | C-DU4-E2-65 | C-DU6-E2-65 |
|---|---|---|---|---|
| Non-yielding length (mm) | Transition | *120* | 120 | 120 |
| | Embedment | *320* | 320 | 320 |
| | Stroke | *68* | 136 | 204 |
| Yielding length (mm) | | *4584* | 4448 | 4312 |
| Radius (mm) | | *80* | 80 | 80 |
| Outer casing depth (mm) | | *65* | 65 | 65 |
| Stiffeners | | *No* | No | No |

**Table 3-9: Single bay configuration unstiffened stroke length sensitivity results**

| Specimen | | | C-DU2-E2-65 | C-DU4-E2-65 | C-DU6-E2-65 |
|---|---|---|---|---|---|
| Failure mode | | | *Global buckling* | Global buckling | Global buckling |
| Material yield (kN) | | | *191.4* | 191.4 | 191.4 |
| Specimen yield (kN) | | | *209.6* | 201.9 | 201.9 |
| Compression adjustment factor, $\beta$ | | | *0.77* | 0.77 | 1.00 |
| Percent strain $\beta$ occurs, $\varepsilon_{sc}$ (%) | | | *0.15* | 0.16 | 0.14 |
| Stroke length (mm) | Actuator end | Initial | *68.89* | 104.23 | 175.0 |
| | | Final | *74.06** | 110.18* | 178.0* |
| | Freestanding frame end | Initial | *74.80* | 95.72 | 176.0 |
| | | Final | *76.55** | 101.68* | 184.0* |
| Global buckling safety factor | | | *1.55* | 1.55 | 1.55 |
| Local buckling | Minor axis (Equation 2-27) | | *1.01* | 1.01 | 1.01 |
| | Demand to capacity ratio (Equation 2-28) | | *1.23* | 1.23 | 1.23 |

* Unloaded displacement

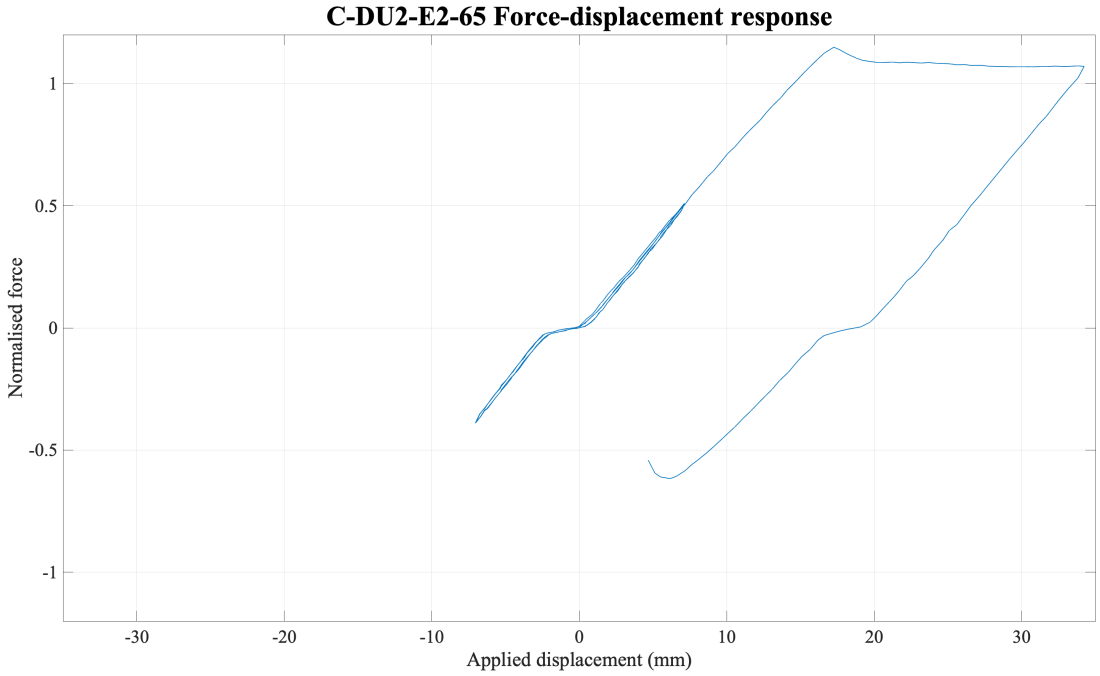
C-DU2-E2-65 Force-displacement response
Normalised force
Applied displacement (mm)
1
0.5
0
-0.5
-1
-30
-20
-10
0
10
20
30

a)

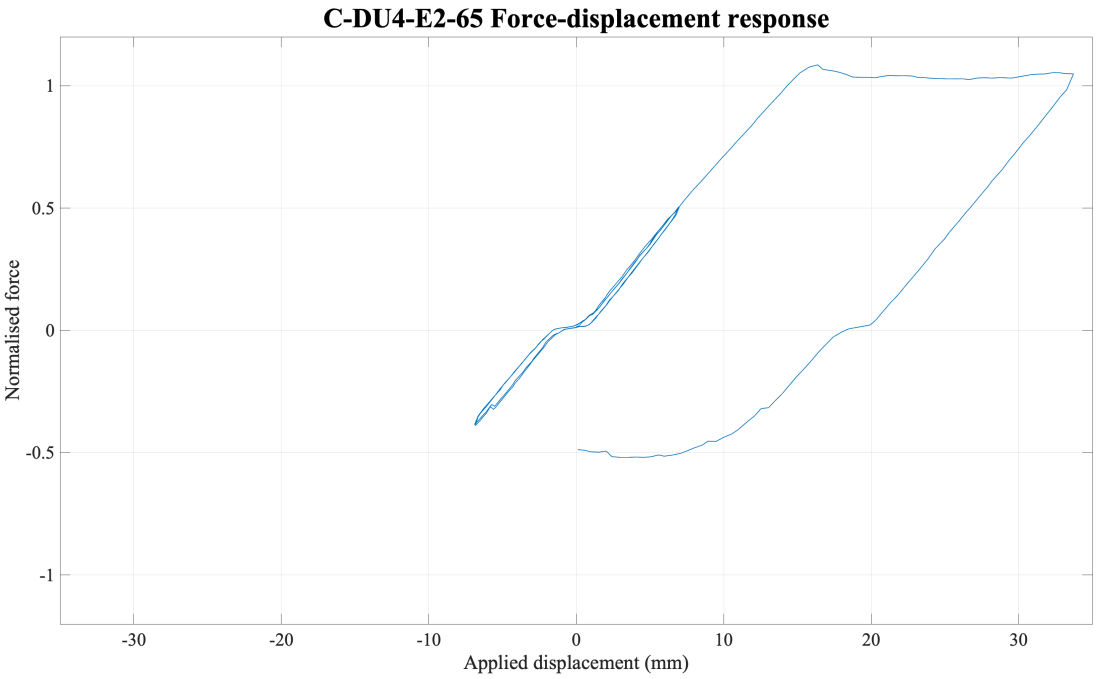
C-DU4-E2-65 Force-displacement response
Normalised force
Applied displacement (mm)
1
0.5
0
-0.5
-1
-30
-20
-10
0
10
20
30

b)

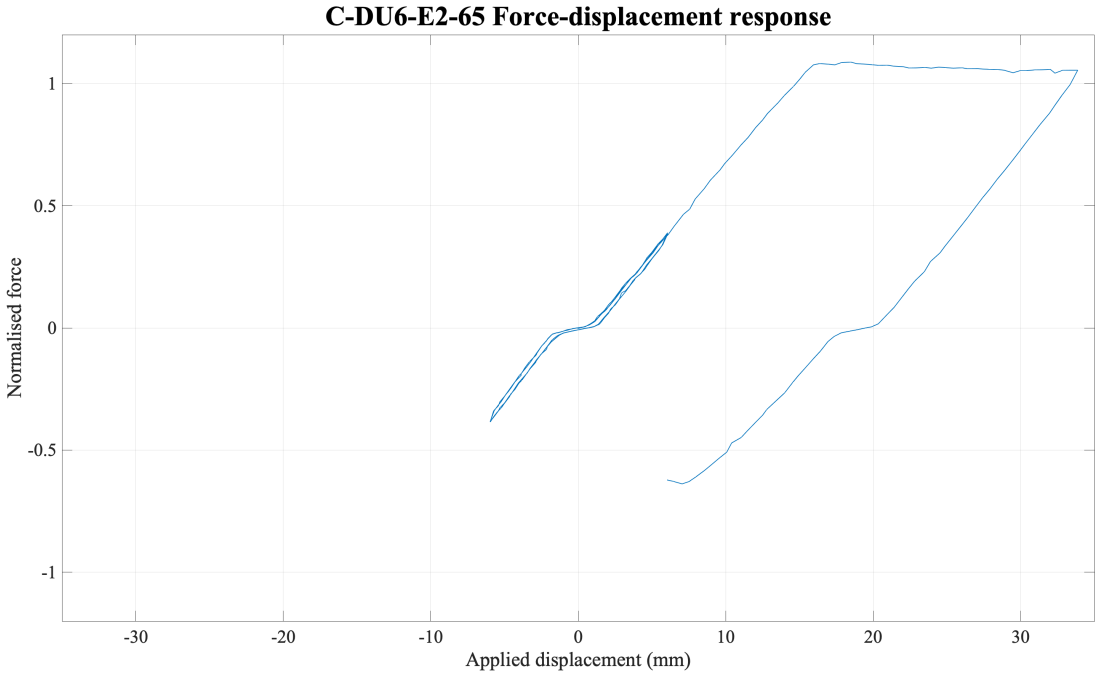


c)

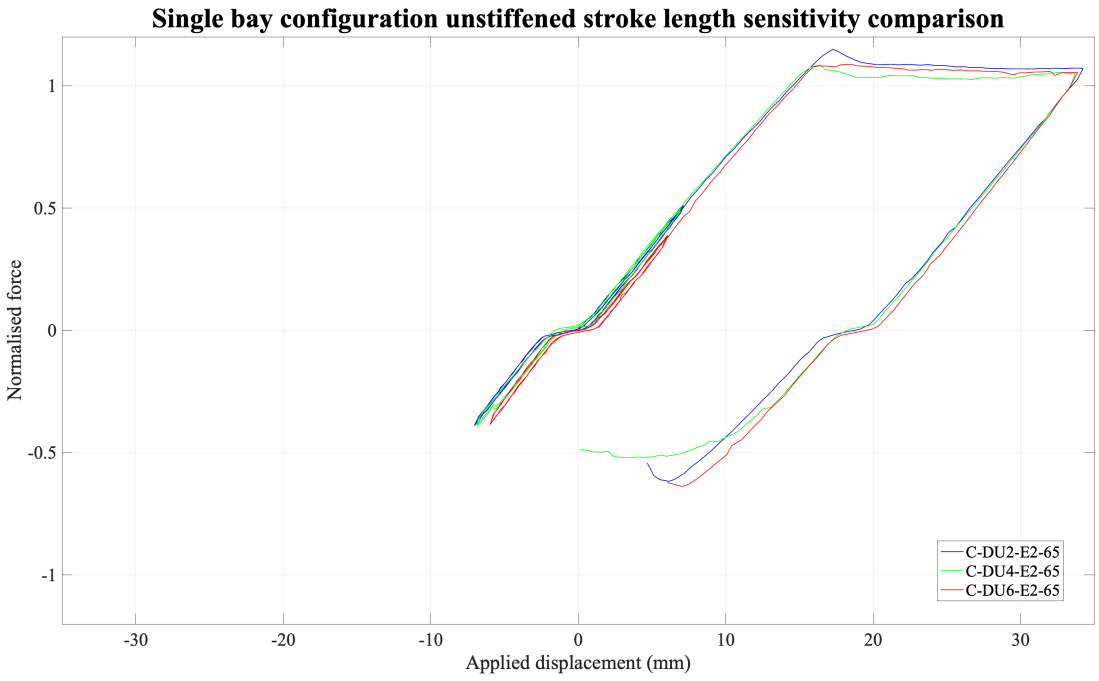


d)

**Figure 3-22: Single bay configuration unstiffened stroke length sensitivity a) Specimen C-DU2-E2-65 b) Specimen C-DU4-E2-65 c) Specimen C-DU6-E2-65 d) Comparison of sensitivity**


a) b)

**Figure 3-23: a) C-DU4-E2-65 no damage to core b) C-DU6-E2-65 global buckling**

Unstiffened SB configurations responded similarly to the V configuration, differing only by stroke and yielding core length but sharing the same global buckling safety factor, minor axis local buckling ratio and DCR, 1.55, 1.01 and 1.23, respectively (Table 3-9). All specimens underwent global buckling within the first 0.5 x drift compression cycle (Figure 3-23 b)). Similar to the V configuration, C-DU2-E2-65 and C-DU6-E2-65 performed similarly, with C-DU6-E2-65 engaging globally only marginally prior to C-DU2-E2-65 (Figure 3-22). Specimen C-DU4-E2-65 responded with a gradual plateau in applied load, whereas C-DU2-E2-65 and C-DU6-E2-65 both displayed sharp declines (Figure 3-22). All specimen tests were aborted after global buckling engagement due to out of plane deflection safety concerns.

**Table 3-10: V configuration stiffened stroke length sensitivity specimen key geometrical features**

| **Specimen** | | **C-VS2-E2-200-R10** | **C-VS4-E2-200-R10** | **C-VS6-E2-200-R10** |
|---|---|---|---|---|
| Non-yielding length (mm) | Transition | 120 | 120 | 120 |
| | Embedment | 320 | 320 | 320 |
| | Stroke | 44 | 88 | 132 |
| Yielding length (mm) | | 2232 | 2144 | 2056 |
| Radius (mm) | | 10 | 10 | 10 |
| Outer casing depth (mm) | | 200 | 200 | 200 |
| Stiffeners | | Yes | Yes | Yes |

**Table 3-11: V configuration stiffened stroke length sensitivity results**

| Specimen | | | C-VS2-E2-200-R10* | C-VS4-E2-200-R10* | C-VS6-E2-200-R10* |
|---|---|---|---|---|---|
| Failure mode | | | Local buckling | Local buckling | Local buckling |
| Material yield (kN) | | | 175.9 | 175.9 | 175.9 |
| Specimen yield (kN) | | | 229.9 | 232.2 | 232.9 |
| Compression adjustment factor, $\beta$ | | | 2.11 | 2.06 | 1.98 |
| Percent strain $\beta$ occurs, $\varepsilon_{sc}$ (%) | | | 3.94 | 4.10 | 3.21 |
| Stroke length (mm) | Actuator end | Initial | Not recorded | Not recorded | Not recorded |
| | | Final | | | |
| | Freestanding frame end | Initial | | | |
| | | Final | | | |
| Global buckling safety factor | | | 0.03 | 0.03 | 0.03 |
| Local buckling | Minor axis (Equation 2-27) | | 0.00 | 0.00 | 0.00 |
| | Demand to capacity ratio (Equation 2-28) | | 0.27 | 0.27 | 0.27 |

* 10 mm radii

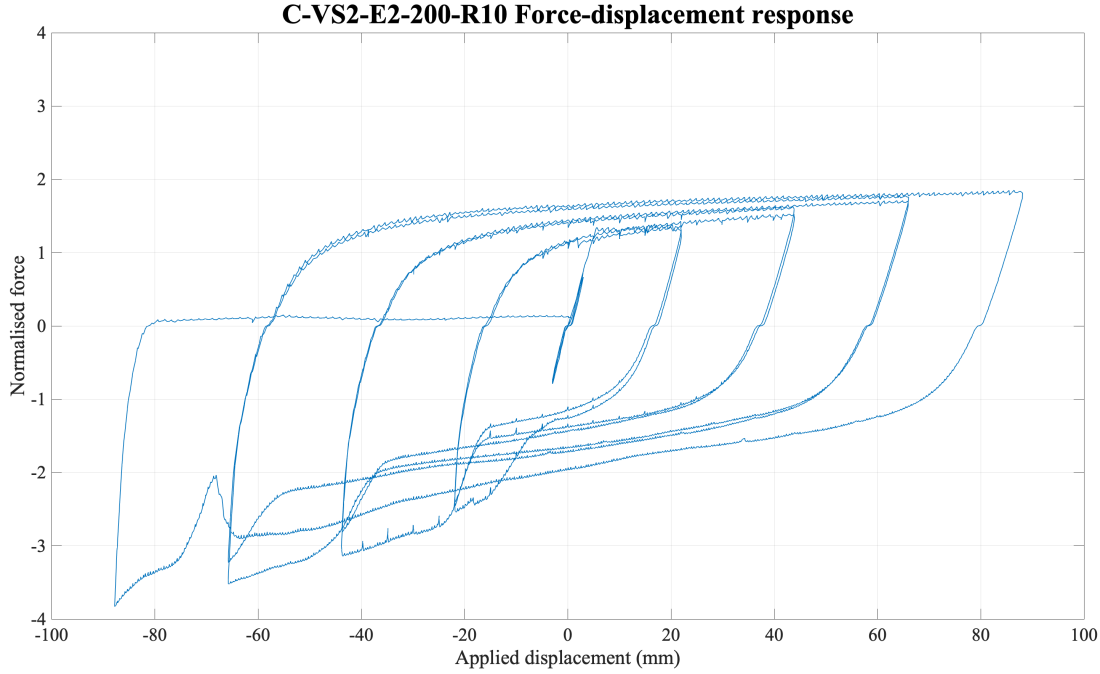


a)

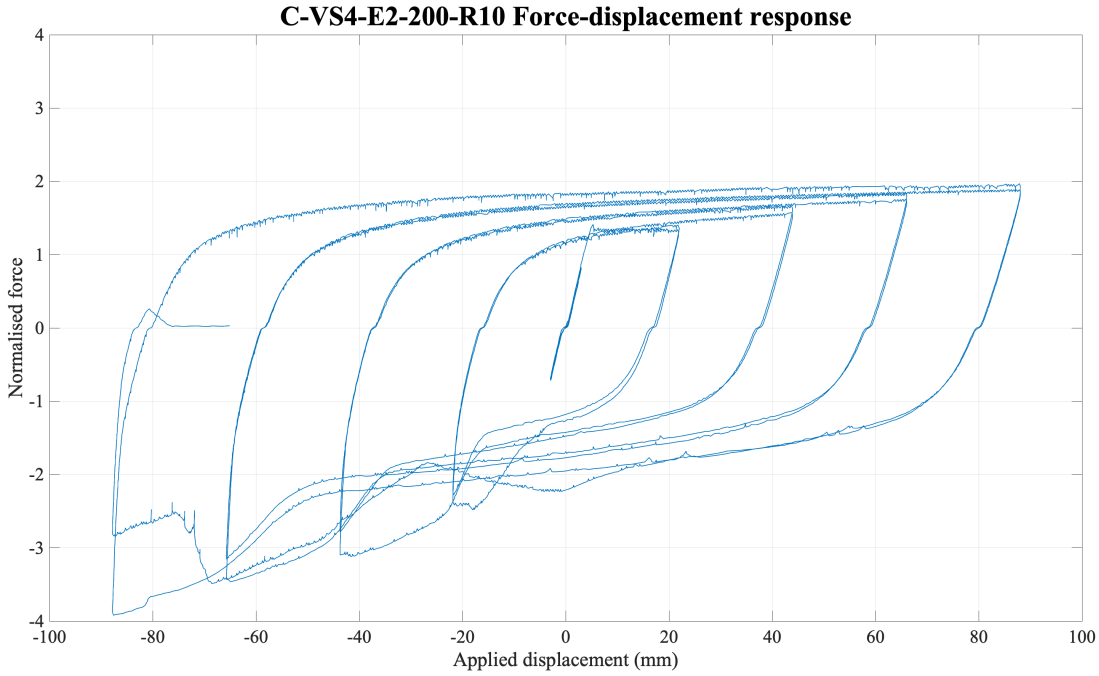
C-VS4-E2-200-R10 Force-displacement response
Normalised force
Applied displacement (mm)
4
3
2
1
0
-1
-2
-3
-4
-100
-80
-60
-40
-20
0
20
40
60
80
100

b)

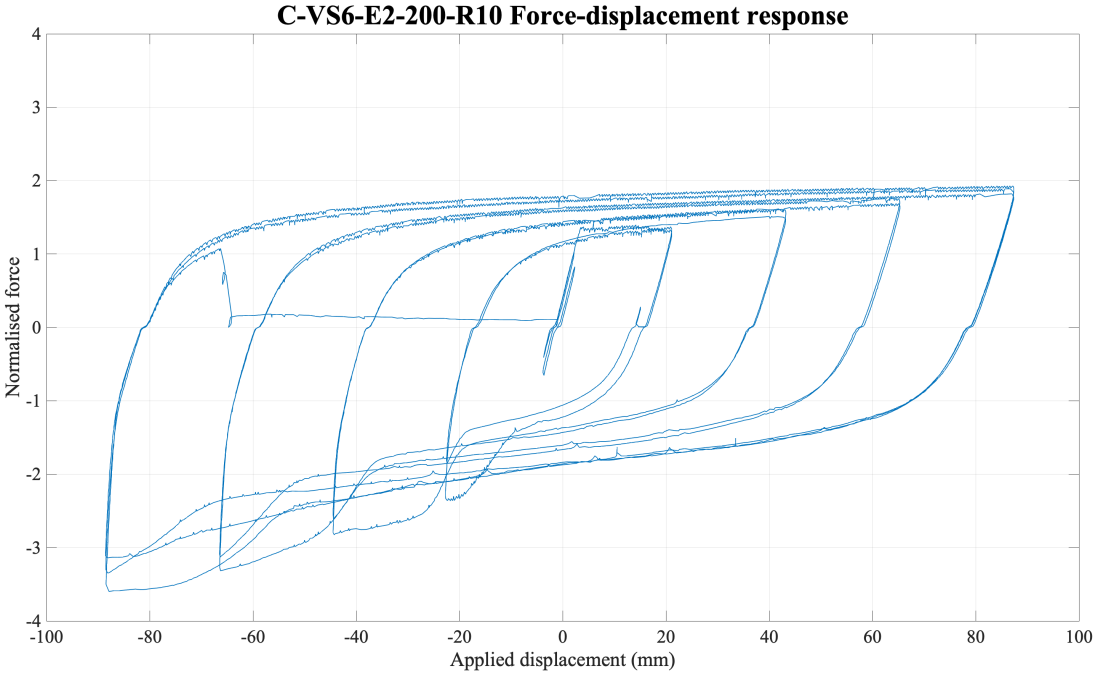
C-VS6-E2-200-R10 Force-displacement response
Normalised force
Applied displacement (mm)
4
3
2
1
0
-1
-2
-3
-4
-100
-80
-60
-40
-20
0
20
40
60
80
100

c)

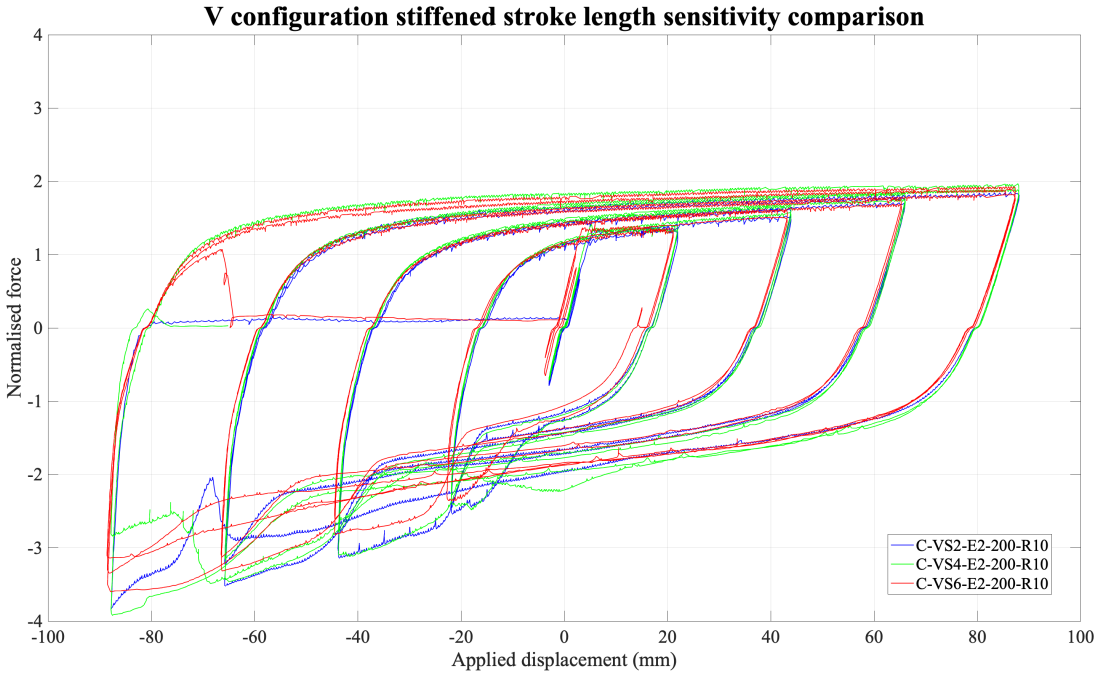


d)

**Figure 3-24: V configuration stiffened stroke length sensitivity a) Specimen C-VS2-E2-200-R10 b) Specimen C-VS4-E2-200-R10 c) Specimen C-VS6-E2-200-R10 d) Comparison of sensitivity**


a) b) c)

**Figure 3-25: Local buckling a) C-VS2-E2-200-R10 b) C-VS4-E2-200-R10 c) C-VS6-E2-200-R10**

The stiffened V configuration specimens were all designed with 10 mm yielding-transition radii. All specimens failed by high mode local buckling at the radii, within the bearing region (Figure 3-25). Local buckling occurred at both ends of the specimen, however concentration at one end occurred once local buckling deflection was significant to lock with the restraining mechanism. All specimens alike shared the same global buckling safety factor, minor axis local buckling ratio and DCR with 0.03, 0.00 and 0.27, respectively (Table 3-11). Based on these ratios, local and global

buckling should be suppressed, however local buckling governed. It is assumed that the yielding-transition radii was the contributing factor to local buckling, this is discussed in Section 3.6.

As the local buckling is contained within the restraining mechanism, when local buckling is engaged it was observed that the member response in the compression cycle increased significantly to accommodate the plastic deformation (squashing/folding) of the steel core. The higher compression force was typically observed near the end of each cycle, when the applied displacement was at maximum, disrupting balanced hysteresis and increasing the maximum normalised force from approximately 1.3 to 2.0 (Figure 3-24). Specimens C-VS2-E2-200-R10, C-VS4-E2-200-R10 and C-VS6-E2-200-R10 all observed local buckling through increase in applied load in the compression cycle of 0.5 x drift. When fracture of the core was imminent a sharp decline in compression strength was observed. Specimen C-VS6-E2-200-R10 was the only specimen to fail within the tension loading cycle, failing suddenly. Overall C-VS2-E2-200-R10 and C-VS4-E2-200-R10 performed similarly, with C-VS2-E2-200-R10 marginally responding with increased applied displacement in compression prior to failure than C-VS4-E2-200-R10. All specimens failed within the 2.0 x drift cycle, undergoing sustained cyclic behaviour without failure albeit without balanced hysteresis behaviour. Based on similar hysteretic performance, the member behaviour was observed to be insensitive to the stroke length.

**Table 3-12: Single Bay configuration stiffened stroke length sensitivity specimen key geometrical features**

| **Specimen** | | **C-DS2-E2-200-R10*** | **C-DS4-E2-200-R10*** | **C-DS6-E2-200-R80** |
|---|---|---|---|---|
| Non-yielding length (mm) | Transition | 120 | 120 | 120 |
| | Embedment | 320 | 320 | 320 |
| | Stroke | 68 | 136 | 204 |
| Yielding length (mm) | | 4585 | 4448 | 4312 |
| Radius (mm) | | 10 | 10 | 80 |
| Outer casing depth (mm) | | 200 | 200 | 200 |
| Stiffeners | | Yes | Yes | Yes |

**Table 3-13: Single bay configuration stiffened stroke length sensitivity results**

| Specimen | | | C-DS2-E2-200-R10* | C-DS4-E2-200-R10* | C-DS6-E2-200-R80 |
|---|---|---|---|---|---|
| Failure mode | | | Local buckling | Local buckling | Local buckling |
| Material yield (kN) | | | 175.9 | 175.9 | 191.4 |
| Specimen yield (kN) | | | 249.6 | 240.3 | 203.0 |
| Compression adjustment factor, $\beta$ | | | 2.24 | 2.04 | 1.44 |
| Percent strain $\beta$ occurs, $\varepsilon_{sc}$ (%) | | | 2.23 | 2.29 | 3.15 |
| Stroke length (mm) | Actuator end | Initial | Not recorded | Not recorded | 174.0 |
| | | Final | | | 148.0 |
| | Freestanding frame end | Initial | | | 178.0 |
| | | Final | | | 178.0 |
| Global buckling safety factor | | | 0.10 | 0.10 | 0.10 |
| Local buckling | Minor axis (Equation 2-27) | | 0.00 | 0.00 | 0.00 |
| | Demand to capacity ratio (Equation 2-28) | | 0.27 | 0.27 | 0.27 |

* 10 mm radii

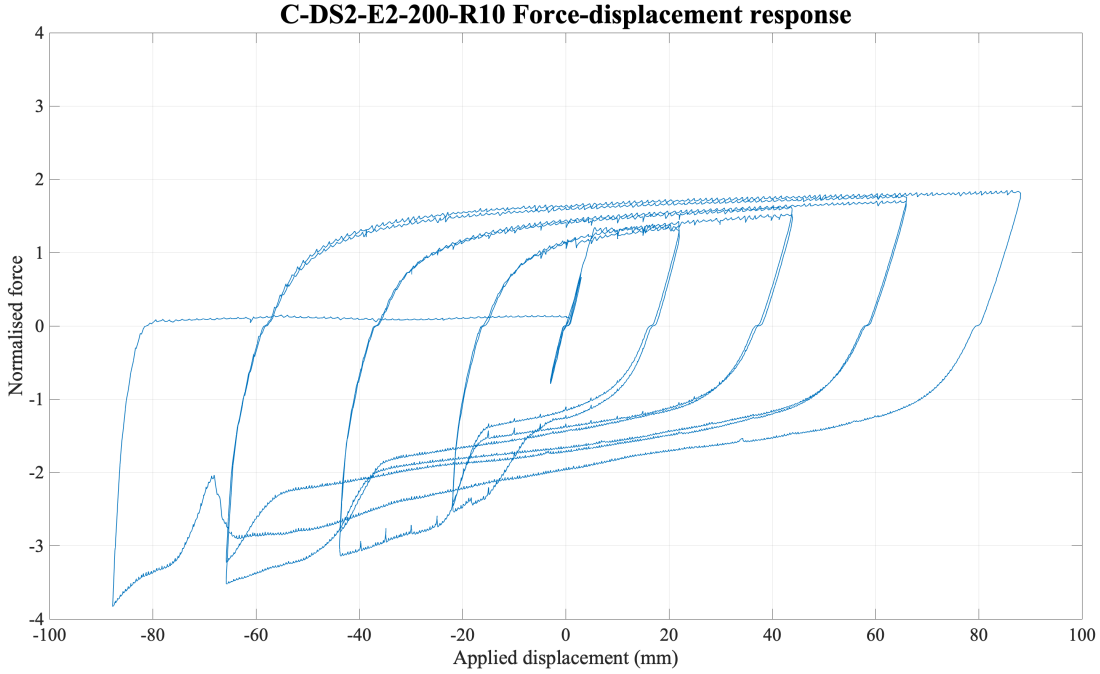


a)

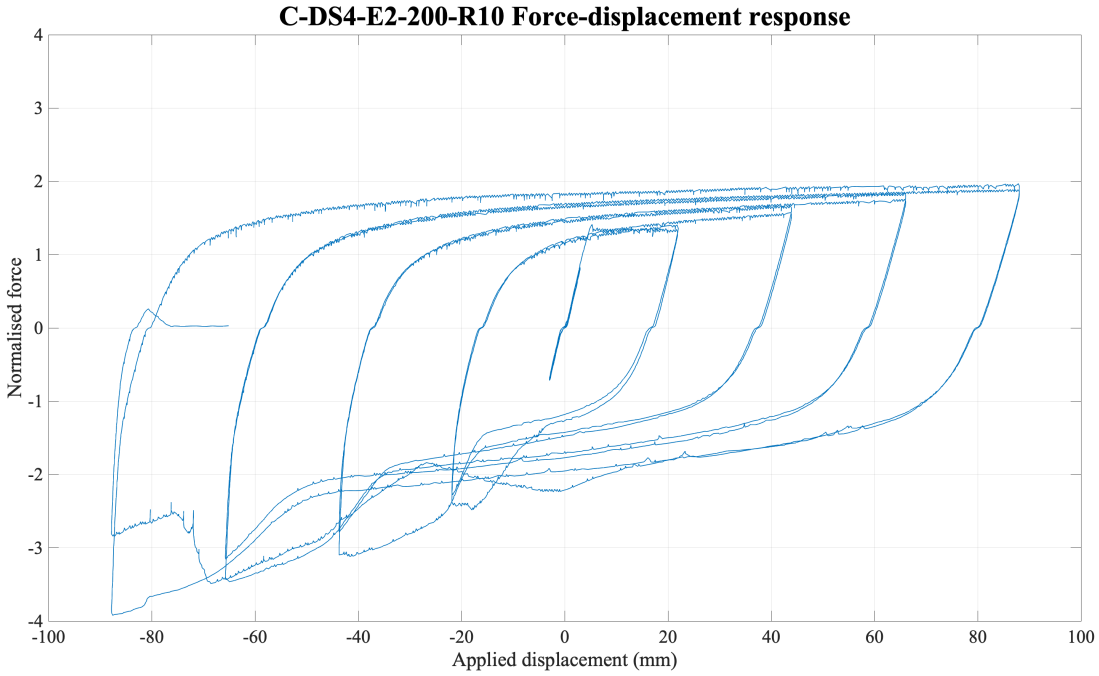
C-DS4-E2-200-R10 Force-displacement response
Normalised force
Applied displacement (mm)
4
3
2
1
0
-1
-2
-3
-4
-100
-80
-60
-40
-20
0
20
40
60
80
100

b)

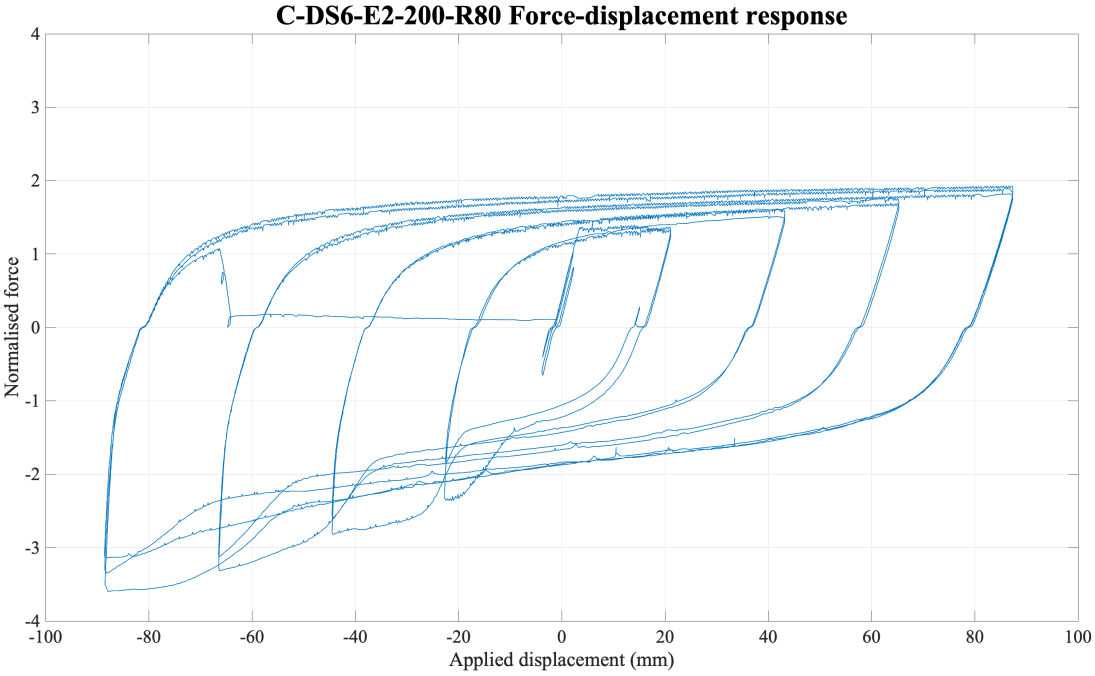
C-DS6-E2-200-R80 Force-displacement response
Normalised force
Applied displacement (mm)
4
3
2
1
0
-1
-2
-3
-4
-100
-80
-60
-40
-20
0
20
40
60
80
100

c)

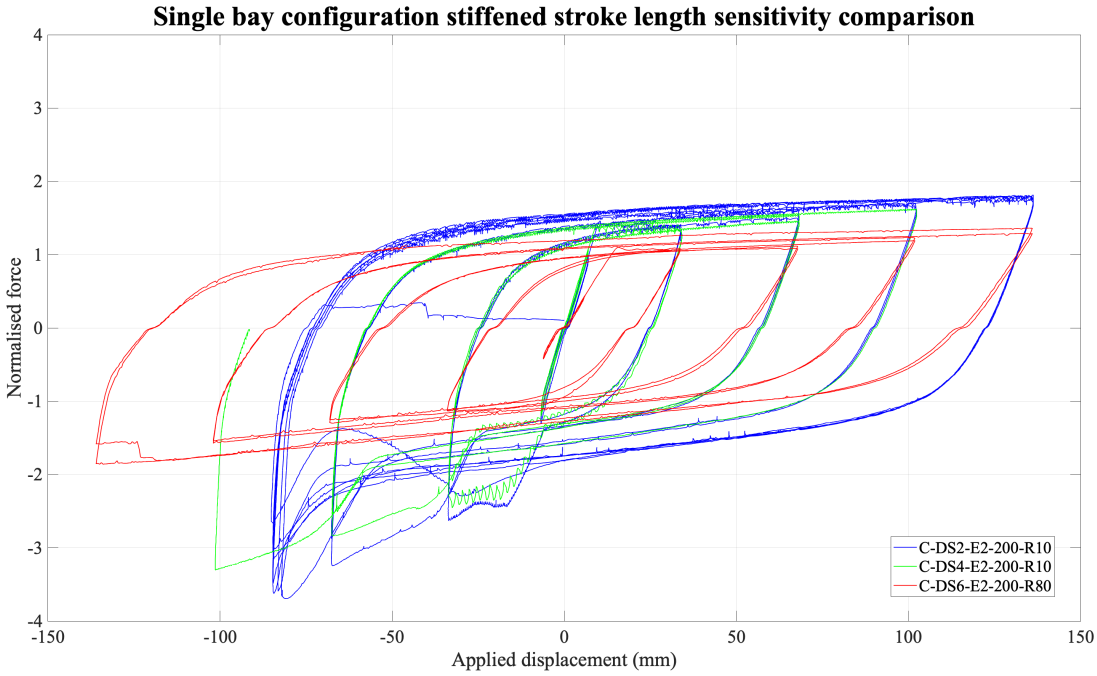


d)

**Figure 3-26: Single bay configuration stiffened stroke length sensitivity a) Specimen C-DS2-E2-200-R10 b) Specimen C-DS4-E2-200-R10 c) Specimen C-DS6-E2-200-R80 d) Comparison of sensitivity**


a) b) c)

**Figure 3-27: Local buckling and fracture a) C-DS2-E2-200-R10 b) C-DS4-E2-200-R10 c) C-DS6-E2-200-R80**

As with the V configuration stiffened specimens, the SB stiffened specimens all failed through local buckling. The global buckling safety factor, minor axis local buckling ratio and DCR for all specimens were 0.10, 0.00 and 0.27, respectively (Table 3-13). Specimens C-DS2-E2-200-R10 and C-DS4-E2-200-R10 were designed with 10 mm yielding-transition radii, whereas C-DS2-E2-200-R80 (which was tested in a different test block) was redesigned to have an 80 mm yielding-transition radii, based on the stiffened specimen results (VS and DS).

Specimens C-DS2-E2-200-R10 and C-DS4-E2-200-R10 behaved similarly to the V configuration counterparts, failing through local buckling at the yielding-transition

radii (Figure 3-27) and a larger compression member response on local buckling engagement. Both specimens failed prior to reaching the maximum displacement cycle. It was observed that the hysteretic performance (Figure 3-26), as with the VS stiffened specimens, displayed behaviours insensitive to stroke length. Specimen C-DS6-E2-200-R80 performed superiorly, with local buckling fracture occurring outside the yielding-transition region. Specimen C-DS6-E2-200-R80 showed promise of meeting the minimum qualification requirements, failing in the second unloading 2.0 x drift compression cycle (Figure 3-26). Specimen C-DS6-E2-200-R80 displayed stable hysteresis until the cycle of failure.

The presence of stiffeners suppressed the dominant mode of failure, increasing the cyclic response and overall maximum member capacity in compression. Stiffened specimens lacked visual identification of failure, and as such, could pose the risk of sudden undesirable failure without warning. All stiffened specimens exhibited localised high mode buckling, whereas the VU specimens displayed low mode localised buckling. Unstiffened specimens were also more susceptible to global buckling, which was dependent on the yielding length of the member. It can be concluded that, to prevent global buckling, a greater volume of restraining medium is required with increasing yielding core length.

The lower stroke length overall performed more reliably, however they tended to exhibit local buckling within the bearing region for all local buckling failure specimens. The performance of the specimens hysteretically was similar and therefore the behaviour of the specimen is insensitive to the stroke length. The relationship between design drift and the appropriate stroke length could not be determined based on the small test sample and varying influences (yielding-transition radii, bearing region and yielding length), therefore further investigation considering variable influences is recommended.

### 3.5.3 Transition gradient sensitivity

Three different transition gradients were investigated; 1:3, 1:2.5 and 1:1 for SB configuration specimens C-DU2-E2-65-T3, C-DU2-E2-65 and C-DU2-E2-65-T1 respectively. The transition gradients were determined based on a review of proprietary products and New Zealand regulatory specifications for notched regions. The transition region, although not required within international regulatory design documents, is common in BRB design, with the slope dictating the available length for the non-yielding and yielding regions, as well as the distribution of stresses from the yielding region.

All specimens engaged global buckling in the first compression loading cycle post yield, with testing aborted due to out of plane deflection safety concerns. Any relationship between member responses, stress-strain relationship attributed to the transition region was not obtained within the test results or on dissection (Figure 3-29). All specimens performed with respect to their steel capacity, with C-DU2-E2-

65 exhibiting the highest ultimate tensile strength and compression capacity prior to global buckling initiation, followed by C-DU2-E2-65-T1 and C-DU2-E2-65-T3 (Figure 3-28, Table 3-15). Further investigation is required into this relationship, with stiffened specimens recommended to supress global buckling initiation.

**Table 3-14: Single Bay configuration unstiffened transition gradient sensitivity specimen key geometrical features**

| **Specimen** | | **C-DU2-E2-65-T3** | **C-DU2-E2-65** | **C-DU2-E2-65-T1** |
|---|---|---|---|---|
| Transition ratio (height:length) | | 1:3 | *1:2.5* | 1:1 |
| Non-yielding length (mm) | Transition | 140 | *120* | 50 |
| | Embedment | 320 | *320* | 320 |
| | Stroke | 68 | *68* | 68 |
| Yielding length (mm) | | 4544 | *4584* | 4724 |
| Radius (mm) | | 80 | *80* | 80 |
| Outer casing depth (mm) | | 65 | *65* | 65 |
| Stiffeners | | No | *No* | No |

**Table 3-15: Single bay configuration unstiffened transition gradient sensitivity results**

| **Specimen** | | | **C-DU2-E2-65-T3** | **C-DU2-E2-65** | **C-DU2-E2-65-T1** |
|---|---|---|---|---|---|
| Failure mode | | | Local** and global buckling | *Global buckling* | Global buckling |
| Material yield (kN) | | | 205.0 | *191.4* | 191.4 |
| Specimen yield (kN) | | | 213.3 | *209.6* | 204.0 |
| Compression adjustment factor, $\beta$ | | | 0.75 | *0.77* | 0.84 |
| Percent strain $\beta$ occurs, $\varepsilon_{sc}$ (%) | | | 0.15 | *0.15* | 0.15 |
| Stroke length (mm) | Actuator end | Initial | 77.00 | *68.89* | 70.55 |
| | | Final | 76.80* | *74.06** | 79.19* |
| | Freestanding frame end | Initial | 69.95 | *74.80* | 57.40 |
| | | Final | 79.98* | *76.55** | 58.65* |
| Global buckling safety factor | | | 1.55 | *1.55* | 1.55 |
| Local buckling | Minor axis (Equation 2-27) | | 1.01 | *1.01* | 1.01 |
| | Demand to capacity ratio (Equation 2-28) | | 1.23 | *1.23* | 1.23 |

* Unloaded displacement

** Hinge formed within stroke region

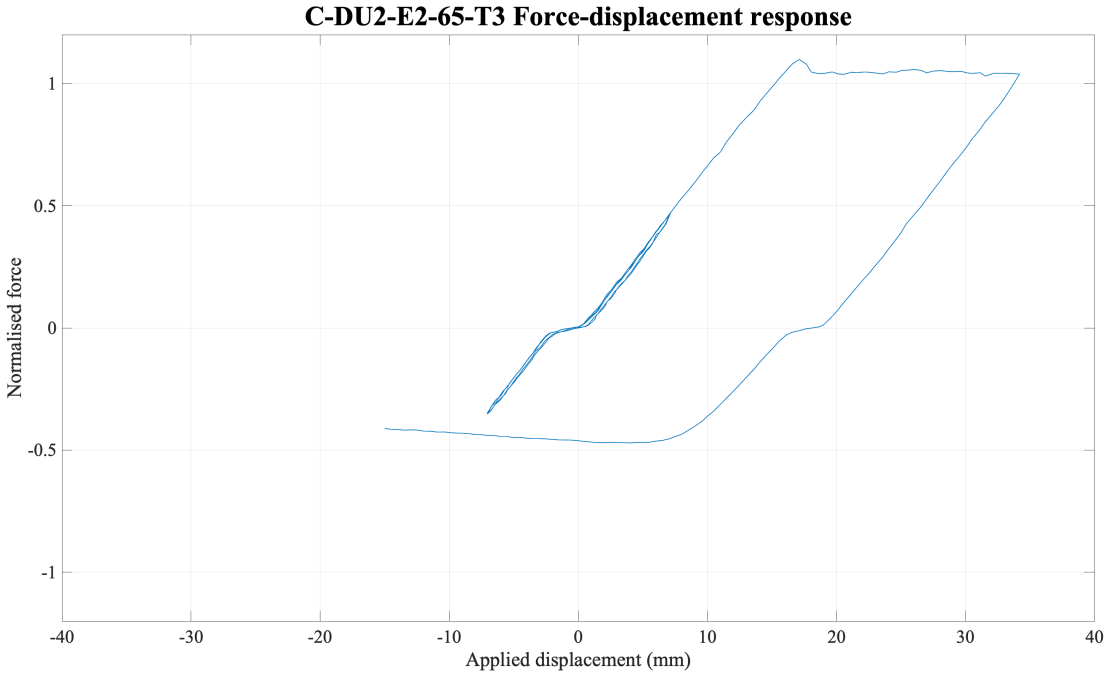
C-DU2-E2-65-T3 Force-displacement response
Normalised force
Applied displacement (mm)
1
0.5
0
-0.5
-1
-40
-30
-20
-10
0
10
20
30
40

a)

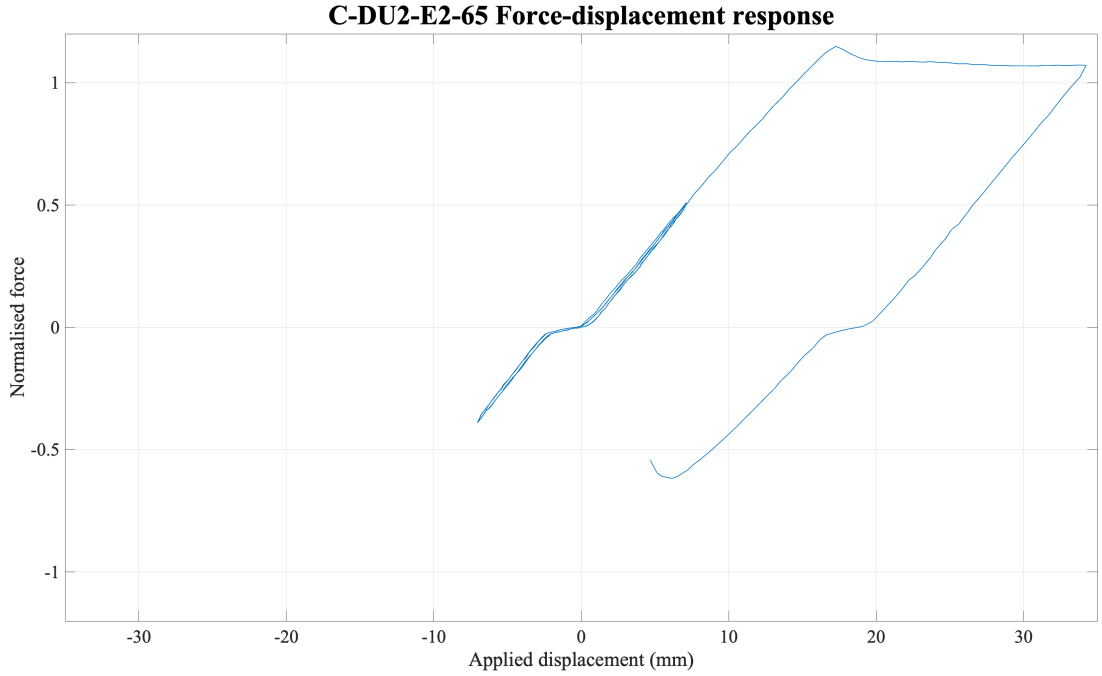
C-DU2-E2-65 Force-displacement response
Normalised force
Applied displacement (mm)
1
0.5
0
-0.5
-1
-30
-20
-10
0
10
20
30

b)

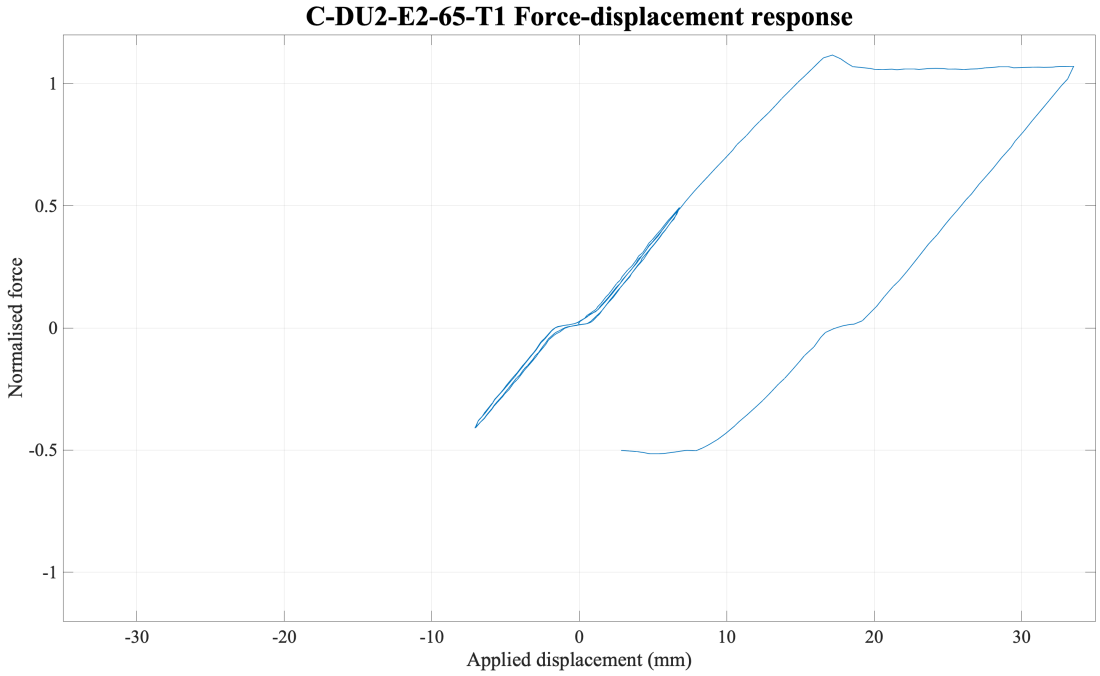


c)

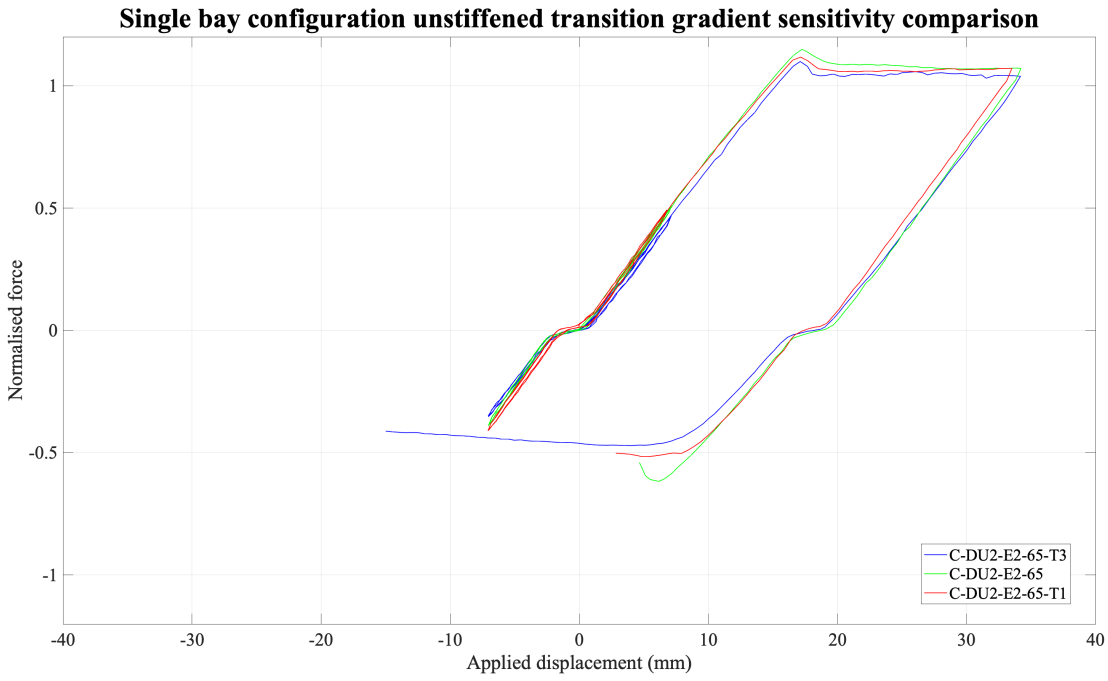


d)

**Figure 3-28: Single bay configuration unstiffened transition gradient sensitivity a) Specimen C-DU2-E2-65-T3 b) Specimen C-DU2-E2-65 c) Specimen C-DU2-E2-65-T1 d) Comparison of sensitivity**

a) b)

**Figure 3-29: C-DU2-E2-65 Dissection a) Damaged restraining medium b) Fractured core**

### 3.5.4 Embedment length influence sensitivity

The embedment length is typically designed with respect to connection requirements, preventing torsion and rotation of the connection. The embedment length was investigated within this program to evaluate the overall influence the length has on the performance and sensitivity of the member (irrespective of connection influence).

**Table 3-16: V configuration unstiffened embedment length sensitivity specimen key geometrical features**

| **Specimen** | | **C-VU2-E1-65** | **C-VU2-E2-65** | **C-VU2-E3-65** |
|---|---|---|---|---|
| Non-yielding length (mm) | Transition | 120 | *120* | 120 |
| | Embedment | 160 | *320* | 480 |
| | Stroke | 44 | *44* | 44 |
| Yielding length (mm) | | 2552 | *2232* | 1912 |
| Radius (mm) | | 80 | *80* | 80 |
| Outer casing depth (mm) | | 65 | *65* | 65 |
| Stiffeners | | No | *No* | No |

**Table 3-17: V configuration unstiffened embedment length sensitivity results**

| Specimen | | | C-VU2-E1-65 | C-VU2-E2-65 | C-VU2-E3-65 |
|---|---|---|---|---|---|
| Failure mode | | | Local buckling | *Local buckling* | Local buckling |
| Material yield (kN) | | | 195.1 | *195.1* | 195.1 |
| Specimen yield (kN) | | | 220.9 | *221.5* | 216.8 |
| Compression adjustment factor, $\beta$ | | | 1.09 | *1.05* | 1.08 |
| Percent strain $\beta$ occurs, $\varepsilon_{sc}$ (%) | | | 1.72 | *0.99* | 2.30 |
| Stroke length (mm) | Actuator end | Initial | 47.97 | *51.81* | 47.25 |
| | | Final | 90.94 | *32.12* | 38.82 |
| | Freestanding frame end | Initial | 47.99 | *51.79* | 49.17 |
| | | Final | 51.85 | *107.92* | 105.42 |
| Global buckling safety factor | | | 0.51 | *0.51* | 0.51 |
| Local buckling | Minor axis (Equation 2-27) | | 1.01 | *1.01* | 1.01 |
| | Demand to capacity ratio (Equation 2-28) | | 1.23 | *1.23* | 1.23 |

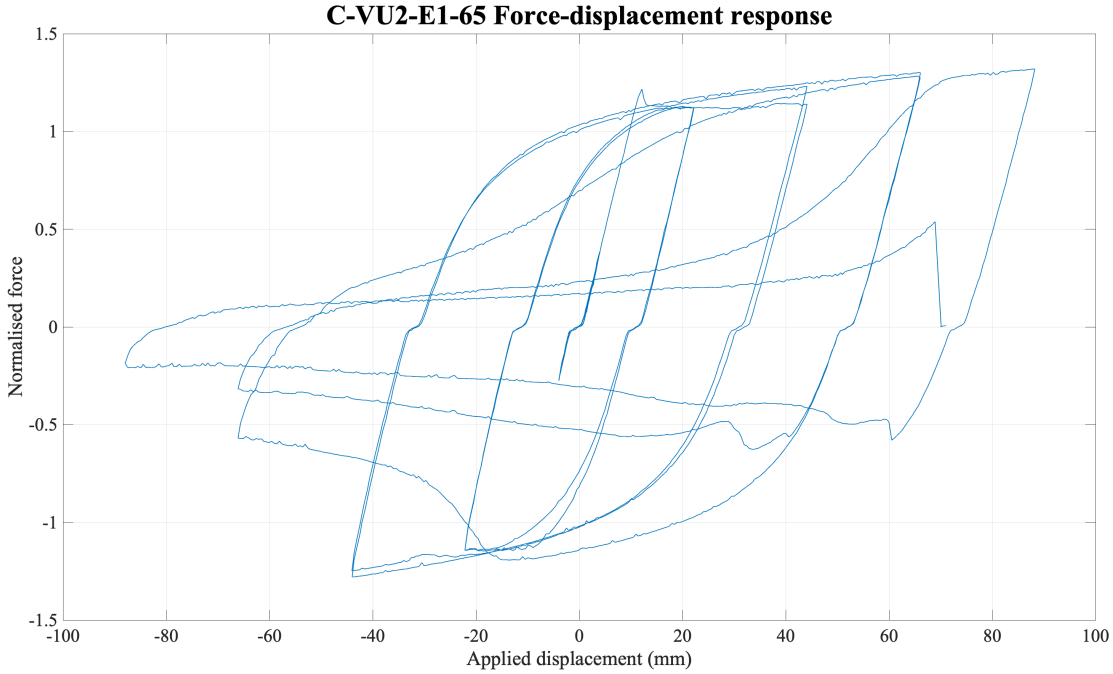


a)

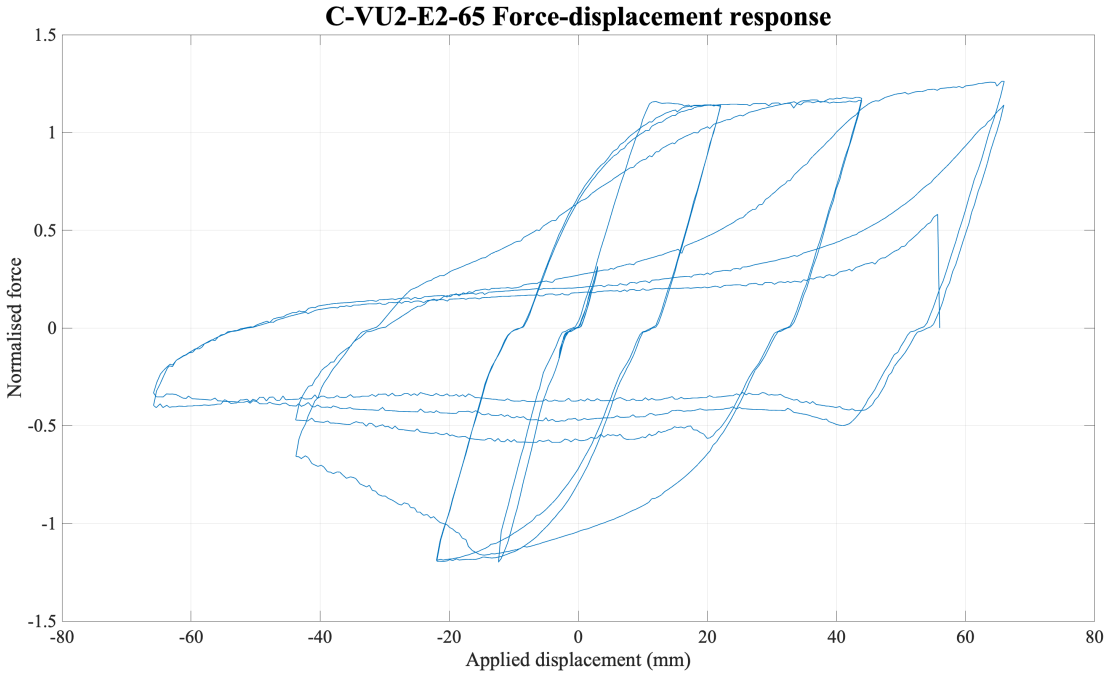
C-VU2-E2-65 Force-displacement response
Normalised force
Applied displacement (mm)
1.5
1
0.5
0
-0.5
-1
-1.5
-80
-60
-40
-20
0
20
40
60
80

b)


C-VU2-E3-65 Force-displacement response
Normalised force
Applied displacement (mm)
1.5
1
0.5
0
-0.5
-1
-1.5
-80
-60
-40
-20
0
20
40
60
80

c)

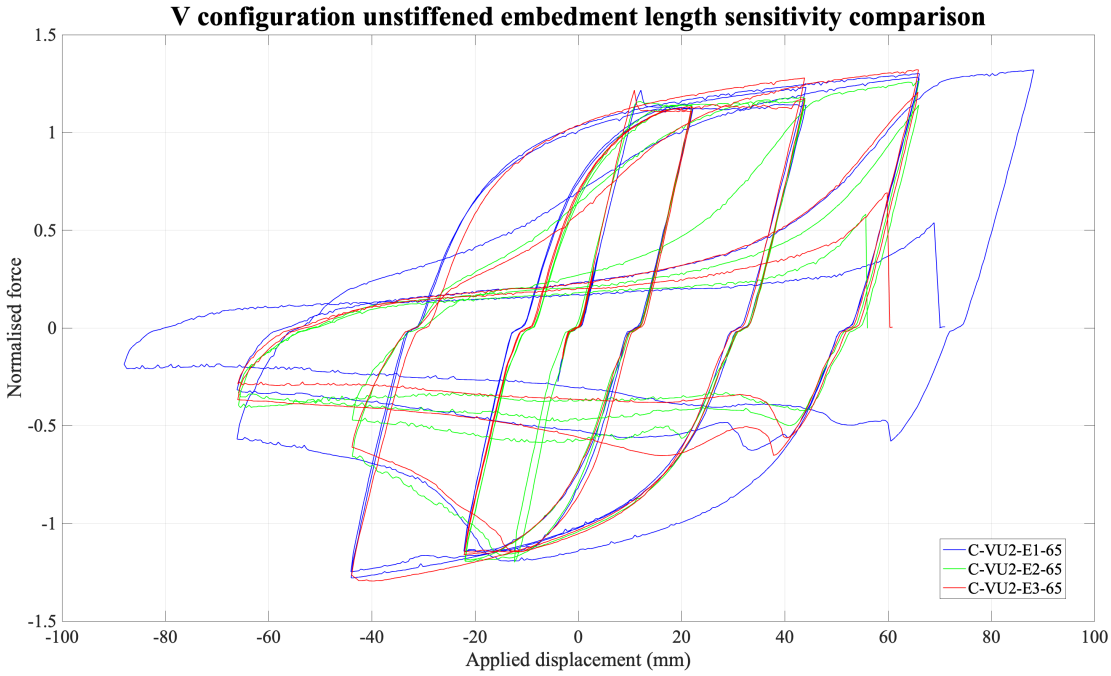


d)

**Figure 3-30: V configuration unstiffened embedment length sensitivity a) Specimen C-VU2-E1-65 b) Specimen C-VU2-E2-65 c) Specimen C-VU2-E3-65 d) Comparison of sensitivity**

Three V configuration specimens were tested; C-VU2-E1-65, C-VU2-E2-65 and C-VU2-E3-65 with varying embedment lengths equal to the non-yielding width, two times and three times the non-yielding width. It is important to note that with increase in embedment, the yielding core length is reduced. All specimens had equal global buckling safety factor, minor axis local buckling ratio and DCR, with values of 0.51, 1.01 and 1.23, respectively (Table 3-17).

All specimens underwent local buckling failure. Specimen C-VU2-E1-65 performed the greatest experimental cycles, engaging local buckling in the first compression cycle of 1.5 x drift, failing through fracture in the second 2 x drift tension cycle (Figure 3-30). Specimen C-VU2-E1-65 underwent 3$^{rd}$ mode local buckling. The compression force, although lower on local buckling engagement, degraded at a slower rate than the other two specimens (Figure 3-30). Specimen C-VU2-E2-65 engaged local buckling in the first compression cycle of 1.0 x drift, and C-VU2-E3-65 engaged on the second compression cycle. Both specimens failed within the second tension cycle of 1.5 x drift (Figure 3-30). Specimen C-VU2-E2-65 underwent 1$^{st}$ mode local buckling and small elastic global buckling. The specimen exhibited faster compression strength degradation, although sustaining this degradation for a further cycle than C-VU2-E3-65.

Specimen C-VU2-E3-65 was the only specimen to present minor and major axis local buckling, 2nd and 1st mode respectively. Whether the engagement of both minor and major axis local buckling was a result of the longer embedment length or the shorter yielding core is unknown, and it is recommended this be investigated further. The observed trend was that the shorter the embedment length (and longer the yielding core) the stronger performance in cyclic loading, with higher mode local buckling engaged.

**Table 3-18: Single bay configuration unstiffened embedment length sensitivity specimen key geometrical features**

| Specimen | | C-DU2-E1-65 | C-DU2-E2-65 | C-DU2-E3-65 |
|---|---|---|---|---|
| Non-yielding length (mm) | Transition | 120 | *120* | 120 |
| | Embedment | 160 | *320* | 480 |
| | Stroke | 68 | *68* | 68 |
| Yielding length (mm) | | 4904 | *4584* | 4264 |
| Radius (mm) | | 80 | *80* | 80 |
| Outer casing depth (mm) | | 65 | *65* | 65 |
| Stiffeners | | No | *No* | No |

**Table 3-19: Single bay configuration unstiffened embedment length sensitivity results**

| Specimen | | | C-DU2-E1-65 | C-DU2-E2-65 | C-DU2-E3-65 |
|---|---|---|---|---|---|
| Failure mode | | | Global buckling | *Global buckling* | Global buckling |
| Material yield (kN) | | | 191.4 | *191.4* | 191.4 |
| Specimen yield (kN) | | | 203.1 | *209.6* | 205.7 |
| Compression adjustment factor, $\beta$ | | | 1.00 | *0.69* | 0.77 |
| Percent strain $\beta$ occurs, $\varepsilon_{sc}$ (%) | | | 0.69 | *0.14* | 0.15 |
| Stroke length (mm) | Actuator end | Initial | 70.86 | *68.89* | 67.68 |
| | | Final | 72.57* | *74.06** | 66.66* |
| | Freestanding frame end | Initial | 75.25 | *74.80* | 74.14 |
| | | Final | 79.47* | *76.55** | 86.80* |
| Global buckling safety factor | | | 1.55 | *1.55* | 1.55 |
| Local buckling | Minor axis (Equation 2-27) | | 1.01 | *1.01* | 1.01 |
| | Demand to capacity ratio (Equation 2-28) | | 1.23 | *1.23* | 1.23 |

* Unloaded displacement


C-DU2-E1-65 Force-displacement response
Normalised force
Applied displacement (mm)
1
0.5
0
-0.5
-1
-30
-20
-10
0
10
20
30

a)

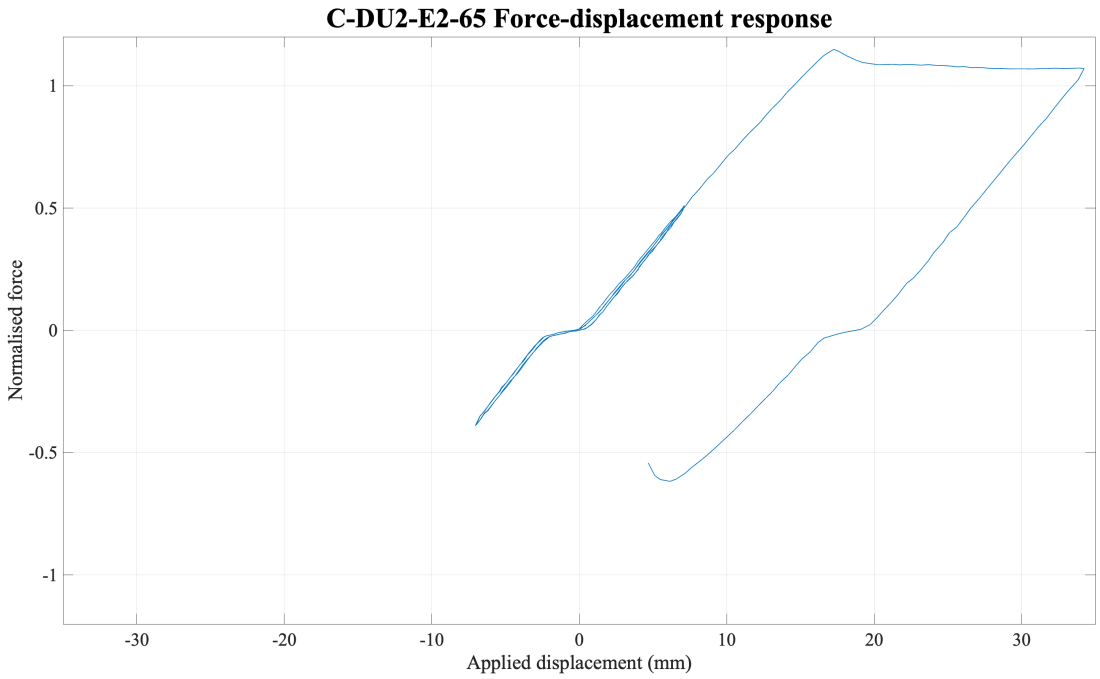
C-DU2-E2-65 Force-displacement response
Normalised force
Applied displacement (mm)
1
0.5
0
-0.5
-1
-30
-20
-10
0
10
20
30

b)

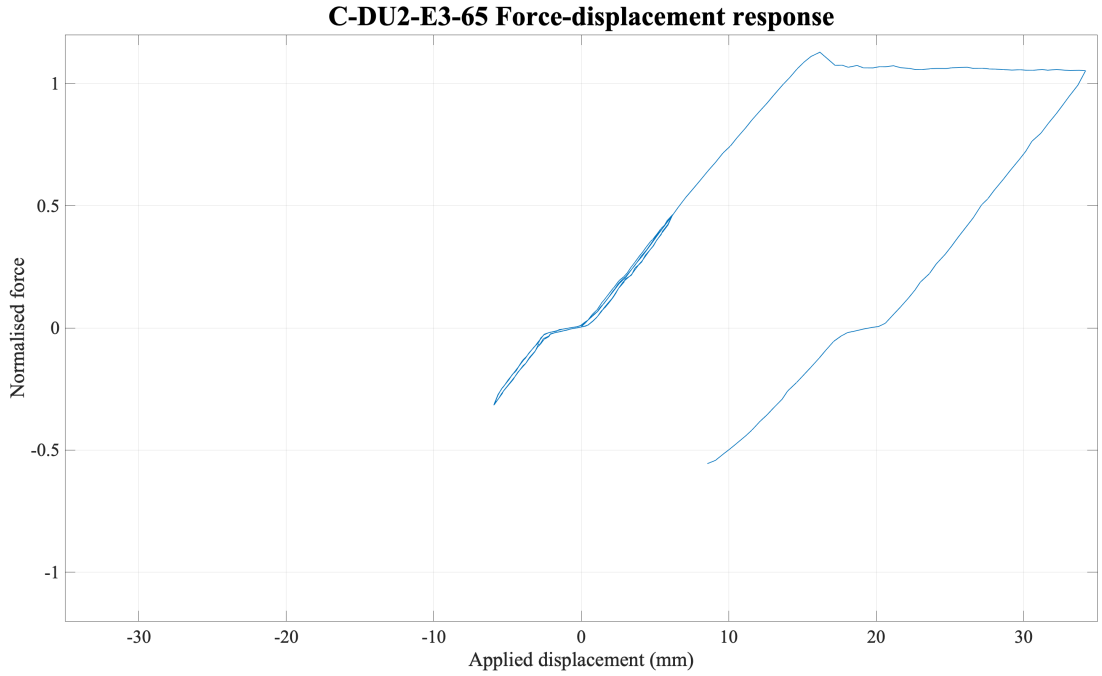


c)

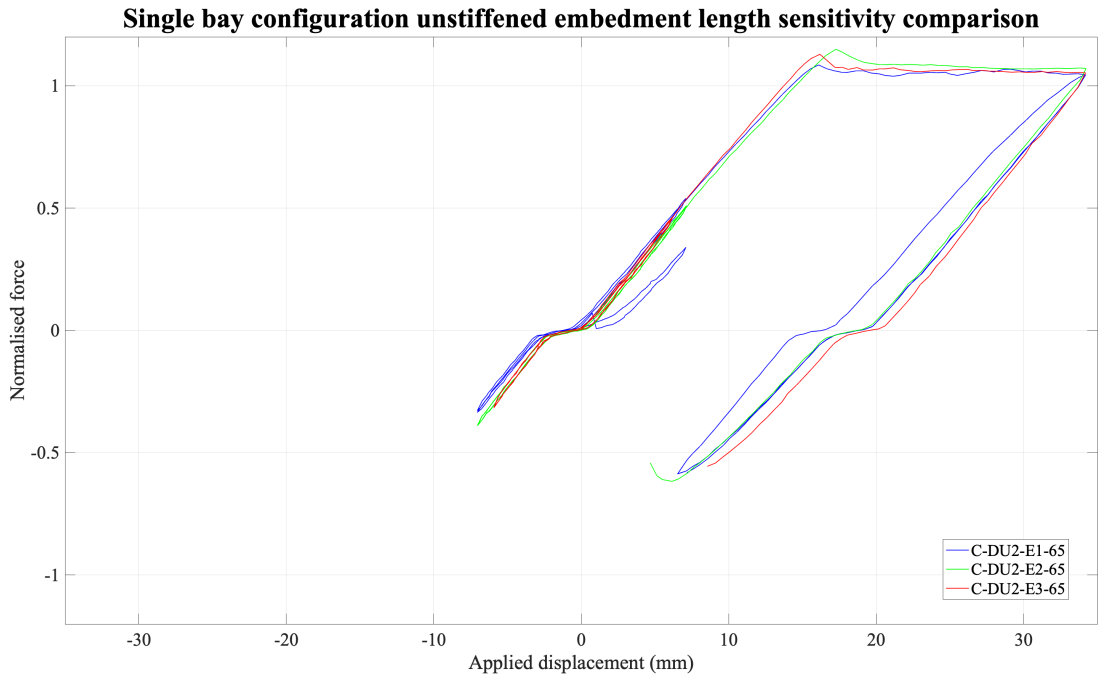


d)

**Figure 3-31: Single bay configuration unstiffened embedment length sensitivity a) Specimen C-DU2-E1-65 b) Specimen C-DU2-E2-65 c) Specimen C-DU2-E3-65 d) Comparison of sensitivity**

Three SB configuration specimens, C-DU2-E1-65, C-DU2-E2-65 and C-DU2-E3-65 were also evaluated for embedment length sensitivity (Table 3-19). All specimens

underwent global buckling within the first compression cycle post yield, resulting in the test being aborted. Higher ultimate tensile strength (UTS) was presented by C-DU2-E2-65, whose embedment length was two times the non-yielding width, with C-DU2-E1-65 obtaining the lowest UTS with an embedment equal to the non-yielding length (Figure 3-31). There is insufficient evidence to speculate the embedment lengths sensitivity, and as with the transition region sensitivity, it is recommended that further testing be carried out on stiffened specimens to supress the tendency to global buckling.

### 3.5.5 Nominally identical specimen response

Three nominally identical specimens were evaluated for variability in response.

**Table 3-20: V configuration stiffened nominally identical specimen key geometrical features**

| Specimen | | C-VS2-E2-200-R80A | C-VS2-E2-200-R80B | C-VS2-E2-200-R80C |
|---|---|---|---|---|
| Non-yielding length (mm) | Transition | 120 | 120 | 120 |
| | Embedment | 320 | 320 | 320 |
| | Stroke | 44 | 44 | 44 |
| Yielding length (mm) | | 2232 | 2232 | 2232 |
| Radius (mm) | | 80 | 80 | 80 |
| Outer casing depth (mm) | | 200 | 200 | 200 |
| Stiffeners | | Yes | Yes | Yes |

**Table 3-21: V configuration stiffened nominally identical results**

| Specimen | | | C-VS2-E2-200-R80A | C-VS2-E2-200-R80B | C-VS2-E2-200-R80C |
|---|---|---|---|---|---|
| Failure mode | | | DNF | DNF | DNF |
| Material yield (kN) | | | 225.6 | 225.6 | 225.6 |
| Specimen yield (kN) | | | 215.8 | 217.6 | 221.5 |
| Strain hardening adjustment factor, $\omega$ | | | 1.21 | 1.24 | 1.25 |
| Compression adjustment factor, $\beta$ | | | 1.42 | 1.41 | 1.34 |
| Percent strain $\beta$ occurs, $\varepsilon_{sc}$ (%) | | | 3.94 | 3.94 | 3.94 |
| Stroke length (mm) | Actuator end | Initial | 47.12 | 50.28 | 43.12 |
| | | Final | 21.25 | 33.00 | 48.76 |
| | Freestanding frame end | Initial | 49.92 | 50.32 | 45.86 |
| | | Final | 38.15 | 28.74 | 6.75 |
| Global buckling safety factor | | | 0.03 | 0.03 | 0.03 |
| Local buckling | Minor axis (Equation 2-27) | | 0.00 | 0.00 | 0.00 |
| | Demand to capacity ratio (Equation 2-28) | | 0.25 | 0.25 | 0.25 |

DNF: Did not fail, passed AISC 341 minimum requirements for BRB qualification

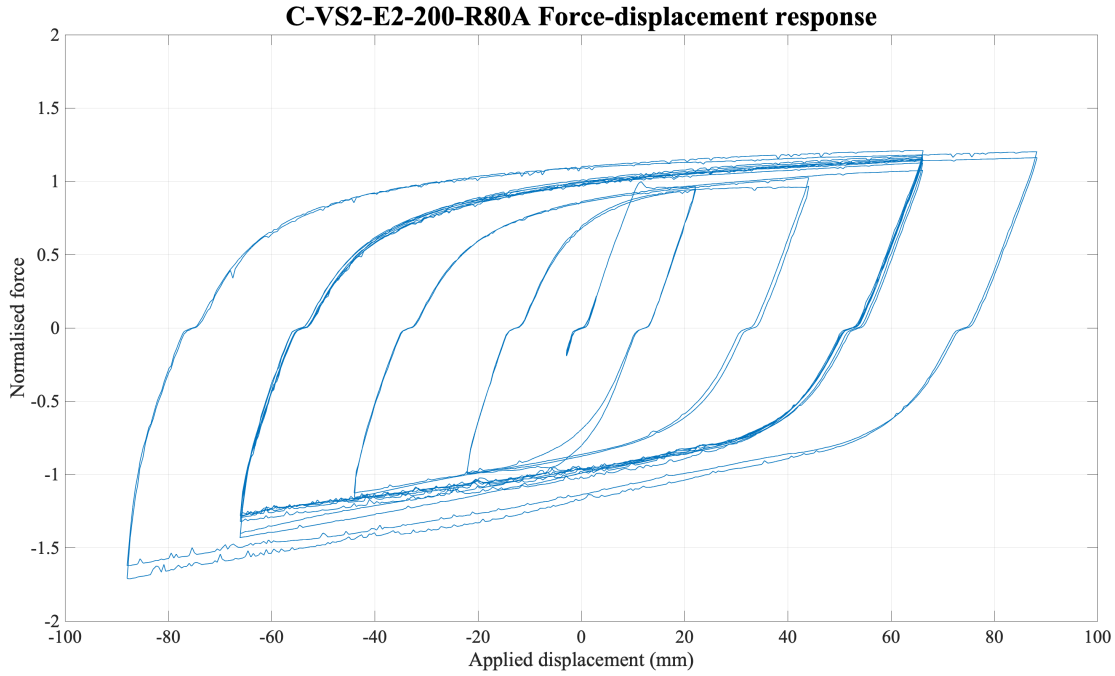
C-VS2-E2-200-R80A Force-displacement response
Normalised force
Applied displacement (mm)
2
1.5
1
0.5
0
-0.5
-1
-1.5
-2
-100
-80
-60
-40
-20
0
20
40
60
80
100

a)

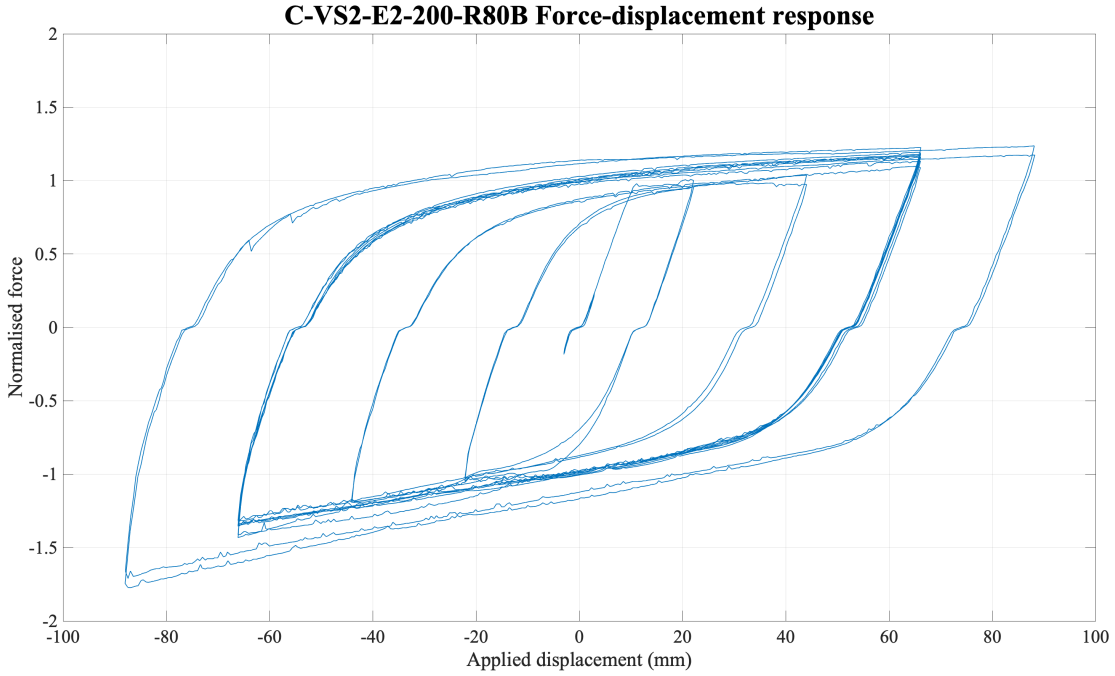
C-VS2-E2-200-R80B Force-displacement response
Normalised force
Applied displacement (mm)
2
1.5
1
0.5
0
-0.5
-1
-1.5
-2
-100
-80
-60
-40
-20
0
20
40
60
80
100

b)

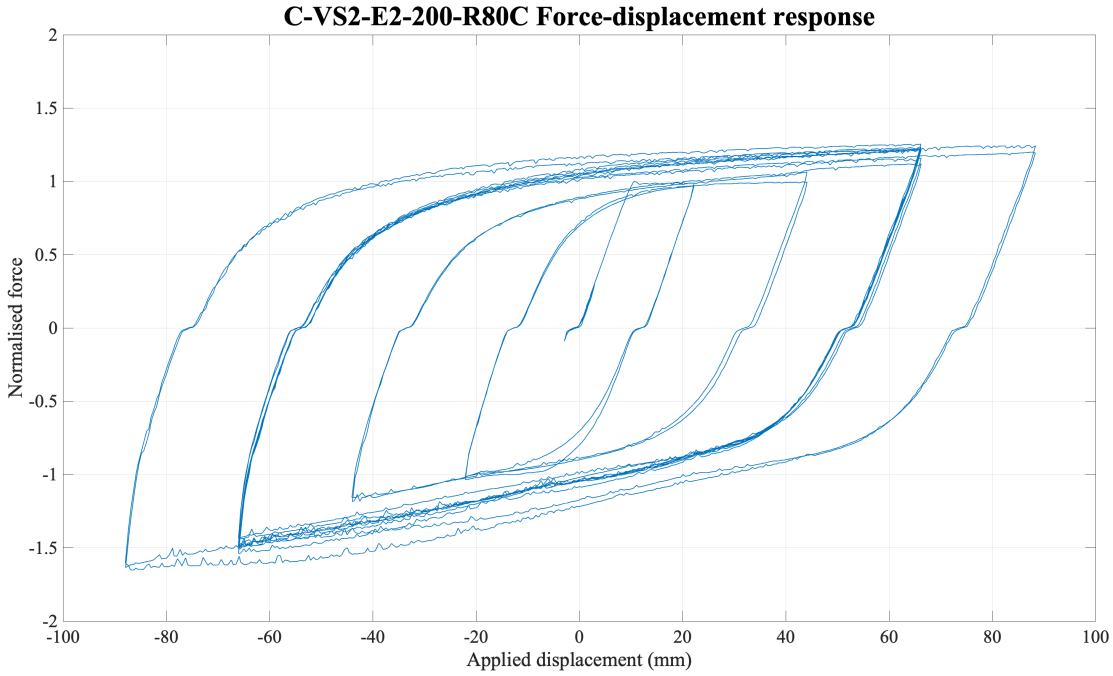


c)

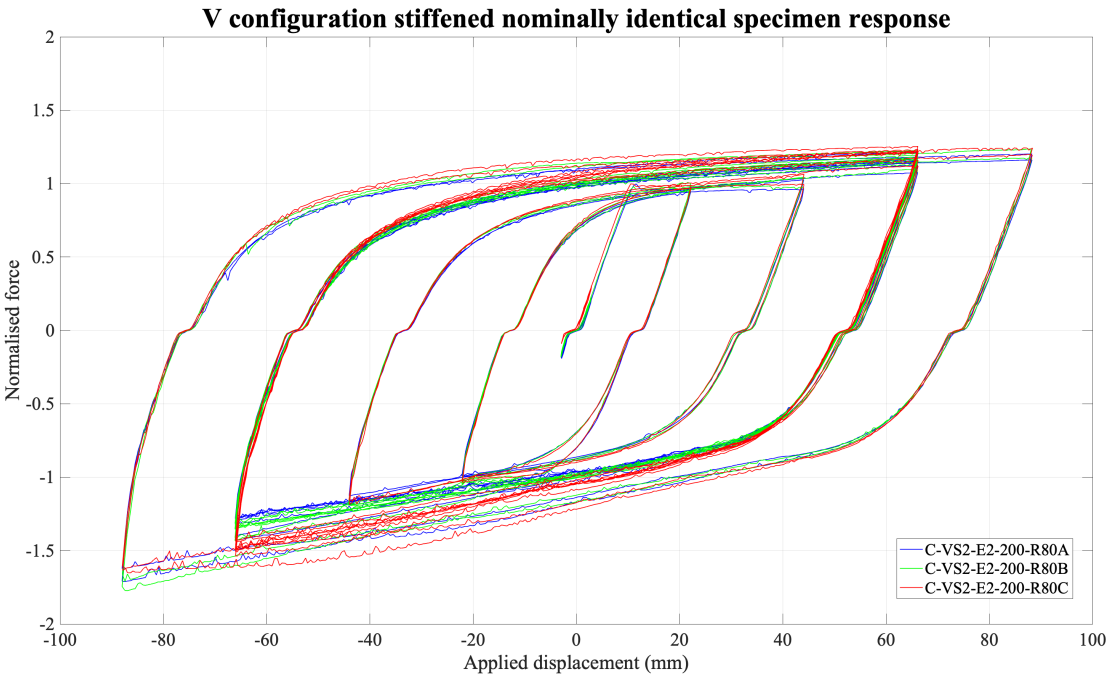


d)

**Figure 3-32: V configuration stiffened nominally identical a) Specimen C-VS2-E2-200-R80A b) Specimen C-VS2-E2-200-R80B c) Specimen C-VS2-E2-200-R80C d) Comparison of sensitivity**

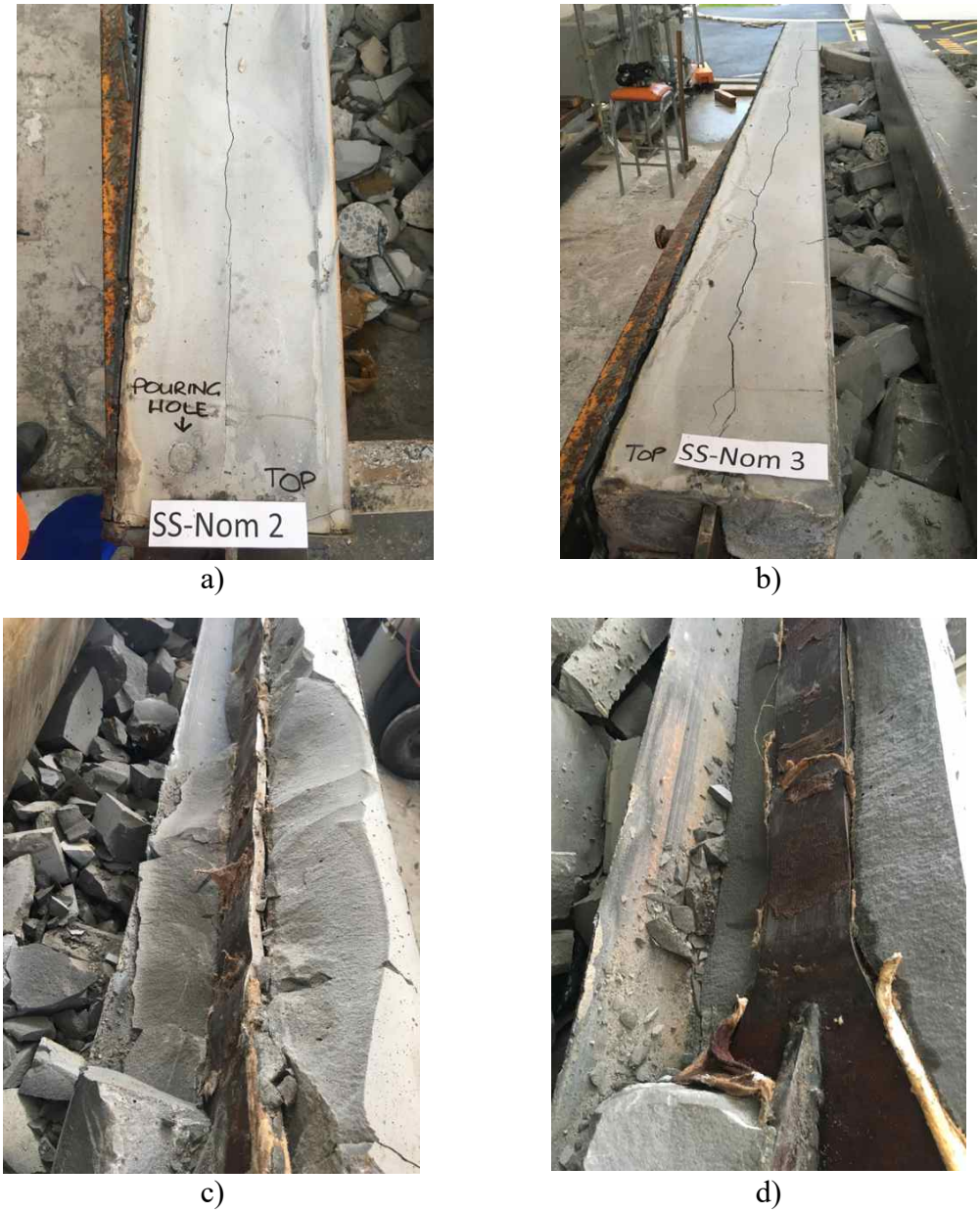


a) b)

c) d)

**Figure 3-33: Nominal dissection a) C-VS2-E2-200-R80B, restraining medium fracture down core line b) C-VS2-E2-200-R80C, restraining medium fracture down core line c) C-VS2-E2-200-R80B buckling wavelength d) C-VS2-E2-200-R80C buckling wavelength**

The identical V configuration specimens were tested; C-VS2-E2-200-R80A, C-VS2-E2-200-R80B and C-VS2-E2-200-R80C. All specimens passed the minimum experimental criteria set out by AISC 341 for BRB member qualification. On dissection (Figure 3-33) all specimens exhibited high mode local buckling wavelength distributed throughout the full yielding core length, commencing at both ends within the bearing region. The yielding cores were mapped to measure the wavelength distribution, with all specimens distributed similarly (see Section 3.6). Specimens C-VS2-E2-200-R80A and C-VS2-E2-200-R80B engaged both stroke regions throughout qualification, however C-VS2-E2-200-R80C displayed little stroke movement at the actuator end, with stroke displacement primarily concentrated at the freestanding end. Specimen C-VS2-E2-200-R80C marginally passed qualification, with an increase in

compression capacity (and deviation from the hysteresis curve) in the final 2.0 x drift compression cycle, performing stably on repetitive 1.5 x drift cycles to meet the required cumulative inelastic ductility (CID) (Figure 3-32). This instability is likely attributed to the unequal stoke engagement and it is expected that if further 2.0 x drift cycles were imposed, the specimen would have failed through local buckling.

The strain hardening adjustment factors ($\phi_{os}$) for C-VS2-E2-200-R80A, C-VS2-E2-200-R80B and C-VS2-E2-200-R80C were 1.21, 1.24 and 1.25, respectively (Table 3-21). All specimens performed similarly with respect to tension loading with C-VS2-E2-200-R80A exhibiting a slightly lower tension response than C-VS2-E2-200-R80B and C-VS2-E2-200-R80C, and this response directly relates to the CID. The actual and theoretical CID (calculated with respect to AISC 341) for each specimen is presented in Figure 3-34 and Figure 3-35. It was observed that the theoretical CID for each specimen was grossly overestimated. As this is a requirement for minimum qualification, calculation of the CID while experimental verification is being undertaken is recommended, by basing design of the BRB on the theoretical CID, potential under performance in practice could result.

The compression adjustment factor ($\beta$) is a key response to measure not only the difference between the compression and tension capacities, but is also a means of judging the unbonding medium performance. Specimens C-VS2-E2-200-R80A, C-VS2-E2-200-R80B and C-VS2-E2-200-R80C presented compression adjustment factors of 1.42, 1.41 and 1.34 respectively (Table 3-21). Based on the minimum qualification criteria set out in AISC 341, all tests did not satisfy $\beta < 1.3$ and therefore do not meet the minimum acceptance requirements for BRB application use. A high ($> 1.0$) compression adjustment factor indicates poor debonding and ability to develop a debonding gap, resulting in high compression forces. Although all specimens passed the minimum experimental criteria, the reliability of the debonding gap is questionable and therefore these specimens are not appropriate for practical application. It is also important to note that C-VS2-E2-200-R80C, although presenting a lower compression adjustment factor of the three specimens, was also deviating from stability in the final 2.0 x drift cycle.

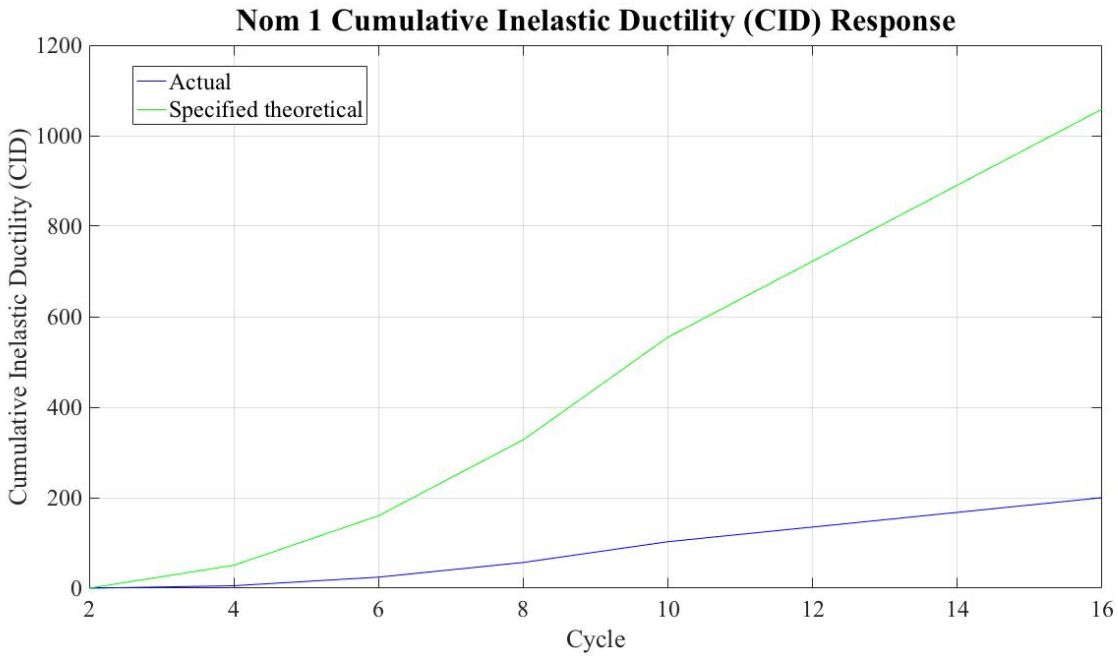


**Figure 3-34: Specimen C-VS2-E2-200-R80A specified vs. actual cumulative inelastic ductility response**

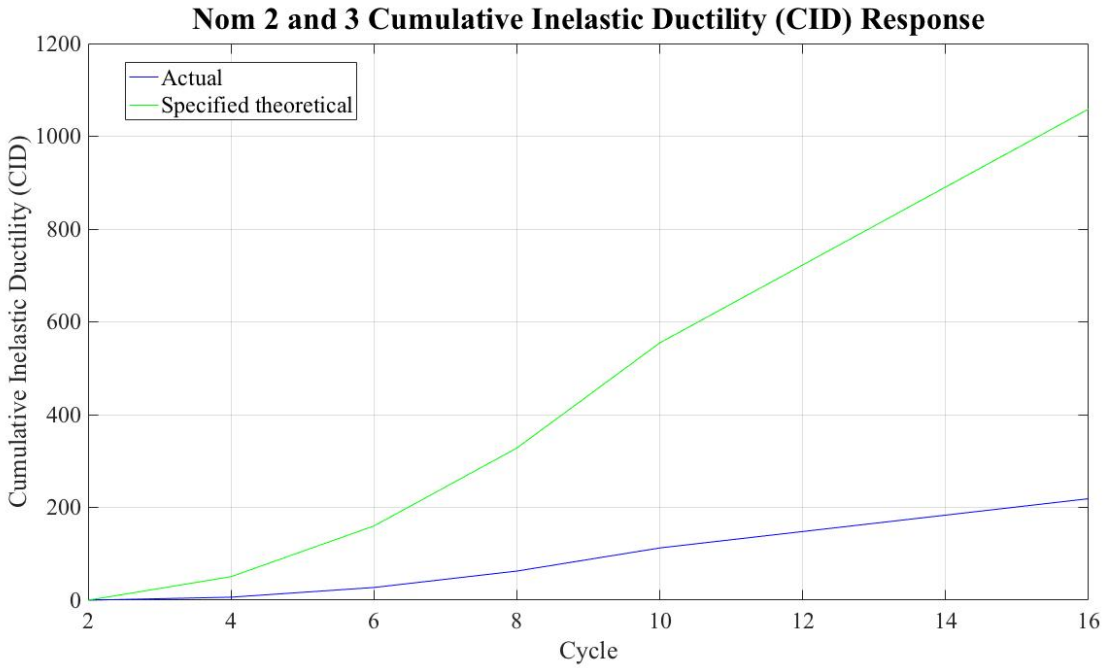


**Figure 3-35: Specimen C-VS2-E2-200-R80B and C-VS2-E2-200-R80C specified vs. actual cumulative inelastic ductility response**

### 3.5.6 Eccentric loading unrestrained non-yielding region response sensitivity

Eccentric testing was investigated to evaluate rotational response of the BRB. The eccentric testing was carried out within two different configurations, fixed-fixed at both ends for stiffened specimens, and the use of horizontal spherical pins at each end for unstiffened specimens. The use of a horizontal spherical bearing (as used in concentric testing) was required as unstiffened specimens are vulnerable to local

buckling in the stroke region at the Euler buckling load. This was observed in a loading rig test using an already tested DU specimen, and this specimen buckled within the stroke region at the Euler buckling load in the fixed-fixed (fully fixed at both ends) configuration. The applied eccentricity and fixed-fixed orientation results develop a significant moment unlikely to occur in practice. The eccentric testing was conducted to evaluate what response the member has in an unlikely/failure inducing circumstance, irrespective of frame and connection influence.

**Table 3-22: V configuration unstiffened eccentric stroke length sensitivity specimen key geometrical features**

| **Specimen** | | **E-VU2-E2-65** | **E-VU4-E2-65** | **E-VU6-E2-65** |
|---|---|---|---|---|
| Non-yielding length (mm) | Transition | 120 | 120 | 120 |
| | Embedment | 320 | 320 | 320 |
| | Stroke | 44 | 88 | 132 |
| Yielding length (mm) | | 2232 | 2144 | 2056 |
| Radius (mm) | | 80 | 80 | 80 |
| Outer casing depth (mm) | | 65 | 65 | 65 |
| Stiffeners | | No | No | No |

**Table 3-23: V configuration unstiffened eccentric stroke length sensitivity results**

| **Specimen** | | | **E-VU2-E2-65** | **E-VU4-E2-65** | **E-VU6-E2-65** |
|---|---|---|---|---|---|
| Failure mode | | | Local and global buckling | Global buckling and rotation | Local hinge |
| Material yield (kN) | | | 225.6 | 225.6 | 225.6 |
| Specimen yield (kN) | | | 210.69 | 239.57 | 239.57 |
| Compression adjustment factor, $\beta$ | | | 1.05 | 0.50 | 1.38 |
| Percent in-plane strain $\beta$ occurs, $\varepsilon_{sc}$ (%) | | | 0.99 | 1.03 | 0.15 |
| End type | | | Pin | Pin | Pin |
| Stroke length (mm) | Actuator end | Initial | 48.00 | 60.4 | 104.7 |
| | | Final | 92.01 | NA | NA |
| | Freestanding frame end | Initial | 48.01 | 58.66 | 107.64 |
| | | Final | 41.47 | NA | NA |
| Global buckling safety factor | | | 0.51 | 0.51 | 0.51 |
| Local buckling | Minor axis (Equation 2-27) | | 1.01 | 1.01 | 1.01 |
| | Demand to capacity ratio (Equation 2-28) | | 1.23 | 1.23 | 1.23 |

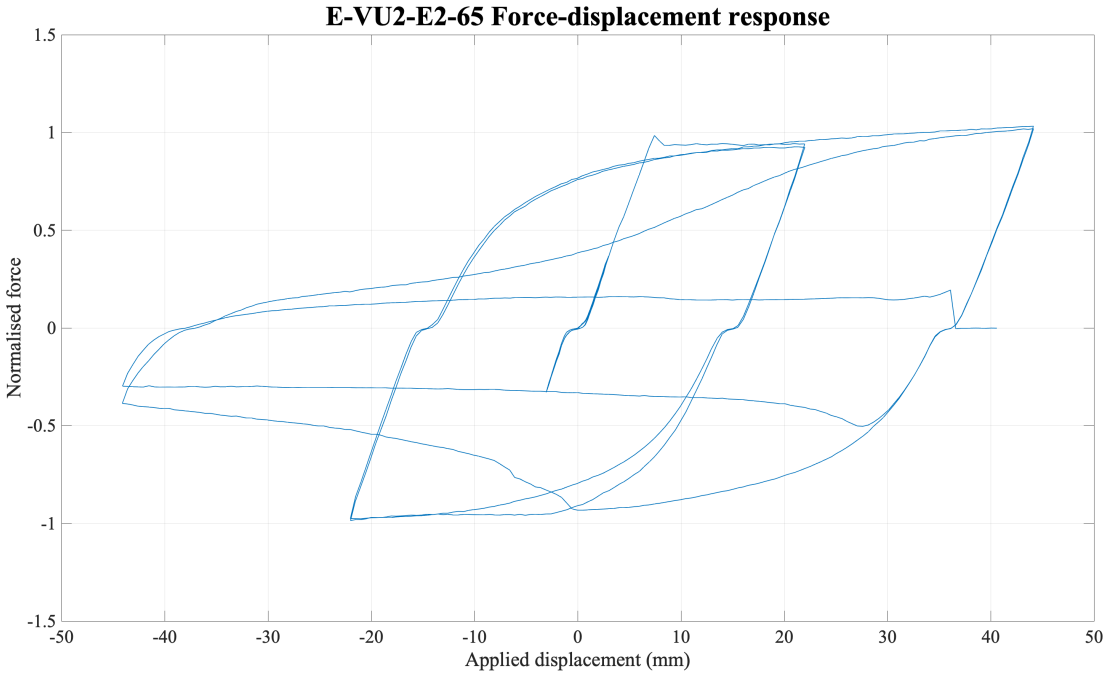
E-VU2-E2-65 Force-displacement response
Normalised force
Applied displacement (mm)
1.5
1
0.5
0
-0.5
-1
-1.5
-50
-40
-30
-20
-10
0
10
20
30
40
50

a)

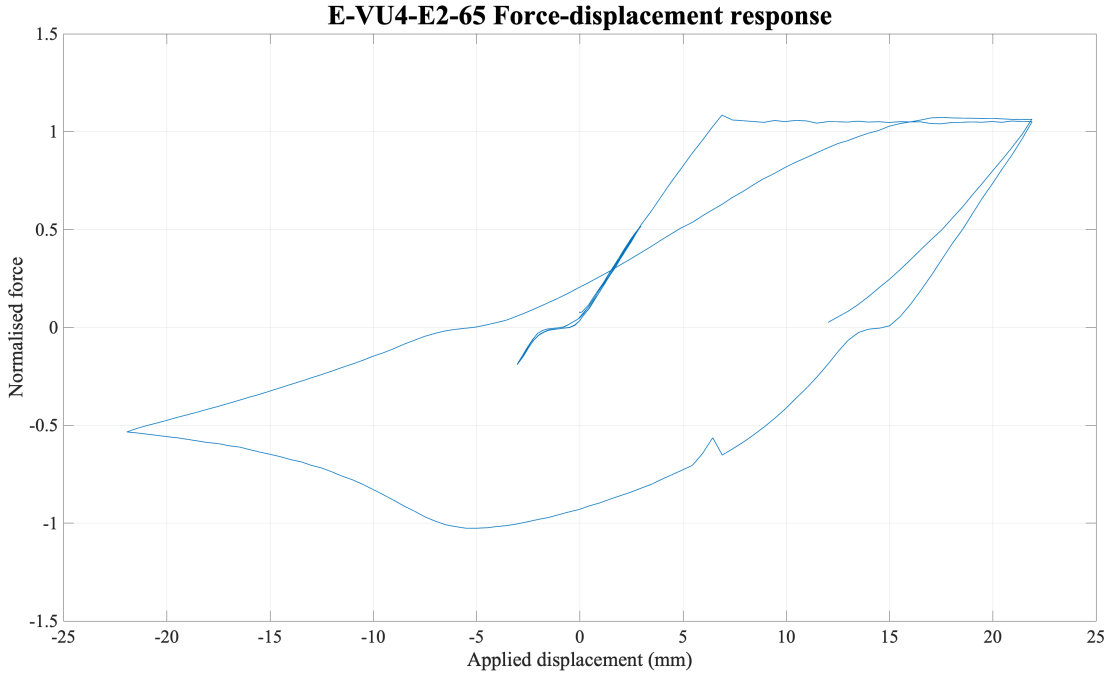
E-VU4-E2-65 Force-displacement response
Normalised force
Applied displacement (mm)
1.5
1
0.5
0
-0.5
-1
-1.5
-25
-20
-15
-10
-5
0
5
10
15
20
25

b)

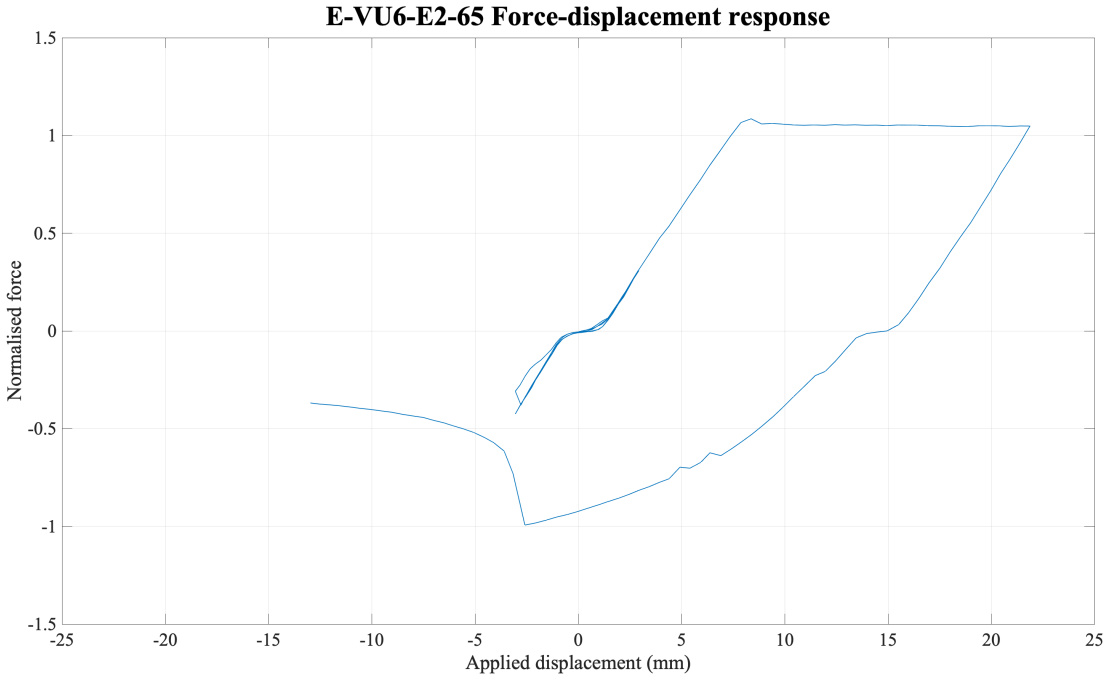


c)

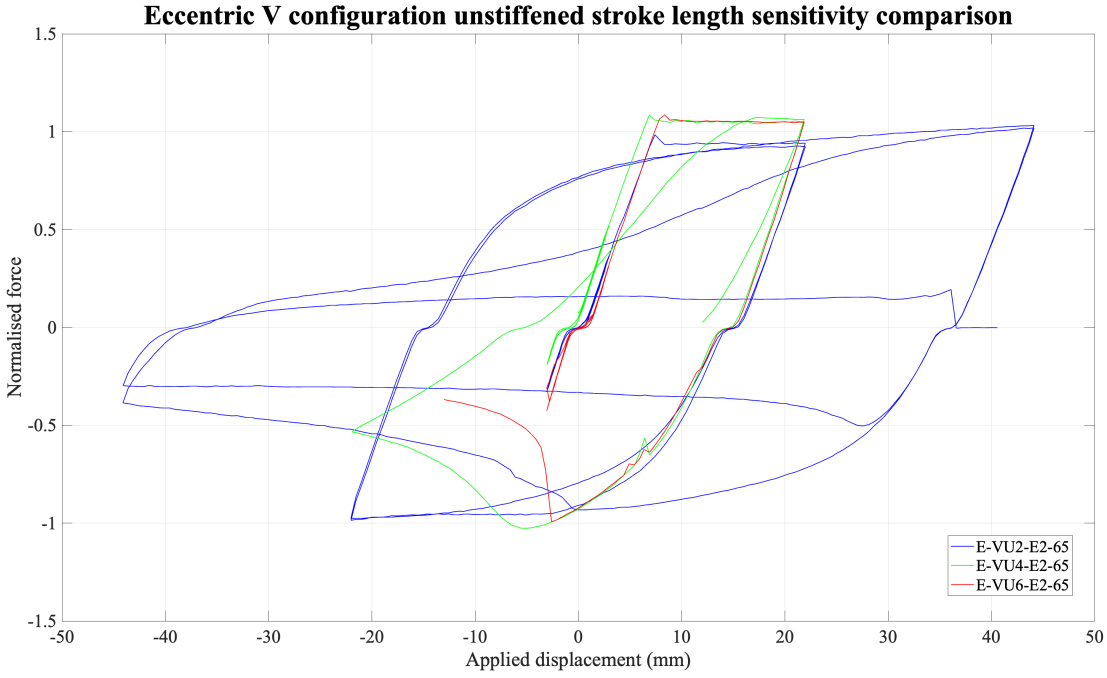


d)

**Figure 3-36: V configuration unstiffened eccentric stroke length sensitivity a) Specimen E-VU2-E2-65 b) Specimen E-VU4-E2-65 c) Specimen E-VU6-E2-65 d) Comparison of sensitivity**

The unstiffened V configuration specimens performed similarly to the concentric specimens. Instability in compression capacity occurred within the same cycle (1 x

drift) as the concentric specimens, however the eccentric specimens degraded in tension capacity, whereas the concentric specimens retained full capacity. The material yield of the eccentric specimens occurred at approximately 7 mm, whereas the concentric specimens occurred at approximately 10 mm. Failure was in the tension cycle through core fracture within the bearing region. The unstiffened eccentric specimens were more venerable within tension loading than the concentric counterparts.

**Table 3-24: Single bay configuration unstiffened eccentric stroke length sensitivity specimen key geometrical features**

| Specimen | | E-DU2-E2-65 | E-DU4-E2-65 | E-DU6-E2-65 |
|---|---|---|---|---|
| Non-yielding length (mm) | Transition | 120 | 120 | 120 |
| | Embedment | 320 | 320 | 320 |
| | Stroke | 68 | 136 | 204 |
| Yielding length (mm) | | 4584 | 4448 | 4312 |
| Radius (mm) | | 80 | 80 | 80 |
| Outer casing depth (mm) | | 65 | 65 | 65 |
| Stiffeners | | No | No | No |

**Table 3-25: Single bay configuration unstiffened eccentric stroke length sensitivity results**

| Specimen | | | E-DU2-E2-65 | E-DU4-E2-65 | E-DU6-E2-65 |
|---|---|---|---|---|---|
| Failure mode | | | Global buckling and rotation | Global buckling and rotation | Global buckling, rotation and local hinge |
| Material yield (kN) | | | 191.4 | 191.4 | 191.4 |
| Specimen yield (kN) | | | 198.52 | 194.25 | 201.91 |
| Compression adjustment factor, $\beta$ | | | 0.91 | 0.99 | 0.80 |
| Percent in-plane strain $\beta$ occurs, $\varepsilon_{sc}$ (%) | | | 0.15 | 0.16 | 0.14 |
| End type | | | Pin | Pin | Pin |
| Stroke length (mm) | Actuator end | Initial | 69.88 | 111.9 | 183.58 |
| | | Final | Not recorded | Not recorded | Not recorded |
| | Freestanding frame end | Initial | 70.53 | 103.78 | 187.14 |
| | | Final | Not recorded | Not recorded | Not recorded |
| Global buckling safety factor | | | 1.55 | 1.55 | 1.55 |
| Local buckling | Minor axis (Equation 2-27) | | 1.01 | 1.01 | 1.01 |
| | Demand to capacity ratio (Equation 2-28) | | 1.23 | 1.23 | 1.23 |

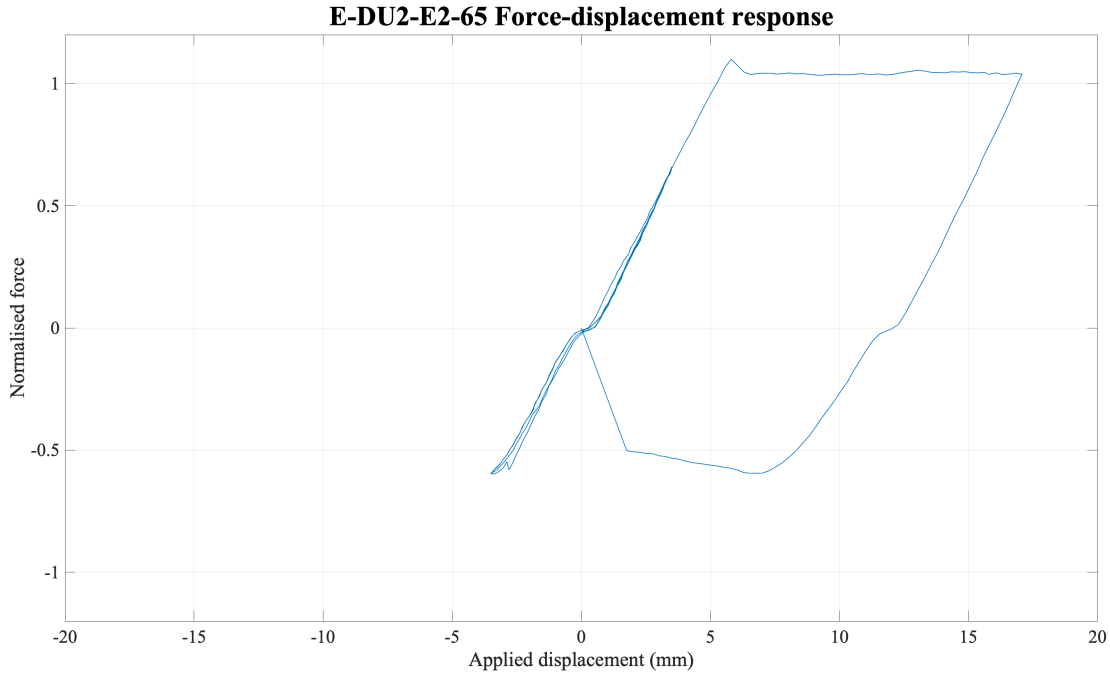
E-DU2-E2-65 Force-displacement response
Normalised force
Applied displacement (mm)
1
0.5
0
-0.5
-1
-20
-15
-10
-5
0
5
10
15
20

a)

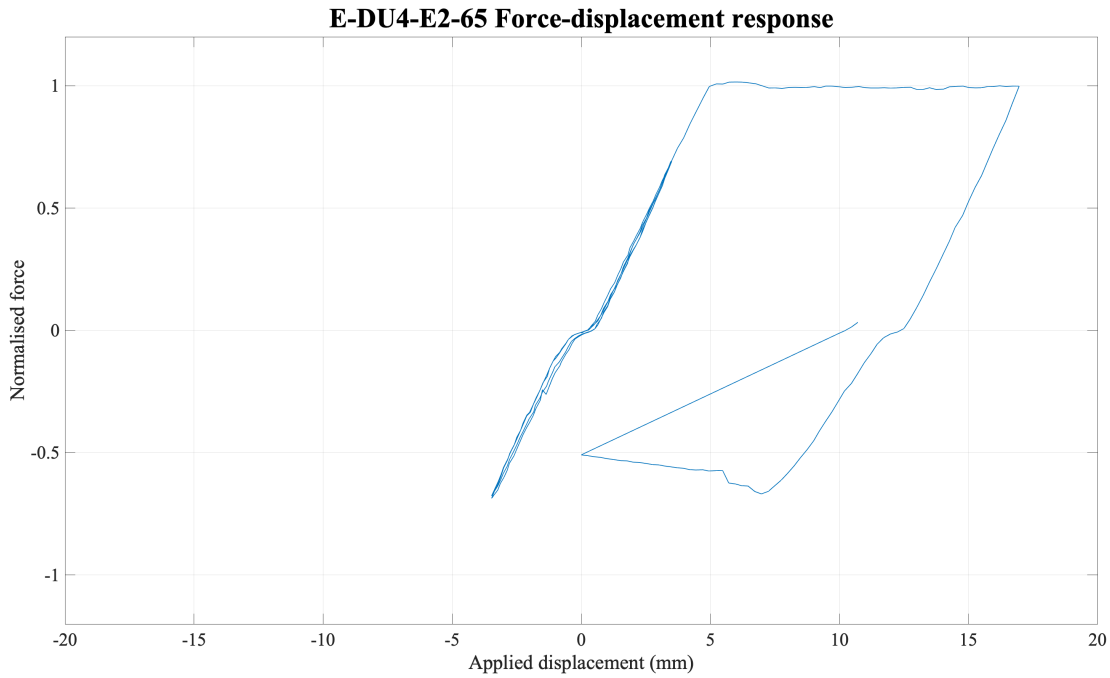
E-DU4-E2-65 Force-displacement response
Normalised force
Applied displacement (mm)
1
0.5
0
-0.5
-1
-20
-15
-10
-5
0
5
10
15
20

b)

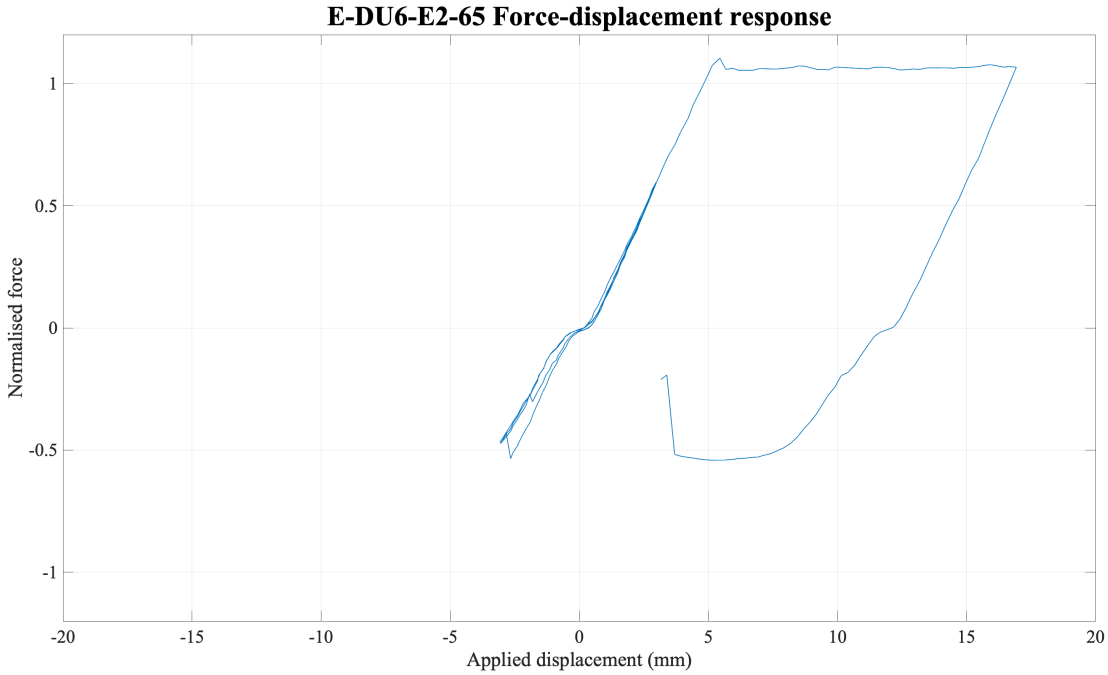


c)

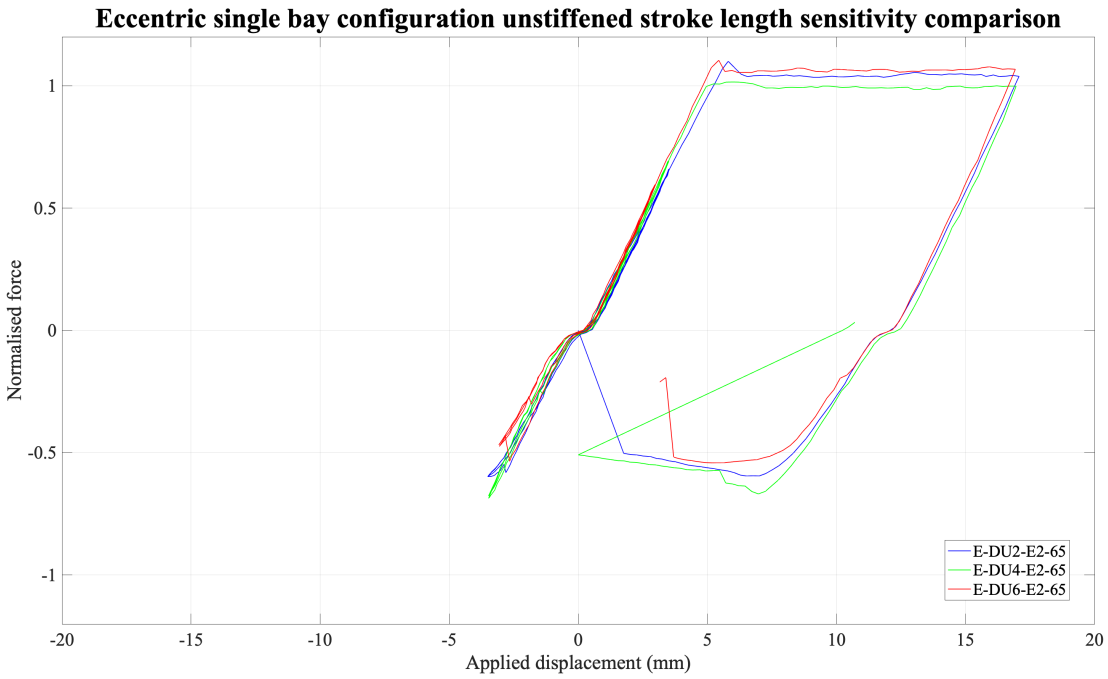


d)

**Figure 3-37: Single bay configuration unstiffened eccentric stroke length sensitivity a) Specimen E-DU2-E2-65 b) Specimen E-DU4-E2-65 c) Specimen E-DU6-E2-65 d) Comparison of sensitivity**

The unstiffened SB specimens underwent global buckling within the 0.5 x drift cycle. Along with global buckling, the specimens underwent rotation away from the point of

buckling. The tests were stopped in all cases due to safety. As observed in the V configuration unstiffened specimens, the specimen yield occurred at approximately 5 mm, whereas the concentric specimens occurred at 10 mm. This confirms that when stiffeners are not present, the specimens are more susceptible to tension degradation when out-of-plane strain is present.

**Table 3-26: V configuration stiffened eccentric stroke length sensitivity specimen key geometrical features**

| **Specimen** | | **E-VS2-E2-200** | **E-VU4-E2-200** | **E-VU6-E2-200** |
|---|---|---|---|---|
| Non-yielding length (mm) | Transition | 120 | 120 | 120 |
| | Embedment | 320 | 320 | 320 |
| | Stroke | 44 | 88 | 132 |
| Yielding length (mm) | | 2232 | 2144 | 2056 |
| Radius (mm) | | 80 | 80 | 80 |
| Outer casing depth (mm) | | 200 | 200 | 200 |
| Stiffeners | | Yes | Yes | Yes |

**Table 3-27: V configuration stiffened eccentric stroke length sensitivity results**

| **Specimen** | | | **E-VS2-E2-200** | **E-VS4-E2-200** | **E-VS6-E2-200** |
|---|---|---|---|---|---|
| Failure mode | | | Local buckling | Local buckling | Local buckling |
| Material yield (kN) | | | 225.6 | 205.0 | 205.0 |
| Specimen yield (kN) | | | 249.95 | 220.29 | 218.90 |
| Compression adjustment factor, $\beta$ | | | 1.47 | 1.32 | 1.28 |
| Percent in-plane strain $\beta$ occurs, $\varepsilon_{sc}$ (%) | | | 2.96 | 3.08 | 3.21 |
| End type | | | Fixed | Fixed | Fixed |
| Stroke length (mm) | Actuator end | Initial | 45.56 | 60.35 | 103.35 |
| | | Final | 92.24 | Not recorded | 168.89 |
| | Freestanding frame end | Initial | 50.09 | 47.52 | 88.14 |
| | | Final | 6.46 | Not recorded | 27.25 |
| Global buckling safety factor | | | 0.03 | 0.03 | 0.03 |
| Local buckling | Minor axis (Equation 2-27) | | 0.00 | 0.00 | 0.00 |
| | Demand to capacity ratio (Equation 2-28) | | 0.28 | 0.28 | 0.28 |

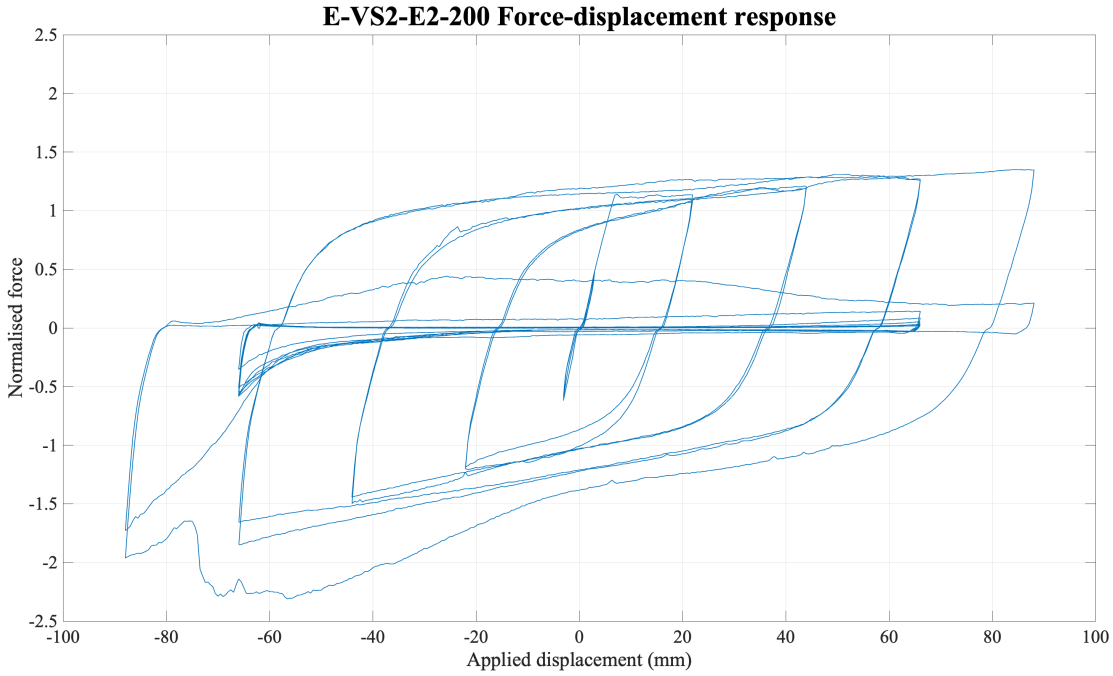
E-VS2-E2-200 Force-displacement response
Normalised force
Applied displacement (mm)
2.5
2
1.5
1
0.5
0
-0.5
-1
-1.5
-2
-2.5
-100
-80
-60
-40
-20
0
20
40
60
80
100

a)

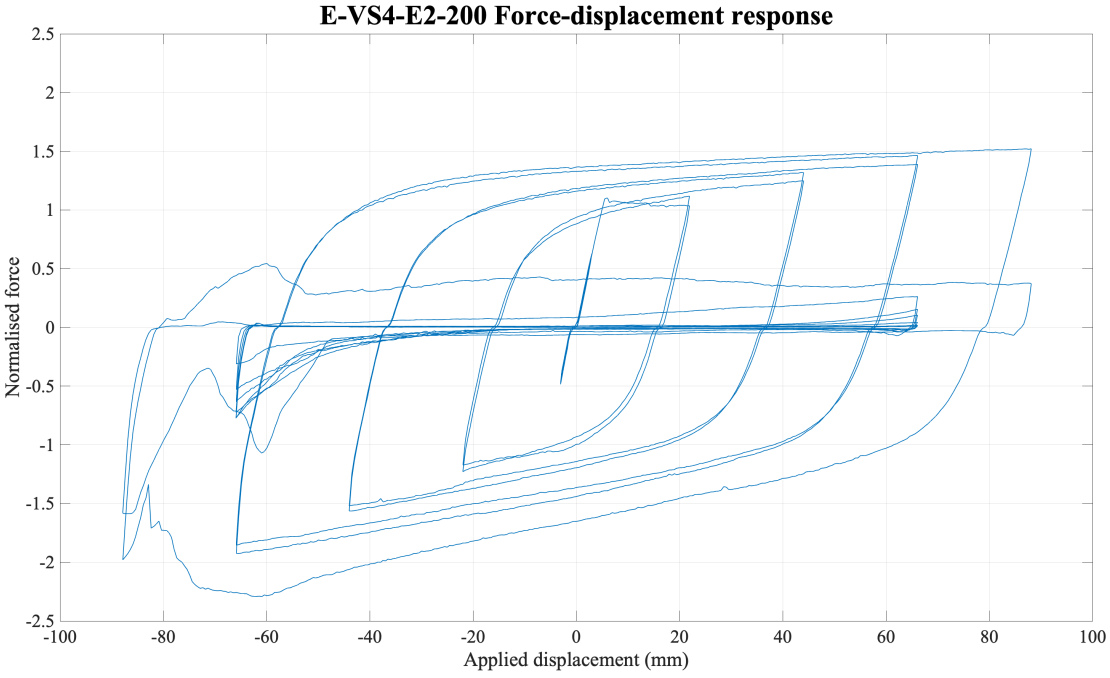
E-VS4-E2-200 Force-displacement response
Normalised force
Applied displacement (mm)
2.5
2
1.5
1
0.5
0
-0.5
-1
-1.5
-2
-2.5
-100
-80
-60
-40
-20
0
20
40
60
80
100

b)

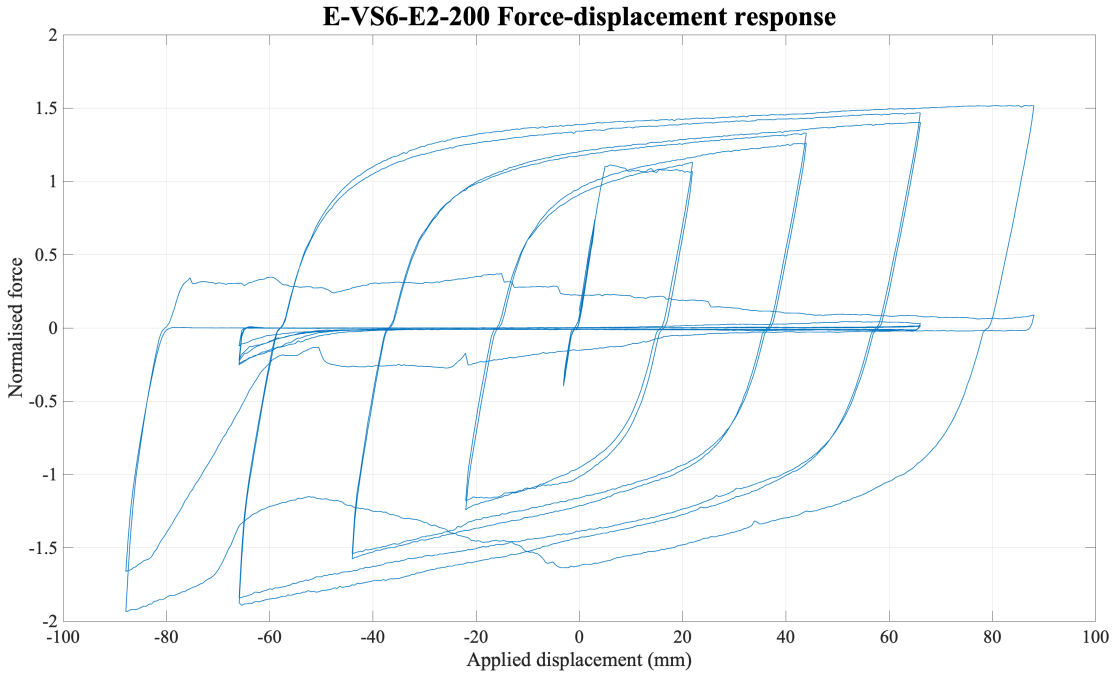


c)

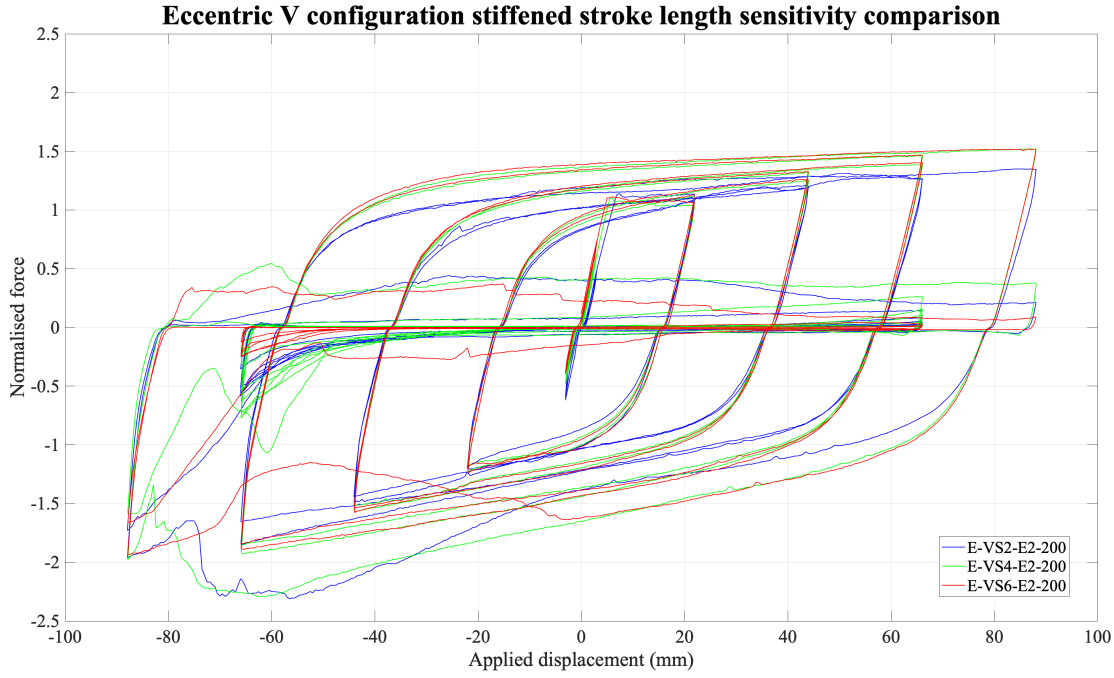


d)

**Figure 3-38: V configuration stiffened eccentric stroke length sensitivity a) Specimen E-VS2-E2-200 b) Specimen E-VS4-E2-200 c) Specimen E-VS6-E2-200 d) Comparison of sensitivity**

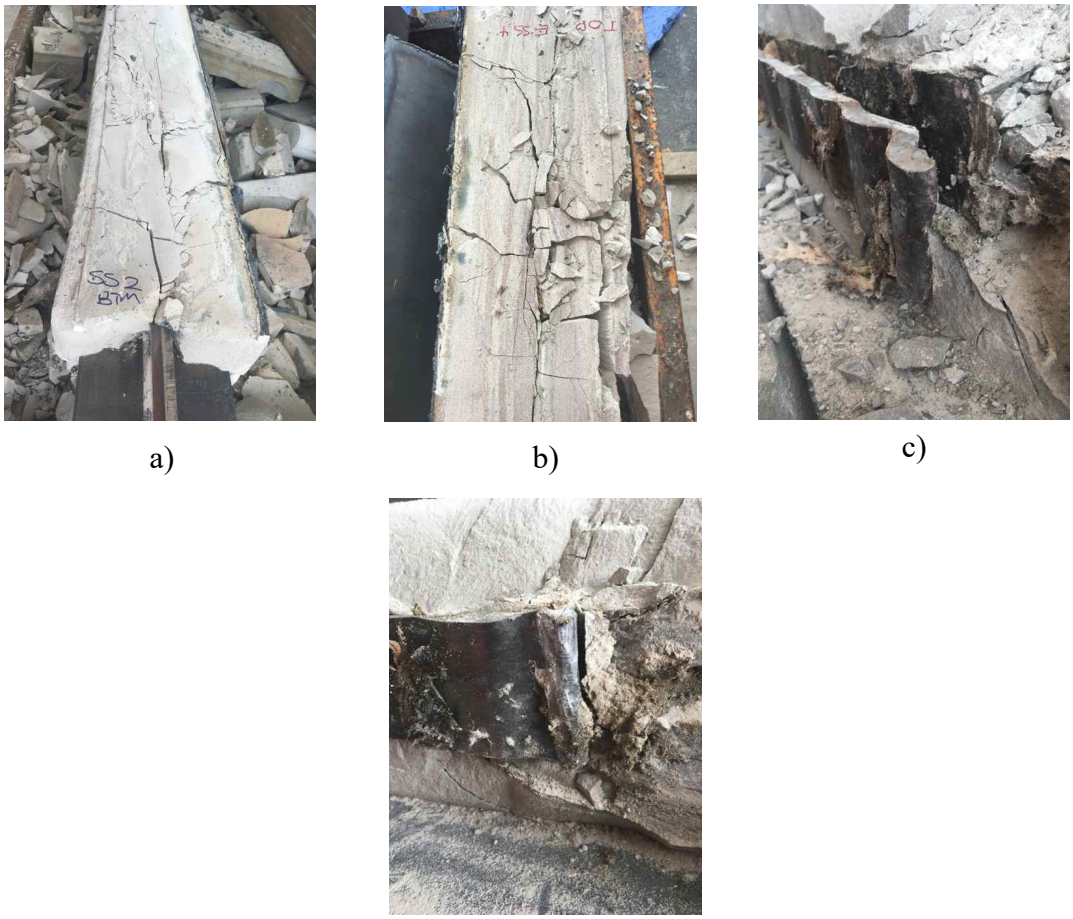

a) b) c)

d)

**Figure 3-39: a) E-VS2-E2-200 restraining medium damage b) E-VS4-E2-200 restraining medium damage c) E-VS2-E2-200 core fracture d) E-VS4-E2-200 core fracture**

The stiffened V configuration eccentric specimens all contained 80 mm radii in the transition-yielding region, in comparison to the concentric specimens which contained 10 mm. Fracture occurred in E-VS4-E2-200 and E-VS6-E2-200 within the bearing region, prior to the radii, through folding of the core. All specimens sustained continual cycling to large displacements, although capacity was tending to 0 kN in both tension and compression. The specimens remained stable within compression at greater strains than the concentric specimens, even with the additional strain from fixed connections and eccentricity. Although failure occurred within all specimens, it can be concluded that the 80 mm radii performed better than the 10 mm radii concentric specimens.

**Table 3-28: Single bay configuration stiffened eccentric stroke length sensitivity specimen key geometrical features**

| Specimen | | E-DS2-E2-200 | E-DS4-E2-200 | E-DS6-E2-200 |
|---|---|---|---|---|
| Non-yielding length (mm) | Transition | 120 | 120 | 120 |
| | Embedment | 320 | 320 | 320 |
| | Stroke | 68 | 136 | 204 |
| Yielding length (mm) | | 4584 | 4448 | 4312 |
| Radius (mm) | | 80 | 80 | 80 |
| Outer casing depth (mm) | | 200 | 200 | 200 |
| Stiffeners | | Yes | Yes | Yes |

**Table 3-29: Single bay configuration stiffened eccentric stroke length sensitivity results**

| Specimen | | | E-DS2-E2-200 | E-DS4-E2-200 | E-DS6-E2-200 |
|---|---|---|---|---|---|
| Failure mode | | | Local buckling | Local buckling | Local buckling |
| Material yield (kN) | | | 191.4 | 191.4 | 191.4 |
| Specimen yield (kN) | | | 199.38 | 194.93 | 207.12 |
| Compression adjustment factor, $\beta$ | | | 1.80 | 1.50 | 1.23 |
| Percent in-plane strain $\beta$ occurs, $\varepsilon_{sc}$ (%) | | | 2.97 | 2.29 | 1.58 |
| End type | | | Fixed | Fixed | Fixed |
| Stroke length (mm) | Actuator end | Initial | 71.81 | 91.95 | 182.00 |
| | | Final | Not recorded | Not recorded | 135.00 |
| | Freestanding frame end | Initial | 65.44 | 108.06 | 161.00 |
| | | Final | Not recorded | Not recorded | 76.00 |
| Global buckling safety factor | | | 0.10 | 0.10 | 0.10 |
| Local buckling | Minor axis (Equation 2-27) | | 0.00 | 0.00 | 0.00 |
| | Demand to capacity ratio (Equation 2-28) | | 0.28 | 0.28 | 0.28 |

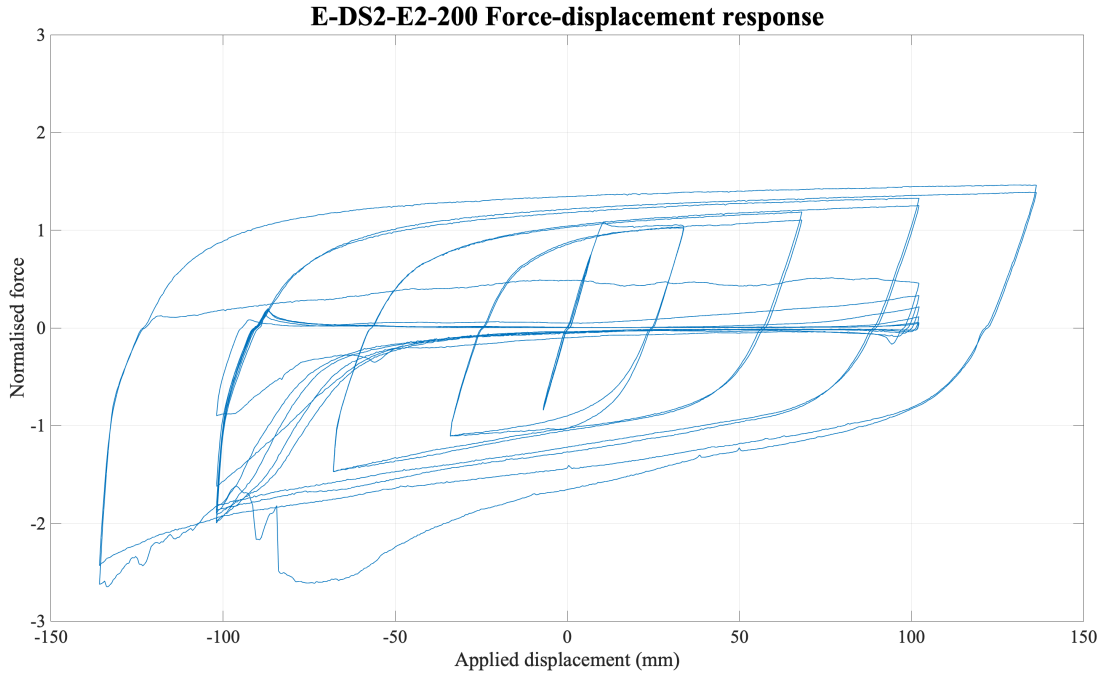
E-DS2-E2-200 Force-displacement response
Normalised force
Applied displacement (mm)
3
2
1
0
-1
-2
-3
-150
-100
-50
0
50
100
150

a)

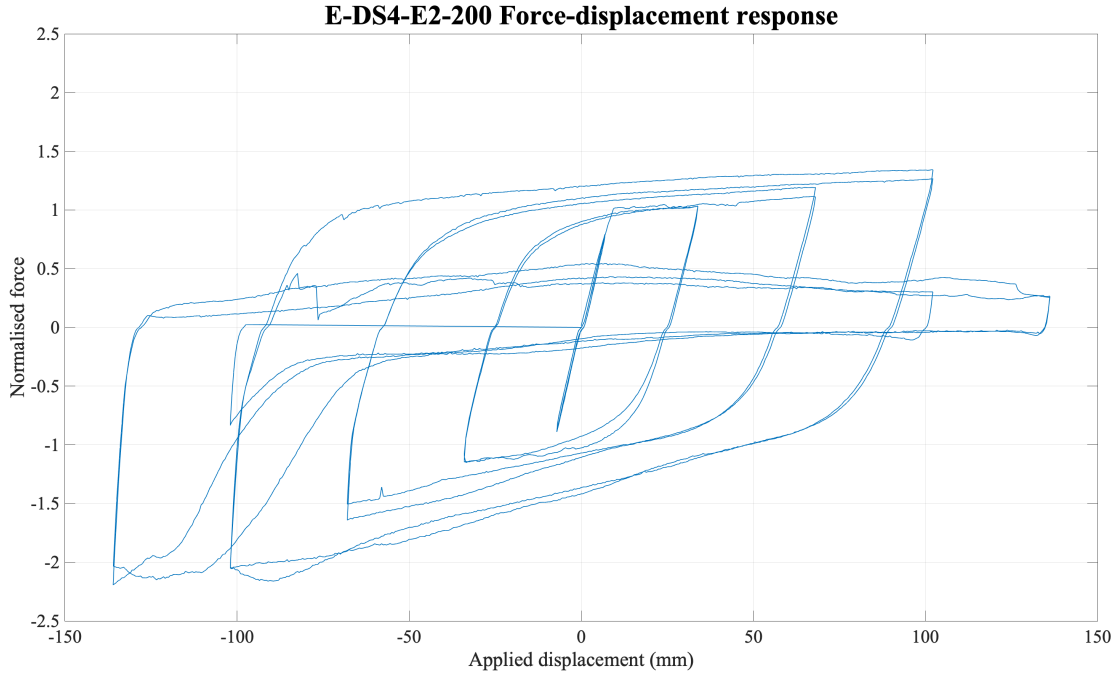
E-DS4-E2-200 Force-displacement response
Normalised force
Applied displacement (mm)
2.5
2
1.5
1
0.5
0
-0.5
-1
-1.5
-2
-2.5
-150
-100
-50
0
50
100
150

b)

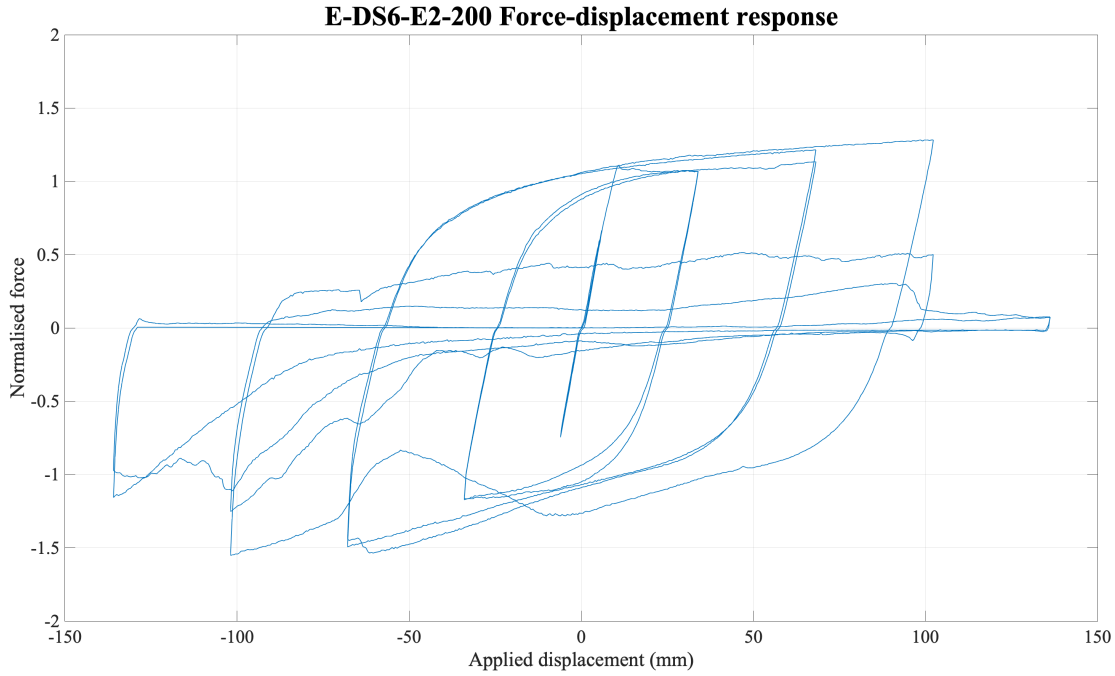


c)

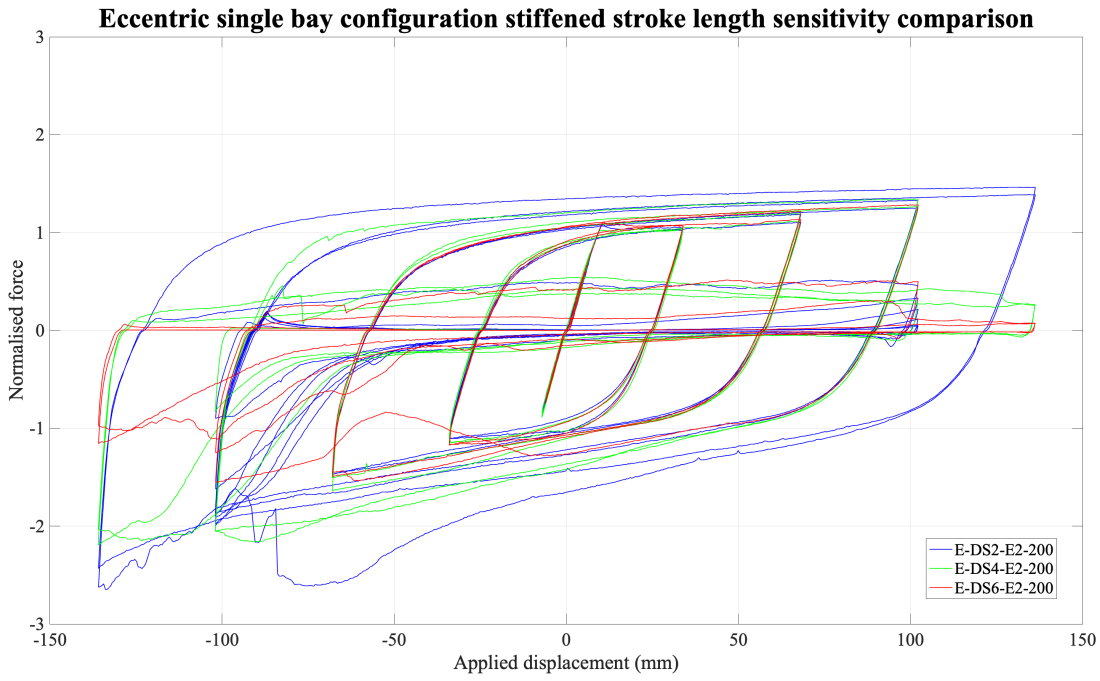


d)

**Figure 3-40: Single bay configuration stiffened eccentric stroke length sensitivity a) Specimen E-DS2-E2-200 b) Specimen E-DS4-E2-200 c) Specimen E-DS6-E2-200 d) Comparison of sensitivity**

a) b) c)

**Figure 3-41: Core deformation a) E-DS2-E2-200 core fracture b) E-DS4-E2-200 core fracture c) E-DS4-E2-200 core deformation**

The stiffened SB configuration specimens alike the V configuration failed through local buckling within the bearing region. The E-DS2-E2-200 and E-DS4-E2-200 failed through fracture of the core. The compression capacity degraded prior to the tension, however unlike the concentric specimens which retained tension capacity when compression capacity became unstable, the eccentric specimens degraded in both tension and compression together, cycling at load tensing to 0 kN for multiple cycles prior to fracture.

## 3.6 General comments

Member qualification of BRBs is carried out through cyclic loading. It was found through the first test conducted (C-VU2-E2-65) that when compression is loaded prior to tension (yielding cycle) global buckling was initiated. This test was re-started with tension-applied displacement (global buckling was not permanent), with the specimen performing as expected and undergoing local buckling. All tests were carried out with tension engaged first. This alludes to the need for tension to be engaged to initiate the debonding gap; without it, there is no debonding gap and the member behaves in a composite manner. To date, tests have been carried out in compression first, however these are low in number and further investigation is required to confirm if this flaw in the testing regime can be exploited by BRB providers providing skewed representation of performance or if it is unique to this testing regime.

Pre-tensioning of the specimens to less than first yield prior to commencing the test regime (with the compression cycle carried out first in the program) should be investigated, and if successful, should be applied to all BRBs pre-installation. Further discussion and investigation into this phenomenon is required to provide reliability of the BRB members performance in both tension and compression initial engagement.

The testing regime itself along with non-explicit specification for first engagement also presented ambiguity with regards to the applied displacement with respect to design drift. AISC 341 allows interpolation of results such that qualification testing is not required for all BRB designs (lengths, double core, etc.) and the tests themselves do not need to be carried out at full scale. This poses the risk of not adequately evaluating the specific design requirements for each application and also for misuse

with regards to variation in core numbers and also connection sizing. It is recommended that an explicit testing regime (and subsequent design requirements) be introduced such that each application of the BRB is verified along with its surrounding elements.

It was observed in all specimens which underwent global buckling, rotation of the specimen occurred. This rotation was amplified within the eccentric tests. The 1.5 global buckling safety factor, omitted from design should be used in evaluation of design. Furthermore, the governing mode, global or local from the evaluated safety factors should be used as the governing mode in specimen design.

Local buckling was initiated in all (local buckling failure) specimens in the outer thirds of the yielding core, primarily the bearing region. In all specimens, the bearing region length equated to the stroke length. For longer stroke specimens that failed through local buckling within the bearing region, a smaller bearing region length could push the local buckling into the restrained portion of the yielding core, inducing higher mode and distributed wavelength. An investigation into the bearing region length sensitivity with respect to stroke length is recommended.

It was found that the performance (and qualification) of the specimens was sensitive to the yielding to transition region radii. Figure 3-42 shows the performance of two specimens (C-VS2-E2-200-R80A and C-VS2-E2-200-R10), with the only variance the yielding to transition radii. It was observed that with a larger radius (in conjunction with BS 5400-10, H.23) the local buckling initiation moved from the radii into the bearing region. A lower tension and compression force was required to meet the applied displacement, resulting in lower compression overstrength. The local buckling wavelength was distributed along the full yielding core, rather than being localised from the radii, this also contributed to stable and balanced hysteresis loops. BS 5400-10, H.23 is recommended as the minimum radii criteria for BRB design.

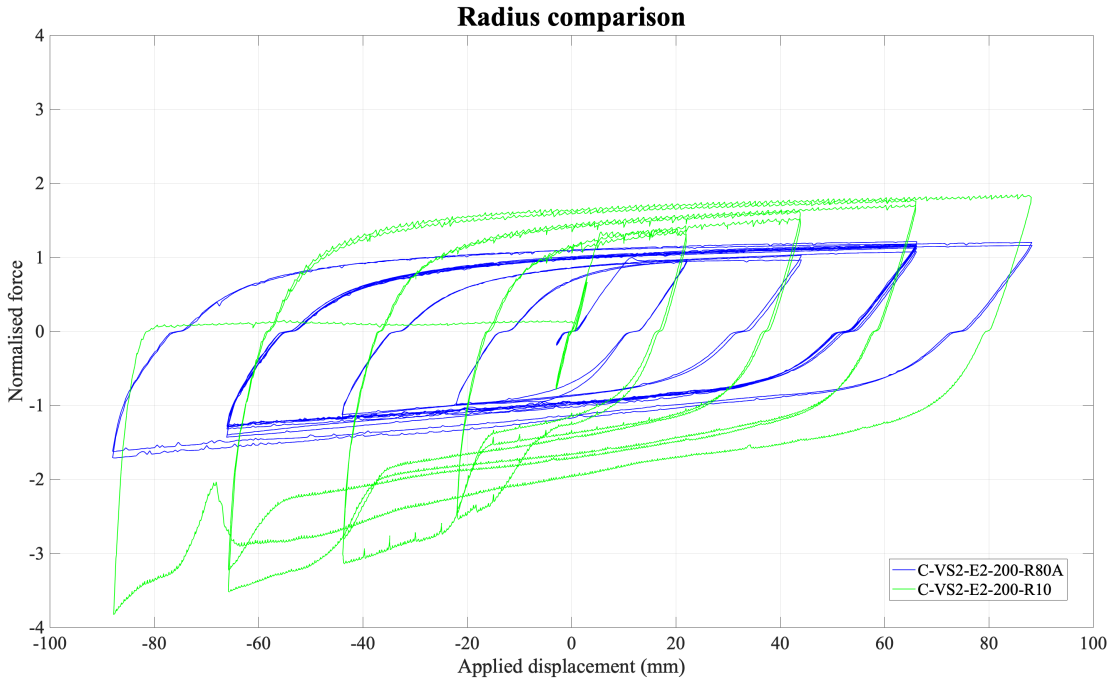


**Figure 3-42: Yielding region to transition radii comparison**

The nominal specimens yielding cores were mapped post dissection. This allowed the wavelengths of the minor axis to be captured. Mapping was commenced from the first visual indication of local buckling (within the bearing region). The results of the mapping can be found in Appendix F, with C-VS2-E2-200-R80A exhibiting an average wavelength of 62.29 mm, C-VS2-E2-200-R80B 62.00 mm and C-VS2-E2-200-R80C displaying two fewer waves than C-VS2-E2-200-R80A and C-VS2-E2-200-R80B at 65.76 mm. All specimens underwent minor and major axis buckling. The buckling wavelengths will be used to evaluate and validate the numerical modelling within the next chapter.

It is important to note that only C-VS2-E2-200-R80A, C-VS2-E2-200-R80B and C-VS2-E2-200-R80C successfully completed the AISC 341 testing regime out of the 37 specimens evaluated. Although successful, the compression overstrength factors of these specimens exceeded 1.3, and therefore do not meet the minimum qualification criteria for BRB application. The observed behaviour of the specimens indicated subsequent 2.0 x drift cycles passed the minimum criteria, or higher drift engagement would have resulted in specimen instability. The practicality of reducing the loading protocol from 2.0 x drift to 1.5 x drift for the remaining cycles until CID is reached should be investigated as instability failure may be supressed.

# 4 Theoretical and Numerical Modelling

## 4.1 Introduction

Within New Zealand experimental verification is not required for implementation of a buckling restrained brace (BRB) design. First principle calculations are typically presented to validate the BRBs behaviour for peer review and structural compliance. The following chapter details the development of a theoretical and numerical BRB model, evaluating the reliability of first principle relationships and quantification through empirical means.

The numerical model was developed using finite element analysis (FEA) software Abaqus/CAE 2017. The FEA model was designed using the specification for nominally identical experimental specimens. The purpose of the FEA model was to evaluate the reliability of designing and testing the BRB within the software, removing the need to verify the design through experimental means. Due to the limiting capacity and availability of testing facilities within New Zealand, a numerical approach to design is desired.

Initially the FEA model were developed empirically to evaluate the need for experimental calibration, with previous models within literature limited to the core and semi-empirical methods, developed based on experimental results. The empirical models were insufficient at capturing the BRB response, and calibration to experimental results was investigated for completion.

The theoretical model explores the use of an elastic foundation on an elastic-plastic bar with differing cross-sections. The theoretical model is intended to predict the magnitude of first buckling (tension and/or compression) and subsequent backbone curve. This model only considers elastic behaviour of the bar (core) and can be used in conjunction with the restraining mechanism, or the two forming components (restraining medium or outer casing). The theoretical magnitude of first buckling will be compared to the nominally identical experimental specimen results in Chapter 3 (specimens C-VS2-E2-200-R80A, C-VS2-E2-200-R80B and C-VS2-E2-200-R80C).

## 4.2 Numerical model

Numerical modelling using finite element analysis (FEA) software Abaqus/CAE 2017 was carried out to investigate suitability of evaluating the BRB performance. This method is cost effective in comparison to experimental analysis; however, the present author does not believe it should replace experimental verification regardless of the demand. To date, the yielding region of composite BRBs have been evaluated, where full BRB models of all-steel BRBs have been successful. The composite models previously developed were semi-empirical, imposing constraints to qualify the FEA model to that of previous experimental testing. The FEA models in the following

sections will be developed empirically with no additional constraints applied, and where unsuccessful, semi-empirical methods will be explored. The models themselves will be evaluated with respect to the successful nominal specimen experimental testing and also alongside one another.

### 4.2.1 Model definition

A single model was developed, with varying material definition complexity to evaluate BRB response. Due to symmetry, half of the model was developed, and appropriate mid-span boundary conditions introduced. The model was geometrically based on the successful nominal experimental specimens. Four variations of the model were evaluated. The first variation (M1) represented simple isotropic strain hardening of the steel core and plastic response of the restraining medium.

The second variation (M2) extended the steel plasticity profile based on steel tensile test results. The restraining medium was reduced to an elasto-plastic model to aid convergence. The third variation (M3) expands the steel plasticity profile to combined isotropic kinematic hardening, calibrated with respect to nominal specimen experimental hysteretic response. The fourth and final variation (M4) expanded the backstress relationships developed within M3 incorporating additional isotropic hardening parameters. All models were processed in dynamic explicit double time.

### 4.2.2 Geometric definition

All models were developed using the geometrical specification of the nominal specimens (Figure 4-1). The outer casing was specified as a 200 mm x 200 mm S4R (conventional stress-displacement shell with four nodes and reduced integration) with an assigned uniform thickness of 4 mm. The outer casing was assumed to be uniform in nature and did not consider the longitudinal weld and C-section lips present in the experimental testing specimens. The core and stiffeners were modelled as a S4R shell, excluding the stiffener welds and the core-transition region radii. The core and stiffeners were assigned a thickness of 10 mm. The unbonding medium of 2 mm thickness was modelled as a void surrounding the core, stiffeners and bearing region in all planes. The bearing region was also specified as a void. The grout-restraining medium occupies the remaining volume between the unbonding medium and outer casing inner surface and is modelled as a C3D8R element (continuum stress-displacement three-dimensional solid with eight nodes and reduced integration).

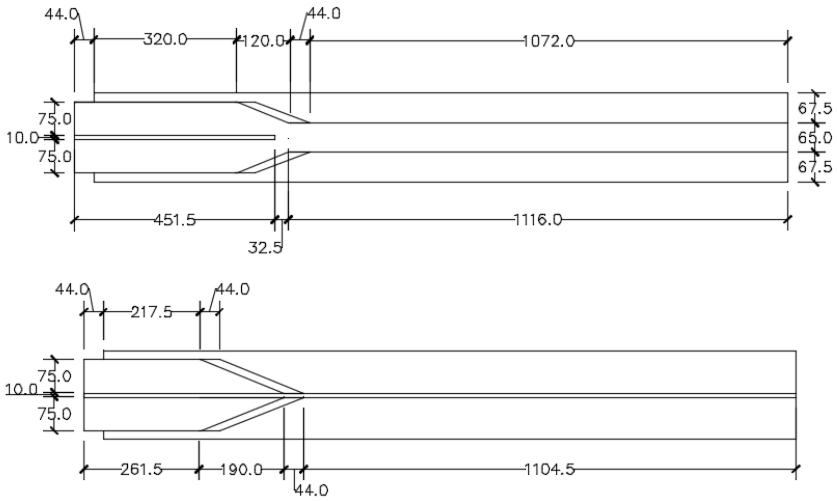


(c)

**Figure 4-1: Model schematic**

### 4.2.3 Material definition

#### *4.2.3.1 Steel*

The core and outer casing were defined as steel, based on the average tensile testing results of Easy Steel One (Table 4-1) and the mill certificate supplied for the outer casing. The true stress ($\sigma_{true}$) and plastic strain ($\varepsilon_p$) were calculated as follows:

$$\sigma_{true} = \sigma_{nom}(1 + \varepsilon_{nom}) \quad \text{(Equation 4-1)}$$

$$\varepsilon_p = \ln(1 + \sigma_{nom}) - \frac{\sigma_{true}}{E} \quad \text{(Equation 4-2)}$$

where: $\sigma_{nom} > f_y$

M1 used a two point steel definition system, based on the yield stress and ultimate tensile stress (Table 4-1). This was expanded for M2 to include additional points for the core based on the tensile results (Table 4-2).

**Table 4-1: Summary of steel material properties M1**

| | Material property | Average nominal stress, $\sigma_{nom}$ (MPa) | Average nominal strain, $\varepsilon_{nom}$ | True stress, $\sigma_{true}$ (MPa) | Plastic strain, $\varepsilon_p$ |
|---|---|---|---|---|---|
| **Core** | Yield stress, $f_y$ | 347.05 | 0.0017 | 347.62 | 0 |
| | Ultimate tensile stress, $f_{ult}$ | 493.10 | 0.1150 | 549.81 | 0.106 |

**Table 4-2: Summary of steel material properties M2**

| | **Material property** | **Average nominal stress, $\sigma_{nom}$ (MPa)** | **Plastic strain, $\varepsilon_p$** |
|---|---|---|---|
| **Core** | Yield stress, $f_y$ | 347.05 | 0 |
| | | 351.25 | 0.001 |
| | | 361.76 | 0.002 |
| | | 361.46 | 0.003 |
| | | 361.46 | 0.004 |
| | | 362.56 | 0.005 |
| | | 362.66 | 0.006 |
| | | 362.86 | 0.007 |
| | | 363.06 | 0.009 |
| | | 362.76 | 0.01 |
| | | 362.26 | 0.011 |
| | | 362.06 | 0.012 |
| | | 361.36 | 0.013 |
| | | 361.16 | 0.014 |
| | | 361.36 | 0.015 |
| | | 362.06 | 0.016 |
| | | 362.66 | 0.017 |
| | | 363.66 | 0.018 |
| | | 363.46 | 0.019 |
| | | 362.16 | 0.028 |
| | | 397.70 | 0.038 |
| | | 426.13 | 0.047 |
| | | 446.85 | 0.057 |
| | | 465.27 | 0.066 |
| | | 476.08 | 0.075 |
| | | 484.88 | 0.085 |
| | | 484.38 | 0.093 |
| | | 488.59 | 0.102 |
| | Ultimate tensile stress, $f_{ult}$ | 493.10 | 0.106 |
| **Outer Casing** | Yield stress, $f_y$ | 308.00 | 0 |
| | Ultimate tensile stress, $f_{ult}$ | 432.00 | 0.297 |

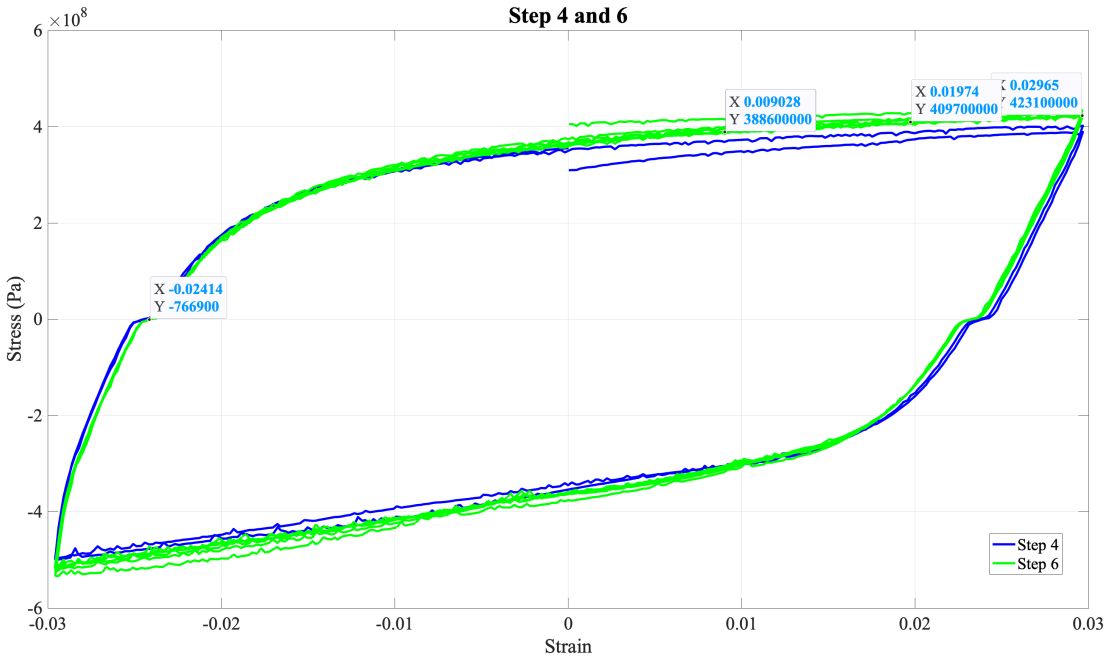


**Figure 4-2: C-VS2-E2-200-R80C Stress-strain response at 1.5 x drift**

In addition to the plastic strain points, M3 and M4 were expanded to include combined kinematic hardening of the core. The combined hardening parameter allows capture of both the cyclic and monotonic behaviour of the steel. This allows capture of the Bauschinger effect, which is characterised by the reduction in yield stress upon load reversal post plastic deformation. The addition of the kinematic hardening factors calculated through backstress evaluation allows the non-linear shape to be captured. Backstresses were calculated based on the cyclic response at 1.5 x drift of C-VS2-E2-200-R80C (Figure 4-2). The isotropic hardening factors were calculated as follows:

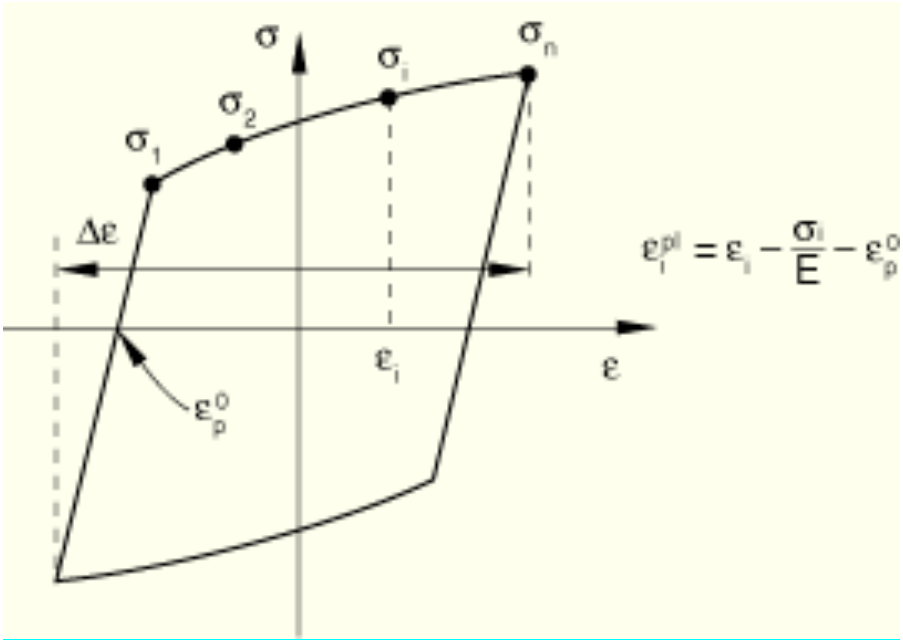


**Figure 4-3: Backstress calculation from stress-strain response**

$$\sigma_0 = f_y$$

$$\varepsilon_i^{pl} = \varepsilon_p$$

$$\varepsilon_i^{pl} = \varepsilon_i - \frac{\sigma_i}{E} - \varepsilon_p^o \qquad \text{Equation 4-3}$$

$$\alpha = \frac{C}{\gamma}\left(1 - e^{-\gamma\varepsilon_i^{pl}}\right) + \alpha_1 e^{-\gamma\varepsilon_i^{pl}} \qquad \text{Equation 4-4}$$

$$\alpha_i = \sigma_i - \frac{(\sigma_0 + \sigma_n)}{2} \qquad \text{Equation 4-5}$$

$$C = \frac{\sigma_i - \sigma_0}{\varepsilon_i^{pl}} \qquad \text{Equation 4-6}$$

where:
$\alpha$ = backstress
$C$ = kinematic hardening modulus
$\gamma$ = kinematic hardening parameter

**Table 4-3: Core backstress factors**

| $C$ (Pa) | 910000000 | 1330000000 | 1495000000 | 1454000000 |
|---|---|---|---|---|
| $\gamma$ | 152 | 375 | 55 | 74 |

In addition to the backstress factors, M4 incorporated two additional factors for cyclic loading, $Q$ and $b$. $Q$, an isotropic hardening factor is based on the yield stress of the

material, taken as 120 MPa. *b* represents the rate in which isotropic hardening stabilises, the lower this value, the slower the rate of stabilisation, *b* was taken as 5.

#### *4.2.3.2 Grout*

The restraining medium was defined as grout, based on the average of the 28-day and day of test compression cylinder strength tests for all three nominal specimens (Appendix E). The average compression cylinder strength was taken as 50.71 MPa and was evaluated to determine the concrete damage plasticity model based on the Drucker-Prager Hardening theory. The Drucker-Prager Hardening theory is used to evaluate elastic-plastic materials in which the compressive yield strength is greater than the tensile strength. The theory allows for hardening and softening of the material isotropically and generally allows for volume change with inelastic behaviour.

**Table 4-4: Concrete damaged plasticity, compressive behaviour state**

| Yield stress (Pa) | Inelastic strain |
|---|---|
| 20284000 | 0 |
| 38032500 | 0.00020394 |
| 50710000 | 0.00115059205030138 |
| 45075555.56 | 0.00395163737804567 |
| 20172222.2 | 0.00708277 |
| 507100 | 0.01052915 |

The restraining medium was specified with a uniform distribution and mass density of 2200 kg/m$^3$, isotropic in nature and undergoing long-term viscoelasticity. The Young's modulus and Poisson's ratios for elastic behaviour were specified as 34138769763.75 Pa and 0.2 respectively. For the concrete damaged plasticity specification, three states are considered; compression, plastic and tensile. The compressive behaviour is determined using the Drucker-Prager Hardening theory and the resulting values are summarised in Table 4-4. The plastic state requires the minimum specification of the dilation angle, 30°; the flow potential eccentricity which is the rate in which the hyperbolic flow potential approaches its asymptote, 0.1; the ratio of initial equibiaxial compressive yield stress required to initiate the uniaxial compressive yield stress, 1.16; the ratio of the second stress invariant on the tensile meridian to the compressive meridian, 0.6666; and the viscosity parameter, 0. The tensile behaviour is specified as GFI, defining post-cracking behaviour. The yield stress and fracture energy are taken as 2500000 Pa and 50 J, respectively.

The concrete damage plasticity model was only considered within M1, within M2 - M4, the restraining medium was represented by an elasto-plastic definition, where the plasticity of the medium was not captured.

### 4.2.4 Material density and contact definition

Each part (core, restraining medium, outer casting, etc.) was independently meshed to form a material density. The core had the most refined (most dense mesh) as it was the part with the highest value in required output. The restraining medium was less dense than the core, but of higher density than the coarse outer casing. For all models the core and outer casing underwent linear meshing (quad-dominant), with the restraining medium quadratic meshing (tet) (Figure 4-4). Isolated nodes within key areas; yielding-transition junction, stiffener origin and stroke were used for output.

The interaction between the parts was classified as general contact between all surface pairs. This general contact was assigned a tangential frictionless behaviour with the normal behaviour pressure-overclosure specified as “hard” contact. By assigning a frictionless contact interaction, no additional stresses will be developed when a part moves against another part, and all surfaces in contact slide freely without friction. The “hard” pressure-overclosure uses a penalty contact enforcement within the analysis.

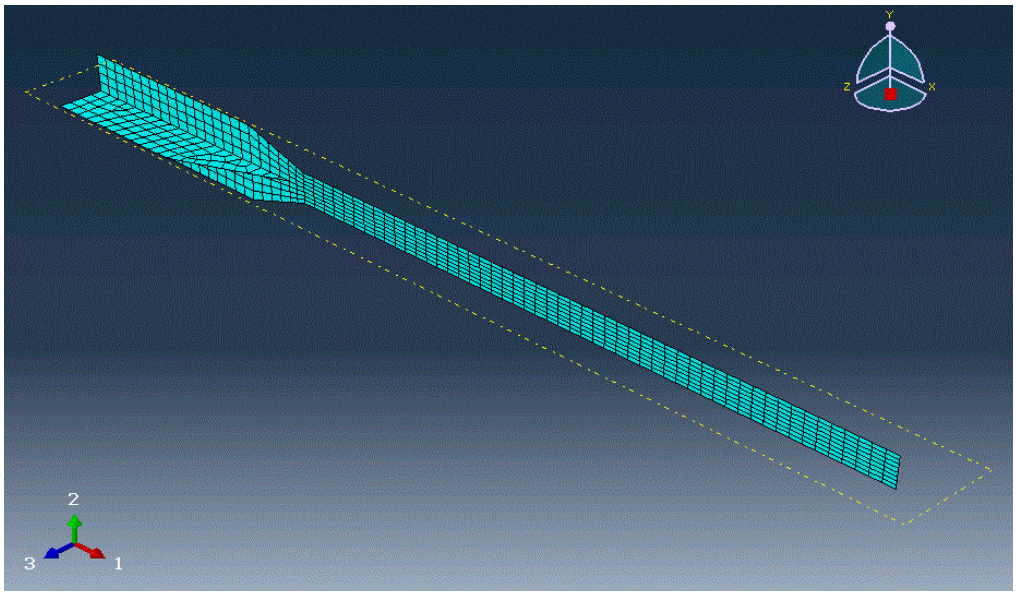


(a)

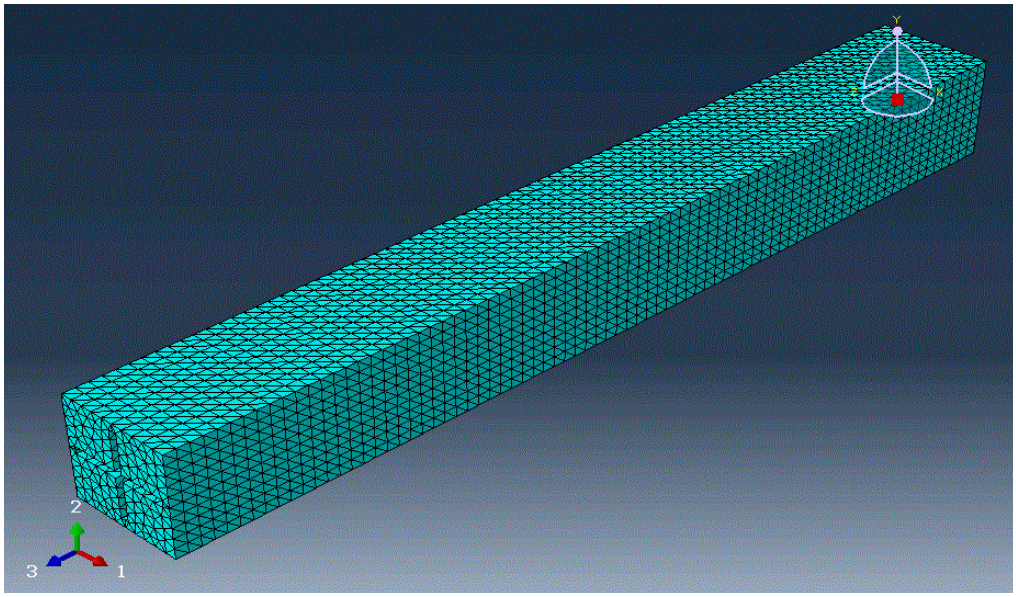


(b)

**Figure 4-4: Mesh density (a) core (b) restraining medium**

### 4.2.5 Boundary conditions and loading

The analysis of the given models was carried out over three steps; the initial set up step, gravity and amplitude steps. Within these steps, boundary conditions are established, and in some cases are step-specific. Each step considers a different load or displacement control and the following sub-sections detail these.

#### *4.2.5.1 Boundary conditions*

Boundary conditions were applied throughout the initial, gravity and amplitude steps at the "midspan" end of all parts, displacement application point "actuator" and the outer casing base. The midspan boundary condition (present within all steps) was applied to represent the midpoint of the BRB and also the model simplification due to symmetry that only half the specimen requires modelling. This boundary condition can be summarised as restrained from displacement in the U3 plane and rotation in the U1 and U2 planes.

The actuator, which is a point 10 mm from the centre of the core stroke, is the position in which the displacement loading occurs in the amplitude step. The actuator is kinematically coupled to the core end, such that uniform distribution of the dynamic explicit loading occurs. This point is fixed from displacement and rotation in all directions. Within the gravity-loading step, the outer casing base corners are restrained from displacement within the U2 plane. This boundary condition restricts the model from displacing in the U2 plane under gravity loading, capturing the gravity effects on the model.

#### *4.2.5.2 Load specification*

The gravity step was controlled by the application of a gravity load, -9.81 m/s$^2$ applied to all parts of the model in the U2 direction through a smooth step (Figure 4-5). The gravity load was uniform, and the smooth step was instigated instantaneously at the start of the gravity step. The gravity load, once applied, was continuous throughout the subsequent amplitude step.

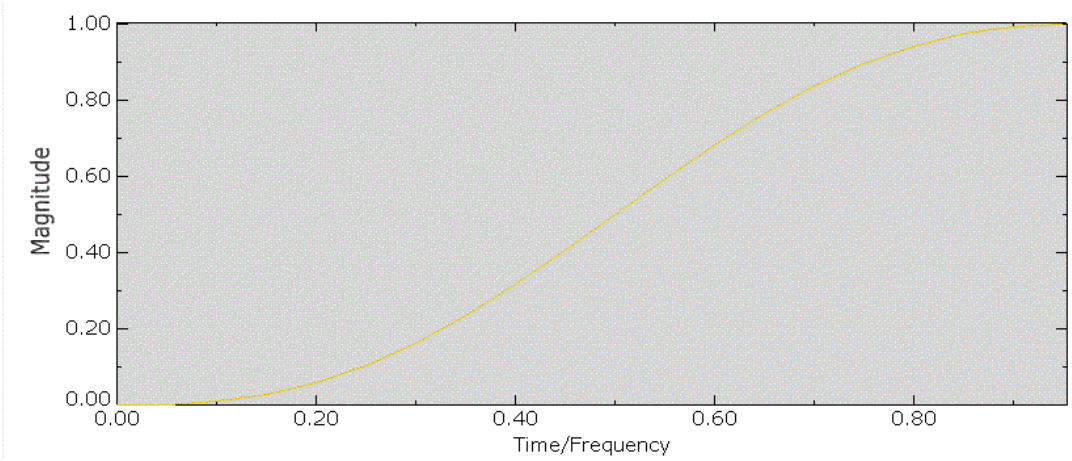


**Figure 4-5: Smooth step application of gravity load**

The application of a displacement-controlled loading program was applied in the amplitude step. This programme was applied in the U3 direction at the actuator point. The displacement programme was uniform in distribution and as a result of the actuator-core coupling, was applied evenly across the core and stiffener edge. The displacement programme was the same as that applied in experimental testing and can be found in Appendix B. The displacement programme was smoothed to reduce sudden interaction errors (Figure 4-6).

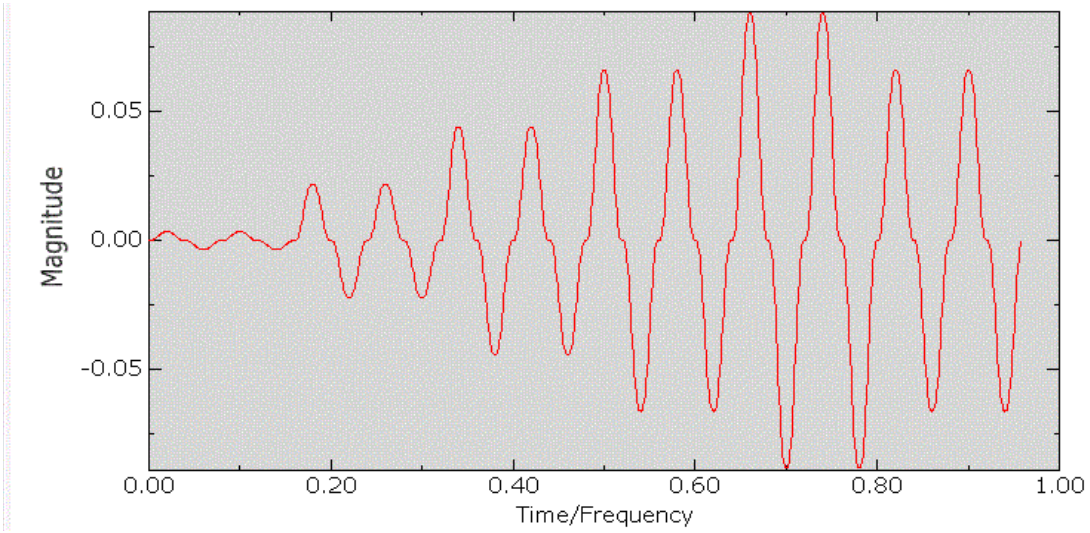


**Figure 4-6: Displacement programme, smoothed, applied in amplitude cycle**

### 4.2.6 Analysis application

Three linear steps are considered within the dynamic, explicit analysis; initial, gravity and amplitude. Prior to this application, the natural frequency must be determined for the model. This is carried out through linear perpetration with a natural frequency, $f$, a time period of 2.9 s was adopted for the amplitude step based on the ninth mode buckling of the core. The time period for the gravity step is calculated by:

$$time\ period = 10 \times \frac{1}{f}$$

A total number of 44 steps are considered within analysis, occurring at 0 mm displacement and the peak of each cycle in tension in compression. Due to the computational time for the model to run, subsequent mid-steps were not evaluated. Non-linear geometry is considered in each step with full analysis of the model carried out with double precision.

### 4.2.7 Evaluation of results

#### *4.2.7.1 Model 1*

M1 was unable to successfully complete the full displacement programme, however it completed the two yielding cycles, failing through instability prior to compression unloading. The model exhibited the highest stress within the bearing region (gap), with Abaqus/CAE 2017 aborting due to the inability to converge this region (Figure 4-7). The stiffeners also displayed contact stress with the restraining medium at the loading end, with the outer casing also showing signs of stress within this region. The restraining medium remained constant in stress distribution through the completed cycles. The yielding force of the core was recorded at 149.382 kN, 1.46 times lower than the average experimental yield, 218.30 kN.

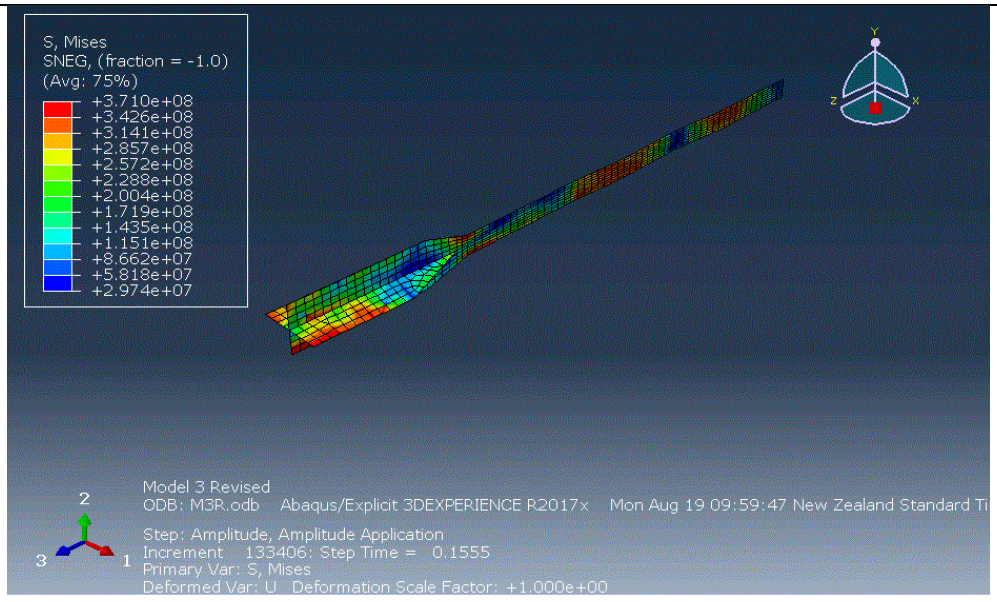


Core

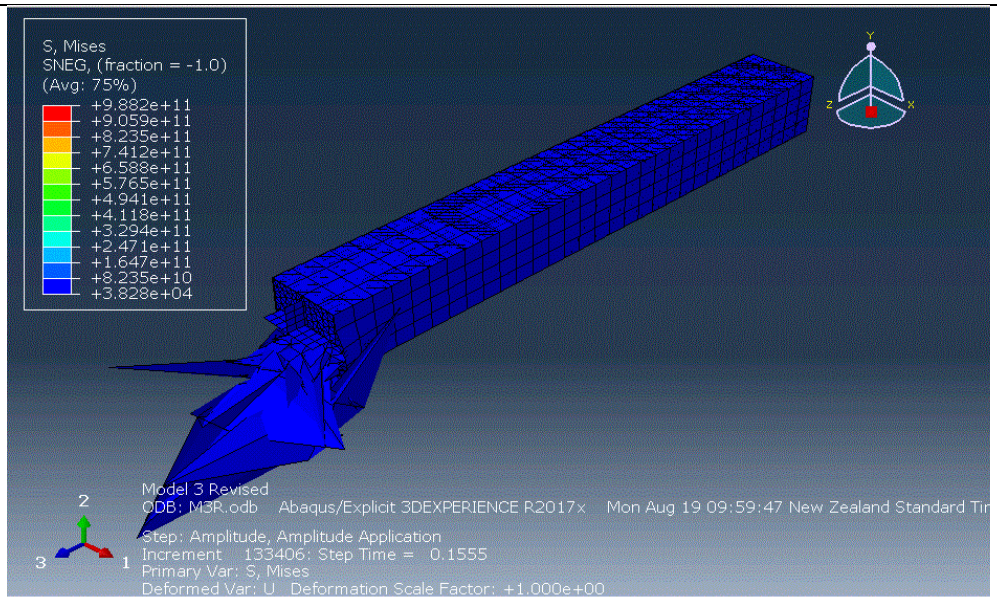


Restraining Medium

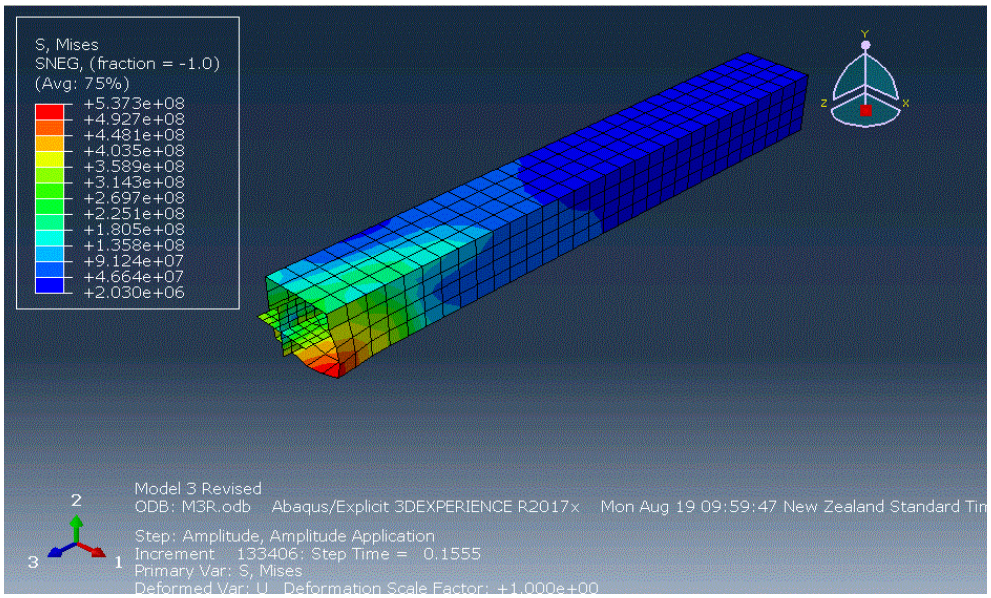


Core and Outer Casing

**Figure 4-7: M1 failure**

#### *4.2.7.2 Model 2*

M2 considered an elasto-plastic material definition for the restraining medium. The restraining medium and outer casing remained elastic throughout the loading protocol, with plasticity localised to the core part only. The steel model was expanded to include multiple stress-plastic strain points with respect to the tensile testing. M2 was unsuccessful in completing the full loading protocol, however completed up and including 2 x drift cycle. The response degraded/softened in tension (Figure 4-8) alluding to cyclic strain hardening occurring and calibration to experimental results required to capture the steel hardening profile.

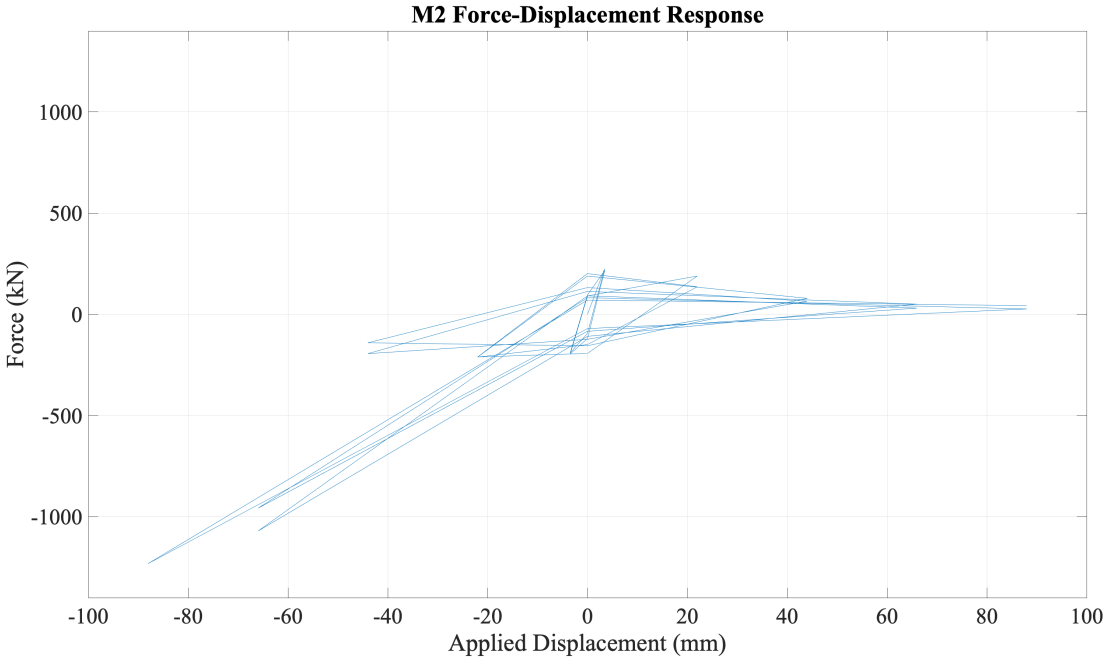


**Figure 4-8: M2 Force-Displacement Response**

#### *4.2.7.3 Model 3*

M3 introduced material calibration of the steel core through the evaluation of backstresses. This model is referred to as a semi-empirical model. Four kinematic hardening backstress properties were used, calibrated from the 1.5 x drift cycles of C-VS2-E2-200-R80C, these properties are represented as $C$, kinematic hardening modulus and $\gamma$, kinematic hardening parameter. These factors represent the Bauschinger effect, the reduced yield stress upon reverse cyclic loading. Through application of the Bauschinger effect, both the tension and compression hardening can be represented, with the tension and compression loads stabilising and maintained at higher strains.

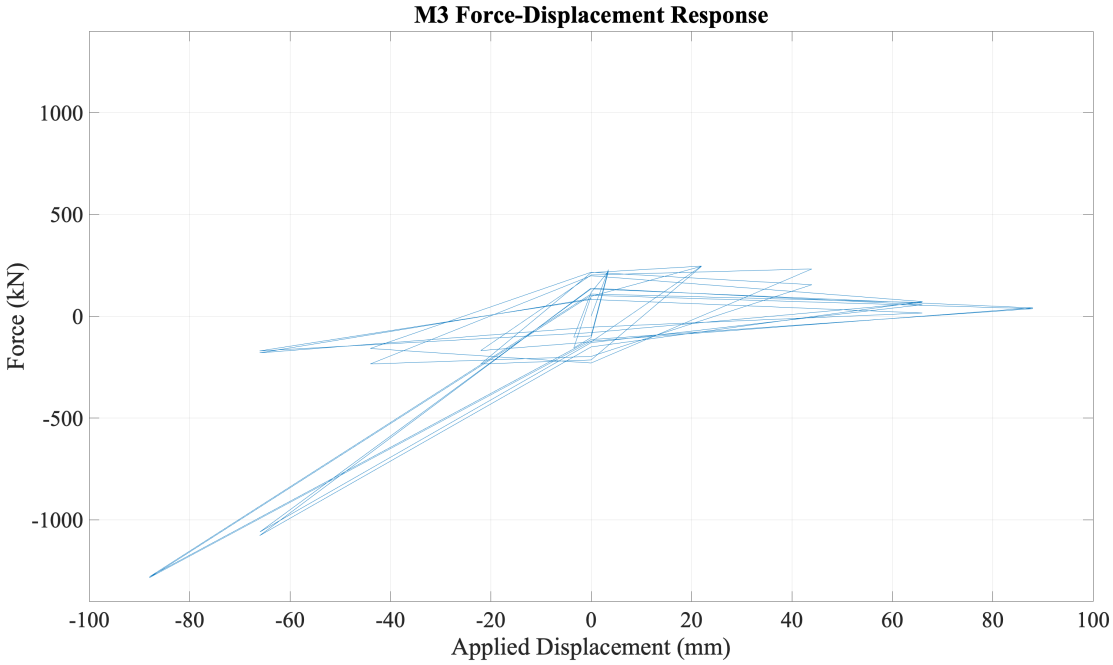


**Figure 4-9: M3 Force-Displacement Response**

Figure 4-9 shows the force-displacement output. The tension response, although softening, has improved when compared to M2. The output, although not fully capturing the cyclic hardening of the steel core in the higher displacements, is forming a hysteretic response tending to that observed experimentally. The compression hardening has been captured up too 1.5 x drift, with a significant increase in load at 2.0 x drift.

#### *4.2.7.4 Model 4*

M4 introduced isotropic hardening cyclic material stabilisation factors, $Q$ and $b$, to reduce the rate of softening of tension response and to stabilise both the tension and compression outputs.

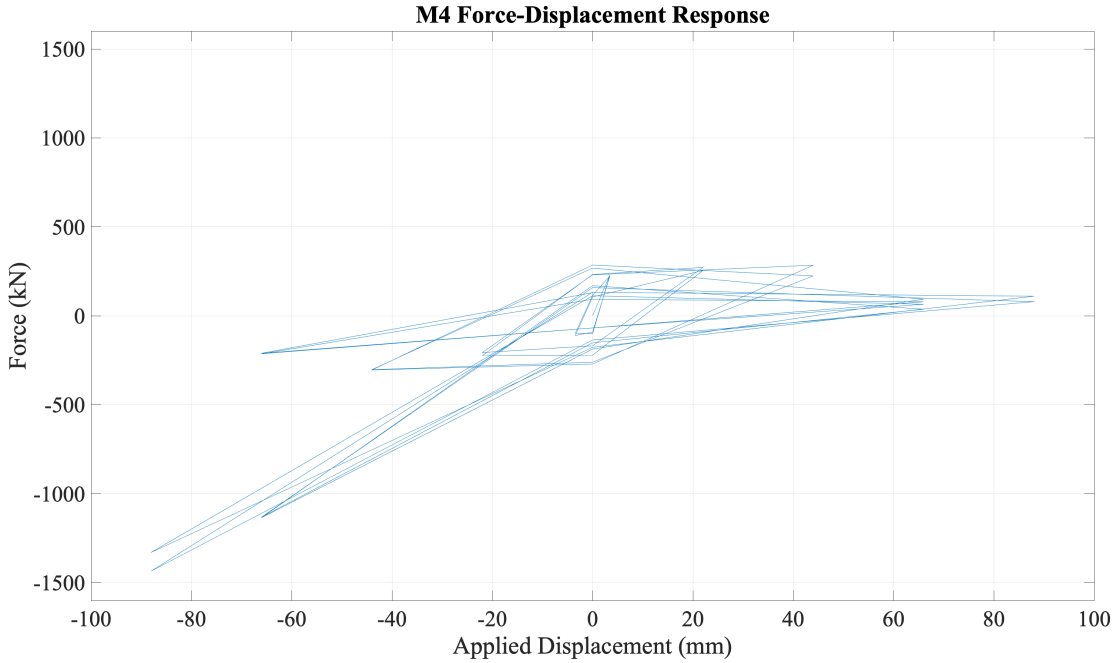


**Figure 4-10: M4 Force-Displacement Response**

Figure 4-10 shows the force-displacement output of M4. The cycles up to and including 1.0 x drift have stabilised, with softening occurring in tension at the 1.5 x drift cycle. The first 1.5 x drift compression cycle has stabilised, with degradation occurring in the subsequent. A comparison between the FEA and experimental response is demonstrated within Figure 4-11, with up to 1.0 x drift adequately captured by M4. It can also be observed that the elastic yield (initial cycle) is equivalent to M4 core yield. It is recommended that further experimental testing of BRBs to calibrate the backstresses be carried out, with cycling at a higher drift (such as 3.0 x drift) to capture a larger range for calibration, and different material stabilisation factors investigated.

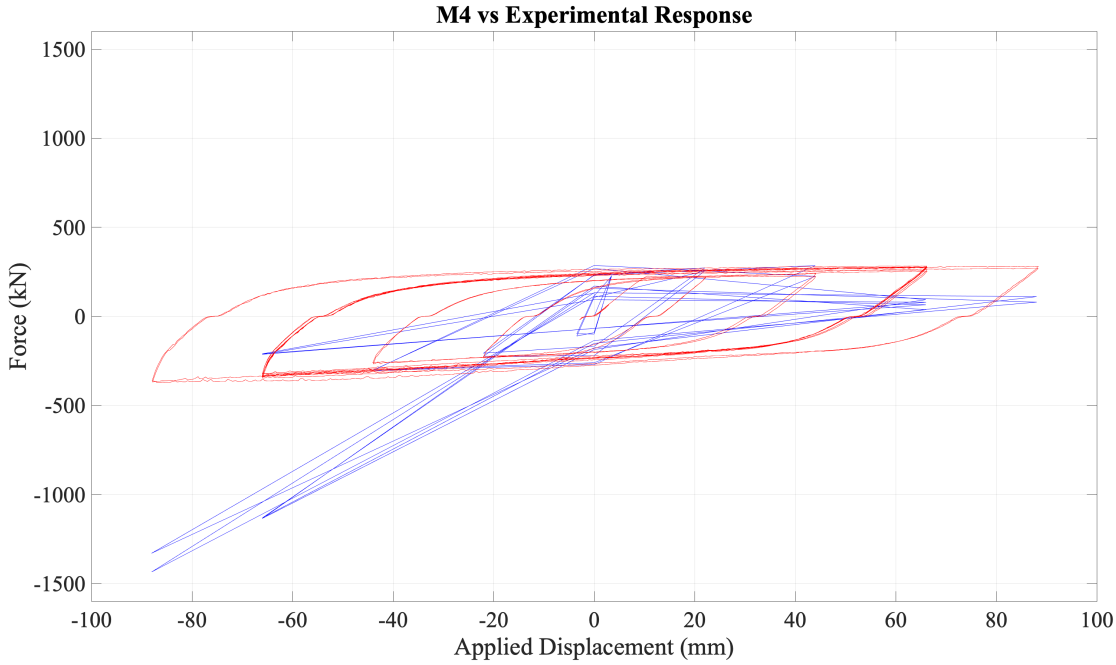


**Figure 4-11: M4 verses C-VS2-E2-200-R80C**

### 4.2.8 Numerical modelling general comments

The empirical and semi-empirical numerical modelling was unsuccessful in adequately predicting BRB performance and behaviour. M4 provided a reasonable approximation up to 1.0 x drift. With further investigation into the relationship between kinematic strain hardening models and backstress calculations with respect to BRBs is required to capture the hardening within the latter cycles and identify areas of vulnerability. The material definition of the restraining medium, although common in practice, was unable to capture the response and behaviour when interacting independently of the core and outer casing elements (non-composite behaviour).

Within New Zealand, there is a demand to adequately predict the BRB performance, response and behaviour through empirical numerical modelling. This has been shown through M1 and M2 to be problematic. It is recommended that experimental testing be carried out for all BRB designs, to validate and also highlight any performance constraints.

Semi-empirical methods have been developed with success (Lin P-C et al., 2015; Takeuchi T et al., 2012), and these models were developed based on experimental results. Takeuchi *et al.* developed their model based on a local buckling wavelength approximately 4 times the core plate width, determined from experimental results. This wavelength was imposed through the use of boundary conditions, influencing the models behaviour. Additional boundary conditions were not imposed on the semi-empirical models M3 and M4, rather using material definition calibrated to

experimental specimens. The successfully developed semi-empirical models within literature only considered the yielding core, ignoring the bearing region and non-yielding regions. The boundary conditions imposed are based on the full member and are assumed to be representative of the yielding region alone. The relationships found through semi-empirical methods are only applicable to the specified design and as such material calibration, although specific, has a wider range of application than a single design.

## 4.3 Theoretical model

Theoretical models were developed to evaluate the accuracy in predicting the compression strength at core yield (0.2 % core strain), and in conjunction with (Saxey B & Daniels M) detailed in Section 2.3.1, the expected maximum compression strength at 2 % core strain. It is important to note that the theoretical models are not intended to be used as a primary design tool, however in the case where experimental verification has not been evaluated for already implemented BRB, the theoretical models can provide a basic force-displacement relationship with respect to specific BRB variables.

The theoretical models were developed using the equilibrium and energy methods. Both methods were used to demonstrate the progression of influence when the number of contributing variables (core geometry, restraining mechanism, etc.) within the equation increases. By increasing the number of influencing variables, the sensitivity, performance of the BRB and deviation of the two methods can be visualised.

The equilibrium method was used to demonstrate a simple and methodical approach to BRB behaviour. This method assumes equilibrium, however it does not account for situations where solutions do not exist. The energy method was used due to its approximation of elastic solutions where exact solutions of a system may not exist. The non-complex solution of the energy method also allows rapid evaluation of a BRB design where a number of variables are present. Both methods consider elastic behaviour only and assume the BRB is symmetric in two planes.

### 4.3.1 Case one – pinned column with axial load

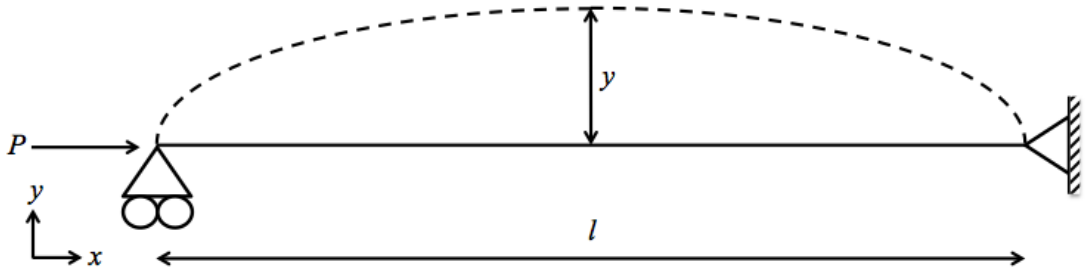


**Figure 4-12: Pinned column with axial load**

The progression of the models originates from an axially loaded pinned column (Figure 4-12). The equilibrium method considers a second order linear, homogeneous condition where the solutions are controlled by the boundary conditions. Moment equilibrium is assumed throughout. The energy method assumes an initial buckling shape of the column and evaluates the internal buckling strain energy equal to that of the external work produced by the applied axial load. Both methods produce the fundamental Euler equation for column buckling, Equation 4-7.

$$P = \frac{\pi^2 EI}{l^2} \qquad \text{Equation 4-7}$$

where:

$P$ Axial load
$E$ Young's modulus of column
$I$ Second moment area of column
$l$ Length of column

### 4.3.2 Case two – pinned column with axial load and elastic foundation

Case one is expanded to include the restraining mechanism, by the use of a uniformly distributed load (UDL) (***equilibrium method,*** Figure 4-13) or an elastic foundation (***energy method,*** Figure 4-14). This can be used to evaluate the restraining medium, outer casing, or both restraining mechanism variables and their contribution to restraining the elastic BRB core. The equilibrium method is solved with respect to the deflection of the column based on the applied/critical axial load. Alternatively, the energy method is solved with respect to the critical load of the column based on an assumption of the number of sine waves present in the column deflection. Both methods are summarised below.

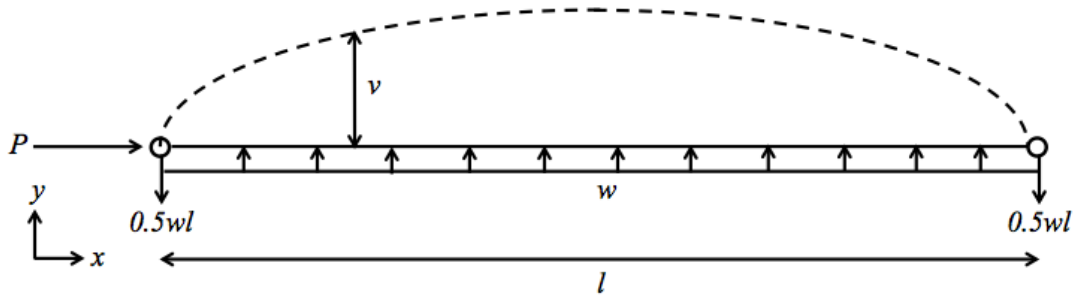


**Figure 4-13: Pinned column with axial load and uniformly distributed load, equilibrium method**

The ***equilibrium method*** assumes moment of equilibrium of the bar with the moment developed by the applied load (sum of all moments equals zero), and is summarised as:

$$-Pv - \frac{wlx}{2} + \frac{wx^2}{2} = EI\frac{d^2v}{dx^2} \qquad \text{Equation 4-8}$$

where:

$v$ $y$ axis deflection at length $x$
$w$ Uniformly distributed load
$x$ Distance along length, $l$

$$\alpha^2 = \frac{P}{EI} \qquad \textbf{(4-a)}$$

Equation 4-8 and ***(4-a)*** are rearranged:

$$\frac{d^2v}{dx^2} + \alpha^2 v = \frac{w\alpha^2}{2P}(x^2 - lx) \qquad \textbf{(4-b)}$$

***(4-b)*** is solved for deflection, $v$. The critical axial load, $P_{crit}$, is determined with respect to a critical allowable displacement.

$$v = \frac{w}{\alpha^2 P}\left[\cos\alpha x + \left(\frac{1-\cos\alpha l}{\sin\alpha l}\right)\sin\alpha x\right] + \frac{w}{2P}\left(x^2 - lx - \frac{2}{\alpha^2}\right) \qquad \text{Equation 4-9}$$

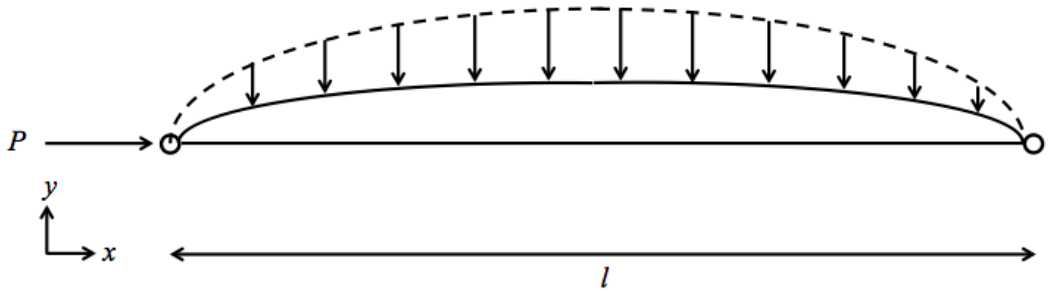


**Figure 4-14: Pinned column with axial load and elastic foundation, energy method**

The ***energy method*** assumes:

$$external\ work = bar\ strain\ energy + total\ deformation\ energy\ of\ elastic\ medium$$

The bar strain energy in bending ($U_b$) is:

$$\Delta U_b = \frac{EI}{2}\int_0^l \left(\frac{d^2y}{dx^2}\right)^2 dx \qquad \text{Equation 4-10}$$

An initial deflection, $y$, is assumed as:

$$y = \sum a_n \sin\frac{n\pi x}{l} \qquad \textbf{(4-c)}$$

$$\Delta U_b = \frac{\pi^4 EI}{4l^3}\sum_{n=1}^{n=\infty} n^4 a_n^2 \qquad \text{Equation 4-11}$$

where:

$a$ Maximum deflection (amplitude) of that mode

$n$ Number of half sine waves

The total deformation energy of the elastic medium ($U_f$) is:

$$\Delta U_f = 0.5\beta_e y^2 \qquad \text{Equation 4-12}$$

where:

$\beta_e$ Modulus of foundation, N/m$^2$

$\frac{k}{a}$ = spring constant of individual supports per distance between supports

$$\Delta U_f = \frac{\beta_e}{2}\int_0^l y^2 dx \qquad \textbf{(4-d)}$$

***(4-d)*** becomes:

$$\Delta U_f = \frac{\beta_e l}{4}\sum_{n=1}^{n=\infty} n^2 a_n^2 \qquad \text{Equation 4-13}$$

The external work ($T$) is:

$$\Delta T = P\lambda \qquad \text{Equation 4-14}$$

where:

$\lambda$ External deflection

$\lambda = 0.5\left(\frac{dy}{dx}\right)^2 dx$

$$\Delta T = \frac{P\pi^2}{4l}\sum_{n=l}^{n=\infty} n^2 a_n^2 \qquad \text{Equation 4-15}$$

$$external\ work = bar\ strain\ energy + total\ deformation\ energy\ of\ elastic\ medium$$

$$\Delta T = \Delta U_b + \Delta U_f \qquad \text{Equation 4-16}$$

Solving for $P$, with $n$ taken as 1:

$$P = \frac{\pi^2 EI}{l^2}\left(m^2 + \frac{\beta_e l^4}{m^2\pi^4 EI}\right) \qquad \text{Equation 4-17}$$

where:

$m$ Integer

$\frac{\beta_e l^4}{\pi^4 EI} = m^2(m+1)^2$

### 4.3.3 Case three – pinned column of varying cross-section with axial load

To include the varying cross-sectional area throughout the steel core, both methods were initially evaluated without the inclusion of a uniformly distributed load, or elastic foundation. A pin-pin column, symmetric at mid-span (Figure 4-15 b)) can be initially approximated by a fixed-free end column (Figure 4-15 a)) for ease of calculation.

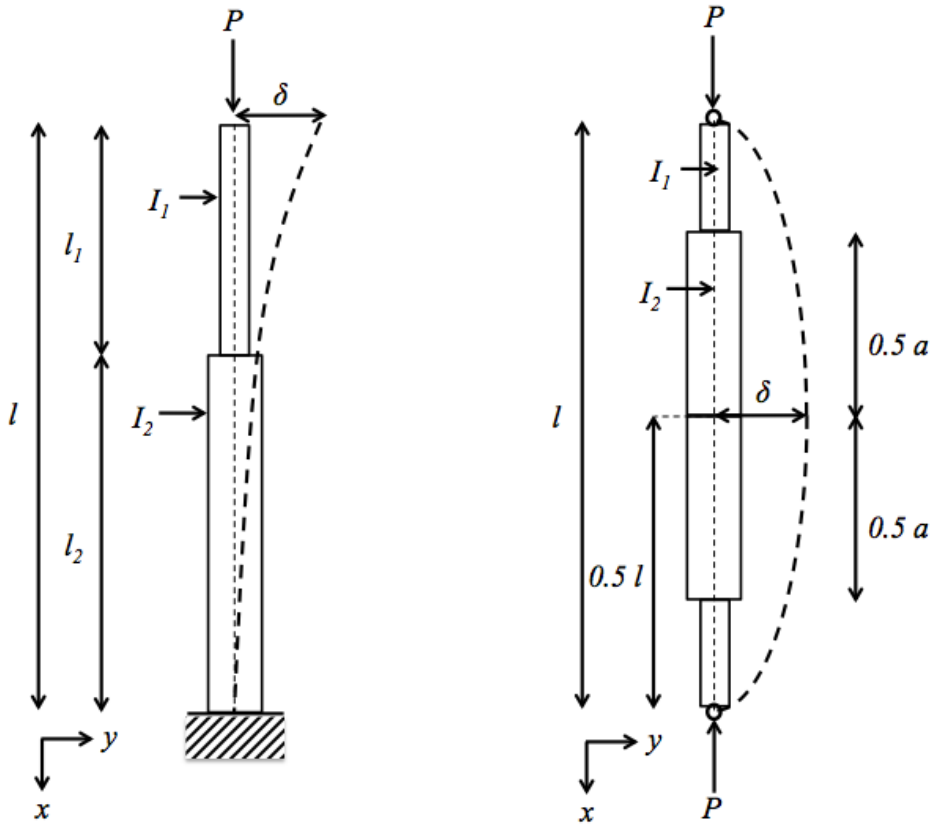


**Figure 4-15: a) Fixed-free column with varying cross-sectional area b) Pin-pin symmetric column with varying cross-sectional area**

The ***equilibrium method*** considers a second order linear, non-homogeneous condition where the solutions are controlled by boundary conditions. To accommodate the non-homogeneous nature of the fundamental equation, the second order equation is solved in two steps. The first step considers the equation as homogeneous, removing the non-homogeneity on the right-hand side of the equation and solving for zero. The second step assumes a particular integral, which is substituted and solved within the original fundamental equation. The final solution below is determined by including both the homogeneous complementary function and particular integral solution, solving for constants using the initial boundary conditions. This solution however is transcendental, a real or complex solution and trial and error is required to determine the final solution.

$$-EI_1\frac{d^2y_1}{dx^2} = P(\delta - y_1) \qquad \text{Equation 4-18}$$

where:

$I_1$ Second moment of area of section 1
$\delta$ Maximum $y$ deflection
$y_1$ $y$ deflection due to section 1

$$-EI_2\frac{d^2y_2}{dx^2} = P(\delta - y_2) \qquad \text{Equation 4-19}$$

where:

$I_2$ Second moment of area of section 2

$y_2$ $y$ deflection due to section 2

$$\alpha_1^2 = \frac{P}{EI_1} \qquad \textbf{(4-f)}$$

$$\alpha_2^2 = \frac{P}{EI_2} \qquad \textbf{(4-g)}$$

$$y_1 = A\cos\alpha_1 x + B\sin\alpha_1 + \delta \qquad \text{Equation 4-20}$$

where:

$A$ $-B\tan\alpha_1 l$

$B$ $\frac{\delta\cos\alpha_2 l_2\cos\alpha_1 l}{\sin\alpha_1 l_1}$

$$y_2 = \delta(1-\cos\alpha_2 x) \qquad \text{Equation 4-21}$$

At $\frac{dy}{dx}$, where $x = l_2$, $y_1$ and $y_2$ have equal tangents, resulting in the transcendental equation:

$$\tan\alpha_1\, l_1 \tan\alpha_2 l_2 = \frac{\alpha_1}{\alpha_2} \qquad \text{Equation 4-22}$$

where:

$l_1$ Length of section 1

$l_2$ Length of section 2

By substituting in the equivalent length of the pin-pin column, $\frac{a}{2}$ for $l_2$ and $\frac{l}{2}$ for $l$, the critical load can be summarised as:

$$P_{crit} = \frac{mEI_2}{l^2} \qquad \text{Equation 4-23}$$

Where m is a numerical factor that has been determined by (Timoshenko S. P & Gere J. M, 1989), and is summarised in Table 4-5.

**Table 4-5: Values of factor m (Timoshenko S. P & Gere J. M, 1989)**

| $\frac{I_1}{I_2}$ | $\frac{a}{l}$ | | | |
|---|---|---|---|---|
| | **0.2** | **0.4** | **0.6** | **0.8** |
| 0.01 | 0.15 | 0.27 | 0.60 | 2.26 |
| 0.1 | 1.47 | 2.40 | 4.50 | 8.59 |
| 0.2 | 2.80 | 4.22 | 6.69 | 9.33 |
| 0.4 | 5.09 | 6.68 | 8.51 | 9.67 |
| 0.6 | 6.98 | 8.19 | 9.24 | 9.78 |
| 0.8 | 8.55 | 9.18 | 9.63 | 9.84 |

The ***energy method*** is less arduous than the equilibrium method. An initial deflection of the column is assumed, *y*, and using integrals to represent the change in cross-sectional area the following relationship is solved (Figure 4-16). It is assumed due to symmetry that the internal energy for both halves is equal.

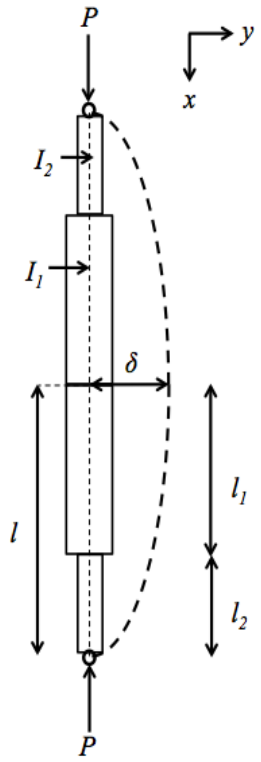


**Figure 4-16: Pin-pin axially loaded column with varying cross sectional area**

$$external\ work = bar\ strain\ energy$$

$$y = \delta \sin\frac{\pi x}{2l} \qquad \text{Equation 4-24}$$

The bar strain internal energy is:

$$\Delta U_b = \frac{P^2}{2EI}\int y^2 dx \qquad \text{Equation 4-25}$$

$$\Delta U_b = \frac{P^2\delta^2}{2EI_2}\left[\int_0^{l_2} \sin^2\frac{\pi x}{2l}dx + \frac{I_2}{I_1}\int_{l_2}^{l} \sin^2\frac{\pi x}{2l}dx\right] \qquad \textbf{\textit{(4-h)}}$$

Solving ***(4-h)*** provides the bar strain internal energy:

$$\Delta U_b = \frac{P^2\delta^2}{2EI_2}\left[\frac{l}{2\pi}\sin\pi\frac{l_2}{l}\left(\frac{I_2}{I_1}-1\right)+\frac{l_2}{2} + \frac{I_2}{I_1}\left(\frac{l-l_2}{2}\right)\right] \qquad \text{Equation 4-26}$$

The external work, Equation 4-14, becomes:

$$\Delta T = \frac{P\delta^2}{2}\int \frac{dy}{dx}dy \qquad \text{Equation 4-27}$$

By substituting and rearranging the derivative of *y*:

$$\Delta T = \frac{P\delta^2}{2}\int_0^l \frac{\pi^2}{4l^2}\cos^2\frac{\pi x}{2l}dx \qquad \textbf{\textit{(4-i)}}$$

$$\Delta T = \frac{P\delta^2\pi^2}{16l} \qquad \text{Equation 4-28}$$

Equating Equation 4-26 and Equation 4-28 provides the critical load for a pinned column axially loaded with varying cross-section area.

$$P = \frac{\pi^2 E I_2}{8l} \frac{1}{\left[\frac{l}{2\pi}\sin\pi\frac{l_2}{l}\left(\frac{I_2}{I_1}-1\right)+\frac{l_2}{2}+\frac{I_2}{I_1}\left(\frac{l-l_2}{2}\right)\right]} \qquad \text{Equation 4-29}$$

### 4.3.4 Case four – pinned column of varying cross-section with axial load and elastic foundation

Case four is an extension of case three with the additional application of an elastic foundation (Figure 4-17). The equilibrium method does not provide exact solutions when addressing varying cross-sectional area and is therefore not considered within case four. The ***energy method*** is simple in application and follows the same principle as case three above. The initial deflection is assumed as Equation 4-24.

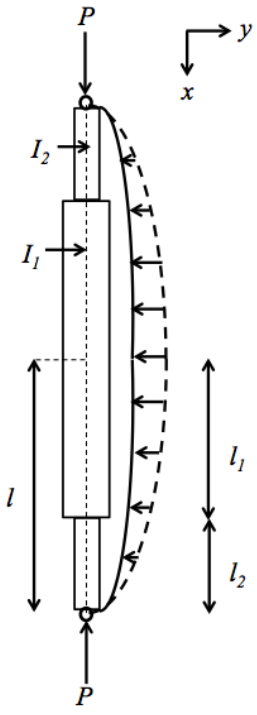


**Figure 4-17: Pinned column with axial load, elastic foundation and varying cross-sectional area**

The bar strain energy and external work can be taken as Equation 4-26 and Equation 4-28 respectively. The elastic medium energy is calculated below and shown in Equation 4-31.

$$\Delta U_f = \frac{\beta_e \delta^2}{2}\int_0^l \sin^2\frac{\pi x}{2l}\,dx \qquad \textbf{(4-j)}$$

$$\Delta U_f = \frac{\beta_e \delta^2}{2}\left[\frac{2l}{\pi}\left(\frac{\pi l}{4l}\right)\right] \qquad \text{Equation 4-30}$$

$$\Delta U_f = \frac{\beta_e \delta^2 l}{4} \qquad \text{Equation 4-31}$$

Solving Equation 4-16:

$$\frac{P\pi^2}{4l} = \frac{2P^2}{EI_2}\left[\frac{l}{2\pi}\sin\pi\frac{l_2}{l}\left(\frac{I_2}{I_1}-1\right)+\frac{l_2}{2} + \frac{I_2}{I_1}\left(\frac{l-l_2}{2}\right)\right]+\beta_e l \qquad \text{Equation 4-32}$$

### 4.3.5 Theoretical model representation

To compare the differing complexities present within each model, the models are calculated with respect to the geometrical and material properties of the experimentally tested nominal specimens. The average yield load and maximum compression loads of the nominal specimens are included for comparison. The stroke

is ignored, with two different lengths considered; the yielding core and the full length for the uniform bar case. The yielding core to transition region length and yielding core to non-yielding region length (transition and embedment regions) for varying bar cases. Both major and minor axis cases are considered for each case.

Stiffeners are present throughout the non-yielding region, with the average second moment of area for the transition region taken as the cross-sectional area at the centroid (approximately 80 mm from the yielding core to transition region radii). The centroid of the non-yielding region lies within the embedment region, and the subsequent second moment of area is calculated with this cross-sectional area.

The average yield of the nominal specimens from experimental testing is 218.3 kN, 97 % of the measure material yield of 225.6 kN from tensile testing. The average maximum compression capacity (stable) from the nominal specimens is 374.1 kN, and the average restraining medium compression strength is 50.7 MPa. Throughout nominal specimen testing, each specimen underwent both major and minor axis local buckling.

**Table 4-6: Theoretical evaluation using yielding core geometry, major axis**

| | | Equation | | | | | |
|---|---|---|---|---|---|---|---|
| | | **4-3** | **4-5** | **4-13** | **4-19** | **4-25** | **4-28** |
| **Case** | | **One** | **Two** | | **Three** | | **Four** |
| **Theoretical** | **Compression yield $P_{crit}$ (kN)** | 95.2 | 5130.0 | 3217.0 | 101.1 | 66.3 | 234.8 |
| | **Maximum compression $P_{crit,max}$ (kN)** | 137.1 | 7387.2 | 4632.5 | 145.6 | 95.5 | 338.1 |
| **Experimental** | **Yield strength $P_{Nom,avgfy}$ (kN)** | 218.3 | 218.3 | 218.3 | 218.3 | 218.3 | 218.3 |
| | **Maximum compression $P_{Nom,avgc}$ (kN)** | 374.1 | 374.1 | 374.1 | 374.1 | 374.1 | 374.1 |
| | **$\beta_{0.2\%}$** | 0.42 | 22.60 | 14.17 | 0.45 | 0.29 | 1.03 |
| | **$P_{crit}$ / $P_{Nom}$** | 0.37 | 20.00 | 12.50 | 0.40 | 0.26 | 0.90 |
| **$I$ ($m^4$)** | **$I_1$** | $2.29 \times 10^{-7}$ | $2.29 \times 10^{-7}$ | $2.29 \times 10^{-7}$ | $2.00 \times 10^{-9}$ | $2.29 \times 10^{-7}$ | $2.29 \times 10^{-7}$ |
| | **$I_2$** | | | | $2.29 \times 10^{-7}$ | $2.00 \times 10^{-9}$ | $2.00 \times 10^{-9}$ |

where $P_{crit,max} = \phi_{os} \times \beta_{2\%} \times P_{crit}$

$\phi_{os} = 1.2$

$\beta_{0.2\%}$ = 1.04
$\beta_{2\%}$ = 1.20

The four cases were evaluated, with results summarised in Table 4-6, Table 4-7, Table 4-8 and Table 4-9. The modulus of foundation was taken as 50.7 MPa where applicable, and the maximum theoretical compression load was determined based on the relationship, Equation 2-2:

$$N_{brace}^{oc} = \phi\beta\phi_{os}\phi_{om}f_yA_{sc}$$

where:

$\phi$ = 1.0

$\beta$ = Equation 2-8, $\beta = 4.97\varepsilon_{sc} + 1.10$

where: $\varepsilon_{sc}$ = 2 %, equivalent to 2.0 $\delta_{ui}$

$\phi_{os}$ = Equation 2-4, $\phi_{os} = 20.63\varepsilon_{sc} + 1.15$

where: $\varepsilon_{sc}$ = 0.2 %, assuming the ratio between tension and compression remains constant post yield

$\phi_{om}$ = 1.0

$f_yA_{sc}$ = $P_{crit}$

For evaluating the compression load at yield, the experimental load at yield in tension was modified through application of the compression overstrength factor (Equation 2-8) at $\varepsilon_{sc}$ = 0.2 %.

Two lengths were considered for Case one, the yielding core and full member length, along with both the major and minor axis geometry. Case one (Equation 4-7), evaluated using the yielding core length in the major axis (Table 4-6) underestimating the compression yield load and maximum compression load, with theoretical to experimental ratios of 0.42 and 0.37 respectively. In the minor axis (Table 4-7), Case one was significantly smaller than both the compression yield and maximum compression load, with theoretical to experimental ratios of 0.01 for both loads.

The opposite to that of using the yielding core full length was true when using the full member length, with the theoretically predicted compression yield and maximum compression load being significantly greater than that observed experimentally. In the major axis (Table 4-8) the theoretical to experimental ratios for compression yield and maximum compression load are 5.45 and 4.77 respectively, and in the minor axis (Table 4-9) 5.30 and 4.63 respectively.

**Table 4-7: Theoretical evaluation using yielding core geometry, minor axis**

| | | Equation | | | | | |
|---|---|---|---|---|---|---|---|
| | | **4-3** | **4-5** | **4-13** | **4-19** | **4-25** | **4-28** |
| **Case** | | **One** | **Two** | | **Three** | | **Four** |
| **Theoretical** | **Compression yield $P_{crit}$ (kN)** | 2.3 | 1858.3 | 482.5 | 4.5 | 1.8 | 234.8 |
| | **Maximum compression $P_{crit,max}$ (kN)** | 3.3 | 2676.0 | 694.8 | 6.5 | 2.6 | 338.1 |
| **Experimental** | **Yield strength $P_{Nom,avgfy}$ (kN)** | 218.3 | 218.3 | 218.3 | 218.3 | 218.3 | 218.3 |
| | **Maximum compression $P_{Nom,avgc}$ (kN)** | 374.1 | 374.1 | 374.1 | 374.1 | 374.1 | 374.1 |
| $\frac{P_{crit}}{\beta_{0.2\%}P_{Nom,avgfy}}$ | | 0.01 | 8.19 | 2.13 | 0.02 | 0.01 | 1.03 |
| $\frac{P_{crit,max}}{P_{Nom,avgc}}$ | | 0.01 | 7.15 | 1.86 | 0.02 | 0.01 | 0.90 |
| $I$ $(m^4)$ | $I_1$ | $5.42 \times 10^{-9}$ | $5.42 \times 10^{-9}$ | $5.42 \times 10^{-9}$ | $2.00 \times 10^{-9}$ | $5.42 \times 10^{-9}$ | $2.29 \times 10^{-7}$ |
| | $I_2$ | | | | $5.42 \times 10^{-9}$ | $2.00 \times 10^{-9}$ | $2.00 \times 10^{-9}$ |

The equilibrium method (Equation 4-9) for Case two considers a pinned column, with an axial load and UDL, converged to approximately 2 mm deflection (the thickness of the unbonding medium on one side of the core). In all cases the buckling capacity was overestimated, with the BRB member length and buckling within the major axis (Table 4-8) performing the best, with theoretical to experimental ratios of 2.87 and 2.51 for compression yielding and maximum compression load, respectively. The energy method (Equation 4-17) for Case two (elastic foundation) assumed that the critical load will occur when the core forms half a sine wave. As with the equilibrium method, all results were overestimated, with the yielding core length within the minor axis (Table 4-7) performing the best, with theoretical to experimental ratios of 2.13 and 1.86 for compression yield and maximum compression load respectively.

By introducing the variation in cross-sectional area in Case three, the predicted capacities within the major axis become more realistic (Table 4-6 and Table 4-8). The equilibrium method predicts larger values than the energy method, with theoretical to experimental ratios of 0.45 and 0.40 compared to 0.29 and 0.26 for compression yield

and maximum compression loads respectively. The minor axis in both the equilibrium (Equation 4-23) and energy method (Equation 4-29) (Table 4-7 and Table 4-9) underestimate the critical load significantly, with ratios between 0.01 – 0.02.

**Table 4-8: Theoretical evaluation using average core geometry, major axis**

| | | Equation | | | | | |
|---|---|---|---|---|---|---|---|
| | | **4-3** | **4-5** | **4-13** | **4-19** | **4-25** | **4-28** |
| **Case** | | **One** | **Two** | | **Three** | | **Four** |
| **Theoretical** | **Compression yield $P_{crit}$ (kN)** | 1238.1 | 651.8 | 16934.2 | 154.4 | 50.8 | 18833.5 |
| | **Maximum compression $P_{crit,max}$ (kN)** | 1782.9 | 938.6 | 24385.2 | 222.3 | 73.2 | 27120.2 |
| **Experimental** | **Yield strength $P_{Nom,avgfy}$ (kN)** | 218.3 | 218.3 | 218.3 | 218.3 | 218.3 | 218.3 |
| | **Maximum compression $P_{Nom,avgc}$ (kN)** | 374.1 | 374.1 | 374.1 | 374.1 | 374.1 | 374.1 |
| $\frac{P_{crit}}{\beta_{0.2\%}P_{Nom,avgfy}}$ | | 5.45 | 2.87 | 74.60 | 0.68 | 0.22 | 83.00 |
| $\frac{P_{crit,max}}{P_{Nom,avgc}}$ | | 4.77 | 2.51 | 65.18 | 0.59 | 0.20 | 72.49 |
| $I$ $(m^4)$ | $I_1$ | $5.79 \times 10^{-6}$ | $5.79 \times 10^{-6}$ | $5.79 \times 10^{-6}$ | $2.73 \times 10^{-5}$ | $2.29 \times 10^{-7}$ | $2.29 \times 10^{-7}$ |
| | $I_2$ | | | | $2.29 \times 10^{-7}$ | $2.73 \times 10^{-5}$ | $2.73 \times 10^{-5}$ |

Case four applying the energy method for a pinned column with axial load and elastic foundation with varying cross-sectional area (Equation 4-32) performed the best of the four cases. Both major and minor axis critical loads are equal for the two lengths considered, with the average geometry BRB length (yielding core-non-yielding region) significantly overestimating the critical load (Table 4-8 and Table 4-9). While the yielding core-transition region length (Table 4-6 and Table 4-7) provides a reasonable approximation of BRB performance observed within experimental testing of the nominal specimens, with theoretical to experimental ratios of 1.03 and 0.90 for compression yield and maximum compression load, respectively.

**Table 4-9: Theoretical evaluation using average core geometry, minor axis**

| | | Equation | | | | | |
|---|---|---|---|---|---|---|---|
| | | **4-3** | **4-5** | **4-13** | **4-19** | **4-25** | **4-28** |
| **Case** | | **One** | **Two** | | **Three** | | **Four** |
| **Theoretical** | **Compression yield $P_{crit}$ (kN)** | 1203.9 | 7058.6 | 16685.1 | 3.7 | 1.2 | 18833.5 |
| | **Maximum compression $P_{crit,max}$ (kN)** | 1733.6 | 10164.4 | 24026.5 | 5.3 | 1.7 | 27120.2 |
| **Experimental** | **Yield strength $P_{Nom,avgfy}$ (kN)** | 218.3 | 218.3 | 218.3 | 218.3 | 218.3 | 218.3 |
| | **Maximum compression $P_{Nom,avgc}$ (kN)** | 374.1 | 374.1 | 374.1 | 374.1 | 374.1 | 374.1 |
| $\frac{P_{crit,max}}{\beta_{0.2\%}P_{Nom,avgfy}}$ | | 5.30 | 31.10 | 73.50 | 0.02 | 0.01 | 83.00 |
| $\frac{P_{crit,max}}{P_{Nom,avgc}}$ | | 4.63 | 27.17 | 64.22 | 0.01 | 0.01 | 72.49 |
| $I$ $(m^4)$ | $I_1$ | $5.63 \times 10^{-6}$ | $5.63 \times 10^{-6}$ | $5.63 \times 10^{-6}$ | $2.73 \times 10^{-5}$ | $5.42 \times 10^{-9}$ | $2.29 \times 10^{-7}$ |
| | $I_2$ | | | | $5.42 \times 10^{-9}$ | $2.73 \times 10^{-5}$ | $2.73 \times 10^{-5}$ |

It is recommended that Case four, considering the yielding core and transition region length be used to evaluate BRB designs. The critical load in Case four can be used to adequately approximate the first compression yield of the specimen (Figure 4-18). In addition, by application of the compression overstrength and material overstrength factors determined by (Saxey B & Daniels M), the maximum compression load can be determined.

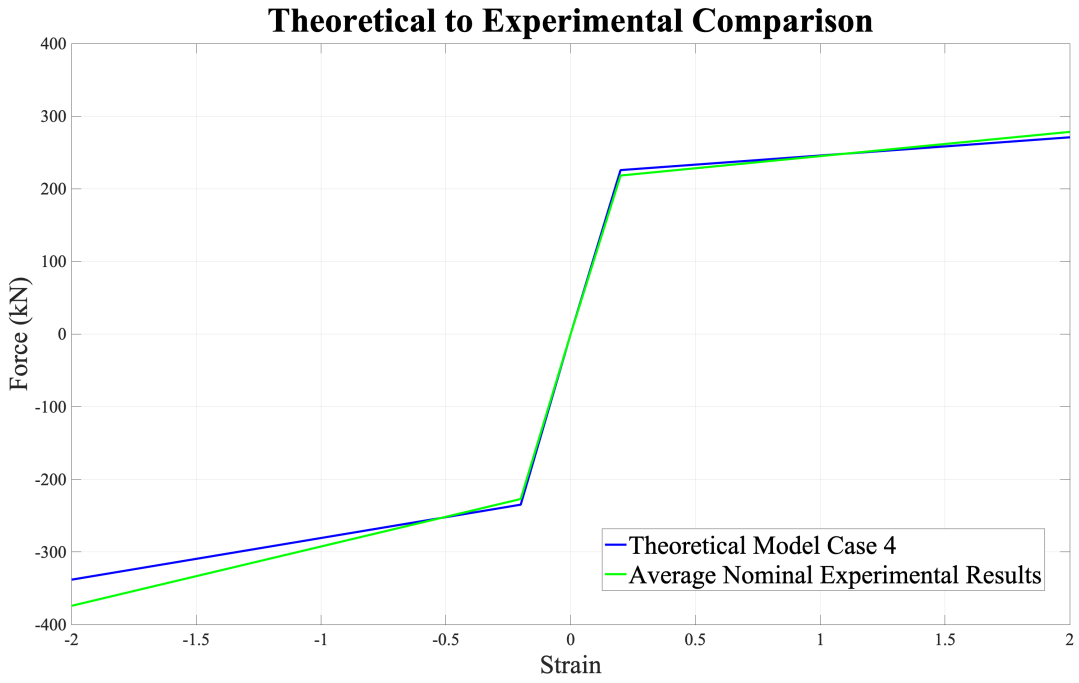


**Figure 4-18: Theoretical model Case 4 verses average nominal experimental results**

## 4.4 Theoretical model sensitivity analysis

Case four, Equation 4-32, is independent of deflection, solved through convergence of the external work to internal work with respect to the critical load. The restraining medium, $\beta_e$ (elastic foundation factor), can be modified to evaluate its contribution to the critical load. Figure 4-19 shows the relationship between the restraining medium and the critical load.

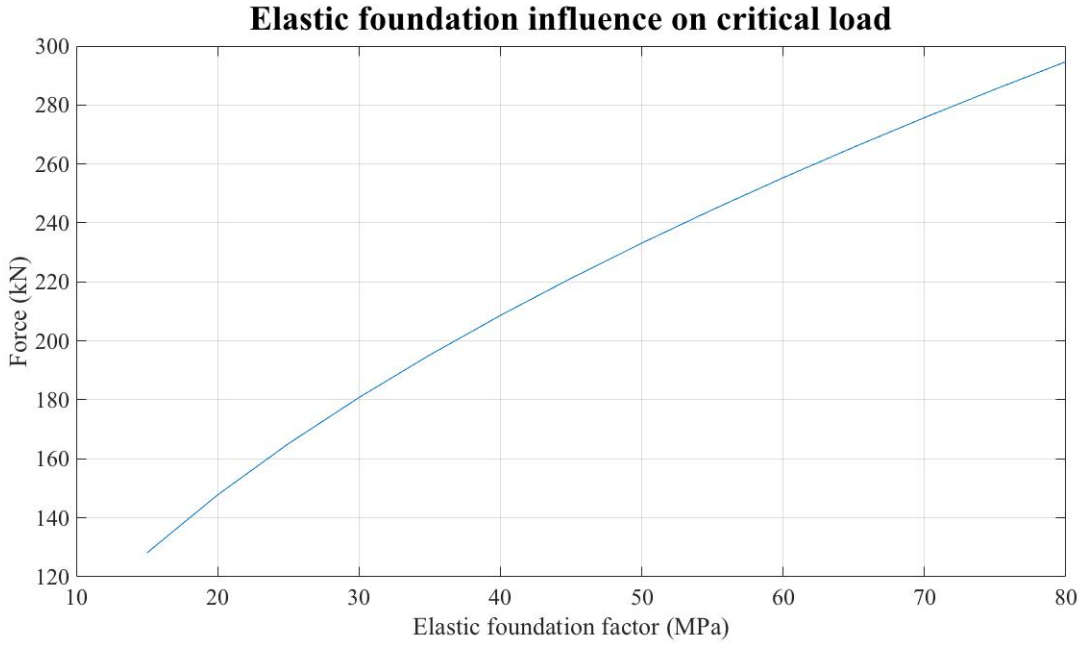


**Figure 4-19: Relationship between restraining medium and critical load**

The critical load (compression yield load) increases as the restraining medium compression strength increases. Where this load is greater than the outer casing Euler buckling load, global buckling will govern. The relationship presented in Figure 4-19 can be approximated by the polynomial equation $P = -0.0149{\beta_e}^2 + 3.9174\beta_e + 75.164$. The thickness of the restraining medium is not considered within Equation 4-32, with the elastic foundation factor taken as equal to the restraining medium compression strength. This equation only considers elastic behavior of the BRB, and it is assumed the flexural strength of the restraining medium is engaged when the steel core moves from elastic to plastic. It is recommended that further research expanding this equation into the plastic region be considered. This will allow the sensitivity of the grout thickness to be evaluated, as well as its influence on the core buckling wavelength.

# 5 Conclusions

This chapter presents key findings from the present thesis, along with theories and relationships within the design of Buckling Restrained Braces (BRBs). Future work and recommendations are also included for completion.

## 5.1 Purpose of research

This research was carried out to compile the available resources for design of BRBs, allowing design of BRB specimens and evaluating their performance. Numerical modelling through finite element analysis was also investigated, as a means of design and performance evaluation. A theoretical model was developed to provide boundaries of capacity when designing BRBs. This body of research together was to encompass the information freely available and used by practitioners, highlighting areas requiring further investigation and those sound for use.

## 5.2 Outcomes of research

The outcomes of this research are detailed in the following subsections with respect to theories and relationships of the BRB. These are, where applicable, to provide guidance when designing the BRB and also highlight any key areas to observe within BRB design, testing and implementation. The subsections follow a similar format to the previous chapters, detailing the key factors in the three fundamental elements; core, unbonding medium and restraining mechanism.

### 5.2.1 Core

The core is the key element, most susceptible to geometrical design variation. It is recommended that the core contain a yielding portion, transition region and non-yielding region.

### 5.2.2 Yielding region

The yielding region is the key dissipating element of the BRB. It was found that susceptibility to localised buckling was more prominent in the regions close to the bearing and non-yielding region. It is been recommended that 2/3 wp-wp be used when proportioning the yielding region, however it was found within this research that buckling was more prone when this guidance was followed. The yielding region length should be evaluated experimentally to confirm compliance, as the general design guidance may be influenced by other design parameters.

### 5.2.3 Yielding to transition region radii

The yielding to transition radii has not been addressed within literature and was investigated within this research. It was found through experimental testing that NZS 3404 minimum radii (10 mm) was inappropriate for BRB design when the bearing

region was larger the 10 mm. BS 5400-10, H.23 highlights the additional stress magnification when a small radii is used in proportion to the yielding width and non-yielding width. This stress magnification can be suppressed, provided the point of magnification is adequately restrained by the restraining mechanism, lying outside the bearing region. BS 5400-10 should be adopted as a method of determining the appropriate radii. It was also found that with a larger radius, and subsequent stress magnification of 1.0 there was a reduction in the compression overstrength factor, resulting in a flatter, more stable and balanced hysteresis curve.

### 5.2.4 Stroke

The stroke region is the non-restrained portion of the core. The stroke was not found to influence the hysteretic response of the experimental specimens, with three specimens of differing strokes evaluated. The stroke was found to engage non-symmetrically within experimental testing. Where space is restricted within BRB-connection design, this should be considered, as connection-outer casing interaction may occur.

### 5.2.5 Restraining mechanism

The restraining mechanism restrains the core from global and local buckling. When evaluating the restraining mechanism, both modes of buckling must be evaluated, with the governing, critical. Equation 2-26, Equation 2-27 and Equation 2-28 should be used to evaluate the restraining mechanism design.

It was found through the theoretical model that the restraining medium thickness is critical for local buckling engagement and preventing global buckling. It was found that when the restraining medium compression strength increased, so did the expected first yield of the core. This relationship can be summarised by:

$$P = -0.0149\beta^2 + 3.9174\beta + 75.164$$

### 5.2.6 Stiffeners

Stiffeners are commonly used to provide additional stiffness to the non-yielding regions. It was found that stiffeners provide a higher specimen yield when eccentricities and additional forces are present. When stiffeners are not present, the specimen yield can occur at half that strain as with stiffeners. It is recommended that stiffeners be adopted for all BRB design.

### 5.2.7 Experimental qualification

BRB qualification is typically carried out through experimental testing. It was observed within the first experimental test (C-VU2-E2-65), that when the cyclic loading protocol engages compression first, global buckling occurs. This alludes to the need for tension to be engaged to initiate the debonding gap, as without it, the member will behave in a composite manner. The first engagement cycle, compression

or tension should be specified on qualified specimens, and where tension is engaged first or the cyclic loading protocol is unknown, the member should be pre-tensioned to below first yield pre-installation.

Within international experimental verification guidance, interpolation may be used on an already verified specimen to up to 1.5 times that of the verified. The SB specimens were 1.54 times the V configuration specimens (just outside the interpolation range). However the yielding core lengths were 2.0 times the V configuration. The V and SB configuration specimens behaved significantly different, particularly when un-stiffened. Clarification is required within international standards as to what the interpolation range equates too, is it an isolated region, applied uniformly over the full specimen etc.?

### 5.2.8 Numerical modelling

It was found that empirical methods are inadequate for evaluating BRB design. The use of semi-empirical methods can be used; however, experimental qualification is required to calibrate the results. It was observed that the isotropic hardening parameters under cyclic loading were insufficient in capturing the full loading protocol, sufficient only to 1.0 x drift. However, with further experimental cyclic loading to calibrate at higher strains, and a range of BRBs evaluated to capture the range and variation between the steel cyclic plasticity, a general semi-empirical approach could be adopted.

## 5.3 Future work and recommendations

It is recommended by the present author that experimental verification be mandatory for all BRB designs. This includes those specimens which are qualified based on AISC 341 interpolation range. By qualifying each design, sensitivity trends and confidence within the member can be achieved.

Within the current loading protocols (AISC 341 and BSJ) it is recommended that the following be investigated as future work, to provide robustness, and clarify any ambiguity:

- Evaluation of BRB performance with respect to compression and tension initial engagement
- Investigation into the current loading protocol and its effects on member performance when the use of higher drift cycles is implemented
- Effects of scaling on member response
- Effects of interpolation and BRB performance
- Evaluation and explicit boundaries with respect to design (verification) based on drift versus core strain development
- The presence of stiffeners and how this affects performance and design
- Stroke length minimum guidance.

Along with experimental qualification, future investigations into the sensitivity of the following BRB design regions is recommended:

- Design and sensitivity of the bearing region
- Stroke and bearing region relationship

Finally, it is recommended that the numerical model be expanded to capture the cyclic hardening profile of the steel core.

# 6 References


American Institute of Steel Construction. (2010). ANSI/AISC 341-10 Seismic Provisions for Structural Steel Buildings. In: American Institute of Steel Construction.

American Institute of Steel Construction. (2016). ANSI/AISC 341-16 Seismic Provisions for Structural Steel Buildings. In: American Institute of Steel Construction.

American Society of Civil Engineers. (2016). *Minimum Design Loads and Associated Criteria for Buildings and Other Structures (ASCE/SEI 7-16)*. USA: American Society of Civil Engineers

Andrews B. M, Fahnestock L. A, & Song J. (2009). Ductility capacity models for buckling-restrained braces. *Journal of Constructional Steel Research, 65*(8-9), 1712-1720. doi:DOI 10.1016/j.jcsr.2009.02.007

Andrews B. M, Song J, & Fahnestock L. A. (2009). Assessment of buckling-restrained braced frame reliability using an experimental limit-state model and stochastic dynamic analysis. *Earthquake Engineering and Engineering Vibration, 8*(3), 373-385. doi:10.1007/s11803-009-9013-8

Asgarian B, & Shokrgozar H. R. (2009). BRBF response modification factor. *Journal of Constructional Steel Research, 65*(2), 290-298. doi:DOI 10.1016/j.jcsr.2008.08.002

Benzoni G, & Innamorato D. (2007). *Star Seismic Brace Tests, Mercy San Juan Hospital Project*. Retrieved from

Black C. J, Makris N, & Aiken I. D. (2004). Component testing, seismic evaluation and characterization of buckling-restrained braces. *Journal of Structural Engineering, 130*(6), 880-894. doi:10.1061/(asce)0733-9445(2004)130:6(880)

British Standards Institute. (1980). Steel, concrete and composite bridges - Part 10: Code of practice for fatigue. In *BS 5400: Part 10: 1980*: British Standards Institute.

British Standards Institute. (2004). BS EN 1998-1:2004 Eurocode 8: Design of structures for earthquake reisitance. In *Part 1: General rules, seismic actions and rules for buildings*. London, United Kingdom: British Standards Institute.

Canadian Standards Authority. (2014). S16-14 Design of steel structures. In: Canadian Standards Authority.

Carden L. P, Itani A. M, & Buckle I. G. (2006). Seismic performance of steel girder bridges with ductile cross frames using buckling-restrained braces. *Journal of Structural Engineering, 132*(3), 338-345. doi:10.1061/(asce)0733-9445(2006)132:3(338)

Choi H, & Kim J. (2006). Energy-based seismic design of buckling-restrained braced frames using hysteretic energy spectrum. *Engineering Structures, 28*(2), 304-311. doi:http://dx.doi.org/10.1016/j.engstruct.2005.08.008

Chou C-C, & Chen S-Y. (2010). Subassemblage tests and finite element analyses of sandwiched buckling-restrained braces. *Engineering Structures, 32*(8), 2108-2121. doi:10.1016/j.engstruct.2010.03.014

Chou C-C, Liu J-H, & Pham D-H. (2012). Steel buckling-restrained braced frames with single and dual corner gusset connections: Seismic tests and analyses. *Earthquake Engineering and Structural Dynamics, 41*(7), 1137-1156. doi:10.1002/eqe.1176

CoreBrace. (2011). Preliminary design In. Utah: CoreBrace.

CoreBrace. (2013a). Bolted CoreBrace BRB Tables. In. Utah: CoreBrace.
CoreBrace. (2013b). Welded CoreBrace BRB Tables. In. Utah: CoreBrace.
CoreBrace. (2014). Pinned CoreBrace BRB Tables. In. Utah: CoreBrace.
CoreBrace. (2016). Preliminary Design Aids. In. Utah: CoreBrace.
Corte G. D, D'Aniello M, Landolfo R, & Mazzolani F. M. (2011). Review of steel buckling-restrained braces. *Steel Construction, 4*(2), 85-93.
Cowie K (2018). [Steel Construction New Zealand BRB Design Guide].
Cowie K, MacRae G, & Clifton C. (2016). Developments of guidelines for engineers designing and specifying buckling restrained braced frames. *SESOC Journal, 29*(1).
D'Aniello M, Corte G. D, & Mazzolani F. M. (2006). Steel Buckling Restrained Braces. *Seismic Upgrading of Reinforced Concrete Buildings by Advanced Techniques*.
Denso. (2011). *Denso Tape Data Sheet*.
Dunai L. (2011). *Type testing of buckling restrained braces according to EN 15129 EWC800*. Retrieved from Budapest Univeristy of Technology and Economics:
European Standards Committee. (2010). EN 15129:2009 Anti-seismic devices. In: European Standards Committee.
Federal Emergency Management Agency, & SAC Joint Ventrue. (2000). *Recommended Seismic Design Criteria for New Steel Moment-Frame Buildings (FEMA 350)*. Washington, D.C
Fussell A. (2010). An Overview of Buckling Restrained Braced Frames. *Steel construction New Zealand*.
Humar J, Adams J, Tremblay R, Rogers C. A, & Halchuk S. (2010). *Proposals for the seismic design provisions of the 2010 national building code of Canada*. Paper presented at the 9th U.S National and 10th Canadian Conference on Earthquake Engineering, Toronto, Canada.
Iwata M, & Murai M. (2006). Buckling-restrained brace using steel mortar planks; performance evaluation as a hysteretic damper. *Earthquake Engineering and Structural Dynamics, 35*(14), 1807-1826. doi:10.1002/eqe.608
Jones A. S. (2011). *Low cost, light-weight buckling restrained braces for low rise buildings.* (Master of Engineering). Univeristy of Auckland,
Jones A. S (2014). [Sensitivity Study].
Jones A. S (2015). [Proprietary Design].
Jones A. S, Lee C-L, & MacRae G. A. (2016). *Design and Behaviour of Buckling Restrained Braces*.
Kersting R. A, Fahnestock L. A, & Lopez W. A. (2015). *NEHRP Seismic Design Technical Brief No. 11 - Seismic design of steel buckling-restrained braced frames, a guide for practicing engineers*. Retrieved from NEHRP:
Kim J, & Choi H. (2004). Behavior and design of structures with buckling-restrained braces. *Engineering Structures, 26*(6), 693-706. doi:http://dx.doi.org/10.1016/j.engstruct.2003.09.010
Kim J, & Seo Y. (2003). Seismic design of steel structures with buckling-restrained knee braces. *Journal of Constructional Steel Research, 59*(12), 1477-1497. doi:http://dx.doi.org/10.1016/S0143-974X(03)00100-7
Lin P-C, Tsai K-C, Chang C-A, Hsiao Y-Y, & Wu A-C. (2015). Seismic design and testing of buckling-restrained braces with a thin profile. *Earthquake Engineering and Structural Dynamics*(45), 339-358.
Lin P-C, Tsai K-C, Wang K-J, Yu Y-J, Wei C-Y, Wu A-C, . . . Roeder C. W. (2012). Seismic design and hybrid tests of a full-scale three-story buckling-restrained

braced frame using welded end connections and thin profile. *Earthquake Engineering and Structural Dynamics, 41*(5), 1001-1020. doi:10.1002/eqe.1171

Lin P-C, Tsai K-C, Wu A-C, & Chuang M-C. (2013). User Guide for BOD: Buckling-Restrained Brace and Connection Design Procedures.

Lopez W. A, & Sabelli R. (2004). *Seismic Design of Buckling-Restained Braced Frames*. Retrieved from Structural Steel Education Council Technical Information and Product Service:

Lopez-Almansa F, Castro-Medina J. C, & Oiler S. (2012). A numerical model of the structural behavior of buckling-restrained braces. *Engineering Structures, 41*, 108-117. doi:DOI 10.1016/j.engstruct.2012.03.045

Mahin S, Uriz P, Aiken I, Field C, & E., K. (2004). Seismic performance of buckling restrained braced frame systems. *13th World Conference on Earthquake Engineering*.

Mirtaheri M, Gheidi A, Zandi A. P, Alanjari P, & Samani H. R. (2011). Experimental optimization studies on steel core lengths in buckling restrained braces. *Journal of Constructional Steel Research, 67*(8), 1244-1253. doi:10.1016/j.jcsr.2011.03.004

Program on Improved Seismic Safety Provisions. (2003). *NEHRP Recommended Provisions for Seismic Regulations for New Buildings and Other Structures (FEMA 450)*. Washington, D.C: National Institute of Building Services

Robinson K. *Buckling restrained braces - an overview*. Retrieved from StarSeismic:

Robinson K. (2013). *Buckling restrained braces - standards developments and innovative applications*. Paper presented at the Steel Innovations Conference Christchurch, New Zealand.

Sabelli R. (2000). *Research on improving the design and analysis of earthquake-resistant steel-braced frames*. Retrieved from NEHRP:

Saxey B, & Daniels M. *Characterization of overstrength factors for buckling restrained braces*. Retrieved from B Saxey:

Sitler B (2016, 19 February). [Takeuchi Lab BRB Research].

Standards Australia. (2007). Metallic materials - Tensile testing at ambient temperature. In *AS 1391*: Standards Australia.

Standards Australia, & Standards New Zealand. (2011). AS/NZS 3678 Structural steel - Hot-rolled plates, floorplates and slabs. In: Standards Australia & Standards New Zealand.

Standards New Zealand. (1986). NZS 3112.1 Methods for test for concrete. In: Standards New Zealand.

Standards New Zealand. (1997). NZS 3404 Steel Structures Standard. In *Part 1*: Standards New Zealand.

Standards New Zealand. (2004). NZS 1170.5 Structural Design Action Part 5: Earthquake actions - New Zealand. In: Standards New Zealand.

Structural Engineers Association of Northern California. (2001). Recommended Provisions for Buckling-Restrained Braced Frames. In: Structural Engineers Association of Northern California,.

Structure Magazine. (2015). Wilshire Grand. Retrieved from http://www.structuremag.org/?p=8854e

Takeuchi T, Hajjar J. F, Matsui R, Nishimoto K, & Aiken I. D. (2012). Effect of local buckling core plate restraint in buckling restrained braces. *Engineering Structures, 44*(0), 304-311. doi:http://dx.doi.org/10.1016/j.engstruct.2012.05.026

Takeuchi T, & Wada A. (2017). *Buckling-Restrained Braces and Applications*. Japan: The Japan Society of Seismic Isolation.

Timoshenko S. P, & Gere J. M. (1989). *Theory of Elastic Stability* (Second ed.). New York: McGraw-Hill.

Tremblay R, Bolduc P, Neville R, & DeVall R. (2006). Seismic testing and performance of buckling-restrained bracing systems. *Canadian Journal of Civil Engineering, 33*(2), 183-198. doi:10.1139/l05-103

Tremblay R, Poncet L, Bolduc P, Neville R, & DeVall R. (2004). *Testing and design of buckling restrained braces for canadian application*. Paper presented at the 13th World Conference on Earthquake Engineering, Vancouver, Canada.

Tsai K-C, Lai J-W, Hwang Y-C, Lin S-L, & Weng C-H. (2004). Research and application of double-core buckling restrained braces in Taiwan. *13th World Conference on Earthquake Engineering*.

Univeristy of California Davis. (2018). Univeristy of California, Davis: Plant and Envronmental Science Building. Retrieved from http://www.plantsciences.ucdavis.edu/plantsciences/undergrad_students/facilities.htm

University of Canterbury. (2018). Univeristy of Canterbury: Rutherford Regional Science and Innovation Centre. Retrieved from http://www.canterbury.ac.nz/science/why-uc-science/world-class-facilities/

Urban Land. (2018). Wilshire Grand: L.A's Transformative Tower. Retrieved from https://urbanland.uli.org/development-business/wilshire-grand-l-s-transformative-tower/

Watanabe A, Hitomi Y, Saeki E, Wada A, & Fujimoto M. (1988). Properties of brace encased in buckling-restraining concrete and steel tube. *Proceedings of the Ninth World Conference on Earthquake Engineering*.

Wijanto S. (2012). *Behaviour and Design of Generic Buckling Restrained Brace Systems.* (Master of Engineering). Univeristy of Auckland,

Zaboli B, Clifton G. C, & Cowie K. (2017). *Out-of-plane stability of gusset plates using a simplified notional load yeild line method*. Paper presented at the New Zealand Society of Earthquake Engineering.

# Appendix A – Specimen Summary

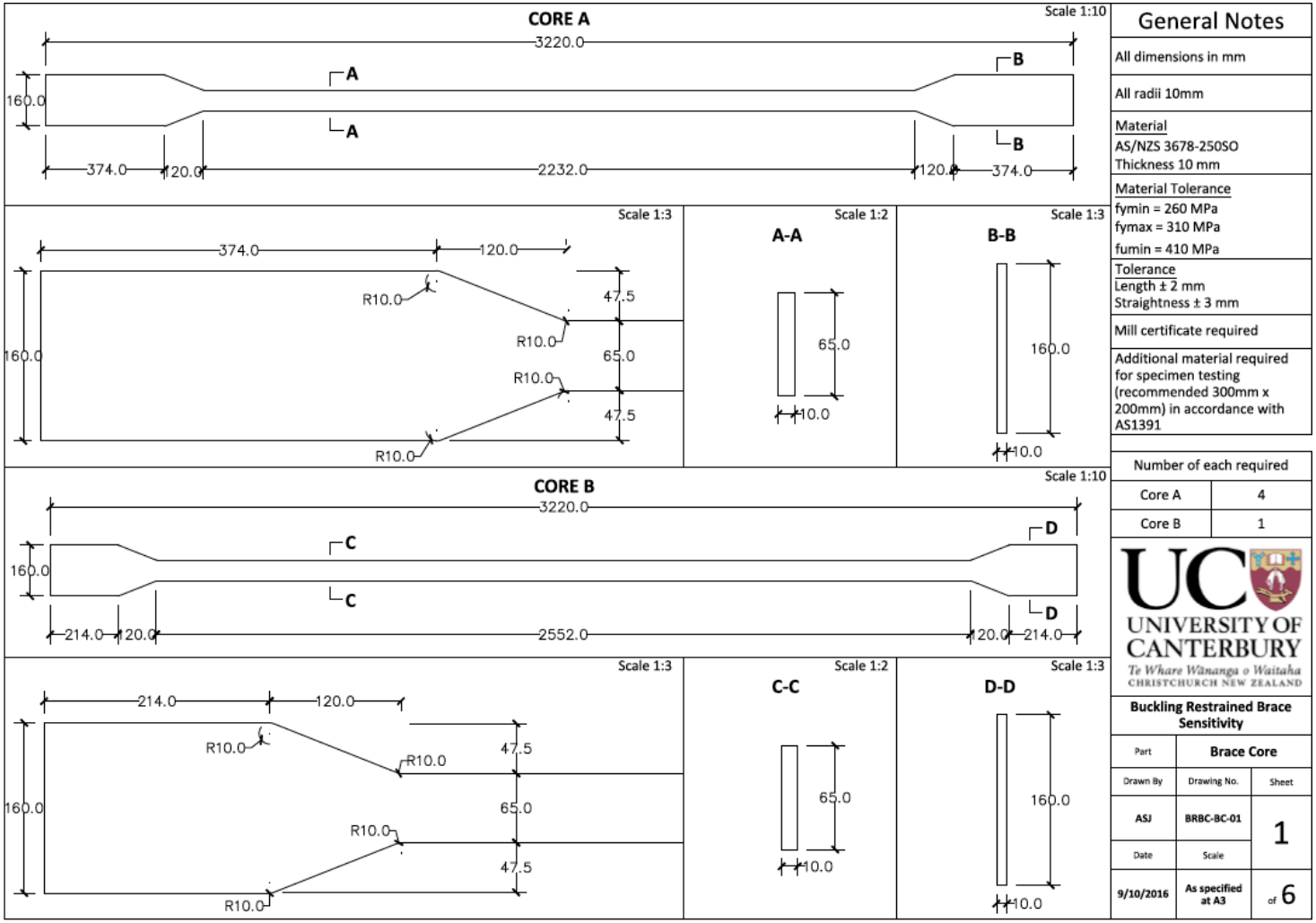


**Figure A. 1: Core technical drawing example**

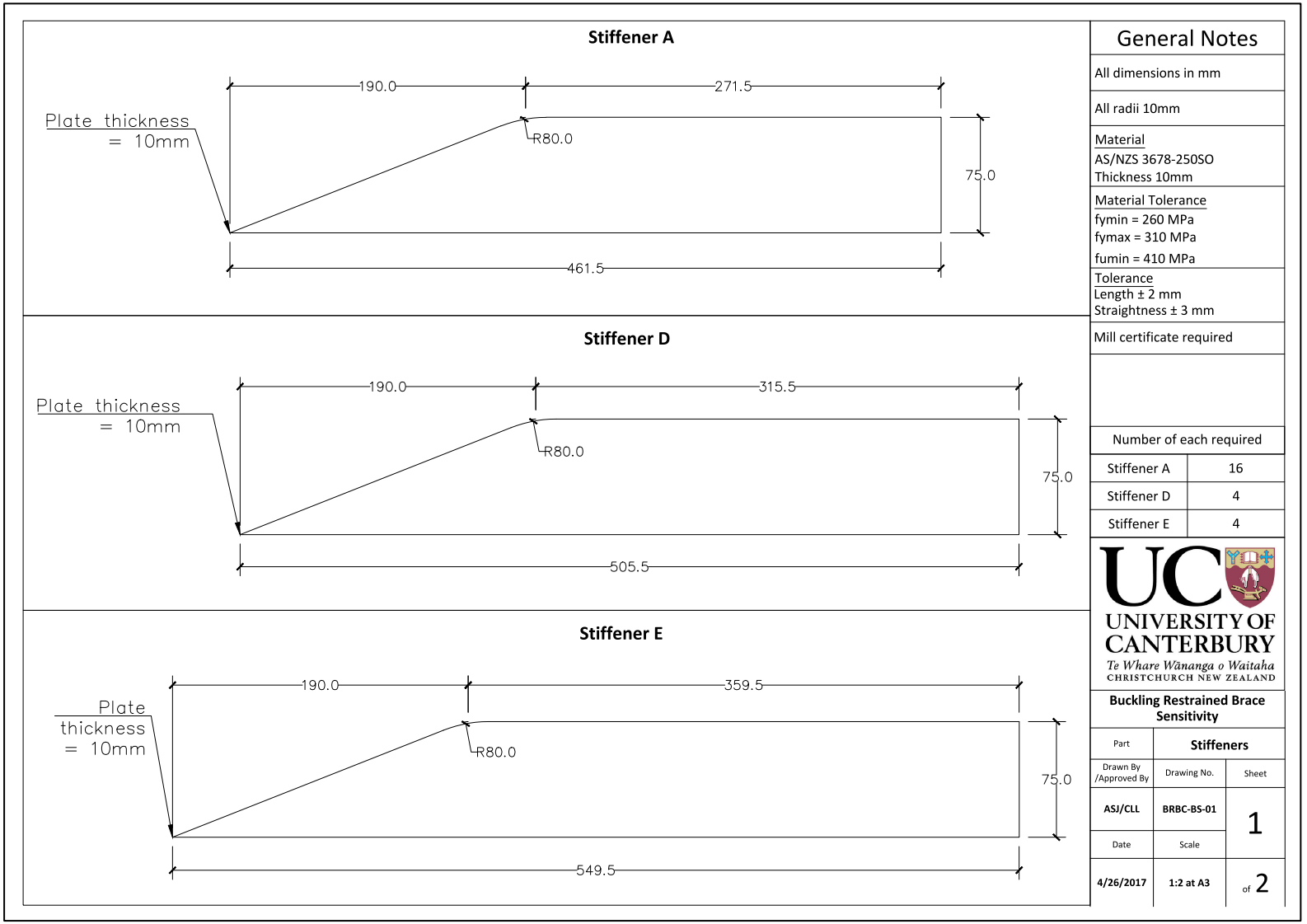


**Figure A. 2: Stiffener technical drawing example**

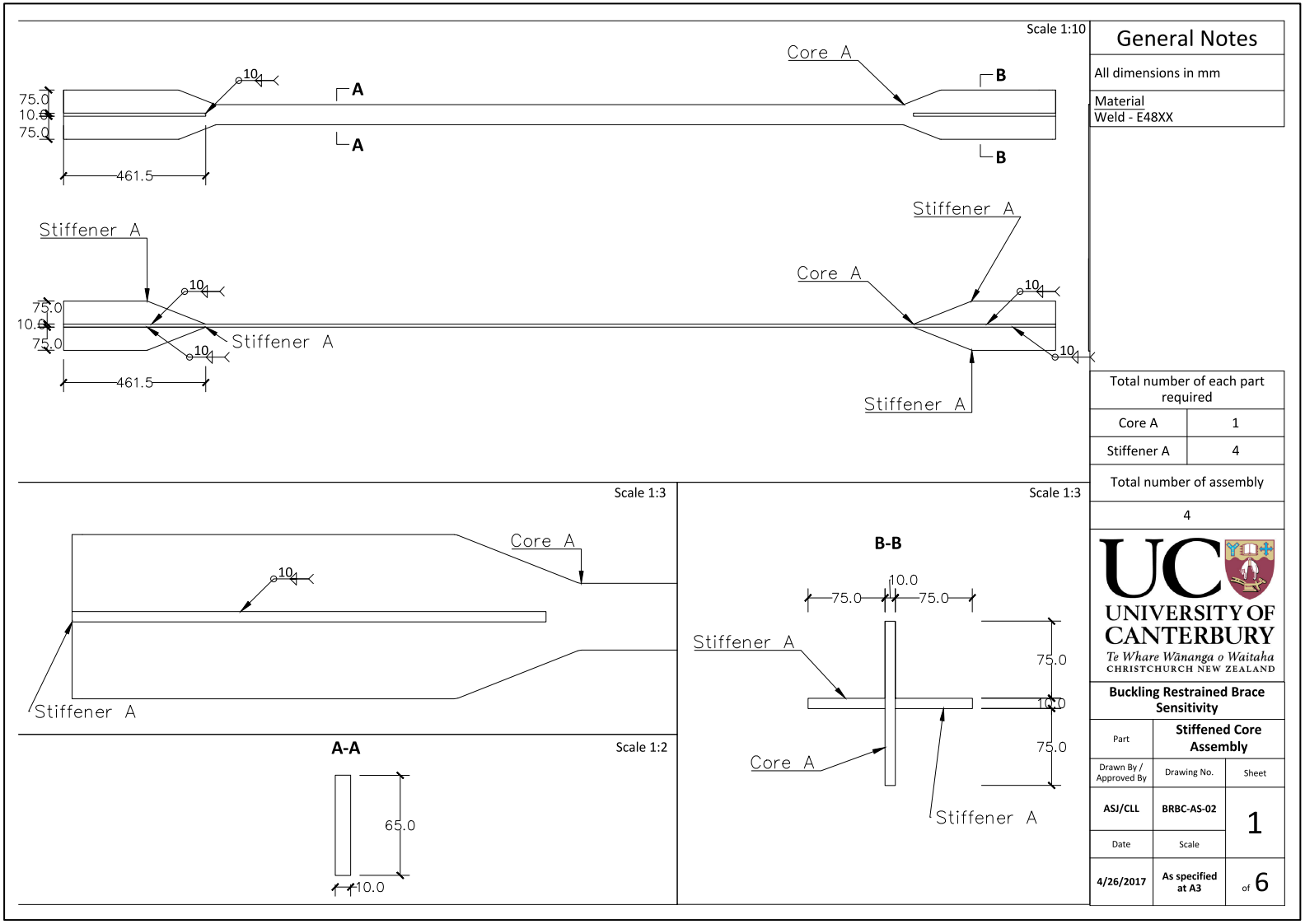


**Figure A. 3: Assembly technical drawing example**

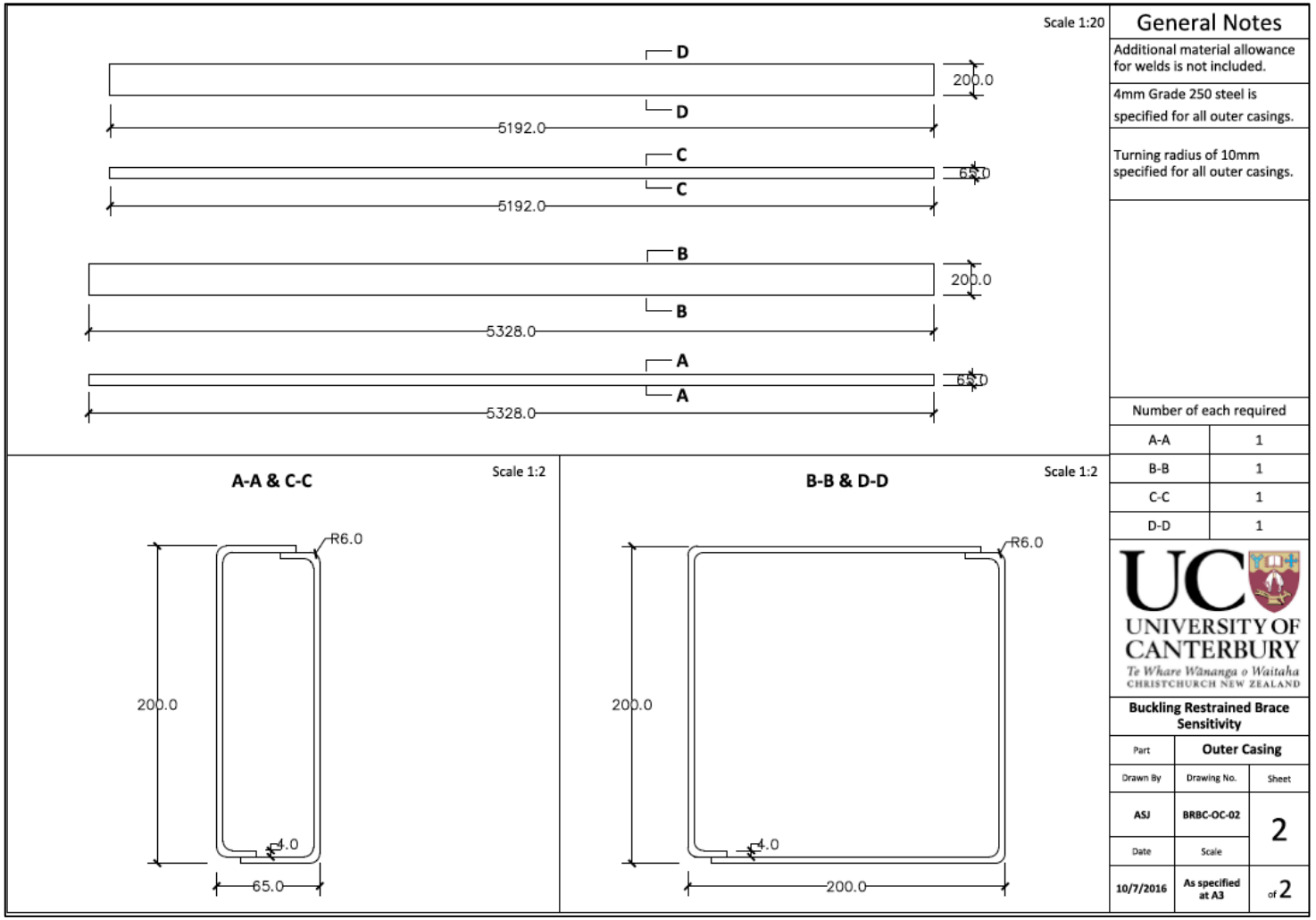


**Figure A. 4: Outer casing technical drawing example**

**Table A. 1: Specimen summary one**

| Specimen reference | Specimen features | Brace length wp-wp (mm) | Region length (mm) | | | | Outer casing length (mm) | Core thickness (mm) | Radius (mm) | Region width (mm) | |
|---|---|---|---|---|---|---|---|---|---|---|---|
| | | | Non-yielding (each end) | | | Yielding | | | | Yielding, $b_c$ | Non-yielding, $b_{ny}$ |
| | | | Transition | Embedment | Un-restrained | | | | | | |
| C-VU2-E2-70 | Grad 1:2.5 Emb 2 x $b_{ny}$ | 4400 | 120 | 320 | 44 | 2232 | 3112 | 10 | 80 | 65 | 160 |
| C-VU2-E1-65 | Grad 1:2.5 Emb $b_{ny}$ | 4400 | 120 | 160 | 44 | 2552 | 3112 | 10 | 80 | 65 | 160 |
| C-VU2-E2-65 | Grad 1:2.5 Emb 2 x $b_{ny}$ | 4400 | 120 | 320 | 44 | 2232 | 3112 | 10 | 80 | 65 | 160 |
| C-VU2-E3-65 | Grad 1:2.5 Emb 3 x $b_{ny}$ | 4400 | 120 | 480 | 44 | 1912 | 3112 | 10 | 80 | 65 | 160 |
| C-VU2-E2-60 | Grad 1:2.5 Emb 2 x $b_{ny}$ | 4400 | 120 | 320 | 44 | 2232 | 3112 | 10 | 80 | 65 | 160 |
| C-VU4-E2-65 | Grad 1:2.5 Emb 2 x $b_{ny}$ | 4400 | 120 | 320 | 88 | 2144 | 3024 | 10 | 80 | 65 | 160 |
| C-VU6-E2-65 | Grad 1:2.5 Emb 2 x $b_{ny}$ | 4400 | 120 | 320 | 132 | 2056 | 2936 | 10 | 80 | 65 | 160 |
| C-VS2-E2-200-R10 | Grad 1:2.5 Emb 2 x $b_{ny}$ | 4400 | 120 | 320 | 44 | 2232 | 3112 | 10 | 10 | 65 | 160 |
| C-VS4-E2-200-R10 | Grad 1:2.5 Emb 2 x $b_{ny}$ | 4400 | 120 | 320 | 88 | 2144 | 3024 | 10 | 10 | 65 | 160 |
| C-VS6-E2-200-R10 | Grad 1:2.5 Emb 2 x $b_{ny}$ | 4400 | 120 | 320 | 132 | 2056 | 2936 | 10 | 10 | 65 | 160 |
| C-VS2-E2-200-R80A | Grad 1:2.5 Emb 2 x $b_{ny}$ | 4400 | 120 | 320 | 44 | 2232 | 3112 | 10 | 80 | 65 | 160 |
| C-VS2-E2-200-R80B | Grad 1:2.5 Emb 2 x $b_{ny}$ | 4400 | 120 | 320 | 44 | 2232 | 3112 | 10 | 80 | 65 | 160 |
| C-VS2-E2-200-R80C | Grad 1:2.5 Emb 2 x $b_{ny}$ | 4400 | 120 | 320 | 44 | 2232 | 3112 | 10 | 80 | 65 | 160 |

| | | | | | | | | | | | |
|---|---|---|---|---|---|---|---|---|---|---|---|
| C-DU2-E2-70 | Grad 1:2.5 Emb 2 x $b_{ny}$ | 6800 | 120 | 320 | 68 | 4584 | 5464 | 10 | 80 | 65 | 160 |
| C-DU2-E1-65 | Grad 1:2.5 Emb $b_{ny}$ | 6800 | 120 | 160 | 68 | 4904 | 5464 | 10 | 80 | 65 | 160 |
| C-DU2-E3-65 | Grad 1:2.5 Emb 3 x $b_{ny}$ | 6800 | 120 | 480 | 68 | 4264 | 5464 | 10 | 80 | 65 | 160 |
| C-DU2-E2-60 | Grad 1:2.5 Emb 2 x $b_{ny}$ | 6800 | 120 | 320 | 68 | 4584 | 5464 | 10 | 80 | 65 | 160 |
| C-DU2-E2-65-T3 | Grad 1:3 Emb 2 x $b_{ny}$ | 6800 | 140 | 320 | 68 | 4544 | 5464 | 10 | 80 | 65 | 160 |
| C-DU2-E2-65 | Grad 1:2.5 Emb 2 x $b_{ny}$ | 6800 | 120 | 320 | 68 | 4584 | 5464 | 10 | 80 | 65 | 160 |
| C-DU2-E2-65-T1 | Grad 1:1 Emb 2 x $b_{ny}$ | 6800 | 50 | 320 | 68 | 4724 | 5464 | 10 | 80 | 65 | 160 |
| C-DU4-E2-65 | Grad 1:2.5 Emb 2 x $b_{ny}$ | 6800 | 120 | 320 | 136 | 4448 | 5328 | 10 | 80 | 65 | 160 |
| C-DU6-E2-65 | Grad 1:2.5 Emb 2 x $b_{ny}$ | 6800 | 120 | 320 | 204 | 4312 | 5192 | 10 | 80 | 65 | 160 |
| C-DS2-E2-200-R10 | Grad 1:2.5 Emb 2 x $b_{ny}$ | 6800 | 120 | 320 | 68 | 4584 | 5464 | 10 | 10 | 65 | 160 |
| C-DS4-E2-200-R10 | Grad 1:2.5 Emb 2 x $b_{ny}$ | 6800 | 120 | 320 | 136 | 4448 | 5328 | 10 | 10 | 65 | 160 |
| C-DS6-E2-200-R80 | Grad 1:2.5 Emb 2 x $b_{ny}$ | 6800 | 120 | 320 | 204 | 4312 | 5192 | 10 | 80 | 65 | 160 |
| E-VU2-E2-65 | Grad 1:2.5 Emb 2 x $b_{ny}$ | 4400 | 120 | 320 | 44 | 2232 | 3112 | 10 | 80 | 65 | 160 |
| E-VU4-E2-65 | Grad 1:2.5 Emb 2 x $b_{ny}$ | 4400 | 120 | 320 | 88 | 2144 | 3024 | 10 | 80 | 65 | 160 |
| E-VU6-E2-65 | Grad 1:2.5 Emb 2 x $b_{ny}$ | 4400 | 120 | 320 | 132 | 2056 | 2936 | 10 | 80 | 65 | 160 |
| E-VS2-E2-200 | Grad 1:2.5 Emb 2 x $b_{ny}$ | 4400 | 120 | 320 | 44 | 2232 | 3112 | 10 | 80 | 65 | 160 |
| E-VS4-E2-200 | Grad 1:2.5 Emb 2 x $b_{ny}$ | 4400 | 120 | 320 | 88 | 2144 | 3024 | 10 | 80 | 65 | 160 |

| | | | | | | | | | | | |
|---|---|---|---|---|---|---|---|---|---|---|---|
| E-VS6-E2-200 | Grad 1:2.5 Emb 2 x $b_{ny}$ | 4400 | 120 | 320 | 132 | 2056 | 2936 | 10 | 80 | 65 | 160 |
| E-DU2-E2-65 | Grad 1:2.5 Emb 2 x $b_{ny}$ | 6800 | 120 | 320 | 68 | 4584 | 5464 | 10 | 80 | 65 | 160 |
| E-DU4-E2-65 | Grad 1:2.5 Emb 2 x $b_{ny}$ | 6800 | 120 | 320 | 136 | 4448 | 5328 | 10 | 80 | 65 | 160 |
| E-DU6-E2-65 | Grad 1:2.5 Emb 2 x $b_{ny}$ | 6800 | 120 | 320 | 204 | 4312 | 5192 | 10 | 80 | 65 | 160 |
| E-DS2-E2-200 | Grad 1:2.5 Emb 2 x $b_{ny}$ | 6800 | 120 | 320 | 68 | 4584 | 5464 | 10 | 80 | 65 | 160 |
| E-DS4-E2-200 | Grad 1:2.5 Emb 2 x $b_{ny}$ | 6800 | 120 | 320 | 136 | 4448 | 5328 | 10 | 80 | 65 | 160 |
| E-DS6-E2-200 | Grad 1:2.5 Emb 2 x $b_{ny}$ | 6800 | 120 | 320 | 204 | 4312 | 5192 | 10 | 80 | 65 | 160 |

where:
Grad = Transition region slope (vertical:horizontal)
Emb = Embedment length based on ratio of non-yielding width
wp – wp = Workpoint to workpoint length

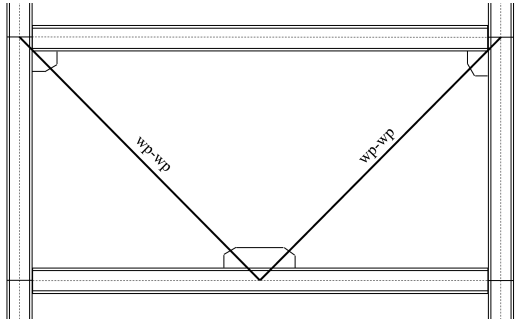


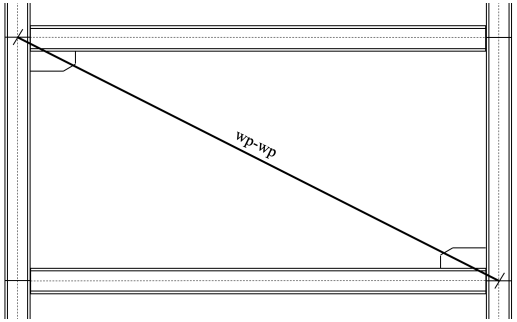


Naming convention

C = Concentric configuration
E = Eccentric configuration
V = V brace configuration
D = Single bay configuration
U = Unstiffened specimen
S = Stiffened specimen

Example:
*C-DS6-E2-200-R80*
Concentric configuration – Single bay configuration, stiffened, 6% un-restrained non-yieding length – Embedment two times non-yielding width – Outer casing depth 200 mm – Radius 80 mm

*C-DU2-E2-65-T1*

Concentric configuration – Single bay configuration, unstiffened, 2% un-restrained non-yielding length – Embedment two times non-yielding width – Outer casing depth 65 mm – Transition gradient 1:1

**Table A. 2: Specimen summary two**

| Specimen reference | Outer casing dimensions (mm) | | | | Global safety factor[a] | Minor axis safety factor[b] | Major axis safety factor[c] | Demand to capacity ratio[d] | Loading protocol | Pre-tension weight (kg) |
|---|---|---|---|---|---|---|---|---|---|---|
| | Width | Thickness (width) | Depth | Thickness (depth) | | | | | | |
| C-VU2-E2-70 | 200 | 4 | 70 | 4 | 0.435 | 0.802 | 0.716 | 1.175 | S1 | 70.0 |
| C-VU2-E1-65 | 200 | 4 | 65 | 4 | 0.513 | 1.008 | 0.707 | 1.233 | S2 | 70.0 |
| C-VU2-E2-65 | 200 | 4 | 65 | 4 | 0.513 | 1.008 | 0.707 | 1.233 | S1 | 70.0 |
| C-VU2-E3-65 | 200 | 4 | 65 | 4 | 0.513 | 1.008 | 0.707 | 1.233 | S1 | 70.0 |
| C-VU2-E2-60 | 200 | 4 | 60 | 4 | 0.614 | 1.213 | 0.696 | 1.296 | S1 | 70.0 |
| C-VU4-E2-65 | 200 | 4 | 65 | 4 | 0.513 | 1.008 | 0.707 | 1.233 | S1 | 70.0 |
| C-VU6-E2-65 | 200 | 4 | 65 | 4 | 0.513 | 1.008 | 0.707 | 1.233 | S1 | 70.0 |
| C-VS2-E2-200-R10 | 200 | 4 | 200 | 4 | 0.034 | Undefined | 0.509 | 0.275 | S1 | NA |
| C-VS4-E2-200-R10 | 200 | 4 | 200 | 4 | 0.034 | Undefined | 0.509 | 0.275 | S1 | NA |
| C-VS6-E2-200-R10 | 200 | 4 | 200 | 4 | 0.034 | Undefined | 0.509 | 0.275 | S1 | NA |
| C-VS2-E2-200-R80A | 200 | 4 | 200 | 4 | 0.034 | Undefined | 0.509 | 0.275 | S1 | 154.5 |
| C-VS2-E2-200-R80B | 200 | 4 | 200 | 4 | 0.034 | Undefined | 0.509 | 0.275 | S1 | 154.5 |
| C-VS2-E2-200-R80C | 200 | 4 | 200 | 4 | 0.034 | Undefined | 0.509 | 0.275 | S1 | 154.5 |
| C-DU2-E2-70 | 200 | 4 | 70 | 4 | 1.312 | 0.802 | 0.716 | 1.175 | L1 | 70.0 |
| C-DU2-E1-65 | 200 | 4 | 65 | 4 | 1.547 | 1.008 | 0.707 | 1.233 | L1 | 103.8 |
| C-DU2-E3-65 | 200 | 4 | 65 | 4 | 1.547 | 1.008 | 0.707 | 1.233 | L2 | 101.4 |
| C-DU2-E2-60 | 200 | 4 | 60 | 4 | 1.849 | 1.213 | 0.696 | 1.296 | L1 | 70.0 |
| C-DU2-E2-65-T3 | 200 | 4 | 65 | 4 | 1.547 | 1.008 | 0.707 | 1.233 | L1 | 70.0 |
| C-DU2-E2-65 | 200 | 4 | 65 | 4 | 1.547 | 1.008 | 0.707 | 1.233 | L1 | 70.0 |
| C-DU2-E2-65-T1 | 200 | 4 | 65 | 4 | 1.547 | 1.008 | 0.707 | 1.233 | L1 | 84.5 |
| C-DU4-E2-65 | 200 | 4 | 65 | 4 | 1.547 | 1.008 | 0.707 | 1.233 | L1 | 103.8 |
| C-DU6-E2-65 | 200 | 4 | 65 | 4 | 1.547 | 1.008 | 0.707 | 1.233 | L2 | 103.8 |
| C-DS2-E2-200-R10 | 200 | 4 | 200 | 4 | 0.101 | Undefined | 0.509 | 0.275 | L1 | NA |
| C-DS4-E2-200-R10 | 200 | 4 | 200 | 4 | 0.101 | Undefined | 0.509 | 0.275 | L1 | NA |

| | | | | | | | | | | |
|---|---|---|---|---|---|---|---|---|---|---|
| C-DS6-E2-200-R80 | 200 | 4 | 200 | 4 | 0.101 | Undefined | 0.509 | 0.275 | L2 | 202.8 |
| E-VU2-E2-65 | 200 | 4 | 65 | 4 | 0.513 | 1.008 | 0.707 | 1.233 | S1 | 70.0 |
| E-VU4-E2-65 | 200 | 4 | 65 | 4 | 0.513 | 1.008 | 0.707 | 1.233 | S1 | 70.0 |
| E-VU6-E2-65 | 200 | 4 | 65 | 4 | 0.513 | 1.008 | 0.707 | 1.233 | S1 | 70.0 |
| E-VS2-E2-200 | 200 | 4 | 200 | 4 | 0.034 | Undefined | 0.509 | 0.275 | S1 | 118.0 |
| E-VS4-E2-200 | 200 | 4 | 200 | 4 | 0.034 | Undefined | 0.509 | 0.275 | S1 | 118.0 |
| E-VS6-E2-200 | 200 | 4 | 200 | 4 | 0.034 | Undefined | 0.509 | 0.275 | S1 | 118.0 |
| E-DU2-E2-65 | 200 | 4 | 65 | 4 | 1.547 | 1.008 | 0.707 | 1.233 | L1 | 86.9 |
| E-DU4-E2-65 | 200 | 4 | 65 | 4 | 1.547 | 1.008 | 0.707 | 1.233 | L1 | 86.9 |
| E-DU6-E2-65 | 200 | 4 | 65 | 4 | 1.547 | 1.008 | 0.707 | 1.233 | L2 | 86.9 |
| E-DS2-E2-200 | 200 | 4 | 200 | 4 | 0.101 | Undefined | 0.509 | 0.275 | L1 | 168.0 |
| E-DS4-E2-200 | 200 | 4 | 200 | 4 | 0.101 | Undefined | 0.509 | 0.275 | L1 | 168.0 |
| E-DS6-E2-200 | 200 | 4 | 200 | 4 | 0.101 | Undefined | 0.509 | 0.275 | L2 | 168.0 |

where:

[a] Global Safety Factor = Equation 4-7

[b] Minor Axis Safety Factor = Equation 2-27

[c] Major Axis Safety Factor = Equation 2-27

[d] Demand to Capacity Ratio = Equation 2-28

# Appendix B – Loading Protocol

**Table B. 1: Loading protocol**

| Step | Cycle | Deformation | Time step | Applied displacement (mm) | | | |
|---|---|---|---|---|---|---|---|
| | | | | S1 | S2 | L1 | L2 |
| 1 | 1 | $\delta_e$ | 0 | 0 | 0 | 0 | 0 |
| | | | 1 | 3 | 4 | 7 | 6 |
| | | | 2 | 0 | 0 | 0 | 0 |
| | | | 3 | -3 | -4 | -7 | -6 |
| | 2 | $\delta_e$ | 4 | 0 | 0 | 0 | 0 |
| | | | 5 | 3 | 4 | 7 | 6 |
| | | | 6 | 0 | 0 | 0 | 0 |
| | | | 7 | -3 | -4 | -7 | -6 |
| 2 | 1 | 0.5 $\delta_{ui}$ | 8 | 0 | 0 | 0 | 0 |
| | | | 9 | 22 | 22 | 34 | 34 |
| | | | 10 | 0 | 0 | 0 | 0 |
| | | | 11 | -22 | -22 | -34 | -34 |
| | 2 | 0.5 $\delta_{ui}$ | 12 | 0 | 0 | 0 | 0 |
| | | | 13 | 22 | 22 | 34 | 34 |
| | | | 14 | 0 | 0 | 0 | 0 |
| | | | 15 | -22 | -22 | -34 | -34 |
| 3 | 1 | $\delta_{ui}$ | 16 | 0 | 0 | 0 | 0 |
| | | | 17 | 44 | 44 | 68 | 68 |
| | | | 18 | 0 | 0 | 0 | 0 |
| | | | 19 | -44 | -44 | -68 | -68 |
| | 2 | $\delta_{ui}$ | 20 | 0 | 0 | 0 | 0 |
| | | | 21 | 44 | 44 | 68 | 68 |
| | | | 22 | 0 | 0 | 0 | 0 |
| | | | 23 | -44 | -44 | -68 | -68 |
| 4 | 1 | 1.5 $\delta_{ui}$ | 24 | 0 | 0 | 0 | 0 |
| | | | 25 | 66 | 66 | 102 | 102 |
| | | | 26 | 0 | 0 | 0 | 0 |
| | | | 27 | -66 | -66 | -102 | -102 |
| | 2 | 1.5 $\delta_{ui}$ | 28 | 0 | 0 | 0 | 0 |
| | | | 29 | 66 | 66 | 102 | 102 |
| | | | 30 | 0 | 0 | 0 | 0 |
| | | | 31 | -66 | -66 | -102 | -102 |
| 5 | 1 | 2.0 $\delta_{ui}$ | 32 | 0 | 0 | 0 | 0 |
| | | | 33 | 88 | 88 | 136 | 136 |
| | | | 34 | 0 | 0 | 0 | 0 |
| | | | 35 | -88 | -88 | -136 | -136 |
| | 2 | 2.0 $\delta_{ui}$ | 36 | 0 | 0 | 0 | 0 |
| | | | 37 | 88 | 88 | 136 | 136 |
| | | | 38 | 0 | 0 | 0 | 0 |
| | | | 39 | -88 | -88 | -136 | -136 |

| | | | | | | | |
|---|---|---|---|---|---|---|---|
| 6 | As many as required | 1.5 $\delta_{ui}$ | 40 | 0 | 0 | 0 | 0 |
| | | | 41 | 66 | 66 | 102 | 102 |
| | | | 42 | 0 | 0 | 0 | 0 |
| | | | 43 | -66 | -66 | -102 | -102 |
| | | 1.5 $\delta_{ui}$ | 44 | 0 | 0 | 0 | 0 |
| | | | 45 | 66 | 66 | 102 | 102 |
| | | | 46 | 0 | 0 | 0 | 0 |
| | | | 47 | -66 | -66 | -102 | -102 |

where:

Positive applied displacement = Tension

Negative applied displacement = Compression

# Appendix C – Steel Mill Certificates

Please refer to Appendix D for tensile testing of the supplied steel and also a summary of steel allocation to each specimen. Not all mill certificates were supplied on request, those received are presented within this appendix. Vulcan One and Two were received from the same steel consignment; the specific roll for each fabrication set was unspecified. Vulcan One and Two are represented by the same mill certificate as represented in Table C. 1.

**Table C. 1: Vulcan One and Two mill certificate**

| | | | | | | | | | | | | | | | | |
|---|---|---|---|---|---|---|---|---|---|---|---|---|---|---|---|---|
| **Customer** | Vulcan Steel Limited | | | | **Specification** | | | EN 10025-2 S275J0+N AS/NZS 3678 G3 | | | **Certificate No.** | | 160825-ASHEX-3215 | | | |
| **Shipper** | JFE Shoji Trade Corporation | | | | **Product** | | | Hot rolled steel plate | | | **Date** | | 25 August 2016 | | | |
| **Reference No.** | FB 2 – C60180065 | | | | **Dimensions (mm)** | | | 10 x 2400 x 6000 | | | | | | | | |
| **Roll number** | **Heat number** | **Chemical composition percent** | | | | | | | | | | | | **Mechanical test** | | |
| | | C | Si | Mn | P | S | Cu | Ni | Cr | Mo | V | N | CE | Yield | Tensile | Percent |
| | | x 100 | | | x 1000 | | | | | | | x 10000 | x 100 | (MPa) | (MPa) | elongation (%) |
| FG40701 | 06522 | 16 | 25 | 113 | 19 | 2 | 1 | 2 | 4 | 1 | 0 | 26 | 36 | 346 | 510 | 28 |
| FG40702 | 06522 | 16 | 25 | 113 | 19 | 2 | 1 | 2 | 4 | 1 | 0 | 26 | 36 | 346 | 510 | 28 |
| FG40703 | 06522 | 16 | 25 | 113 | 19 | 2 | 1 | 2 | 4 | 1 | 0 | 26 | 36 | 346 | 510 | 28 |
| FG40704 | 06522 | 16 | 25 | 113 | 19 | 2 | 1 | 2 | 4 | 1 | 0 | 26 | 36 | 346 | 510 | 28 |
| FG40705 | 06522 | 16 | 25 | 113 | 19 | 2 | 1 | 2 | 4 | 1 | 0 | 26 | 36 | 346 | 510 | 28 |
| FG40706 | 06522 | 16 | 25 | 113 | 19 | 2 | 1 | 2 | 4 | 1 | 0 | 26 | 36 | 346 | 510 | 28 |
| FG40707 | 06522 | 16 | 25 | 113 | 19 | 2 | 1 | 2 | 4 | 1 | 0 | 26 | 36 | 346 | 510 | 28 |
| FG40708 | 06522 | 16 | 25 | 113 | 19 | 2 | 1 | 2 | 4 | 1 | 0 | 26 | 36 | 346 | 510 | 28 |
| FG40709 | 06522 | 16 | 25 | 113 | 19 | 2 | 1 | 2 | 4 | 1 | 0 | 26 | 36 | 346 | 510 | 28 |
| FG40710 | 06522 | 16 | 25 | 113 | 19 | 2 | 1 | 2 | 4 | 1 | 0 | 26 | 36 | 346 | 510 | 28 |
| FG40711 | 06522 | 16 | 25 | 113 | 19 | 2 | 1 | 2 | 4 | 1 | 0 | 26 | 36 | 346 | 510 | 28 |
| FG40712 | 06522 | 16 | 25 | 113 | 19 | 2 | 1 | 2 | 4 | 1 | 0 | 26 | 36 | 346 | 510 | 28 |
| FM18305 | 06522 | 16 | 25 | 113 | 19 | 2 | 1 | 2 | 4 | 1 | 0 | 26 | 36 | 346 | 510 | 28 |
| FM18306 | 06522 | 16 | 25 | 113 | 19 | 2 | 1 | 2 | 4 | 1 | 0 | 26 | 36 | 346 | 510 | 28 |
| FM08301 | 06793 | 16 | 25 | 117 | 16 | 3 | 1 | 1 | 3 | 1 | 0 | 28 | 36 | 324 | 495 | 32 |

**Table C. 2: Outer casing mill certificate**

| **Customer** | Unspecified | **Specification** | JIS GS101 SS400 | **Certificate No.** | 050222H0184 |
|---|---|---|---|---|---|
| **Shipper** | China Steel Corporation | **Product** | Coil | **Date** | 21 February 2017 |
| **Reference No.** | SA 16773321 | **Dimensions (mm)** | 4 x 1800 x Coil | | |

| **Roll number** | **Heat number** | **Chemical composition percent** | | | | | | | | | | | | **Mechanical test** | | |
|---|---|---|---|---|---|---|---|---|---|---|---|---|---|---|---|---|
| | | C | Si | Mn | P | S | Cu | Ni | Cr | Mo | Al | N | CE | Yield (MPa) | Tensile (MPa) | Percent elongation (%) |
| | | x 100 | | | x 1000 | | | | | | | x 10000 | x 100 | | | |
| T515778 | 5GJ02 | 15 | 1 | 71 | 16 | 5 | NA | NA | NA | NA | 28 | NA | NA | 308 | 432 | 35 |
| T515779 | 5GJ02 | 15 | 1 | 71 | 16 | 5 | NA | NA | NA | NA | 28 | NA | NA | 308 | 432 | 35 |

# Appendix D – Tensile Testing

All testing carried out in accordance with AS 1391 (Standards Australia, 2007).

**Table D. 1: Tensile Testing Summary**

| Specimen | Reference | |
|---|---|---|
| C-VU2-E2-70 | Table D. 2 | Figure D. 2 |
| C-VU2-E1-65 | Table D. 2 | Figure D. 2 |
| C-VU2-E2-65 | Table D. 2 | Figure D. 2 |
| C-VU2-E3-65 | Table D. 2 | Figure D. 2 |
| C-VU2-E2-60 | Table D. 2 | Figure D. 2 |
| C-VU4-E2-65 | Table D. 3 | Figure D. 3 |
| C-VU6-E2-65 | Table D. 3 | Figure D. 3 |
| C-VS2-E2-200-R10 | Table D. 6 | Figure D. 6 |
| C-VS4-E2-200-R10 | Table D. 6 | Figure D. 6 |
| C-VS6-E2-200-R10 | Table D. 6 | Figure D. 6 |
| C-VS2-E2-200-R80A | Table D. 4 | Figure D. 4 |
| C-VS2-E2-200-R80B | Table D. 4 | Figure D. 4 |
| C-VS2-E2-200-R80C | Table D. 4 | Figure D. 4 |
| C-DU2-E2-70 | Table D. 5 | Figure D. 5 |
| C-DU2-E1-65 | Table D. 5 | Figure D. 5 |
| C-DU2-E3-65 | Table D. 5 | Figure D. 5 |
| C-DU2-E2-60 | Table D. 5 | Figure D. 5 |
| C-DU2-E2-65-T3 | Table D. 3 | Figure D. 3 |
| C-DU2-E2-65 | Table D. 5 | Figure D. 5 |
| C-DU2-E2-65-T1 | Table D. 5 | Figure D. 5 |
| C-DU4-E2-65 | Table D. 5 | Figure D. 5 |
| C-DU6-E2-65 | Table D. 5 | Figure D. 5 |
| C-DS2-E2-200-R10 | Table D. 6 | Figure D. 6 |
| C-DS4-E2-200-R10 | Table D. 6 | Figure D. 6 |
| C-DS6-E2-200-R80 | Table D. 5 | Figure D. 5 |
| E-VU2-E2-65 | Table D. 4 | Figure D. 4 |
| E-VU4-E2-65 | Table D. 4 | Figure D. 4 |
| E-VU6-E2-65 | Table D. 4 | Figure D. 4 |
| E-VS2-E2-200 | Table D. 4 | Figure D. 4 |
| E-VS4-E2-200 | Table D. 3 | Figure D. 3 |
| E-VS6-E2-200 | Table D. 3 | Figure D. 3 |
| E-DU2-E2-65 | Table D. 5 | Figure D. 5 |
| E-DU4-E2-65 | Table D. 5 | Figure D. 5 |
| E-DU6-E2-65 | Table D. 5 | Figure D. 5 |
| E-DS2-E2-200 | Table D. 5 | Figure D. 5 |
| E-DS4-E2-200 | Table D. 5 | Figure D. 5 |
| E-DS6-E2-200 | Table D. 5 | Figure D. 5 |

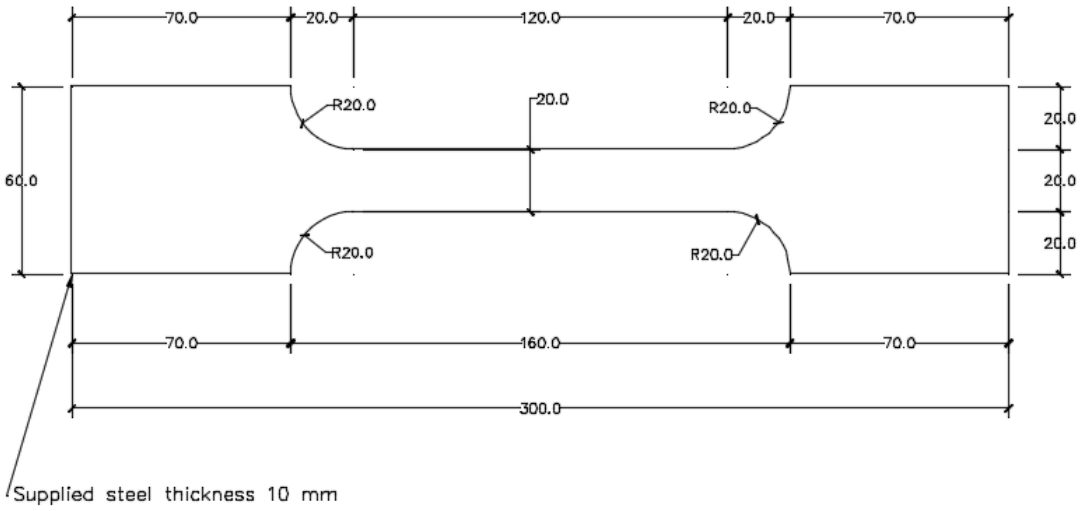


**Figure D. 1: Tensile sample technical drawing**

**Table D. 2: Tensile testing results sample Vulcan One**

| **Specimen** | **Vulcan One** | | |
|---|---|---|---|
| Sample | 1 | 2 | 3 |
| Loading rate, MPa/min | 220.77 | 245.31 | 294.87 |
| Clipgauge | Epsilon | Epsilon | Epsilon |
| Youngs modulus, GPa | 133.94 | 124.88 | 136.6 |
| Strain hardening slope, GPa | 4.57 | 4.75 | 5.71 |
| Yield stress, MPa | 300 | 305.71 | 309.31 |
| Yield strain | 1.83 | 1.09 | 2.66 |
| Original length, mm, $L_o$ | 49.886 | 49.652 | 49.137 |
| Final length, mm, $L_f$ | 60.383 | 60.157 | 59.35 |
| Stress at 0.2% strain, MPa | 300 | 295.195 | 305.105 |
| Average from test bunch (0.2%), MPa | 300.1 | | |

**Table D. 3: Tensile testing results sample Vulcan Two**

| **Specimen** | **Vulcan Two** | | |
|---|---|---|---|
| Sample | 1 | 2 | 3 |
| Loading rate, MPa/min | 382.37 | 367.86 | 396.29 |
| Clipgauge | Epsilon | Epsilon | Epsilon |
| Youngs modulus, GPa | 123.22 | 126.88 | 127.66 |
| Strain hardening slope, GPa | 1.91 | 1.6 | 1.85 |
| Yield stress, MPa | 323.42 | 331.83 | 318.62 |
| Yield strain | 1.96 | 1.27 | 1.49 |
| Original length, mm, $L_o$ | 49.282 | 49.41 | 49.855 |
| Final length, mm, $L_f$ | 60.363 | 60.26 | 60.409 |
| Stress at 0.2% strain, MPa | 308.709 | 318.919 | 318.619 |
| Average from test bunch (0.2%), MPa | 315.4156667 | | |

**Table D. 4: Tensile testing results sample Easy Steel One**

| **Specimen** | **Easy Steel One** | | |
|---|---|---|---|
| Sample | 1 | 2 | 3 |
| Loading rate, MPa/min | 461.11 | 472.3 | 436.82 |
| Clipgauge | Epsilon | Epsilon | Epsilon |
| Youngs modulus, GPa | 157.57 | 161.22 | 322.8 |
| Strain hardening slope, GPa | 0.69 | 6.61 | 4.95 |
| Yield stress, MPa | 355.86 | 361.56 | 112.61 |
| Yield strain | 2.23 | 2.11 | 0.17 |
| Original length, mm, $L_o$ | 49.778 | 49.829 | 49.758 |
| Final length, mm, $L_f$ | 55.487 | 54.305 | 54.088 |
| Stress at 0.2% strain, MPa | 343.544 | 348.649 | 348.949 |
| Average from test bunch (0.2%), MPa | 347.0473333 | | |

**Table D. 5: Tensile testing results sample Easy Steel Two**

| **Specimen** | **Easy Steel Two** | | |
|---|---|---|---|
| Sample | 1 | 2 | 3 |
| Loading rate, MPa/min | 338.4 | 354.63 | 375.91 |
| Clipgauge | Epsilon | Epsilon | Epsilon |
| Youngs modulus, GPa | 123.9 | -128.74 | 140.77 |
| Strain hardening slope, GPa | -0.2 | 0.81 | 2.05 |
| Yield stress, MPa | 293.99 | 316.82 | 277.78 |
| Yield strain | 2.01 | 0.75 | 1.26 |
| Original length, mm, $L_o$ | 49.604 | 49.612 | 49.584 |
| Final length, mm, $L_f$ | 60.409 | 57.471 | 58.321 |
| Stress at 0.2% strain, MPa | 289.79 | 314.715 | 278.979 |
| Average from test bunch (0.2%), MPa | 294.4946667 | | |

**Table D. 6: Tensile testing results sample Gallagher**

| **Specimen** | **Gallagher** | | |
|---|---|---|---|
| Sample | 1 | 2 | 3 |
| Loading rate, MPa/min | 273.18 | 298.44 | 326.15 |
| Clipgauge | Epsilon | Epsilon | Epsilon |
| Youngs modulus, GPa | 109.07 | 104.63 | 104.04 |
| Strain hardening slope, GPa | 2.54 | 2.51 | 2.34 |
| Yield stress, MPa | 280.78 | 294.54 | 295.05 |
| Yield strain | 2.76 | 2.86 | 2.7 |
| Original length, mm, $L_o$ | 49.63 | 49.687 | 49.513 |
| Final length, mm, $L_f$ | 60.409 | 56.206 | 58.953 |
| Stress at 0.2% strain, MPa | 266.266 | 272.523 | 273.023 |
| Average from test bunch (0.2%), MPa | 270.604 | | |

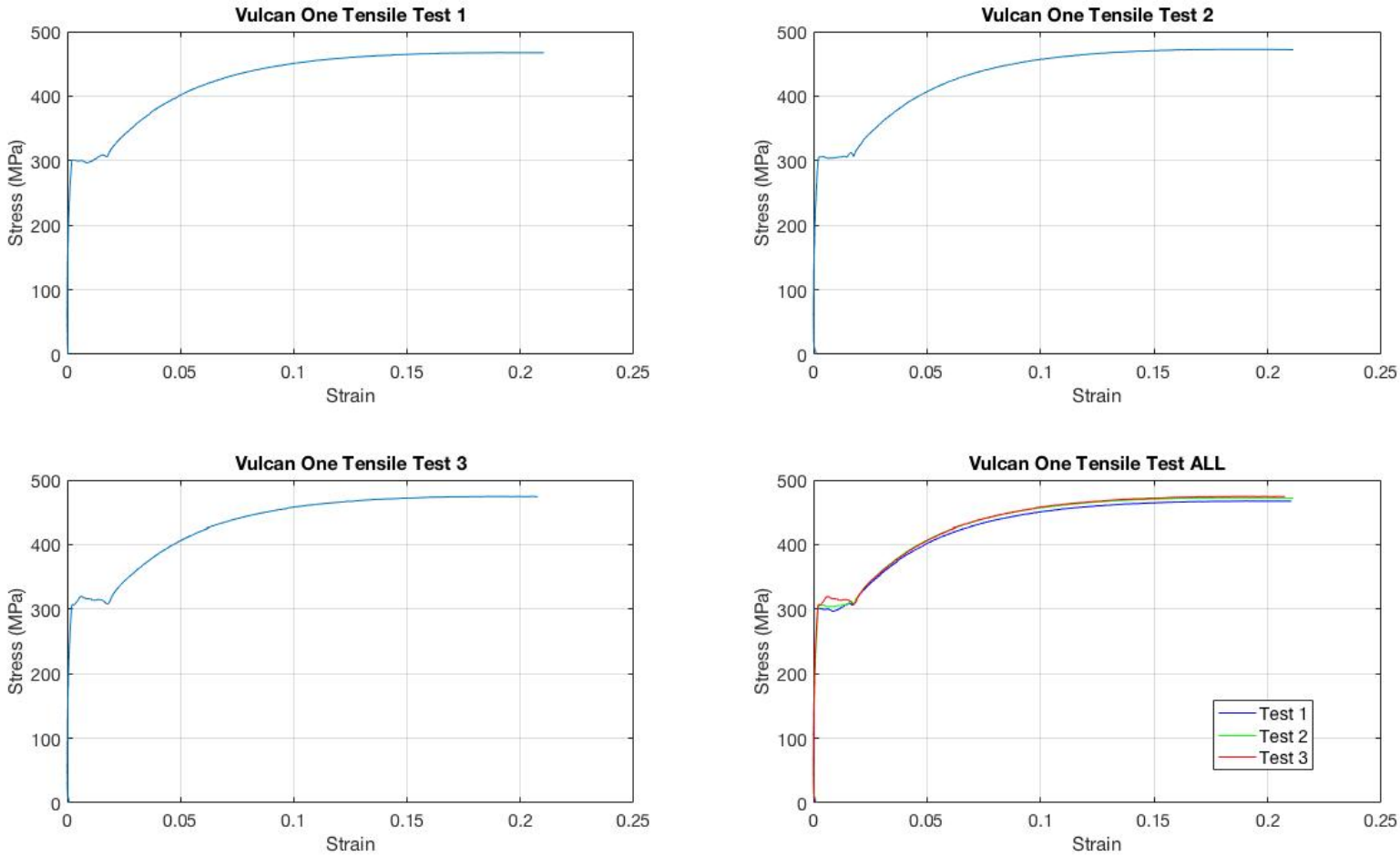


**Figure D. 2: Tensile testing results sample Vulcan One**

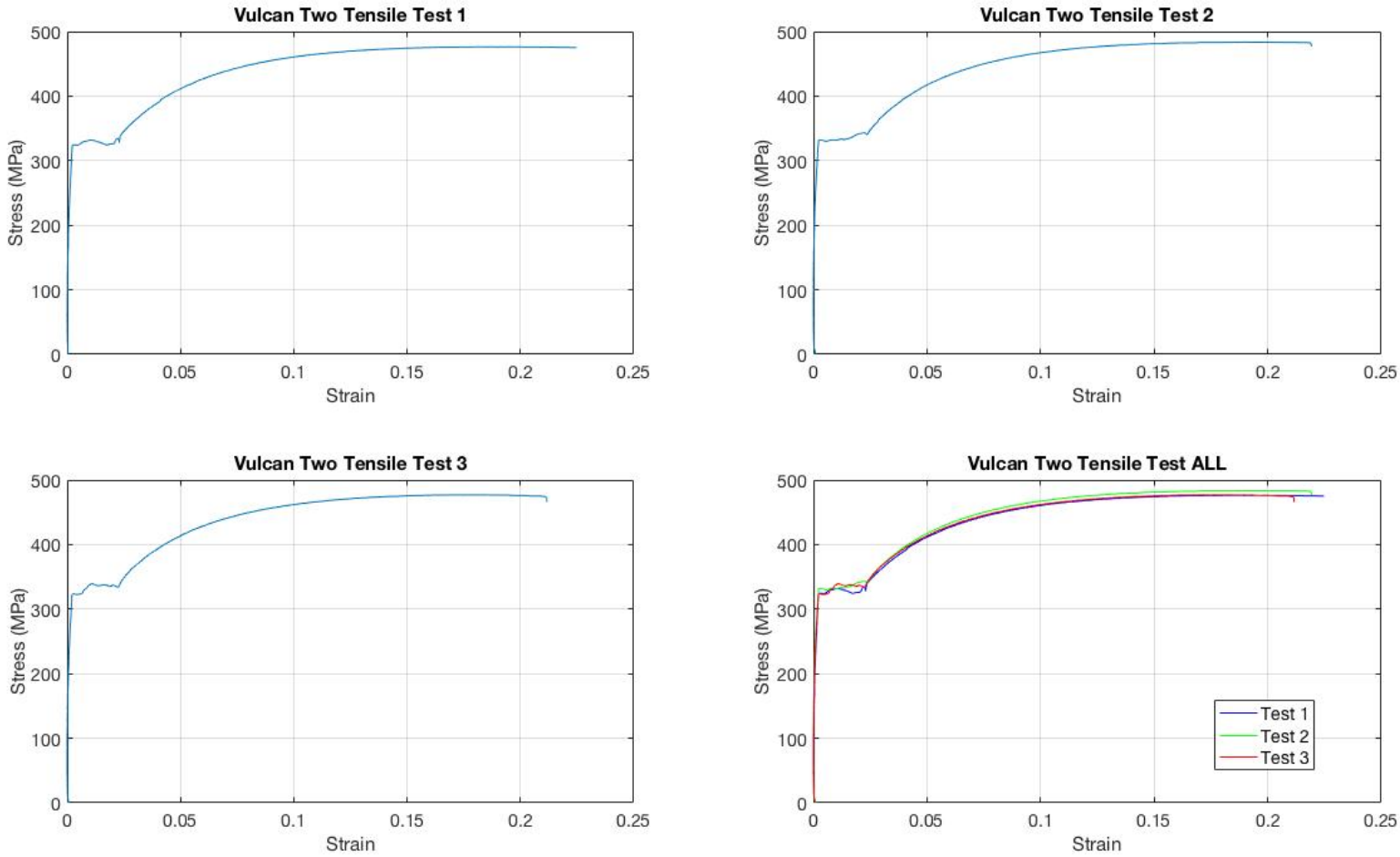


**Figure D. 3: Tensile testing results sample Vulcan Two**

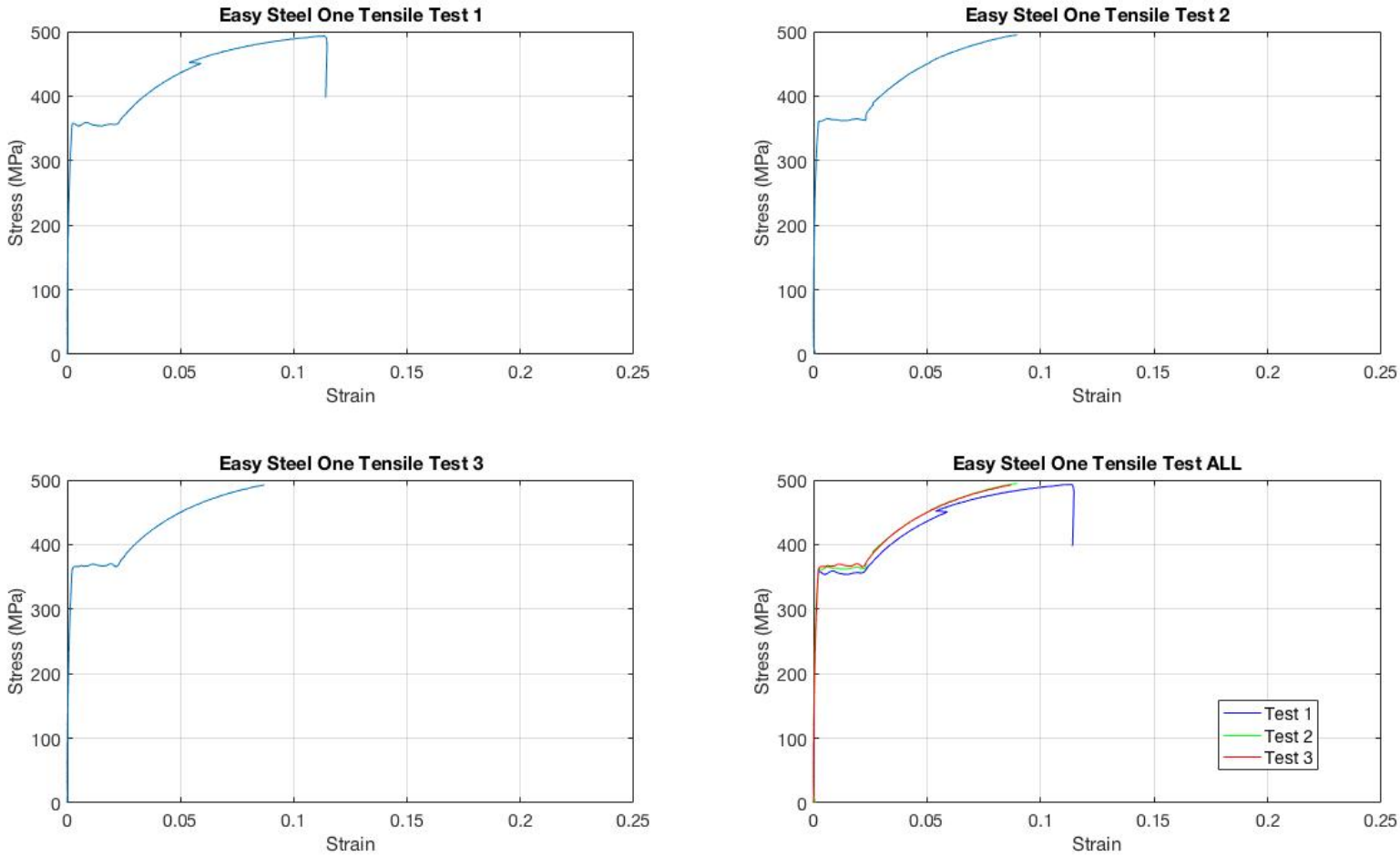


**Figure D. 4: Tensile testing results sample Easy Steel One**

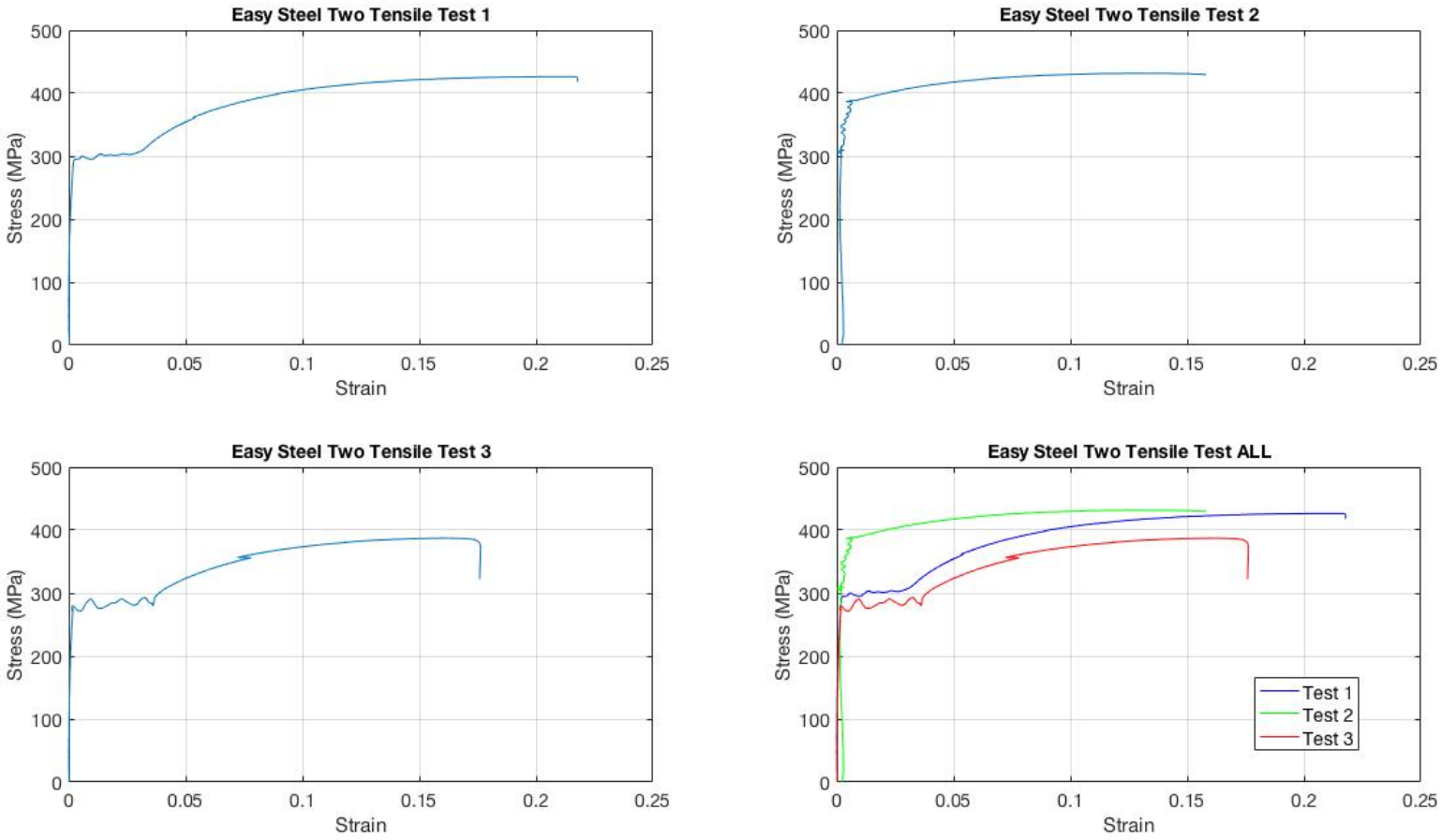


**Figure D. 5: Tensile testing results sample Easy Steel Two**

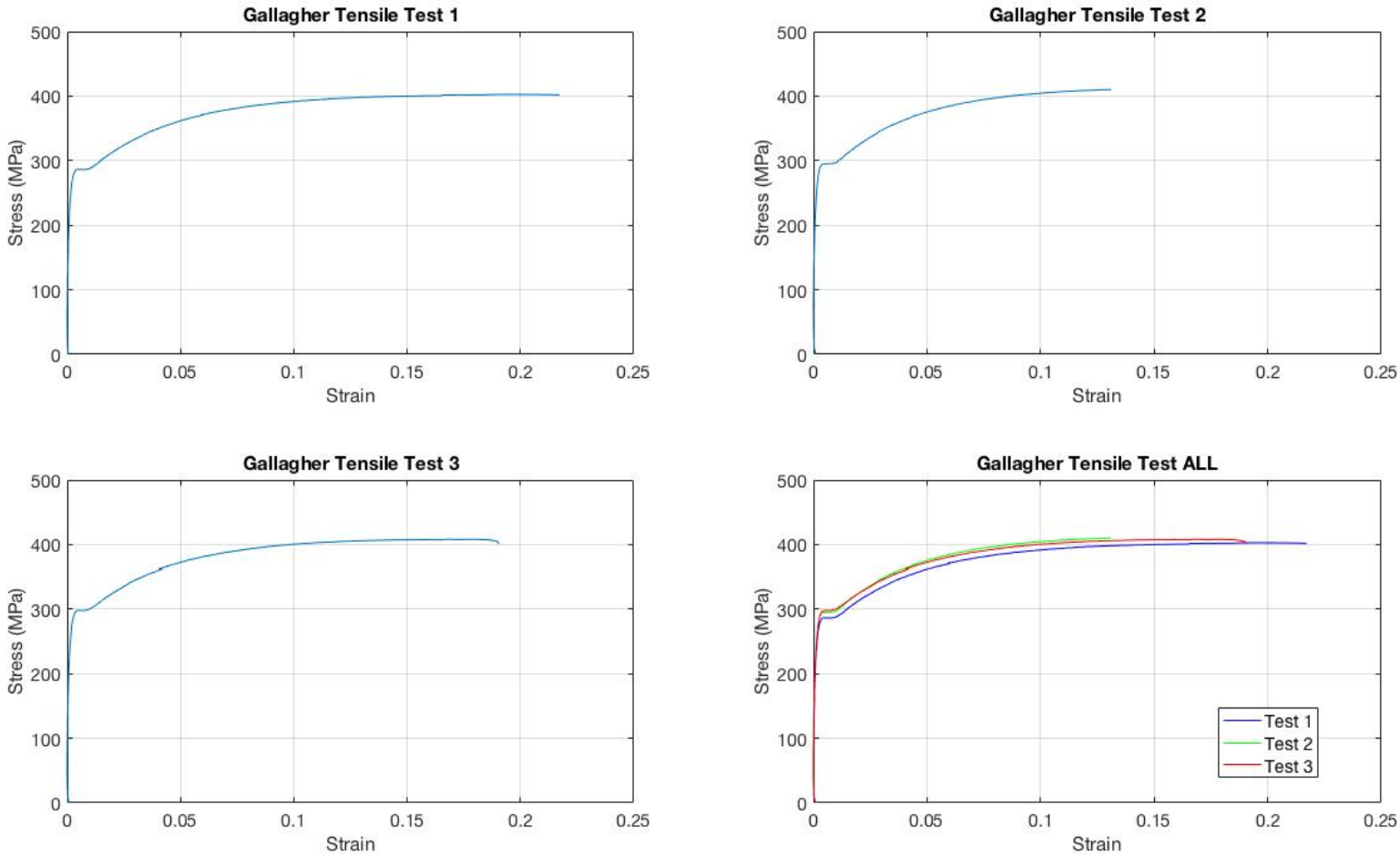


**Figure D. 6: Tensile testing results sample Gallagher**

# Appendix E – Grout Sample Testing

All grout testing was carried out in accordance with NZS 3112 (Standards New Zealand, 1986). Two samples from each specimen were tested, one at 28 days, the other within 24 hours of experimental testing of the specimen.

**Table E. 1: Grout sample test results sample C-VU2-E2-70**

| **Specimen** | | **C-VU2-E2-70** | |
|---|---|---|---|
| | | **28 day test** | **Day of test** |
| Number of days since cast | | 28 | 82 |
| Water bath temperature | ° | 20.40 | 19.20 |
| Top plastered | | No | Yes |
| | | | |
| Top diameter 1 | mm | 50.50 | 51.86 |
| Top diameter 2 | mm | 50.50 | 51.84 |
| Bottom diameter 1 | mm | 50.50 | 50.98 |
| Bottom diameter 2 | mm | 50.50 | 50.89 |
| Height 1 | mm | 101.00 | 103.84 |
| Height 2 | mm | 102.00 | 104.33 |
| | | | |
| Average diameter | mm | 50.50 | 51.39 |
| Average height | mm | 101.50 | 104.09 |
| Height to diameter ratio | | 2.01 | 2.03 |
| | | | |
| Max load | kN | 97.16 | 109.49 |
| Cross-sectional area | $mm^2$ | 2002.96 | 2074.39 |
| **Max compressive strength** | **MPa** | **48.51** | **52.78** |

**Table E. 2: Grout sample test results sample C-VU2-E1-65**

| **Specimen** | **C-VU2-E1-65** | | |
|---|---|---|---|
| | | **28 day test** | **Day of test** |
| Number of days since cast | | 28 | 82 |
| Water bath temperature | ° | 20.40 | 19.20 |
| Top plastered | | No | Yes |
| | | | |
| Top diameter 1 | mm | 50.50 | 50.22 |
| Top diameter 2 | mm | 50.50 | 51.18 |
| Bottom diameter 1 | mm | 51.00 | 50.90 |
| Bottom diameter 2 | mm | 51.00 | 51.56 |
| Height 1 | mm | 100.50 | 102.66 |
| Height 2 | mm | 101.00 | 102.91 |
| | | | |
| Average diameter | mm | 50.75 | 50.97 |
| Average height | mm | 100.75 | 102.79 |
| Height to diameter ratio | | 1.99 | 2.02 |
| | | | |
| Max load | kN | 98.59 | 113.25 |
| Cross-sectional area | $mm^2$ | 2022.84 | 2040.02 |
| **Max compressive strength** | **MPa** | **48.74** | **55.51** |

**Table E. 3: Grout sample test results sample C-VU2-E2-65**

| **Specimen** | **C-VU2-E2-65** | | |
|---|---|---|---|
| | | **28 day test** | **Day of test** |
| Number of days since cast | | 28 | 74 |
| Water bath temperature | ° | 20.40 | 18.80 |
| Top plastered | | No | No |
| | | | |
| Top diameter 1 | mm | 50.00 | 50.00 |
| Top diameter 2 | mm | 50.00 | 50.00 |
| Bottom diameter 1 | mm | 50.00 | 51.00 |
| Bottom diameter 2 | mm | 50.00 | 50.00 |
| Height 1 | mm | 102.00 | 102.00 |
| Height 2 | mm | 102.50 | 103.00 |
| | | | |
| Average diameter | mm | 50.00 | 50.25 |
| Average height | mm | 102.25 | 102.50 |
| Height to diameter ratio | | 2.05 | 2.04 |
| | | | |
| Max load | kN | 90.00 | 80.37 |
| Cross-sectional area | $mm^2$ | 1963.50 | 1983.18 |
| **Max compressive strength** | **MPa** | **45.84** | **40.53** |

**Table E. 4: Grout sample test results sample C-VU2-E3-65**

| **Specimen** | **C-VU2-E3-65** | | |
|---|---|---|---|
| | | **28 day test** | **Day of test** |
| Number of days since cast | | 28 | 76 |
| Water bath temperature | ° | 20.40 | 19.80 |
| Top plastered | | No | Yes |
| | | | |
| Top diameter 1 | mm | 50.00 | 50.48 |
| Top diameter 2 | mm | 50.00 | 50.75 |
| Bottom diameter 1 | mm | 50.50 | 50.94 |
| Bottom diameter 2 | mm | 51.00 | 50.84 |
| Height 1 | mm | 102.50 | 104.29 |
| Height 2 | mm | 103.00 | 104.12 |
| | | | |
| Average diameter | mm | 50.38 | 50.75 |
| Average height | mm | 102.75 | 104.21 |
| Height to diameter ratio | | 2.04 | 2.05 |
| | | | |
| Max load | kN | 71.24 | 123.73 |
| Cross-sectional area | $mm^2$ | 1993.06 | 2023.04 |
| **Max compressive strength** | **MPa** | **35.74** | **61.16** |

**Table E. 5: Grout sample test results sample C-VU2-E2-60**

| **Specimen** | **C-VU2-E2-60** | | |
|---|---|---|---|
| | | **28 day test** | **Day of test** |
| Number of days since cast | | 28 | 84 |
| Water bath temperature | ° | 20.40 | 19.20 |
| Top plastered | | No | Yes |
| | | | |
| Top diameter 1 | mm | 50.00 | 50.80 |
| Top diameter 2 | mm | 50.00 | 50.61 |
| Bottom diameter 1 | mm | 50.00 | 50.80 |
| Bottom diameter 2 | mm | 50.50 | 50.13 |
| Height 1 | mm | 103.50 | 104.44 |
| Height 2 | mm | 102.50 | 104.48 |
| | | | |
| Average diameter | mm | 50.13 | 50.59 |
| Average height | mm | 103.00 | 104.46 |
| Height to diameter ratio | | 2.05 | 2.07 |
| | | | |
| Max load | kN | 104.20 | 126.71 |
| Cross-sectional area | $mm^2$ | 1973.33 | 2009.71 |
| **Max compressive strength** | **MPa** | **52.80** | **63.05** |

**Table E. 6: Grout sample test results sample C-VU4-E2-65**

| **Specimen** | **C-VU4-E2-65** | | |
|---|---|---|---|
| | | **28 day test** | **Day of test** |
| Number of days since cast | | 28 | 62 |
| Water bath temperature | ° | 20.30 | 19.80 |
| Top plastered | | No | Yes |
| | | | |
| Top diameter 1 | mm | 50.00 | 50.53 |
| Top diameter 2 | mm | 50.00 | 50.65 |
| Bottom diameter 1 | mm | 50.00 | 50.83 |
| Bottom diameter 2 | mm | 51.00 | 50.73 |
| Height 1 | mm | 102.00 | 105.76 |
| Height 2 | mm | 102.50 | 105.60 |
| | | | |
| Average diameter | mm | 50.25 | 50.69 |
| Average height | mm | 102.25 | 105.68 |
| Height to diameter ratio | | 2.03 | 2.09 |
| | | | |
| Max load | kN | 101.10 | 93.27 |
| Cross-sectional area | $mm^2$ | 1983.18 | 2017.66 |
| **Max compressive strength** | **MPa** | **50.98** | **46.23** |

**Table E. 7: Grout sample test results sample C-VU6-E2-65**

| **Specimen** | **C-VU6-E2-65** | | |
|---|---|---|---|
| | | **28 day test** | **Day of test** |
| Number of days since cast | | 28 | 63 |
| Water bath temperature | ° | 20.30 | 18.80 |
| Top plastered | | No | Yes |
| | | | |
| Top diameter 1 | mm | 50.00 | 50.53 |
| Top diameter 2 | mm | 50.00 | 50.73 |
| Bottom diameter 1 | mm | 50.50 | 50.73 |
| Bottom diameter 2 | mm | 50.50 | 50.69 |
| Height 1 | mm | 101.00 | 105.65 |
| Height 2 | mm | 101.50 | 105.70 |
| | | | |
| Average diameter | mm | 50.25 | 50.67 |
| Average height | mm | 101.25 | 105.68 |
| Height to diameter ratio | | 2.01 | 2.09 |
| | | | |
| Max load | kN | 112.00 | 117.22 |
| Cross-sectional area | $mm^2$ | 1983.18 | 2016.47 |
| **Max compressive strength** | **MPa** | **56.47** | **58.13** |

**Table E. 8: Grout sample test results sample C-VS2-E2-200-R10**

| **Specimen** | **C-VS2-E2-200-R10** | | |
|---|---|---|---|
| | | **28 day test** | **Day of test** |
| Number of days since cast | | 28 | 43 |
| Water bath temperature | ° | NA | NA |
| Top plastered | | No | No |
| | | | |
| Top diameter 1 | mm | 50.00 | 50.00 |
| Top diameter 2 | mm | 50.00 | 50.50 |
| Bottom diameter 1 | mm | 50.00 | 50.00 |
| Bottom diameter 2 | mm | 50.00 | 50.50 |
| Height 1 | mm | 102.00 | 102.00 |
| Height 2 | mm | 102.50 | 101.50 |
| | | | |
| Average diameter | mm | 50.00 | 50.25 |
| Average height | mm | 102.25 | 101.75 |
| Height to diameter ratio | | 2.05 | 2.02 |
| | | | |
| Max load | kN | 110.77 | 76.20 |
| Cross-sectional area | $mm^2$ | 1963.50 | 1983.18 |
| **Max compressive strength** | **MPa** | **56.41** | **38.42** |

**Table E. 9: Grout sample test results sample C-VS4-E2-200-R10**

| **Specimen** | **C-VS4-E2-200-R10** | | |
|---|---|---|---|
| | | **28 day test** | **Day of test** |
| Number of days since cast | | 28 | 42 |
| Water bath temperature | ° | NA | NA |
| Top plastered | | No | No |
| | | | |
| Top diameter 1 | mm | 50.00 | 50.00 |
| Top diameter 2 | mm | 51.00 | 50.50 |
| Bottom diameter 1 | mm | 51.50 | 50.50 |
| Bottom diameter 2 | mm | 51.00 | 51.00 |
| Height 1 | mm | 101.50 | 103.00 |
| Height 2 | mm | 101.00 | 102.50 |
| | | | |
| Average diameter | mm | 50.88 | 50.50 |
| Average height | mm | 101.25 | 102.75 |
| Height to diameter ratio | | 1.99 | 2.03 |
| | | | |
| Max load | kN | 69.40 | 75.45 |
| Cross-sectional area | $mm^2$ | 2032.82 | 2002.96 |
| **Max compressive strength** | **MPa** | **34.14** | **37.67** |

**Table E. 10: Grout sample test results sample C-VS6-E2-200-R10**

| **Specimen** | **C-VS6-E2-200-R10** | | |
|---|---|---|---|
| | | **28 day test** | **Day of test** |
| Number of days since cast | | 28 | 42 |
| Water bath temperature | ° | NA | NA |
| Top plastered | | No | No |
| | | | |
| Top diameter 1 | mm | 50.00 | 50.00 |
| Top diameter 2 | mm | 50.00 | 50.00 |
| Bottom diameter 1 | mm | 50.00 | 50.00 |
| Bottom diameter 2 | mm | 50.00 | 51.00 |
| Height 1 | mm | 102.00 | 103.00 |
| Height 2 | mm | 102.50 | 103.00 |
| | | | |
| Average diameter | mm | 50.00 | 50.25 |
| Average height | mm | 102.25 | 103.00 |
| Height to diameter ratio | | 2.05 | 2.05 |
| | | | |
| Max load | kN | 89.60 | 120.93 |
| Cross-sectional area | $mm^2$ | 1963.50 | 1983.18 |
| **Max compressive strength** | **MPa** | **45.63** | **60.98** |

**Table E. 11: Grout sample test results sample C-VS2-E2-200-R80A**

| **Specimen** | **C-VS2-E2-200-R80A** | | |
|---|---|---|---|
| | | **28 day test** | **Day of test** |
| Number of days since cast | | 28 | 35 |
| Water bath temperature | ° | 18.90 | 19.80 |
| Top plastered | | Yes | No |
| | | | |
| Top diameter 1 | mm | 50.53 | 50.66 |
| Top diameter 2 | mm | 51.15 | 50.76 |
| Bottom diameter 1 | mm | 51.04 | 50.79 |
| Bottom diameter 2 | mm | 50.91 | 50.86 |
| Height 1 | mm | 106.98 | 108.34 |
| Height 2 | mm | 106.54 | 108.13 |
| | | | |
| Average diameter | mm | 50.91 | 50.77 |
| Average height | mm | 106.76 | 108.24 |
| Height to diameter ratio | | 2.10 | 2.13 |
| | | | |
| Max load | kN | 116.78 | 88.41 |
| Cross-sectional area | $mm^2$ | 2035.42 | 2024.24 |
| **Max compressive strength** | **MPa** | **57.37** | **43.68** |

**Table E. 12: Grout sample test results sample C-VS2-E2-200-R80B**

| **Specimen** | **C-VS2-E2-200-R80B** | | |
|---|---|---|---|
| | | **28 day test** | **Day of test** |
| Number of days since cast | | 28 | 35 |
| Water bath temperature | ° | 18.90 | 19.80 |
| Top plastered | | Yes | No |
| | | | |
| Top diameter 1 | mm | 50.86 | 51.44 |
| Top diameter 2 | mm | 50.81 | 50.60 |
| Bottom diameter 1 | mm | 50.94 | 50.92 |
| Bottom diameter 2 | mm | 50.92 | 50.90 |
| Height 1 | mm | 106.53 | 105.85 |
| Height 2 | mm | 106.49 | 105.84 |
| | | | |
| Average diameter | mm | 50.88 | 50.97 |
| Average height | mm | 106.51 | 105.85 |
| Height to diameter ratio | | 2.09 | 2.08 |
| | | | |
| Max load | kN | 103.53 | 120.75 |
| Cross-sectional area | $mm^2$ | 2033.42 | 2040.02 |
| **Max compressive strength** | **MPa** | **50.91** | **59.19** |

**Table E. 13: Grout sample test results sample C-VS2-E2-200-R80C**

| **Specimen** | **C-VS2-E2-200-R80C** | | |
|---|---|---|---|
| | | **28 day test** | **Day of test** |
| Number of days since cast | | 28 | 33 |
| Water bath temperature | ° | 20.00 | 19.80 |
| Top plastered | | Yes | No |
| | | | |
| Top diameter 1 | mm | 50.32 | 50.62 |
| Top diameter 2 | mm | 50.89 | 50.96 |
| Bottom diameter 1 | mm | 50.90 | 50.95 |
| Bottom diameter 2 | mm | 50.98 | 50.76 |
| Height 1 | mm | 106.31 | 103.89 |
| Height 2 | mm | 105.06 | 103.96 |
| | | | |
| Average diameter | mm | 50.77 | 50.82 |
| Average height | mm | 105.69 | 103.93 |
| Height to diameter ratio | | 2.08 | 2.04 |
| | | | |
| Max load | kN | 98.79 | 89.85 |
| Cross-sectional area | $mm^2$ | 2024.64 | 2028.63 |
| **Max compressive strength** | **MPa** | **48.79** | **44.29** |

**Table E. 14: Grout sample test results sample C-DU2-E2-70**

| **Specimen** | **C-DU2-E2-70** | | |
|---|---|---|---|
| | | **28 day test** | **Day of test** |
| Number of days since cast | | 28 | 64 |
| Water bath temperature | ° | 18.80 | 20.60 |
| Top plastered | | No | Yes |
| | | | |
| Top diameter 1 | mm | 50.00 | 50.77 |
| Top diameter 2 | mm | 50.00 | 51.11 |
| Bottom diameter 1 | mm | 50.50 | 50.84 |
| Bottom diameter 2 | mm | 50.50 | 50.81 |
| Height 1 | mm | 101.50 | 104.49 |
| Height 2 | mm | 101.50 | 104.58 |
| | | | |
| Average diameter | mm | 50.25 | 50.88 |
| Average height | mm | 101.50 | 104.54 |
| Height to diameter ratio | | 2.02 | 2.05 |
| | | | |
| Max load | kN | 85.40 | 140.95 |
| Cross-sectional area | $mm^2$ | 1983.18 | 2033.42 |
| **Max compressive strength** | **MPa** | **43.06** | **69.32** |

**Table E. 15: Grout sample test results sample C-DU2-E1-65**

| **Specimen** | **C-DU2-E1-65** | | |
|---|---|---|---|
| | | **28 day test** | **Day of test** |
| Number of days since cast | | 28 | 50 |
| Water bath temperature | ° | 18.90 | 19.30 |
| Top plastered | | Yes | Yes |
| | | | |
| Top diameter 1 | mm | 50.04 | 50.63 |
| Top diameter 2 | mm | 50.88 | 50.68 |
| Bottom diameter 1 | mm | 50.74 | 50.75 |
| Bottom diameter 2 | mm | 50.92 | 50.81 |
| Height 1 | mm | 105.64 | 105.02 |
| Height 2 | mm | 105.70 | 104.71 |
| | | | |
| Average diameter | mm | 50.65 | 50.72 |
| Average height | mm | 105.67 | 104.87 |
| Height to diameter ratio | | 2.09 | 2.07 |
| | | | |
| Max load | kN | 101.66 | 109.27 |
| Cross-sectional area | $mm^2$ | 2014.48 | 2020.25 |
| **Max compressive strength** | **MPa** | **50.46** | **54.09** |

**Table E. 16: Grout sample test results sample C-DU2-E3-65**

| **Specimen** | **C-DU2-E3-65** | | |
|---|---|---|---|
| | | **28 day test** | **Day of test** |
| Number of days since cast | | 28 | 42 |
| Water bath temperature | ° | 20.00 | 19.50 |
| Top plastered | | Yes | Yes |
| | | | |
| Top diameter 1 | mm | 50.50 | 50.41 |
| Top diameter 2 | mm | 50.59 | 50.81 |
| Bottom diameter 1 | mm | 50.85 | 50.91 |
| Bottom diameter 2 | mm | 50.90 | 50.86 |
| Height 1 | mm | 105.65 | 104.35 |
| Height 2 | mm | 105.10 | 104.08 |
| | | | |
| Average diameter | mm | 50.71 | 50.75 |
| Average height | mm | 105.38 | 104.22 |
| Height to diameter ratio | | 2.08 | 2.05 |
| | | | |
| Max load | kN | 110.93 | 127.59 |
| Cross-sectional area | $mm^2$ | 2019.65 | 2022.64 |
| **Max compressive strength** | **MPa** | **54.93** | **63.08** |

**Table E. 17: Grout sample test results sample C-DU2-E2-60**

| **Specimen** | **C-DU2-E2-60** | | |
|---|---|---|---|
| | | **28 day test** | **Day of test** |
| Number of days since cast | | 28 | 64 |
| Water bath temperature | ° | 18.80 | 20.60 |
| Top plastered | | No | Yes |
| | | | |
| Top diameter 1 | mm | 50.00 | 50.84 |
| Top diameter 2 | mm | 50.00 | 50.77 |
| Bottom diameter 1 | mm | 50.00 | 50.98 |
| Bottom diameter 2 | mm | 50.00 | 50.98 |
| Height 1 | mm | 102.00 | 104.01 |
| Height 2 | mm | 103.50 | 104.37 |
| | | | |
| Average diameter | mm | 50.00 | 50.89 |
| Average height | mm | 102.75 | 104.19 |
| Height to diameter ratio | | 2.06 | 2.05 |
| | | | |
| Max load | kN | 76.47 | 110.15 |
| Cross-sectional area | $mm^2$ | 1963.50 | 2034.22 |
| **Max compressive strength** | **MPa** | **38.95** | **54.15** |

**Table E. 18: Grout sample test results sample C-DU2-E2-65-T3**

| **Specimen** | **C-DU2-E2-65-T3** | | |
|---|---|---|---|
| | | **28 day test** | **Day of test** |
| Number of days since cast | | 28 | 95 |
| Water bath temperature | ° | 20.30 | 20.60 |
| Top plastered | | No | Yes |
| | | | |
| Top diameter 1 | mm | 50.00 | 50.76 |
| Top diameter 2 | mm | 50.00 | 50.39 |
| Bottom diameter 1 | mm | 50.00 | 50.71 |
| Bottom diameter 2 | mm | 50.50 | 50.93 |
| Height 1 | mm | 102.00 | 105.40 |
| Height 2 | mm | 102.00 | 104.38 |
| | | | |
| Average diameter | mm | 50.13 | 50.70 |
| Average height | mm | 102.00 | 104.89 |
| Height to diameter ratio | | 2.03 | 2.07 |
| | | | |
| Max load | kN | 94.69 | 88.85 |
| Cross-sectional area | $mm^2$ | 1973.33 | 2018.66 |
| **Max compressive strength** | **MPa** | **47.98** | **44.01** |

**Table E. 19: Grout sample test results sample C-DU2-E2-65**

| **Specimen** | **C-DU2-E2-65** | | |
|---|---|---|---|
| | | **28 day test** | **Day of test** |
| Number of days since cast | | 28 | 59 |
| Water bath temperature | ° | 18.80 | 19.30 |
| Top plastered | | No | Yes |
| | | | |
| Top diameter 1 | mm | 51.00 | 50.56 |
| Top diameter 2 | mm | 50.50 | 50.67 |
| Bottom diameter 1 | mm | 50.00 | 50.72 |
| Bottom diameter 2 | mm | 50.00 | 50.74 |
| Height 1 | mm | 102.00 | 104.72 |
| Height 2 | mm | 101.50 | 104.45 |
| | | | |
| Average diameter | mm | 50.38 | 50.67 |
| Average height | mm | 101.75 | 104.59 |
| Height to diameter ratio | | 2.02 | 2.06 |
| | | | |
| Max load | kN | 83.16 | 104.53 |
| Cross-sectional area | $mm^2$ | 1993.06 | 2016.67 |
| **Max compressive strength** | **MPa** | **41.72** | **51.83** |

**Table E. 20: Grout sample test results sample C-DU2-E2-65-T1**

| **Specimen** | **C-DU2-E2-65-T1** | | |
|---|---|---|---|
| | | **28 day test** | **Day of test** |
| Number of days since cast | | 28 | 63 |
| Water bath temperature | ° | 18.80 | 19.30 |
| Top plastered | | No | Yes |
| | | | |
| Top diameter 1 | mm | 51.00 | 50.83 |
| Top diameter 2 | mm | 50.50 | 50.77 |
| Bottom diameter 1 | mm | 50.50 | 50.88 |
| Bottom diameter 2 | mm | 50.50 | 50.79 |
| Height 1 | mm | 102.00 | 104.91 |
| Height 2 | mm | 101.50 | 105.15 |
| | | | |
| Average diameter | mm | 50.63 | 50.82 |
| Average height | mm | 101.75 | 105.03 |
| Height to diameter ratio | | 2.01 | 2.07 |
| | | | |
| Max load | kN | 97.12 | 123.40 |
| Cross-sectional area | $mm^2$ | 2012.89 | 2028.23 |
| **Max compressive strength** | **MPa** | **48.25** | **60.84** |

**Table E. 21: Grout sample test results sample C-DU4-E2-65**

| **Specimen** | **C-DU4-E2-65** | | |
|---|---|---|---|
| | | **28 day test** | **Day of test** |
| Number of days since cast | | 28 | 47 |
| Water bath temperature | ° | 20.00 | 20.60 |
| Top plastered | | Yes | Yes |
| | | | |
| Top diameter 1 | mm | 50.83 | 50.86 |
| Top diameter 2 | mm | 50.54 | 50.62 |
| Bottom diameter 1 | mm | 50.75 | 50.65 |
| Bottom diameter 2 | mm | 50.86 | 50.85 |
| Height 1 | mm | 105.90 | 105.11 |
| Height 2 | mm | 105.50 | 105.78 |
| | | | |
| Average diameter | mm | 50.75 | 50.75 |
| Average height | mm | 105.70 | 105.45 |
| Height to diameter ratio | | 2.08 | 2.08 |
| | | | |
| Max load | kN | 91.72 | 108.50 |
| Cross-sectional area | $mm^2$ | 2022.44 | 2022.44 |
| **Max compressive strength** | **MPa** | **45.35** | **53.65** |

**Table E. 22: Grout sample test results sample C-DU6-E2-65**

| **Specimen** | **C-DU6-E2-65** | | |
|---|---|---|---|
| | | **28 day test** | **Day of test** |
| Number of days since cast | | 28 | 46 |
| Water bath temperature | ° | 20.00 | 20.60 |
| Top plastered | | Yes | Yes |
| | | | |
| Top diameter 1 | mm | 50.50 | 50.71 |
| Top diameter 2 | mm | 50.85 | 50.51 |
| Bottom diameter 1 | mm | 50.82 | 50.71 |
| Bottom diameter 2 | mm | 50.83 | 50.81 |
| Height 1 | mm | 106.19 | 105.39 |
| Height 2 | mm | 105.94 | 104.92 |
| | | | |
| Average diameter | mm | 50.75 | 50.69 |
| Average height | mm | 106.07 | 105.16 |
| Height to diameter ratio | | 2.09 | 2.07 |
| | | | |
| Max load | kN | 89.85 | 103.53 |
| Cross-sectional area | $mm^2$ | 2022.84 | 2017.66 |
| **Max compressive strength** | **MPa** | **44.42** | **51.31** |

**Table E. 23: Grout sample test results sample C-DS2-E2-200-R10**

| **Specimen** | **C-DS2-E2-200-R10** | | |
|---|---|---|---|
| | | **28 day test** | **Day of test** |
| Number of days since cast | | 28 | 40 |
| Water bath temperature | ° | NA | NA |
| Top plastered | | No | No |
| | | | |
| Top diameter 1 | mm | 50.00 | 51.00 |
| Top diameter 2 | mm | 50.00 | 50.00 |
| Bottom diameter 1 | mm | 50.00 | 51.00 |
| Bottom diameter 2 | mm | 50.00 | 50.00 |
| Height 1 | mm | 102.00 | 101.00 |
| Height 2 | mm | 102.00 | 101.50 |
| | | | |
| Average diameter | mm | 50.00 | 50.50 |
| Average height | mm | 102.00 | 101.25 |
| Height to diameter ratio | | 2.04 | 2.00 |
| | | | |
| Max load | kN | 138.04 | 63.28 |
| Cross-sectional area | $mm^2$ | 1963.50 | 2002.96 |
| **Max compressive strength** | **MPa** | **70.31** | **31.60** |

**Table E. 24: Grout sample test results sample C-DS4-E2-200-R10**

| **Specimen** | **C-DS4-E2-200-R10** | | |
|---|---|---|---|
| | | **28 day test** | **Day of test** |
| Number of days since cast | | 28 | 36 |
| Water bath temperature | ° | NA | NA |
| Top plastered | | No | No |
| | | | |
| Top diameter 1 | mm | 50.00 | 50.50 |
| Top diameter 2 | mm | 50.00 | 50.50 |
| Bottom diameter 1 | mm | 50.00 | 50.50 |
| Bottom diameter 2 | mm | 50.00 | 50.50 |
| Height 1 | mm | 102.00 | 100.00 |
| Height 2 | mm | 102.00 | 98.00 |
| | | | |
| Average diameter | mm | 50.00 | 50.50 |
| Average height | mm | 102.00 | 99.00 |
| Height to diameter ratio | | 2.04 | 1.96 |
| | | | |
| Max load | kN | 138.04 | 90.63 |
| Cross-sectional area | $mm^2$ | 1963.50 | 2002.96 |
| **Max compressive strength** | **MPa** | **70.31** | **45.25** |

**Table E. 25: Grout sample test results sample C-DS6-E2-200-R80**

| **Specimen** | **C-DS6-E2-200-R80** | | |
|---|---|---|---|
| | | **28 day test** | **Day of test** |
| Number of days since cast | | 28 | 57 |
| Water bath temperature | ° | 18.80 | 19.80 |
| Top plastered | | No | Yes |
| | | | |
| Top diameter 1 | mm | 50.00 | 50.59 |
| Top diameter 2 | mm | 50.00 | 50.62 |
| Bottom diameter 1 | mm | 50.00 | 50.73 |
| Bottom diameter 2 | mm | 50.00 | 50.61 |
| Height 1 | mm | 101.50 | 105.85 |
| Height 2 | mm | 101.50 | 105.73 |
| | | | |
| Average diameter | mm | 50.00 | 50.64 |
| Average height | mm | 101.50 | 105.79 |
| Height to diameter ratio | | 2.03 | 2.09 |
| | | | |
| Max load | kN | 84.84 | 106.84 |
| Cross-sectional area | $mm^2$ | 1963.50 | 2013.88 |
| **Max compressive strength** | **MPa** | **43.21** | **53.05** |

**Table E. 26: Grout sample test results sample E-VU2-E2-65**

| **Specimen** | | **E-VU2-E2-65** | |
|---|---|---|---|
| | | **28 day test** | **Day of test** |
| Number of days since cast | | 28 | 83 |
| Water bath temperature | ° | 18.80 | 20.10 |
| Top plastered | | No | No |
| | | | |
| Top diameter 1 | mm | 50.65 | 50.76 |
| Top diameter 2 | mm | 50.91 | 50.73 |
| Bottom diameter 1 | mm | 50.80 | 50.94 |
| Bottom diameter 2 | mm | 50.85 | 50.88 |
| Height 1 | mm | 103.99 | 104.77 |
| Height 2 | mm | 104.00 | 104.75 |
| | | | |
| Average diameter | mm | 50.80 | 50.83 |
| Average height | mm | 104.00 | 104.76 |
| Height to diameter ratio | | 2.05 | 2.06 |
| | | | |
| Max load | kN | 108.06 | 126.43 |
| Cross-sectional area | $mm^2$ | 2027.03 | 2029.02 |
| **Max compressive strength** | **MPa** | **53.31** | **62.31** |

**Table E. 27: Grout sample test results sample E-VU4-E2-65**

| **Specimen** | | **E-VU4-E2-65** | |
|---|---|---|---|
| | | **28 day test** | **Day of test** |
| Number of days since cast | | 28 | 84 |
| Water bath temperature | ° | 18.80 | 20.10 |
| Top plastered | | No | No |
| | | | |
| Top diameter 1 | mm | 50.42 | 51.20 |
| Top diameter 2 | mm | 50.76 | 50.73 |
| Bottom diameter 1 | mm | 50.89 | 50.80 |
| Bottom diameter 2 | mm | 50.78 | 50.76 |
| Height 1 | mm | 103.34 | 105.08 |
| Height 2 | mm | 103.41 | 105.10 |
| | | | |
| Average diameter | mm | 50.71 | 50.87 |
| Average height | mm | 103.38 | 105.09 |
| Height to diameter ratio | | 2.04 | 2.07 |
| | | | |
| Max load | kN | 111.81 | 97.02 |
| Cross-sectional area | $mm^2$ | 2019.85 | 2032.62 |
| **Max compressive strength** | **MPa** | **55.36** | **47.73** |

**Table E. 28: Grout sample test results sample E-VU6-E2-65**

| **Specimen** | | **E-VU6-E2-65** | |
|---|---|---|---|
| | | **28 day test** | **Day of test** |
| Number of days since cast | | 28 | 93 |
| Water bath temperature | ° | 20.60 | 20.10 |
| Top plastered | | No | No |
| | | | |
| Top diameter 1 | mm | 50.59 | 50.42 |
| Top diameter 2 | mm | 50.67 | 50.74 |
| Bottom diameter 1 | mm | 50.76 | 51.03 |
| Bottom diameter 2 | mm | 50.65 | 51.01 |
| Height 1 | mm | 104.95 | 104.13 |
| Height 2 | mm | 104.92 | 104.50 |
| | | | |
| Average diameter | mm | 50.67 | 50.80 |
| Average height | mm | 104.94 | 104.32 |
| Height to diameter ratio | | 2.07 | 2.05 |
| | | | |
| Max load | kN | 99.56 | 131.93 |
| Cross-sectional area | $mm^2$ | 2016.27 | 2026.83 |
| **Max compressive strength** | **MPa** | **49.38** | **65.09** |

**Table E. 29: Grout sample test results sample E-VS2-E2-200**

| **Specimen** | | **E-VS2-E2-200** | |
|---|---|---|---|
| | | **28 day test** | **Day of test** |
| Number of days since cast | | 28 | 126 |
| Water bath temperature | ° | 18.60 | 20.90 |
| Top plastered | | No | No |
| | | | |
| Top diameter 1 | mm | 50.44 | 50.58 |
| Top diameter 2 | mm | 50.83 | 50.73 |
| Bottom diameter 1 | mm | 50.75 | 50.93 |
| Bottom diameter 2 | mm | 50.80 | 50.87 |
| Height 1 | mm | 102.97 | 104.09 |
| Height 2 | mm | 102.37 | 103.90 |
| | | | |
| Average diameter | mm | 50.71 | 50.78 |
| Average height | mm | 102.67 | 104.00 |
| Height to diameter ratio | | 2.02 | 2.05 |
| | | | |
| Max load | kN | 115.00 | 138.39 |
| Cross-sectional area | $mm^2$ | 2019.26 | 2025.03 |
| **Max compressive strength** | **MPa** | **56.95** | **68.34** |

**Table E. 30: Grout sample test results sample E-VS4-E2-200**

| **Specimen** | | **E-VS4-E2-200** | |
|---|---|---|---|
| | | **28 day test** | **Day of test** |
| Number of days since cast | | 28 | 134 |
| Water bath temperature | ° | 18.60 | 20.60 |
| Top plastered | | No | No |
| | | | |
| Top diameter 1 | mm | 50.67 | 50.54 |
| Top diameter 2 | mm | 50.69 | 50.78 |
| Bottom diameter 1 | mm | 50.85 | 50.83 |
| Bottom diameter 2 | mm | 50.87 | 50.91 |
| Height 1 | mm | 101.91 | 103.50 |
| Height 2 | mm | 102.46 | 103.40 |
| | | | |
| Average diameter | mm | 50.77 | 50.77 |
| Average height | mm | 102.19 | 103.45 |
| Height to diameter ratio | | 2.01 | 2.04 |
| | | | |
| Max load | kN | 87.13 | 166.16 |
| Cross-sectional area | $mm^2$ | 2024.44 | 2024.04 |
| **Max compressive strength** | **MPa** | **43.04** | **82.09** |

**Table E. 31: Grout sample test results sample E-VS6-E2-200**

| **Specimen** | | **E-VS6-E2-200** | |
|---|---|---|---|
| | | **28 day test** | **Day of test** |
| Number of days since cast | | 28 | 131 |
| Water bath temperature | ° | 18.60 | 20.90 |
| Top plastered | | No | No |
| | | | |
| Top diameter 1 | mm | 50.61 | 50.59 |
| Top diameter 2 | mm | 50.32 | 50.58 |
| Bottom diameter 1 | mm | 50.64 | 50.71 |
| Bottom diameter 2 | mm | 50.61 | 50.78 |
| Height 1 | mm | 101.45 | 103.88 |
| Height 2 | mm | 101.84 | 103.76 |
| | | | |
| Average diameter | mm | 50.55 | 50.67 |
| Average height | mm | 101.65 | 103.82 |
| Height to diameter ratio | | 2.01 | 2.05 |
| | | | |
| Max load | kN | 106.10 | 140.00 |
| Cross-sectional area | $mm^2$ | 2006.53 | 2016.07 |
| **Max compressive strength** | **MPa** | **52.88** | **69.44** |

**Table E. 32: Grout sample test results sample E-DU2-E2-65**

| **Specimen** | | **E-DU2-E2-65** | |
|---|---|---|---|
| | | **28 day test** | **Day of test** |
| Number of days since cast | | 28 | 98 |
| Water bath temperature | ° | 20.60 | 20.10 |
| Top plastered | | No | No |
| | | | |
| Top diameter 1 | mm | 50.84 | 50.65 |
| Top diameter 2 | mm | 50.68 | 50.80 |
| Bottom diameter 1 | mm | 50.75 | 50.89 |
| Bottom diameter 2 | mm | 50.92 | 50.81 |
| Height 1 | mm | 104.66 | 107.03 |
| Height 2 | mm | 104.76 | 106.80 |
| | | | |
| Average diameter | mm | 50.80 | 50.79 |
| Average height | mm | 104.71 | 106.92 |
| Height to diameter ratio | | 2.06 | 2.11 |
| | | | |
| Max load | kN | 116.78 | 75.65 |
| Cross-sectional area | $mm^2$ | 2026.63 | 2025.83 |
| **Max compressive strength** | **MPa** | **57.62** | **37.34** |

**Table E. 33: Grout sample test results sample E-DU4-E2-65**

| **Specimen** | | **E-DU4-E2-65** | |
|---|---|---|---|
| | | **28 day test** | **Day of test** |
| Number of days since cast | | 28 | 98 |
| Water bath temperature | ° | 20.60 | 20.10 |
| Top plastered | | No | No |
| | | | |
| Top diameter 1 | mm | 50.72 | 50.77 |
| Top diameter 2 | mm | 50.62 | 50.29 |
| Bottom diameter 1 | mm | 50.92 | 50.81 |
| Bottom diameter 2 | mm | 50.97 | 51.07 |
| Height 1 | mm | 104.40 | 107.49 |
| Height 2 | mm | 104.35 | 107.24 |
| | | | |
| Average diameter | mm | 50.81 | 50.74 |
| Average height | mm | 104.38 | 107.37 |
| Height to diameter ratio | | 2.05 | 2.12 |
| | | | |
| Max load | kN | 115.34 | 97.23 |
| Cross-sectional area | $mm^2$ | 2027.43 | 2021.65 |
| **Max compressive strength** | **MPa** | **56.89** | **48.09** |

**Table E. 34: Grout sample test results sample E-DU6-E2-65**

| **Specimen** | **E-DU6-E2-65** | | |
|---|---|---|---|
| | | **28 day test** | **Day of test** |
| Number of days since cast | | 28 | 98 |
| Water bath temperature | ° | 20.60 | 20.10 |
| Top plastered | | No | No |
| | | | |
| Top diameter 1 | mm | 50.95 | 50.86 |
| Top diameter 2 | mm | 50.62 | 50.48 |
| Bottom diameter 1 | mm | 51.08 | 50.66 |
| Bottom diameter 2 | mm | 51.02 | 51.02 |
| Height 1 | mm | 104.18 | 104.67 |
| Height 2 | mm | 104.36 | 104.71 |
| | | | |
| Average diameter | mm | 50.92 | 50.76 |
| Average height | mm | 104.27 | 104.69 |
| Height to diameter ratio | | 2.05 | 2.06 |
| | | | |
| Max load | kN | 112.80 | 134.54 |
| Cross-sectional area | $mm^2$ | 2036.22 | 2023.24 |
| **Max compressive strength** | **MPa** | **55.40** | **66.50** |

**Table E. 35: Grout sample test results sample E-DS2-E2-200**

| **Specimen** | **E-DS2-E2-200** | | |
|---|---|---|---|
| | | **28 day test** | **Day of test** |
| Number of days since cast | | 28 | 56 |
| Water bath temperature | ° | 18.80 | |
| Top plastered | | No | |
| | | | |
| Top diameter 1 | mm | 50.69 | |
| Top diameter 2 | mm | 51.01 | |
| Bottom diameter 1 | mm | 51.05 | |
| Bottom diameter 2 | mm | 50.95 | |
| Height 1 | mm | 104.81 | |
| Height 2 | mm | 105.01 | NA |
| | | | |
| Average diameter | mm | 50.93 | |
| Average height | mm | 104.91 | |
| Height to diameter ratio | | 2.06 | |
| | | | |
| Max load | kN | 109.38 | |
| Cross-sectional area | $mm^2$ | 2036.82 | |
| **Max compressive strength** | **MPa** | **53.70** | |

**Table E. 36: Grout sample test results sample E-DS4-E2-200**

| **Specimen** | | **E-DS4-E2-200** | |
|---|---|---|---|
| | | **28 day test** | **Day of test** |
| Number of days since cast | | 28 | 63 |
| Water bath temperature | ° | 18.80 | 19.30 |
| Top plastered | | No | Yes |
| | | | |
| Top diameter 1 | mm | 50.68 | 50.55 |
| Top diameter 2 | mm | 50.58 | 50.44 |
| Bottom diameter 1 | mm | 50.77 | 50.98 |
| Bottom diameter 2 | mm | 50.91 | 50.99 |
| Height 1 | mm | 105.06 | 104.55 |
| Height 2 | mm | 105.00 | 104.27 |
| | | | |
| Average diameter | mm | 50.74 | 50.74 |
| Average height | mm | 105.03 | 104.41 |
| Height to diameter ratio | | 2.07 | 2.06 |
| | | | |
| Max load | kN | 104.64 | 134.53 |
| Cross-sectional area | $mm^2$ | 2021.65 | 2022.04 |
| **Max compressive strength** | **MPa** | **51.76** | **66.53** |

**Table E. 37: Grout sample test results sample E-DS6-E2-200**

| **Specimen** | | **E-DS6-E2-200** | |
|---|---|---|---|
| | | **28 day test** | **Day of test** |
| Number of days since cast | | 28 | 76 |
| Water bath temperature | ° | 20.60 | 19.30 |
| Top plastered | | No | Yes |
| | | | |
| Top diameter 1 | mm | 50.76 | 50.97 |
| Top diameter 2 | mm | 50.61 | 50.62 |
| Bottom diameter 1 | mm | 50.73 | 50.07 |
| Bottom diameter 2 | mm | 50.80 | 51.91 |
| Height 1 | mm | 103.35 | 104.29 |
| Height 2 | mm | 103.45 | 104.44 |
| | | | |
| Average diameter | mm | 50.73 | 50.89 |
| Average height | mm | 103.40 | 104.37 |
| Height to diameter ratio | | 2.04 | 2.05 |
| | | | |
| Max load | kN | 129.91 | 100.66 |
| Cross-sectional area | $mm^2$ | 2020.85 | 2034.22 |
| **Max compressive strength** | **MPa** | **64.28** | **49.49** |

# Appendix F - Nominal Specimen Wavelength Mapping

**Table F. 1: Minor axis buckling wavelength C-VS2-E2-200-R80A**

| **Specimen** | **C-VS2-E2-200-R80A** | |
|---|---|---|
| **Minor axis buckling wavelength** | | |
| **Wavelength position** | **Distance (mm)** | **Wavelength distance (mm)** |
| Trough | 20 | |
| Crest | 70 | 50 |
| Trough | 120 | 50 |
| Crest | 190 | 70 |
| Trough | 260 | 70 |
| Crest | 320 | 60 |
| Trough | 380 | 60 |
| Crest | 430 | 50 |
| Trough | 490 | 60 |
| Crest | 560 | 70 |
| Trough | 630 | 70 |
| Crest | 710 | 80 |
| Trough | 780 | 70 |
| Crest | 860 | 80 |
| Trough | 940 | 80 |
| Crest | 1020 | 80 |
| Trough | 1080 | 60 |
| Crest | 1150 | 70 |
| Trough | 1200 | 50 |
| Crest | 1270 | 70 |
| Trough | 1330 | 60 |
| Crest | 1390 | 60 |
| Trough | 1440 | 50 |
| Crest | 1500 | 60 |
| Trough | 1550 | 50 |
| Crest | 1620 | 70 |
| Trough | 1680 | 60 |
| Crest | 1740 | 60 |
| Trough | 1800 | 60 |
| Crest | 1850 | 50 |
| Trough | 1910 | 60 |
| Crest | 1980 | 70 |
| Trough | 2040 | 60 |
| Crest | 2110 | 70 |
| Trough | 2170 | 60 |
| Crest | 2200 | 30 |
| **Average wavelength distance (mm)** | | **62.29** |

**Table F. 2: Minor axis buckling wavelength C-VS2-E2-200-R80B**

| **Specimen** | **C-VS2-E2-200-R80B** | |
|---|---|---|
| **Minor axis buckling wavelength** | | |
| **Wavelength position** | **Distance (mm)** | **Wavelength distance (mm)** |
| Crest | 30 | |
| Trough | 60 | 30 |
| Crest | 90 | 30 |
| Trough | 140 | 50 |
| Crest | 190 | 50 |
| Trough | 240 | 50 |
| Crest | 310 | 70 |
| Trough | 390 | 80 |
| Crest | 470 | 80 |
| Trough | 540 | 70 |
| Crest | 640 | 100 |
| Trough | 720 | 80 |
| Crest | 770 | 50 |
| Trough | 830 | 60 |
| Crest | 880 | 50 |
| Trough | 940 | 60 |
| Crest | 1000 | 60 |
| Trough | 1070 | 70 |
| Crest | 1120 | 50 |
| Trough | 1170 | 50 |
| Crest | 1230 | 60 |
| Trough | 1310 | 80 |
| Crest | 1390 | 80 |
| Trough | 1470 | 80 |
| Crest | 1530 | 60 |
| Trough | 1580 | 50 |
| Crest | 1630 | 50 |
| Trough | 1680 | 50 |
| Crest | 1760 | 80 |
| Trough | 1820 | 60 |
| Crest | 1890 | 70 |
| Trough | 1960 | 70 |
| Crest | 2020 | 60 |
| Trough | 2090 | 70 |
| Crest | 2160 | 70 |
| Trough | 2200 | 40 |
| **Average wavelength distance (mm)** | | **62.00** |

**Table F. 3: Minor axis buckling wavelength C-VS2-E2-200-R80C**

| **Specimen** | **C-VS2-E2-200-R80C** | |
|---|---|---|
| **Minor axis buckling wavelength** | | |
| **Wavelength position** | **Distance (mm)** | **Wavelength distance (mm)** |
| Crest | 30 | |
| Trough | 80 | 50 |
| Crest | 130 | 50 |
| Trough | 200 | 70 |
| Crest | 280 | 80 |
| Trough | 340 | 60 |
| Crest | 440 | 100 |
| Trough | 520 | 80 |
| Crest | 600 | 80 |
| Trough | 670 | 70 |
| Crest | 760 | 90 |
| Trough | 860 | 100 |
| Crest | 930 | 70 |
| Trough | 1000 | 70 |
| Crest | 1050 | 50 |
| Trough | 1110 | 60 |
| Crest | 1180 | 70 |
| Trough | 1260 | 80 |
| Crest | 1330 | 70 |
| Trough | 1410 | 80 |
| Crest | 1460 | 50 |
| Trough | 1520 | 60 |
| Crest | 1560 | 40 |
| Trough | 1640 | 80 |
| Crest | 1710 | 70 |
| Trough | 1780 | 70 |
| Crest | 1840 | 60 |
| Trough | 1900 | 60 |
| Crest | 1950 | 50 |
| Trough | 2000 | 50 |
| Crest | 2050 | 50 |
| Trough | 2110 | 60 |
| Crest | 2170 | 60 |
| Trough | 2200 | 30 |
| **Average wavelength distance (mm)** | | **65.76** |